Fouling by milk constituents and cleaning of modified surfaces

Von der Fakultät für Maschinenbau
der Technischen Universität Carolo-Wilhelmina zu Braunschweig

zur Erlangung der Würde

einer Doktor-Ingenieurin (Dr.-Ing.)

genehmigte Dissertation

von: M.Sc. Cristiane Boxler
aus: Belo Horizonte, Brazil

eingereicht am: 12.06.2014
mündliche Prüfung am: 27.11.2014

Gutachter: Herr Prof. Dr.-Ing. S. Scholl
Herr Prof. Dr. rer. nat. C.-P. Klages
Frau Prof. Dr.-Ing. B. Rademacher

2015

Preface/Acknowledgements

The present work was carried out at the Institute for Chemical and Thermal Process Engineering (ICTV), Technische Universität Braunschweig, between January 2008 and Juni 2012. This research was facilitated with the financial support of Friedrich-Ebert-Stiftung, Max-Buchner-Forschungsstiftung and Deutscher Akademischer Austausch Dienst (DAAD).

I am especially indebted to my supervisor, Prof. Dr.-Ing. Stephan Scholl for his support, his advice and constructive criticisms. I also would like to particularly thank Dr.-Ing. Wolfgang Augustin for his patience, attention to details and fruitful discussions; his enthusiasm and different approach to problems was a great inspiration.

I am grateful to Prof. Dr. rer. nat. Claus-Peter Klages and Prof. Dr.-Ing. Britta Rademacher for their interest in my work and also to Prof. Dr.-Ing. Jürgen Köhler for being the Chairman of the examiners' committee.

I also want to thank Prof. Dr.-Ing. Ulrich Kulozik who gave me the opportunity to come to Germany and to start my doctoral studies at the Technische Universität München.

I wish to express my sincere appreciation to the persons who provided help and suggestions during the development of this work. Special thanks go to Marion Harms-Linke for administrative issues, Karl Karrenführer and the mechanical team in particular Arthur Ermisch for fast technical support, Sabine Knoblauch and Anke Radeleff for helpfulness on lab issues, Karl Pfeil for the electronics lessons and support, Simone Schulze for the ESEM analyses, Christiane Schmidt (Institute of Environmental and Sustainable Chemistry, TU Braunschweig) for ICP-OES analyses and Birgit Gerke (Institut of Physical and Theoretical Chemistry, TU Braunschweig) for SEM pictures.

My appreciation also goes to my colleagues at the ICTV for the friendly working atmosphere and to the motivated students from the Technische Universität Braunschweig and from Brazilian universities (IAESTE exchange program) that worked with me during their study, for their commitment and active support in keeping the experiments progressing to provide data. I acknowledge the short but intense support by Prof. Luis F. Melo and Prof. Joaquim Mendes as well as the colleagues from the Laboratory for Process, Environmental and Energy Engineering, Faculty of Engineering, University of Porto. Thanks for the pleasant moments and interesting discussions.

Further, I wish to express my gratitude to Dipl.-Ing. Ingmar Bialuch for preparation of the DLC-based coatings at Fraunhofer Institute for Surface Engineering and Thin Films, Braunschweig. Heat exchanger plates provided by GEA Ecoflex GmbH, Sarstedt, and whey protein isolate provided by Arla Foods Ingredients Group P/S, Viby are gratefully appreciated.

Finally, I wish to thank my family and Marc for always supporting and encouraging me during the entire course of my study and Jonas for patiente.

Cristiane Boxler. Braunschweig, June 2014.

Table of Contents

Abstract

This work seeks to identify and quantify the influence of surface energetic and topographic properties on the fouling and cleaning of milk constituents. Amorphous hydrogen containing carbon coatings (a-C:X), diamond-like carbon (DLC, a-C:H) and Si doped DLC (a-C:H:Si and a-C:H:Si:O) coatings were used for the investigations. The surfaces were characterized according to their surface free energy, roughness, topography, zeta potential and chemical composition. To obtain insight into fouling and cleaning patterns and mechanisms, experiments were carried out in three different test facilities: batch vessel, flow cell and plate heat exchanger (PHE). Wherein the thermal fouling resistance was monitored and the amount, composition and structure of the deposits as well as the protein content in the cleaning solution were determined. Batch-wise fouling experiments were performed with whey protein (WPI), calcium phosphate (SMUF) and both components combined as well as raw milk at low and high initial surface temperatures of 80 °C and 120 °C (105 °C for calcium phosphate deposition) on diverse coated standard and electropolished stainless steel surfaces. Meanwhile, continuous fouling experiments were carried out in a commercial pilot scale PHE using a calcium phosphate-rich whey protein solution as model fluid. The PHE facility was operated at a product side flow velocity of 0.1 m s^{-1} (Re = 870), heating the solution from a temperature of 62 °C to 85 °C. The cleaning kinetics of WPI plus SMUF soils on the coated surfaces was monitored in a flow cell using 0.25 % w/w and 0.5 % w/w NaOH. The experimental results were fitted using a mathematical model.

The fouling layer formation, composition and structure, as well as its adhesion and cohesion strengths and thus its removal were affected by the surface free energy, surface roughness, the initial surface temperature, the solution composition and the flow conditions. The main surface property influencing the interactions at deposit/surface interface was the polar contribution to surface free energy, particularly the electron donor component (γ^-). A quadratic relationship between γ^- and the final fouling resistance $R_{f,end}$, deposit dry mass or protein and mineral contents could be found. Slightly more fouling built up on electropolished coated surfaces, which were also more difficult to clean, compared to unpolished coated surfaces. The influence of the γ^- on deposition was stronger at the initial surface temperature of 80 °C than at the temperature of 120 °C, in which protein denaturation and precipitation of calcium phosphate are enhanced. In the protein-free solution, the formation of different calcium phosphate aggregates in the first fouling layers could be related to the γ^- component, which possibly also contributed for deposits with different structures from the protein and SMUF-rich protein solutions. On low γ^- surfaces, calcium phosphate will prevail, while protein will attach preferentially to high γ^- surfaces. Crystallization and particulate fouling were more pronounced than protein fouling in the fouling experiments under flow conditions.

The removal patterns as well as the thermal data and cleaning profiles were dependent on the surface properties. On high γ^- surfaces, the soil was almost completely removed and the highest cleaning rate as well as the fastest reduction of the thermal resistance could be measured. Optimum γ^- values for minimal fouling and maximal cleaning effort were suggested.

Kurzfassung

Mit dieser Arbeit wurden die Effekte der energetischen und topographischen Oberflächeneigenschaften auf die Belagbildung und Reinigung von Milchkomponenten identifiziert und quantifiziert. Um die Oberflächeneigenschaften variieren zu können, wurden amorphe wasserstoffhaltige Kohlenstoffschichten (a–C:X), Diamond-like Carbon (DLC, a–C:H) und Si dotiertes DLC (a–C:H:Si und a–C:H:Si:O) für die Untersuchungen verwendet. Die Charakterisierung der Oberflächen erfolgte über die Bestimmung der jeweiligen freien Oberflächenenergie, Rauheit, Topographie, Zetapotential und der chemischen Zusammensetzung. Drei verschiedenen Anlagen: eine diskontinuierliche Laborversuchsanlage, ein Strömungskanal und ein kommerzieller Pilotmaßstab Plattenwärmeübertrager (PHE) wurden für die experimentellen Versuche verwendet. Durch die Erfassung des thermischen Foulingwiderstandverlaufes und die Ermittlung der Belagmasse, –zusammensetzung und –struktur sowie des Proteingehalts in der Reinigungslösung konnten Aussagen über das Fouling– und Reinigungsverhalten sowie die daran beteiligten Mechanismen getroffen werden. Dazu wurden Beläge aus drei Modellstoffsystemen: Molkeproteinisolat (WPI), Calciumphosphat (SMUF) und beide kombiniert sowie Rohmilch, bei initialen Oberflächentemperaturen von 80 °C bzw. 120 °C (oder 105 ° C für das Calciumphosphatfouling) auf verschiedenen beschichteten unbehandelten und elektropolierten Edelstahlsubstrakten in der Batchanlage erzeugt. Die kontinuierlichen Foulingexperimente wurden an der PHE-Anlage durchgeführt, die bei einer produktseitigen Strömungsgeschwindigkeit von 0,1 m s^{-1} (Re = 870) betrieben wurde, wobei die Modelllösung (WPI plus SMUF) in einem Temperaturbereich von 62 °C bis 85 °C erhitzt wurde. Die Reinigungskinetik von WPI plus SMUF Belägen wurde in einem Strömungskanal mittels 0,25 % w/w und 0,5 % w/w NaOH untersucht. Die daraus resultierenden Versuchsergebnisse wurden unter Verwendung eines mathematischen Modells angepasst.

Die Belagbildung, die Belagzusammensetzung und -struktur sowie die Adhäsions– und Kohäsionsfestigkeiten und damit die Entfernung des Belages wurden durch die freie Oberflächenenergie und –rauhheit sowie durch die initiale Oberflächentemperatur, die Lösungszusammensetzung und die Strömungsverhältnisse beeinflusst. Der polare Anteil der freien Oberflächenenergie, insbesondere die Elektronendonorkomponente (γ^-), hat wesentlich die Wechselwirkungen zwischen Belag und Oberfläche beeinflusst. Eine quadratische Beziehung zwischen γ^- und dem Endwert des Foulingwiderstands $R_{f,end}$, Belagmasse oder Protein– und Mineralgehalte im Belag wurde gefunden und ein statisches Modell zur Beschreibung des Zusammenhangs zwischen diesen Parametern wurde vorgeschlagen. Etwas mehr Verschmutzung auf beschichteten elektropolierten Edelstahloberflächen, die auch schwieriger zu reinigen waren, wurde im Vergleich zu beschichteten unbehandelten Edelstahloberflächen festgestellt. Der Einfluss von γ^- an der Belagbildung war stärker bei der initialen Oberflächentemperatur von 80 °C als bei der Temperatur von 120 °C. In der proteinfreien Lösung hing die Bildung von verschiedenen Calciumphosphat–Aggregaten in den ersten Foulingschichten mit der γ^- Komponente zusammen, die auch für Ablagerungen aus Protein sowie aus Protein plus Calciumphosphat mit unterschiedlichen Strukturen beigetragen hat. Auf niedrigen γ^- Oberflächen wuchs ein Belag überwiegend aus Calciumphosphat, während sich auf hohen γ^- Oberflächen Protein bevorzugt ablagerte. Die Beläge unter kontinuierlichen Strömungsbedingungen entstanden mehr aus Kristallisations- und partikulärem Fouling als aus Proteinfouling.

Die Reinigungsmuster sowie der thermische Foulingwiderstand und die Reinigungsprofile waren abhängig von den Oberflächeneigenschaften. Auf hohen γ^- Oberflächen konnte der Belag nahezu vollständig entfernt werden und die höchste Reinigungsrate sowie die schnellste Abnahme des thermischen Foulingwiderstands wurden gemessen. Optimale γ^- Werte für minimales Fouling und maximale Reinigungswirkung wurden daraus abgeleitet.

Nomenclature

$\langle A \rangle$	[m]	mean signal amplitude
A	[m^2]	area, plate heat exchange area
A_{coupon}	[m^2]	coupon area
$A_{plate\ gap}$	[m^2]	transversal surface of the plate gap
A_t	[m^2]	area required to transfer the total heat load
[Ca]	[g L^{-1}]	calcium concentration
C_b	[kg m^{-3}]	concentration of the reaction products in bulk
c_i	[-]	regression coefficient
C_{OH}	[kg m^{-3}]	concentration of hydroxyl ions
$\bar{c}_p$	[J kg^{-1} K^{-1}]	mean specific heat capacity
$c_{protein}$	[g L^{-1}]	protein concentration in the cleaning solution
C_s	[kg m^{-3}]	concentration of the reaction products at the solid surface
C_w	[kg m^{-3}]	concentration of contaminant in equilibrium with solvent
C_x	[kg m^{-3}]	concentration of contaminant removed
D_{app}	[m^2 s^{-1}]	diffusion coefficient
d_h	[m]	hydraulic diameter of particle or of channel in the PHE, $d_h = 2\hat{a}/\phi$
e	[A s]	elementary charge, 1.60×10^{-19} C
$\vec{E}$	[V m^{-1}]	electric field
E_a	[J mol^{-1}]	Activation energy
F	[N]	force to remove the deposit
f(κa)	[-]	Henry function
f_1	[-]	fraction of liquid area in contact with the solid
f_2	[-]	fraction of liquid area in contact with the entrapped air, $f_2 = 1 - f_1$
ΔG	[J]	Gibbs energy
H	[W m^{-2} K^{-1}]	film heat transfer coefficient
K	[-], [s^{-1}]	empirical rate constant
k_a	[s^{-1}]	first order rate constant for surface area reduction
k_B	[J K^{-1}]	Boltzmann's constant, 1.38×10^{-23} J K^{-1}
k_c	[m s^{-1}]	mass transfer coefficient for the reaction products
L	[m]	connecting rod length
L_x	[m]	contact length between the force probe and deposit at the breakage point
m	[kg]	mass of the soil
$\dot{m}$	[kg s^{-1}]	mass flow rate
$\dot{m}_d$	[kg s^{-1}]	rate of deposition
m_f	[g m^{-2}]	mass of deposit per unit heat transfer surface
$m_{protein}$	[g]	protein mass
$\dot{m}_r$	[kg s^{-1}]	rate of removal
n	[-]	refractive index of the liquid
N_A	[mol^{-1}]	Avogadro's number, 6.022×10^{23} mol^{-1}

n_{sample}	[-]	number of measurements or observations of the sample
N_x	[mol]	number of moles of contaminant removed
P	[W]	electric power
$\dot{q}$	[W m^{-2}]	heat flux
$\dot{Q}$	[W]	heat duty
$\vec{q}$	[m^{-1}]	scattering vector
R	[J K^{-1} mol^{-1}]	gas constant, 8.314 J K^{-1} mol^{-1}
r	[-]	ratio between the solid-liquid contact area and its true projection on a horizontal plane
R_a	[µm]	mean roughness
r_c	[g m^{-2} s^{-1}]	cleaning rate
$r_{c,m}$	[g m^{-2} s^{-1}]	constant or maximal cleaning rate
R_f	[m^2 K W^{-1}]	thermal fouling resistance
R_z	[µm]	roughness depth
S_a	[nm]	arithmetic mean deviation
S_{dr}	[%]	surface area ratio
S_y	[nm]	surface maximum height
S_z	[nm]	ten point height
t	[s]	Time
T	[K]	temperature
T_S	[K]	surface temperature
ΔT	[K]	temperature difference between bulk and wall
ΔT_m	[K]	log mean temperature difference (LMTD)
t_c	[h]	time for complete cleaning
t_d	[h]	cleaning time in decay stage
t_r	[s]	reputation time
t_{su}	[s]	sum of cleaning times in swelling and uniform stage
$[TN_b]$	[g L^{-1}]	TN_b concentration
U	[W m^{-2} K^{-1}]	overall heat transfer coefficient
v	[m s^{-1}]	velocity
$\dot{v}$	[m^3 s^{-1}]	volumetric flow rate
V	[L]	total cleaning solution volume
v_E	[m^2 V^{-1} s^{-1}]	electrophoretic mobility
W	[-]	waviness
x	[m]	thickness or distance
x_{bound}	[m]	thickness of the equivalent boundary layer
x_s	[m]	height of the probe above the deposit–surface interface
Y	[N m^{-2}]	critical yield stress that must be exceeded to start removal

Greek

$\tilde{A}$	[-]	removal number ~ Nu
µ	[kg s^{-1}m^{-1}]	dynamic viscosity
$\hat{A}$	[m]	corrugation depth

β	[°]	chevron corrugation inclination angle
γ	[mN m^{-1}]	surface free energy
ε	[-]	medium dielectric constant
θ	[°]	contact angle
θ_s	[°]	scattering angle
κ_s	[N m^{-1}]	resisting interfacial tension
Λ	[m]	corrugation wavelength
λ	[W m^{-1} K^{-1}]	thermal conductivity
λ_0	[m]	wavelength in vacuum
ξ	[s^{-1}]	kinetic constant
ρ	[kg m^{-3}]	density
ρ_f	[kg m^{-3}]	deposit density
τ_w	[Pa]	wall shear stress
Φ	[m]	Doppler phase shift
ϕ	[-]	plate area enlargement factor
Ψ	[-]	dimensionless parameter

Dimensionless numbers

Nusselt number	Nu	$Nu = \frac{h d_h}{\lambda}$
Prandtl number	Pr	$Pr = \frac{\mu \bar{c}_p}{\lambda}$
Reynolds number	Re	$Re = \frac{\rho v d_h}{\mu}$

Superscripts and subscripts

-	electron donor (base)
+	electron acceptor (acid)
0, o	initial
1	liquid
2	solid
3	gas
AB	Acid-Base
clean	clean surface
dis	dispersive
end	final
f	fouled
in	inlet
LW	Lifshitz-van der Waals
out	outlet
pol	polar
PS	product side
r	removal
s	solid
SS	service side
TOT	total

Acronyms / Abbreviations

ACP	amorphous calcium phosphate
AFM	atomic force microscope
ANOVA	analysis of variance
CIP	cleaning in place
CVD	chemical vapor deposition
DLC	diamond-like carbon
DVLO	Derjaguin and Landau, Verwey and Overbeek
EDLC	electropolished plus DLC coated surface
ESEM	environmental scanning electron microscopy
ESICAN	electropolished plus SICAN coated surface
ESICON®	electropolished plus SICON® coated surface
ESS	electropolished stainless steel
IEP	isoelectric point
PECVD	plasma enhanced chemical vapor deposition
PHE	plate heat exchanger
SMUF	simulated milk ultrafiltrate
s	sample standard deviation
SE	standard error
SS	stainless steel
TN_b	bound nitrogen
UHT	ultra-high temperature
WPC	whey protein concentrate, dairy product enriched in whey proteins (60 – 85 %) obtained from milk whey
WPI	whey protein isolate, dairy product enriched in whey proteins (≥ 90 %) and proportionally lower concentration of lactose and minerals than WPC
α-la	α-lactoalbumin
β-lg	β-lactoglobulin

1 Introduction

The dairy industry has been confronted with fouling since the first commercial pasteuriser in the mid-1880s (Westhoff, 1978) and plate heat exchangers were introduced in the 1930s (Visser and Jeurnink, 1997a; Wang et al., 2007) for pasteurizing and sterilizing milk. Since then, diverse technological approaches have been proposed and applied to mitigate milk fouling, although such strategies are limited, need to be adapted to the product or are not effective and sustainable in controlling deposit formation. The control of fouling in the food industry is essential to prevent food contamination and the risk to consumers' health. Therefore, heat transfer systems are regularly cleaned, resulting in: *(i)* loss of production efficiency, due to downtime for cleaning; *(ii)* additional energy and resource consumption, to counter heat transfer inefficiencies caused by fouling, and to heat cleaning solutions; and *(iii)* waste production and the necessity to treat the effluents. While the global production of milk products is consistently increasing on average, milk fouling remains an unresolved issue at present. Owing to the insufficient knowledge about the factors and conditions affecting the incidence of fouling as well as the complexity of deposition and cleaning mechanisms, the heat transfer equipment is often over designed and most CIP systems are operated on a semi-empirical basis. This scenario gives rise to new needs, new technological developments and requirements (Wilson, 2005; Napper, 2007; Guignard et al., 2009) and thus reflects the focus of this research.

The adhesion of particles to surfaces is unavoidable in food processing facilities (Bobe et al., 2007). The attachment, adhesion, retention and removal of foulant components to the surface during the thermal processing of food products are complex processes involving interactions between the surface, the deposit and the foulant or cleaning solution. In addition, these processes are affected by diverse factors. Fig. 1.1 summarizes the influencing factors on deposition, $\dot{m}_d$, and removal, $\dot{m}_r$, of whey protein and calcium phosphate, the main components of milk deposits, during fouling.

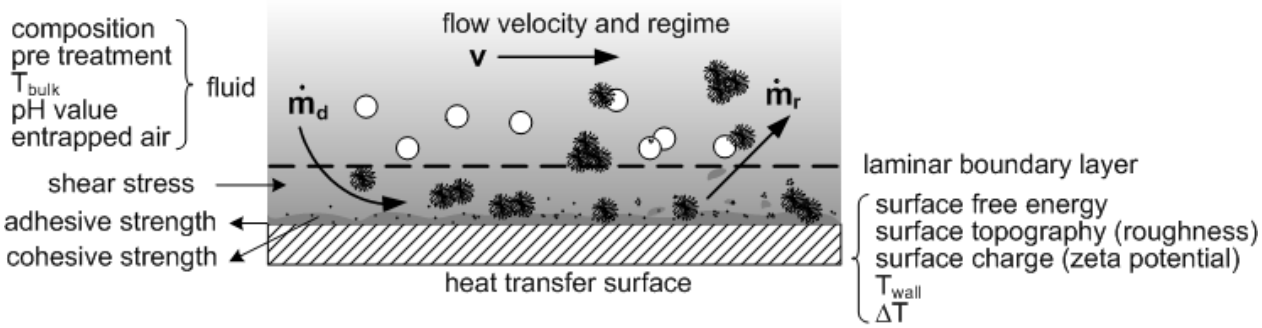

Fig. 1.1. Deposition and removal on a heat transfer surface by a calcium phosphate–rich whey protein solution. ○ native and ✵ denatured β-lactoglobulin, · calcium phosphate nanoclusters, crystals or particulates (adapted from Boxler et al., 2014b)

In order to understand the mechanism of deposit formation and removal, topographic and energetic surface properties have been modified and their effects on parameters such as heat transfer performance, pressure drop, deposit characteristics and properties, deposit adhesive and cohesive strengths and cleaning kinetics have been related. The defined surface modification offers strong potential to avoid or minimize fouling, as well as enhancing the cleanability of the surface, given that the interaction between heat transfer surface and process fluid constituents in the building of the first fouling layers can be altered/changed. The change of the interactions at the interface liquid/deposit might thereby result in longer operational times and shorter cleaning periods. However, an anti-fouling surface, approved for use in the food industry, is easy to clean, resistant in operation and remains effective over the lifetime of a plant is still a challenge (Boxler et al., 2014a).

The aim of the present work is to extend the knowledge about the fouling process occurring during the heat treatment of milk products. For this purpose, the fouling behavior of three model solutions (whey protein, SMUF – a solution that simulates the mineral composition of milk, and a SMUF–rich whey protein solution) on amorphous hydrogen containing carbon coatings, namely a-C:H, a-C:H:Si and a-C:H:Si:O, with different energetic surface properties is to be examined. These coatings show non-cytotoxicity, satisfy corrosion and mitigation standards for food contact and offer superior mechanical properties, thus probably being suitable for many applications in the food industry. The fouling experiments will be carried out under batch conditions and in a pilot scale plate heat exchanger, attempting to approach an industrial situation and permitting the comparison of both processing modes. Previously published studies (as will be discussed in Chapter 2) investigated mainly the influence of process conditions or of surface properties on the formation and composition of whey or milk deposits. However, the simultaneous influence of process and surface related variables on milk fouling is missing. Therefore, further objectives of this work are to quantify and model the relationship between process conditions, surface properties and deposition parameters as well as to find out the particular influencing variables.

The cleaning process is affected by six parameters: temperature, chemistry, cleaning time or duration, fluid mechanical action, type and amount of deposit and surface material or properties, as described in the extended Sinner's circle (Graßhoff, 1998). Here again, many studies have shown the separate influence of process parameters and surface properties (mainly surface material and roughness) on different type of deposits, but no attention has been given on the simultaneous influence of more than one surface property (surface free energy and surface roughness) on cleaning. Thus, another focus of this work concerns the understanding of the cleaning process of milk deposits formed on surfaces with different properties. The combined influence of the surface properties on the cleaning kinetics will be be identified and quantified. For this purpose, reproducible deposits will first be generated on the amorphous hydrogen containing carbon coatings, which are then examined regarding their cleaning behavior.

2 Theoretical Background

In this chapter, aspects of fouling in general and milk fouling in particular are presented. Furthermore, the deposition mechanisms of milk constituents such as proteins and salts are brought to perspective. In this context, influencing factors and fouling mitigation strategies are outlined. Section 2.3 addresses cleaning mechanism and models. Finally, the influence of surface properties on fouling and cleaning of food deposits is discussed.

2.1 Fouling – General concepts

Fouling is the formation and accumulation of unwanted deposits on the surfaces of heat exchangers (Bott, 1995). Soiling also includes the accumulation or presence of residues, cleaning agent residues and residues from rinse water (Maxcy, 1973). The fouling layers lead to a drastic reduction of the equipment thermal efficiency and an increase of the pressure drop in heating systems. Furthermore, the deposits can contaminate the fluids with which they come in contact and promote favorable environmental conditions for the growth of microorganisms and biofilm formation (Marchand et al., 2012). Consequently, additional capital and operating costs and the loss of production opportunities due to production downtime are caused. In the food industry, fouling might also cause a reduction of food quality due to overheating or insufficient heating, resulting in the loss of product quality (Cattaneo et al., 2008) or the potential risk of microbiological contamination (Holsinger et al., 1997). Hence, regular and intensive cleaning procedures are required to remove the deposits, maintain production efficiency and meet hygienic standards and regulations.

2.1.1 Fouling mechanisms and phases

Fouling is a complex process, usually involving various physicochemical sub-processes, which on the other hand are related to the composition and physicochemical characteristics of the fluids in contact with the surface, the properties of the heating surface, design of the heat exchanger, mode of heat transfer, operating conditions (mainly temperature and flow regime) and the type/nature of the fouled layer.

The fouling process can be classified into five groups (Epstein, 1981), depending on the key physical or chemical fouling mechanisms:

1. Crystallization or scaling formation: the precipitation of soluble material from the bulk fluid onto the solid surface due to a reduction in its solubility at the wall temperature. This category also includes the freezing fouling, which is the deposition of solid material from the process fluid itself through cooling down to its freezing point (Bott, 1990);
2. Particulate sedimentation, accumulation or silting: the deposition of finely dispersed insoluble solid particles from the process stream onto a heat transfer surface;
3. Chemical reaction accompanied with product attachment: deposit formed by chemical reactions, such as the decomposition or polymerization of organic matter at the heat transfer surface, in which the surface material itself is not a reactant;

4. Corrosion of the heat transfer surface: corrosion of the substrate resulting in corrosion products, which foul the surface and can foster the attachment of other potential fouling compounds;
5. Biological fouling or biofouling: deposition and growth of microorganisms at the heat transfer surface. The transport of the cells towards a surface, their initial adhesion and the polymer production by the cells leads to the formation of biofilms. The presence of suitable nutrients in a particular environment will determine the survival of the microorganisms, the production of exo-polysaccharides and their consequent growth (Bott, 2011).

A combination of several of the above mechanisms can occur simultaneously, forming a mixed or composite fouling (Epstein, 1981; Bott, 1990; Sheikholeslami, 1999), such as deposits formed in the food industry (Fig. 2.1).

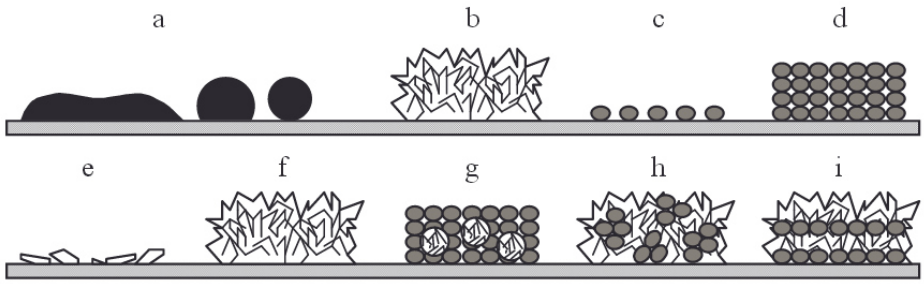

Fig. 2.1. Deposits formed by heating of food products (Kessler, 1996). a: aqueous solutions or fat; b: sugar or low molecular weight carbohydrates, crystal formation by adhesion and agglomeration; c: adsorption of a protein monolayer; d: cross-linked protein agglomerates; e: adsorption of ions or crystals; f: crystallization; g: protein deposits with salt inclusions; h: salt deposits with protein inclusions; i: mixed deposits of protein and salt layers

The overall fouling process consists of a number of sub-processes (Epstein, 1981), encompassing bulk, induction, fouling and aging reactions, as well as diffusion (Sandu and Lund, 1985). The five most important sub-processes are summarized in Fig. 2.2. Here, again an overlap of phases during fouling can occur, such as simultaneous deposition or re-entrapment of particle agglomerate or particulate and removal, or deposit aging, which starts as soon as it has been laid down on the heat transfer surfaces (Epstein, 1981; Bohnet, 1987).

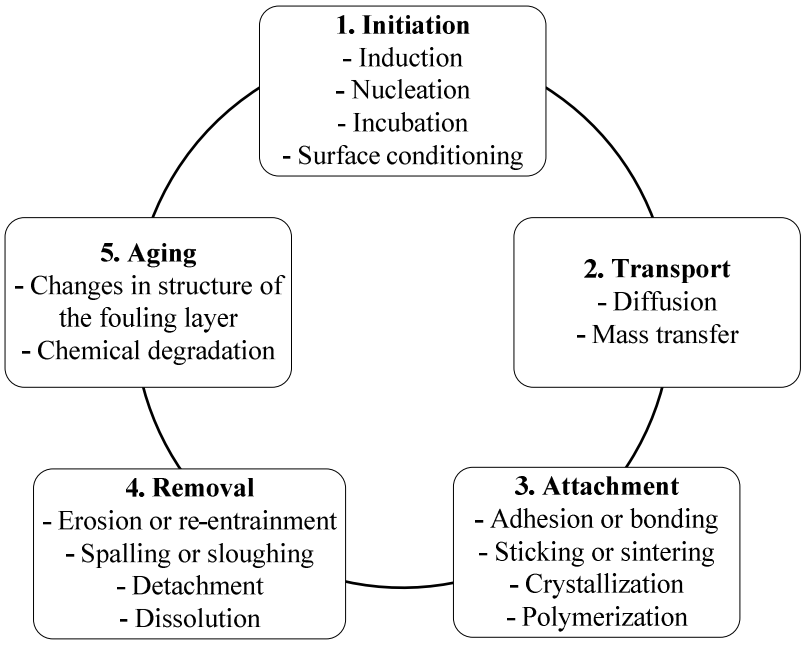

Fig. 2.2. Important phases of fouling (Epstein, 1981; Bohnet, 1987)

2.1.2 Fouling related costs

It is estimated that the worldwide costs due to fouling amount to several billion €/a. In industrial operations, the cost of fouling is in the order of 0.1 – 0.3 % of Gross National Product (GNP) (Garrett-Price et al., 1985; Bohnet, 1987; Chenoweth, 1990; Steinhagen et al., 1993; Xu et al., 2007). In the dairy industry, fouling and the resulting cleaning of the process equipment accounts for about 80 % of the total production costs (Bansal and Chen, 2006). The cost of fouling in the French dairy industry reached 150 million €/a in 1990 and 36 million €/a in the Netherlands in 1986 (Visser and Jeurnink, 1997b). The estimated product loss costs in the Netherlands are around € 3,200/ton deposit (de Jong et al., 2002). An overview of the environmental and ecological impact of the dairy sector (farming and processing) regarding the greenhouse gas emission, primary energy consumption and water use is given by Theilen and Goldbach (2000), Umweltbundesamt (2005) and Guignard et al. (2009). The cleaning of equipment plays a major role in both hygienic and economic considerations and has enormous potential for optimization. About 1.70 kg alkali and 0.60 kg of acid (Spreer, 2005) or 3 kg cleaning and disinfection agents and 1.5 m^3 water (Molkerei Weihenstephan, 2005, 2008; Guignard et al., 2009) are required per ton of processed milk. In Germany, it corresponds to an annual consumption of 70 – 90 million tons of cleaning and disinfection agents and 45 million m^3 water. For other dairy products such as cheese or yoghurt, a specific consumption up to 6 m^3 water per ton product can be estimated (mostly cleaning/rinsing water) (Guignard et al., 2009).

In general, the costs caused by fouling involve:

i. capital expenditure: overdesign of the surface area and extra pumps;
ii. provision of additional equipment to clean the process plant;
iii. loss of production as a result of downtime for cleaning;
iv. energy costs for increased heating demand, sterilization of equipments and the operation of the plant during cleaning;
v. costs with cleaning and disinfection agents and water as a solvent and detergent and steam as an energy source and for sterilization;
vi. disposal or processing for re-use of cleaning chemicals and effluent treatment;
vii. operating costs of anti-fouling devices: employment of biocides to avoid biofouling; purchase and dosing of biocides (Bott, 2011).

2.1.3 Fouling resistance

The fouling resistance, sometimes called the fouling factor, can be defined as the adverse thermal effects of the presence of a deposit on heat transfer surface (Bott, 1995). Fig. 2.3a illustrates the various resistances to heat transfer encountered as heat flows from a hot fluid to a cold fluid (e.g a food product) and the accompanying temperature drops due to the presence of fouling layers.

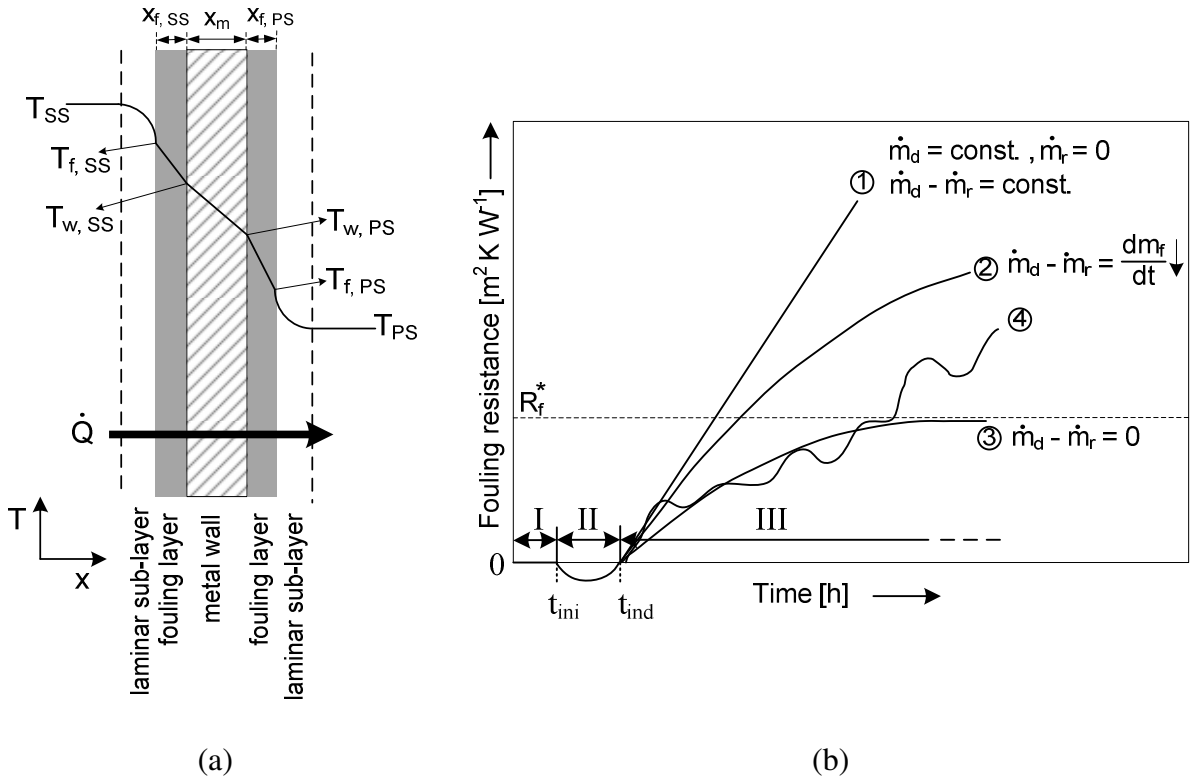

(a) (b)

Fig. 2.3. (a) Idealized distribution of service, product, wall and deposit temperatures across a fouled heat transfer surface of a generalized heat exchanger; (b) Characteristic fouling curves

For a constant heat transfer rate and steady state conditions and assuming the formation of a uniform fouling layer, the heat flow for parallel plates is given by:

$$\dot{Q} = h_{SS} A(T_{SS} - T_{f,SS}) = \frac{\lambda_{f,SS}}{x_{f,SS}} A\left(T_{f,SS} - T_{w,SS}\right) = \frac{\lambda_m}{x_m} A\left(T_{w,SS} - T_{w,PS}\right) = \frac{\lambda_{f,PS}}{x_{f,PS}} A\left(T_{w,PS} - T_{f,PS}\right)$$
$$= h_{PS} A\left(T_{f,PS} - T_{PS}\right) \tag{2.1}$$

The overall temperature driving force to accomplish the heat transfer between the hot and the product fluid streams is the sum of the individual temperature differences. i.e.:

$$(T_{SS} - T_{f,SS}) + \left(T_{f,SS} - T_{w,SS}\right) + \left(T_{w,SS} - T_{w,PS}\right) + \left(T_{w,PS} - T_{f,PS}\right) + \left(T_{f,PS} - T_{PS}\right) \quad \text{or} \quad T_{SS} - T_{PS} \tag{2.2}$$

Then the heat flux for parallel plates with identical heat transfer surface is given by:

$$\dot{q} = U_f \left(T_{SS} - T_{PS}\right) \tag{2.3}$$

The overall heat transfer resistance ($1/U_f$) for the fouled surface is a sum of the individual resistances, namely the resistance of the outer and inner convective heat transfer, the thermal conduction through the heat exchanger and the fouling resistances on the surfaces of the hot and the product fluid streams. Since the heat transfer area remains unchanged, overall heat transfer resistance U_f for the fouled surface is:

$$\frac{1}{U_f} = \frac{1}{h_{SS}} + \frac{x_{f,SS}}{\lambda_{f,SS}} + \frac{x_m}{\lambda_m} + \frac{x_{f,PS}}{\lambda_{f,PS}} + \frac{1}{h_{PS}} \tag{2.4}$$

The thermal impact of fouling is often expressed in terms of the fouling resistance R_f which is defined by the difference between the inverse of the fouled U_f and the clean U_{clean} overall heat transfer coefficient. Assuming no change of the film heat transfer coefficients (h_{SS} and h_{PS}, respectively), considering fouling only on the product side, i.e. $x_{f,SS} = 0$ m and $x_{f,PS} = x_f$ for simplification, the thermal fouling resistance can be written as:

$$R_f = \frac{1}{U_f} - \frac{1}{U_{clean}} = \frac{x_f}{\lambda_f} \tag{2.5}$$

Assuming a uniform coverage of the entire heat transfer surface, the deposit coverage (mass per unit area) m_f in the fouling layer can be expressed by:

$$m_f = x_f \rho_f \approx \rho_f \lambda_f R_f \tag{2.6}$$

At constant density and thermal conductivity of the fouling layer, m_f is directly proportional to R_f. However, it is not usually a good assumption, given that the fouling layer distribuition on the surface is seldom uniform, the values of ρ_f and λ_f are highly dependent

upon the conditions existing at the time of deposition (Knudsen, 1980) and they can vary with deposit aging (Davies et al., 1997).

In most cases, the deposition is simultaneously accompanied by a removal process that is determined by the adhesion and cohesion forces between deposit/heat transfer surface or deposit/deposit and the shear strength of the fouling layer. According to Kern and Seaton (1959), the net rate of fouling or the rate of the increase of solid in the fouling layer thus results from two competing process deposit formation and removal:

$$\frac{dm_f}{dt} = \dot{m}_d - \dot{m}_r \tag{2.7}$$

The progress of a fouling process can be described by a plot of thermal fouling resistance or mass of deposit per unit heat transfer surface against time. The three most characteristic fouling curves, namely linear (1), non-asymptotic or falling rate (2) and asymptotic (3), are shown in Fig. 2.3b. The sawtooth behaviour (4) displays a net rising curve periodically interrupted by drops in the fouling resistance.

The different fouling curves are described as:

(1) Linear fouling: represents a process in which the deposition proceeds at a constant rate and the deposit removal is negligible or the deposition and removal rates have a constant difference. A linear increase of deposit mass and thus also the fouling resistance with time takes place;

(2) Non-asymptotic or falling rate fouling: with increasing of the fouling layer thickness and mass the deposition slows down, without the R_f tending towards a maximum value. This behavior can also be observed when the deposition rate remains constant (and the surface temperature decreases) and the removal rate increases with time;

(3) Asymptotic fouling: a steadily decreasing difference between deposit formation and removal, in which the difference approaches zero as mass of the fouling per unit area and thus R_f approaches a finite value (m_f^* or R_f^*, respectively). Removal of deposit might begin right immediately after the deposition starts.

(4) Sawtooth fouling: a collection of increasing and rising curves, in which the fluctuations of the fouling resistance are caused by a periodically removal of relatively large chunks of deposit. Here, the removal process is determined by: *(i)* low deposit adhesive and cohesive strengths, which can be caused by changes in the deposit structure and chemical degradation; *(ii)* increased shear or thermal stresses; or *(iii)* corrosion of the substrate.

Regarding the time profiles of fouling, three different phases can be distinguished, as suggested in Fig. 2.3b:

I. Delay or initiation period: can be observed before any appreciable fouling is recorded after starting a process. This does not imply that no fouling occurs, although at this time the first fouling layer is formed, e.g. nucleation in crystallization fouling or organic monolayer formation in protein or biological fouling (conditioning of the surface). The initiation phase ends at the initiation time t_{ini};

II. Transition period: deceptively low and even negative values of R_f can be measured, whereby the deposit roughness gives rise to an increase in the convective heat transfer coefficient between the surface and the fluid, compared to that of the clean surface (Albert et al., 2011; Epstein, 1981). In this "roughness controlled phase", variations in the initial temperature profiles, pressure drop and deposit mass can be detectable;

III. Layer growth or fouling phase: the effect of deposit roughness declines in relative importance as the fouling layer thickness increases and R_f becomes large. A compact fouling layer grows up.

Phases I and/or II do not necessarily occur (Bohnet, 1987) and both together are also called the induction phase. The induction phase ends at the induction time t_{ind}. From an industrial perspective, the physicochemical interactions that take place in the induction phase and the formation of the initial fouling layer are very important because they determine the deposit adhesion strength and the cleanability of the surface (Bobe et al., 2007; Boxler et al., 2013a).

2.2 Milk Fouling

The economic importance of the world dairy industry is highlighted in The World Dairy Situation (2010), and for Germany by Wohlfahrt (2012). The worldwide milk production was 703 million tons in 2009, of which ca. 590 million was cow milk, including 120 million tons of liquid milk for direct consumption. In Germany, approximately 30 million tons of cow milk is produced and processed annually, of which 14 million tons, or almost half, is exported. The German dairy industry generated annual sales of around 24 billion € in 2011, making it by far the largest food industry in Germany. In 2011, an average consumer consumed almost 120 kg of dairy products in the form of liquid milk and other products such as cream, butter, yoghurt and cheese. Considering the magnitude of these numbers and the costs due to fouling and cleaning, as indicated in section 2.1, it can be concluded that the understanding of fouling and cleaning mechanisms holds great importance to prevent, avoid or reduce fouling, as well as improving the cleaning efficiency in dairy.

Thermal treatment has long been used for preservation purposes in the processing of dairy products (Westhoff, 1978; Holsinger, 1997). Raw milk is subject to pasteurization for at least 15 seconds at 72 °C (Böhm et al., 2000; Regulation EU No. 605/2010**,** 2010) in order to destroy heat sensitive spoilage and pathogenic bacteria. Further processing steps (UHT treatment - at no less than 135 °C in combination with a suitable holding time (Böhm et al., 2000; Regulation EU No. 605/2010, 2010) or drying) are designed to limit the growth of the thermoduric bacteria that survive the pasteurization. Heating the milk also deactivates enzymes that could degrade the product quality and eliminates non-pathogenic microorganisms that could produce lactic acid or enzymes, leading to off-flavors, thus increasing the product shelf life. Heat treatments also confer various functionalities to dairy ingredients, such as viscosity, gelation, renneting, foaming, and emulsifying properties (Augustin and Udabage, 2007). On the other hand, excessive heating of milk can lead to undesirable alterations in the milk constituents that subsequently influence the functional

properties of the dairy products. One consequence of the thermal treatment is the building up of a fouling layer on the heat transfer surface due to physicochemical changes in the product.

The first published papers on milk fouling deal with the soiling of dairy farm utensils or batch-wise pasteurizers, referred to as milk stone or milk scale, and were presented in the early 1930s (Parker and Johnson, 1930; Tuckey, 1931).

Milk stone is the product resulting from the reactions between an initial film formed on the equipment surface or remnant of deposit that was not readily removed by cleaning, and the chemical constituents of water supply and cleaning detergents with repeated cursory washing/cleaning cycles (Leeder, 1956; Gordon et al., 1968; Maxcy, 1973). The initial milk film is formed by remained phospholipids where heat processing is not involved or remained protein or milk salts due to heating of milk or milk products. The initial film or soil contributes to the accumulation of additional residual, thereby permitting the growth of microorganisms (Gordon et al., 1968; Maxcy, 1973).

Various processes occur during milk fouling, with the numerous interactions among the milk components complicating the observation, understanding and prediction of the fouling mechanism, only allowing for an approximate description. This is due to the fact that milk is a biological and complex medium, whose composition varies seasonally and with the cattle diet. Furthermore, a large number of physical and chemical factors such as the pH, age and pre-treatment of the milk influence the formation, extent and nature of fouling. A general overview of the milk fouling mechanism and the factors affecting it will be presented in the next sections.

The individual milk constituents are involved in varying degrees and phases of the fouling layers' formation and growth due to their different physicochemical properties and especially because of their different heat sensitivity. The raw milk (Table 2.1) and milk deposit (Table 2.2) compositions are significantly different. Lyster (1965) and Jeurnink et al. (1996a) showed that the milk deposit mainly constitutes whey proteins and milk salts. By contrast, the other milk constituents such as casein, lactose and fat play a minor role in the fouling processes (Jeurnink et al., 1996a) and only make a small portion of the deposits, although they together account for over 80 % of the colloidal and soluble compounds in milk. Severe fouling by casein micelles only occurs if the colloidal stability of the casein micelles is reduced, e.g. by lowering the pH or by high pressure treatment (Jeurnink et al., 1996a).

Deposits formed after the heat treatment of milk are classified as type A or type 1 and type B or type 2, depending on the heating temperature. With deposit type A, half of the protein deposit consists of whey protein (Lyster, 1965; Lalande et al., 1985). Both fouling types might also occur simultaneously during High Temperature Short-Time (HTST) pasteurization, performed in the range of 72 °C – 100 °C, or during pasteurization prior to UHT thermal treatment, resulting in a dense deposit with a foam-like structure (Barish and Goddard, 2013).

Table 2.1. Average cow milk composition and size of the major constituents (Walstra and Jenness, 1984; Kessler, 1996; Walstra et al., 1999; Michalski et al., 2004; Töpel, 2004; Lucey and Horne, 2009)

Constituents	Average concentration [% w/w]	Size [nm]	Constituents	Average concentration [% w/w]	Size [nm]
Water	87.5	~ 0.3	Lactose	4.6	1
Total solids	13	--	Minerals	0.8	0.5 (ions)
Proteins	3.4	--	Calcium	0.1 – 0.12	--
Casein micelle	2.8	10 – 600	Magnesium	0.01 – 0.015	--
α_{S1}-casein	1	--	Potassium	0.12 – 0.16	--
α_{S2}-casein	0.26	--	Sodium	0.03 – 0.06	--
β-casein	0.93	--	Carbonate (including CO_2)	~ 0.02	--
κ-casein	0.33	--			
γ-casein	0.08	--	Chloride	0.08 – 0.12	--
minerals	0.2	--	Citrate	0.13 – 0.2	--
Calcium	0.008	--	Total phosphorous (all forms)	0.09 – 0.1	--
Magnesium	0.0004	--			
Inorganic PO_4^-	0.1	--			
Citrate	0.018	--	Inorganic PO_4^-	0.17 – 0.2	--
Whey proteins	0.6	1 – 10	Sulphate	~ 0.01	--
β-lactoglobulin	0.32	1.2 – 6	Fat globule	3.9	100 – 10,000
α-lactoalbumin	0.12	3	Others (vitamins, organic acids, etc)	0.3	--
BSA	0.04	3 – 12			
IgG, IgA, IgM	0.08	--			
Other proteins	0.36	--	pH	6.7	--

PO_4^- = phosphate, BSA = bovine serum albumin, Ig = Immunoglobulin

Table 2.2. Characteristics of milk and whey protein deposits

Original fluid	Deposit type	Process parameters	Composition [% w/w dry basis]	Appearance
Whole milk	Type 1 (Lyster, 1965) or Type A (Burton, 1968)	Pasteurization T = 75 – 100 °C	Protein: 50 – 60 Minerals: 30 – 35 Fat: 4 – 8	Soft, spongy and voluminous structure, white or cream-colored
Whole milk	Type 2 (Lyster, 1965) or Type B (Burton, 1968)	Ultra-heat treatment (UHT) T = 110 – 140 °C	Protein: 15 – 20 Minerals: 70 – 75 Fat: 4 – 8	Brittle and porous, grey
Whey protein	-- (Robbins et al., 1999; Christian et al., 2002; Hooper et al., 2006)	Pasteurization or ultra-heat treatment	depends on the solution compo-sition: WPC, WPI or whey	Soft and spongy structure, white or transparent
Residues from food processing and imperfect cleaning	Milk stone (Leeder, 1956; Kulkarni et al., 1975)	Pasteurization	Protein: 4 – 44 Minerals: 42 – 67 Fat: 4 –18; up 72 °C mainly fat and protein, above 72 °C also minerals	Yellow hard compact or grey porous soft film

A review of the variability on the composition of fouling layers formed from whole and skim milk heated in tubular or plate heat exchangers by diverse studies is summarized by Sadeghinezhad et al. (2013). In general, the protein content of the deposits formed at temperatures to 90 °C matches the classification for deposit type A of Table 2.2, while a lower mineral content (varying from 5 % w/w to 25 % w/w) and a higher fat content (varying to 50 % w/w) in the deposits of different studies was measured. Deposits obtained at temperatures of 110 °C – 140 °C presented a lower mineral composition (varying from normally 20 % w/w to maximal 75 % w/w) than deposit type B (Table 2.2). Milk pretreatment such as heating, homogenization or drying (in the case of reconstituted/recombined milk as model fluid), different processing conditions or equipments' types, geometries or design (including different heating sections of a heat exchanger) mainly influenced the deposit composition (Visser et al., 1997a) of the diverse works (see also Table 2.4) due to changes in chemical and physical or structural properties of the milk components (Davies, 1936; Jeurnink et al., 1996a; Visser and Jeurnink, 1997a; Lee, 2002). The deposit removal from the fouled surface and/or its dissolution procedures and different analytical methods can also result in variability of the deposit composition. Due to the difficulty of storage and avoiding the natural variations of raw milk or whey, whey protein concentrate (WPC) or whey protein isolate (WPI) have been used to obtain reproducible fouling behavior (Lalande et al., 1985; Delplace et al., 1997). However, as highlighted by Robbins et al. (1999), WPC deposits were predominantly proteinaceous at both pasteurization and UHT temperatures (Table 2.2). Given that WPI or WPC pure does not produce a mineral scale at UHT temperatures (Bird and Fryer, 1991; Delplace et al., 1994; Christian et al., 2002), synthetic milk ultrafiltrate or calcium and phosphate solutions have been added to WPI or WPC and thus used as a milk model fluid (Daufin et al., 1987; Christian et al., 2002; Rosmaninho and Melo, 2007).

Deposits formed at low temperature, e.g. by cooling of milk, show different structure, composition and mechanism (Kane and Middlemiss, 1985) and will not be discussed in detail within this work.

2.2.1 Mechanisms of milk fouling

The exact mechanism of milk fouling has not yet been fully understood (Bansal and Chen, 2006). Despite a wide range of works on the literature (Burton, 1968; Jeurnink et al., 1996a; Changani et al., 1997; Visser and Jeurnink, 1997a; Visser et al., 1997; Petit et al., 2013), it is unclear whether mineral or protein fouling form first in the induction phase and whether fouling is primarily caused by the deposition of denatured or aggregated proteins on the heat transfer surface.

Table 2.3 provides an overview of the basic and contradictory postulates of milk fouling mechanism.

Table 2.3. Basic postulates regarding milk fouling mechanisms (adapted from Bansal and Chen, 2006)

Topic	Observation	References
governing bulk reaction	protein denaturation	Lalande et al. (1985), Kessler et al. (1986), Arnebrant et al. (1987), Kessler and Beyer (1991), de Jong et al. (1992), de Jong (1997), Petit et al. (2013)
	protein aggregation	Gotham et al. (1992), Delplace et al. (1997)
first fouling layer	mostly proteinaceous	Delsing and Hiddink (1983), Belmar-Beiny and Fryer (1993), Visser and Jeurnink (1997a), Jimenez et al. (2013)
	mostly mineral	Tissier and Lalande (1986), Daufin et al. (1987), Britten et al. (1988), Foster et al. (1989), Fryer and Belmar-Beiny (1991)
	protein and minerals simultaneously	Daufin et al. (1987), Foster and Green (1990), Boxler et al. (2013b)
	proportion of minerals in deposit increases after long contact times (10 – 60 min)	Daufin et al. (1987), Hege (1984)
fouling mitigation through milk constituents	formation of protein aggregates	de Jong et al. (1992), Delplace et al. (1997)
	absence of precipitable calcium and phosphate ions	Daufin et al. (1987)
controlling step	protein aggregates are not involved in fouling/are absent in the fouling layer	Blanpain-Avet et al. (2012), Jimenez et al. (2013)
	fouling is caused only by protein aggregates	Visser et al. (1997), Mahdi et al. (2009), Jun and Puri (2007)
	fouling depends on protein reactions (in bulk) only	Kessler et al. (1986), de Jong et al. (1992), de Jong and van der Linden (1992), Belmar -Beiny et al. (1993), Delplace et al. (1994, 1997), Schreier and Fryer (1995), Grijspeerdt et al. (2004)
	fouling depends on mass transfer as well as bulk and surface reactions	Georgiadis and Macchietto (2000), Chen et al. (2002), Bansal and Chen (2006)
	fouling depends on bulk as well as surface reactions	Paterson and Fryer (1988), Fryer and Belmar-Beiny (1991), Jeurnink et al. (1996a), Boxler et al. (2013b)

The most accepted deposition stages governing milk fouling are (Belmar-Beiny and Fryer, 1993; Jeurnink et al., 1996a; de Jong, 1997; Bansal and Chen, 2006):

(i) protein denaturation and the formation of insoluble material (aggregated protein) in bulk;

(ii) transport/mass transfer of denatured and aggregated proteins or calcium and phosphate ions to the heat transfer surface;

(iii) adhesion of this material to the surface, initiating the fouling or causing the deposit to grow by further incorporation of proteins and/or calcium ions and calcium phosphate particulates, as well as the entrapment of other milk constituents (such as fat globules) into the fouling layer; and

(iv) possible transfer of proteins or crystals/particulates back to the bulk (re-entrainment).

Based on scanning and transmission electron microscopy and X-ray microanalysis studies by other authors, as well as her mathematical model simulation, Sandu (1989) proposed a three steps mechanism or defects-growth model for milk deposit formation, also reviewed by Grant et al. (1996). In this model (Fig. 2.4), a compact and dense sublayer forms in a relatively short period of time (< 1 min) at metal surface. The sublayer contains mostly calcium phosphate and protein as a binding material. At a given stage, granules (probably of protein) build up randomly at active sites on the sublayer surface. The granules extend into the bulk phase, providing anchors for protein aggregates and leading to the growth of a porous, spongy deposit with low density and high moisture content. With increasing deposit thickness and density, proteins will crosslink and polymerize. Hence, the porous matrix of the deposit consists of proteins, with minerals agglomerated in certain regions. Fat globules and microorganisms are also entrapped inside this matrix. The compact layer continues to grow underneath the spongy deposit (Sandu, 1989) due to deposit aging by thermal reactions and diffusion of species (whey proteins, α- and β-caseins or mineral salts or ions) through the protein matrix to the deposit-metal interface (Sandu, 1989; Changani et al., 1997). Foster et al. (1989), Jeurnink et al. (1996a) and Changani et al. (1997) also describe an upper soft layer. Additionally, Foster and Green (1990), Belmar-Beiny and Fryer (1993) and Blanpain-Avet et al. (2012) demonstrate that the distribution, structure and content of deposit components in the fouling layer changes with depth.

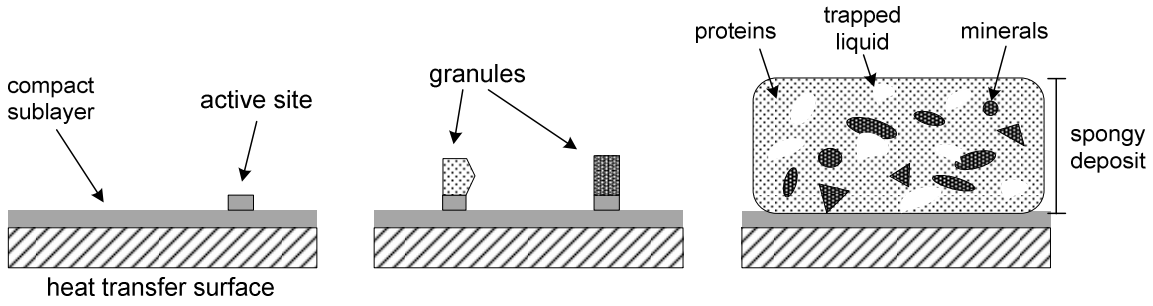

Fig. 2.4. Three stages deposit formation: compact sublayer, granule and spongy deposit (Grant et al., 1996)

Some studies have suggested that protein adsorbs first on the heat exchanger surface due to its high surface activity (Fryer and Belmar-Beiny, 1991), whereas other works have reported that the first layer is largely mineral (see Table 2.3). Maubois (1984) proposed two possible mechanisms: either denatured protein might act as nuclei for crystal growth; or denatured protein becomes adsorbed on the surface of mineral crystals. Through ToF-SIMS[1] analysis, AFM, X-ray microanalysis, X-ray photo-electron spectroscopy and SEM of fouled surfaces, Jimenez et al. (2013) proposed that the protein would be the first deposited during fouling of WPC and WPC plus $CaCl_2$.

Mass balance for denatured protein between the inlet and outlet of a heat exchanger is confusing regarding interaction of different protein stages (unfolded or aggregated) with the surface, as well as their role played on fouling growth (Blanpain-Avet et al., 2012). Recently,

[1] Time-of-Flight Secondary Ion Mass Spectrometry

Blanpain-Avet et al. (2012) and Petit et al. (2013) have shown through Raman spectroscopy and HPLC analysis, respectively, that protein aggregates are not present in the deposit of WPI and WPI plus $CaCl_2$ generated at wall temperature of 85 °C.

The deposit growth is essentially linked to the presence of calcium and phosphate, which provide a link with denatured proteins: β-lactoglobulin alone or aggregated to κ-casein of casein micelles (Daufin et al., 1987). Besides, Daufin et al. (1987) emphasize the role played by calcium complexing substances in the broad sense (phosphates, citrates, soluble proteins, caseins) in influencing the fouling capacity of the fluid. Such a capacity decreases from ultrafiltrate to whey and milk (Daufin et al., 1987), due to the increase of bound calcium, e.g. to the casein micelles.

2.2.2 Fouling modelling/Modelling of milk fouling

Jun and Puri (2005) provide a review of fouling models in dairy processing, which correlate deposit mass or fouling progress with temperature and time of processing, fluiddynamic conditions or whey protein denaturation kinetics. The effects of pH, crystallization fouling (calcium phosphate deposition) and adhesion of further fouling components, as casein or fat, to the surface have been neglected in the developed models (Jun and Puri, 2005). Furthermore, no existing model is able to estimate milk fouling parameters based on energetic and topographic surface properties, which is the focus of this work.

McGuire (1989) and McGuire and Swartzel (1989) proposed a model for protein deposition, considering the influence of the surface free energy:

$$\frac{\partial m}{\partial t} = a \exp\left(-\frac{E_{a,T_s}}{RT_s} - \frac{E_{a,\gamma_s}}{\left|\gamma_s^{TOT} - \gamma_{s,\min}^{TOT}\right|} \right) \tag{2.8}$$

where a is a constant, $\gamma_{s,\min}^{TOT}$ the optimum surface free energy for minimal adhesion of milk protein, $E_{a,Ts}$ and $E_{a,\gamma s}$ are the apparent activation energies required for transformation of an adsorbed specie to a irreversibly adsorbed specie on the surface, where $E_{a,Ts}$ represents the bulk component and $E_{a,\gamma s}$ represents the surface component. $E_{a,Ts}$ and $E_{a,\gamma s}$ can be expressed as:

$$E_{a,T_s} = b_1 + b_2 T \tag{2.9}$$

and

$$E_{a,\gamma_s} = \gamma_{s,\min}^{*} \tag{2.10}$$

where b_1 and b_2 are constants and $\gamma_{s,\min}^{*}$ ist the component of the surface free energy required for the surface reaction.

According to the extended DLVO theory and assuming that the electron acceptor component of the surface free energy $\gamma_s^+ = 0$ mN m^{-1}, Zhao and co-workers derived $\gamma_{s,min}^{TOT}$, on which fouling of $CaSO_4$ (Zhao and Müller-Steinhagen, 2002) and bacterial adhesion (Zhao et al., 2004a) are minimal:

$$\gamma_{s,min}^{TOT} = \gamma_s^{LW} = 1/4\left[\left(\gamma_l^{LW}\right)^{1/2} + \left(\gamma_{foulant}^{LW}\right)^{1/2}\right]^2 \tag{2.11}$$

However, for $\gamma_s^+ > 0$ mN m^{-1} the surface free energy for minimal fouling is:

$$\gamma_{s,min}^{TOT} = \gamma_s^{LW} + 2\left(\gamma_s^+\gamma_s^-\right)^{1/2} = 1/4\left[\left(\gamma_l^{LW}\right)^{1/2} + \left(\gamma_{foulant}^{LW}\right)^{1/2}\right]^2 + 2\left(\gamma_s^+\gamma_s^-\right)^{1/2} \tag{2.12}$$

This means that for a given system foulant/fluid, the optimum surface tension also depends on the polar fractions of the surface free energy, i.e. the electron acceptor and electron donor components: γ_s^+ and γ_s^-. In practical coating processes, it is very difficult to fix γ_s^- values and adjust γ_s^{LW} value to increase interfacial repulsion, i.e. $\Delta G_{s,l,foulant} > 0$ J (Liu and Zhao 2011). Therefore, Liu and Zhao (2011) recently proposed using the γ_s^{LW}/γ_s^- ratio to compare bacterial adhesion and removal on diverse coated surfaces. The authors correlated the γ_s^{LW}/γ_s^- ratio with the number of adhered bacteria and the percentage of their removal in many diagrams, but no model has been proposed.

In the following, the effect of heat treatment on the principal milk constituents, which contribute to milk fouling, will be revised. Sections 2.2.3 and 2.2.4 are concerned with the heat-induced denaturation and aggregation of whey protein, as well as the precipitation of calcium phosphate, respectively. Thereafter, the interaction forces involved on deposit formation will be discussed in section 2.2.5.

2.2.3 Milk protein

The fouling formation is closely connected to protein thermal stability (Skudder et al., 1981; Lalande et al., 1985; Belmar-Beiny et al., 1993). In aqueous solutions, globular proteins are stabilized by electrostatic repulsion. However, heating or pressurizing may cause a change of the protein structure, rendering the peptide chain more mobile. Consequently, segments of different molecules may interact through hydrophobic interactions or by forming hydrogen bonds, leading to protein denaturation and aggregation. If the protein contains cysteine (Cys), such as the whey protein β-lg, intermolecular disulfide bridges may by formed (Nicolai et al., 2011).

Bovine milk protein consists of caseins and whey proteins, whose concentration is presented in Table 2.1. Caseins include four kinds of polypeptide chains (α_{s1}-, α_{s2}-, β-, and κ-caseins) and some derivatives formed by proteolysis of these chains, including γ-caseins and proteose peptones (Fox and Brodkorb, 2008). The casein fractions aggregate to submicelles. These accumulate into micelles (Fig. 2.5a) and are stabilized by colloidal calcium phosphate.

The micelle contains 92 % protein and 8 % inorganic salts (Walstra et al., 1999). Given that the casein micelles are hardly heat-sensitive up to a temperature of 120 °C (Walstra et al., 1999), casein is therefore not the major proteinaceous component in milk deposits, thus playing a secondary role in the fouling process of heat exchangers.

The whey proteins have a compact, globular conformation (Walstra et al., 1999) and have different heat stabilities due to the different denaturation temperatures in diverse environmental conditions: Lactoferin, Lf = 60 – 70 °C; Immunoglobulin, Ig = 70 – 72 °C; Bovine serum albumin, BSA = 52 °C – 64 °C; β-lg = 68 °C – 78 °C and α-la > 72 °C (de Wit and Klarenbeek, 1984; Walstra and Jenness, 1984; Töpel, 2004; Considine et al., 2007). By heating, various protein complexes can be formed. The denatured whey proteins can react with each other (β-lg:β-lg, β-lg:α-la) and with the casein micelle (κ-CN:β-lg at 70 °C – 90 ° C and α_{S2}-CN:β-lg at UHT temperature). β-lg, α-la and BSA show also different isoelectric points IEP: 5.1, 4.2 – 4.5 and 4.7 – 4.9, respectively; and different charge in neutral solution: –15 mV, –2 mV and –18 mV, respectively (Suttiprasit et al., 1992). Even small changes in pH change the association of the proteins; for example, about 70 % of the denatured whey proteins are linked to the casein micelles at pH 6.5. The degree of association decreases with increasing pH, such that only about 30 % are still associated at pH 6.7 (Walstra et al., 1999). At relatively moderate heating temperatures below 100 ° C, the β-lg dominates the composition of the milk deposit. At higher temperatures (T > 110 °C), an increased contribution of caseins, mainly κ-casein and β-casein, is accepted and up to 40 % of the deposit may be composed of casein (Burton, 1988). The presence of denatured α–La possibly contributes to destabilization of the casein micelles (Skudder et al., 1981).

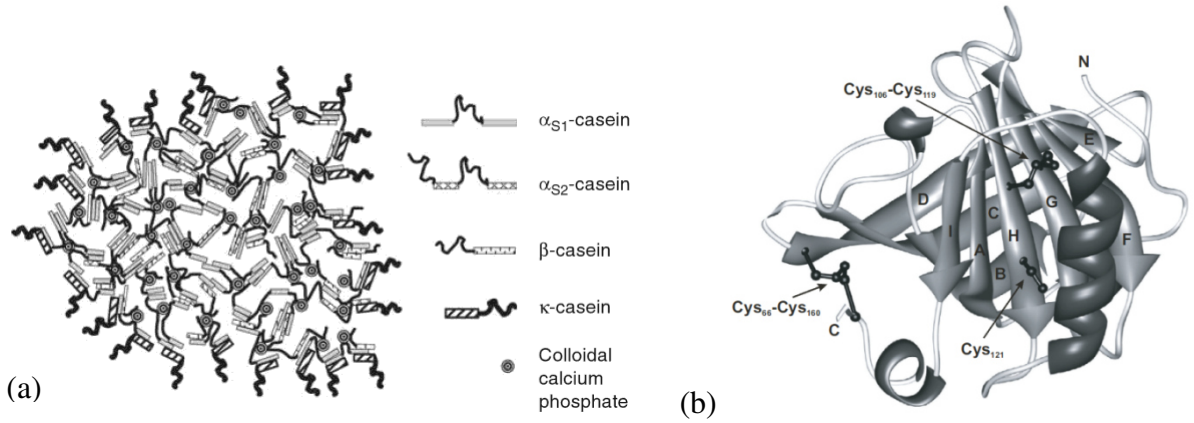

Fig. 2.5. Structure of (a) casein micelle (Horne, 1998) and of (b) β-lactoglobulin (Tolkach and Kulozik, 2007)

Due to its sensitivity to heat, the whey protein β-lg is a key component for the formation of milk deposits (Jeurnink et al., 1996a; de Jong, 1997). The β-lg is a major component of the whey protein fraction in bovine milk, constituting more than 50 % w/w of the total whey protein. It is a typical globular protein of known secondary and tertiary structures (see Fig. 2.5b). The secondary structure of β-lg consists of 6 – 10 % α-helix, 44 – 52 % β-sheet, 8 – 10 % turn and 32 – 35 % of random coil (Tolkach and Kulozik, 2007). The tertiary structure is stabilized by four of the five Cys residues, which form two disulfide bonds

(Cys_{106}-Cys_{119} and Cys_{66}-Cys_{160}). The free thiol group (Cys_{121}) is normally hidden by the α-helix in the native state. 13 genetic variants of β-lg are currently known, whereas two variants, β-lg A and β-lg B, are the most common (Tolkach and Kulozik, 2007). The β-lg A and β-lg B variants occur in almost equal concentration in bovine milk, which differ only in two amino acids and thus have slightly differing primary structures, yet distinct solubilities (de Wit, 2009) and slightly different denaturation and aggregation behaviors (Schokker et al., 2000; Croguennec et al., 2004). Subjecting the β-lg to heat, the protein loses its helical structure, exposing the buried sulphydryl group Csy (de Wit, 1990) and initiating a chain of reactions. As a result, β-lg can interact via thiol-disulfide SH/SS exchange and/or via hydrophobic forces with other milk constituents, leading to the loss of native β-lg and the formation of protein aggregates (van Creamer et al., 2004; Considine et al., 2007). The formation of deposits on heating equipment is one of the undesirable effects of the β-lg denaturation, due to the attachment of denatured protein or protein complexes to the heating surface.

It should be emphasized that the intra- and intermolecular interactions of β-lg, and therefore the extent and rate of β-lg denaturation, is determined by a number of factors (Galani, 1997), such as:

i. pH values during heating (Monahan et al., 1995; Gotham et al., 1992; O'Kennedy, 2006; de Wit, 2009; O'Kennedy and Mounsey, 2009);
ii. heating conditions (temperature, heating rate, isothermal or non-isothermal heating, duration of heating treatment) (Rüegg et al., 1977; Dannenberg and Kessler, 1988; de Wit, 1990; Paulsson and Dejmek, 1990; Monahan et al., 1995; Galani and Apenten, 1999b; Schokker et al., 1999; Oldfield et al., 2000; van Claeys et al., 2001);
iii. concentration of native proteins, including whey proteins in different concentrations, as well as mixtures of whey proteins and casein in different proportions, or the ratio among them (Kessler and Beyer, 1991; Gotham et al., 1992; Verheul et al., 1998; Galani and Apenten, 1999a; Oldfield et al., 2005);
iv. solution ionic strength (Verheul et al., 1998; Unterhaslberger et al., 2006; O'Kennedy and Mounsey, 2009); and
v. ionic composition, particularly concentration of calcium (Anema and McKenna, 1996; Croguennec et al., 2004; Navarra et al., 2007; Petit et al., 2011).

The extent of polymerization and aggregates growth depends on the nature of the protein aggregates (covalent or non-covalent) already formed, pH, rate of heating, residence time and temperature (de Wit, 2009; Petit et al., 2013). The parameters listed not only have an effect on protein denaturation/aggregation, but they will also influence the rate of protein adsorption and consequently fouling layers building up (Visser and Jeurnink, 1997a).

α-la is a compact globular protein, stabilized by four disulfide bonds, which exist mainly as monomers. α-la does not contain a free thiol group (Schokker et al., 2000) and is known to bind calcium (Paulsson and Dejmek, 1990). α-la is more heat-sensitive than β-lg and undergoes a three-state heat-unfolding (Apenten, 1995). However, α-la does not polymerize by itself (Schokker et al., 2000); rather, it forms via disulphide bonds and to a considerable extent via hydrophobic interactions oligomers with other whey proteins or associates with the casein micelle via a β-lg/α-la aggregate (Schokker et al., 2000; Rozzi et al., 2007).

Kinetic data and models of β-lg and α-la denaturation in aqueous and buffer solutions or whey protein solutions during isothermal process at diverse protein and calcium concentrations and pH values have been described frequently in existing research and reviewed by Dannenberg (1986), Schokker et al. (2000), de la Fuente et al. (2002), Oldfield et al. (2005), Considine et al. (2007), Tolkach and Kulozik (2007), de Wit (2009) and Nicolai et al. (2011). Although the changes on the structure of β-lg have been studied intensively, the protein denaturation can be influenced to a lesser or greater extent by interactions with other proteins (other denatured whey proteins, proteins from the casein micelle or other proteins), carbohydrates, fat and minerals. Hence, the kinetic and thermodynamic of β-lg denaturation in dairy or other food products is considerably more complex than purified protein model systems and is less understood (Oldfield et al., 2000; Lowe et al., 2004). Indeed, the mechanism of the structural changes and interactions of the whey proteins by heating at non-isothermal conditions, as occur in industrial processes, such as at different temperature profiles along the heat exchanger, residence times and hydrodynamic conditions (Petit et al., 2013; Bouvier et al., 2014) or by heating through direct steam injection (Oldfield et al., 1998), as well as after heating treatment, viz. during holding (Villamiel et al., 1997, Petit et al., 2013) or storage, have also been less commonly reported in the literature. Moreover, the thermodynamics of interactions with surfaces during heating or information on the protein structural changes after adsorption and deposition on different surfaces are also still lacking.

The heat-induced denaturation of β-lg can be characterized by a three-state model, as shown by the following scheme (Fig. 2.6) and illustrated on Fig. 2.7, and is commonly modelled by formal kinetic means, supposing the denaturation to be a two-stage process (native → denatured → aggregate protein) (Oldfield et al., 1998a; Tolkach and Kulozik, 2007). According to the scheme the native molecule of β-lg (β-lg_N), native dimer ((β-lg_N)$_2$) or native octomer ((β-lg_N)$_8$) dissociates reversibly into native monomers (β-lg_N) at temperatures above 40 °C. In the temperature range between 40 °C and 55 °C, the monomer undergoes an intramolecular transition (R-state, β-lg_R), characterized by minor conformational changes. The β-lg in the R-state is able to form polymers (Pathway I). However, the polymerization rate is negligible (Tolkach and Kulozik, 2007). Native molecules of β-lg subsequently become thermally unstable above a temperature of 65 °C, forming a molten globule state (β-lg_{MG}) in which the unfolding of the α-helix structure occurs and the reactive sulphydryl (-SH) groups and some parts of the hydrophobic core are exposed. In this state, the protein chain is more mobile, but does not completely unfold (reversible unfolded molecules) (Nicolai et al., 2011). Groups in this native state are buried inside, become exposed and may interact with other proteins (Nicolai et al., 2011), leading to aggregation. Above about 70 °C, there is the irreversible thiol-disulfide reaction between unfolded protein and aggregates form (chemical aggregation or polymerization). Non-covalent interactions such as electrostatic, hydrophobic interactions and hydrogen bonding are also involved in the aggregation mechanisms (physical aggregation of unfolded molecules or chemically formed aggregates) (Verheul et al., 1998; de la Fuente et al., 2002). Hence, the unfolded molecules polymerize in intermolecular aggregation, resulting in irreversibly denatured (β-lg_D) and polymerized or aggregated ((β-lg_D)$_n$, (β-lg_D)$_m$) β-lg molecules.

In milk, unfolded β-lg can react in three ways: *(i)* β-lg molecules can self-interact to form aggregates with a free sulphydryl group (Pathway V). Alternatively, unfolded β-lg molecules and/or aggregates can interact to form an aggregate without a free sulphydryl group

(Pathways II and XI), *(ii)* forming a complex with κ-casein via a sulphydryl-disulphide interchange reaction and hydrophobic interactions at the surface of the casein micelle (Pathway III) (Fink and Kessler, 1985; Paulsson and Dejmek, 1990) and *(iii)* forming a complex with the κ-casein or α-la in the milk serum (Jeurnink and de Kruif, 1995; Kim and Lund, 1998b; de la Fuente et al., 2002) (Pathways III or IV) and forming further association of α-la-β-lg complexes with the casein micelle (Oldfield et al., 2005) (Pathway VIII). The β-lg aggregate without a free sulphydryl group would be unable to interact via a thiol-dissulphide interchange (Pathway VII), thus remaining in solution (Oldfield et al., 2005). The contribution of non-covalent interactions is expected to become increasingly influenced by the pH value closer to isoeletric point and/or with higher solution ionic strength, as well as being more important at temperatures between 90 °C and 110 °C (Galani and Apenten, 1999).

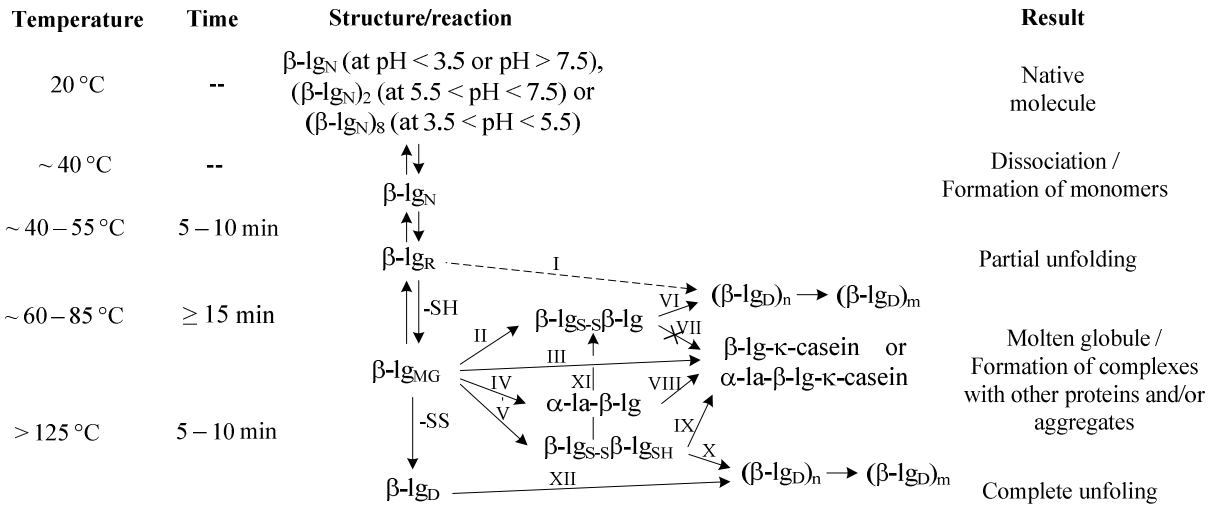

Fig. 2.6. Mechanism of the thermal denaturation of β-lg in a neutral or slightly alkaline pH including the possible complexes with other milk proteins (modified/adapted from Oldfield et al., 2005; Tolkach and Kulozik, 2007 and de Wit, 2009). β-lg$_N$: native β-lg; β-lg$_R$: reversible native β-lg; β-lg$_{MG}$: unfolded molten globule state; β-lg$_D$: denatured β-lg respectively composed of n or m β-lg units

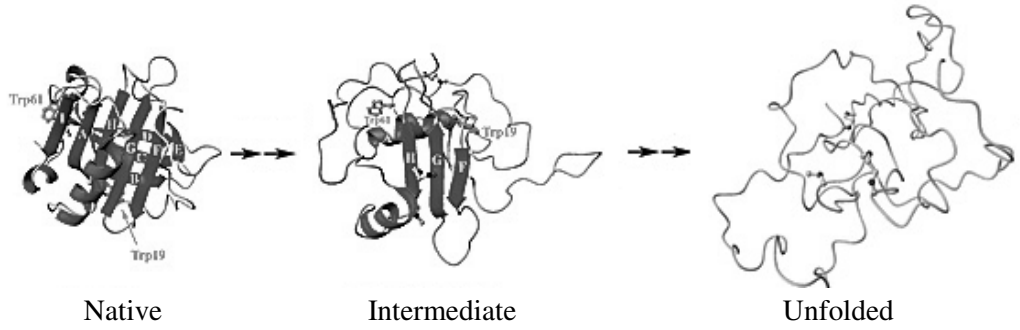

Fig. 2.7. Stages of β-lactoglobulin denaturation (Kuwata et al., 2001)

Schokker et al. (2000) propose a mechanism of formation and aggregation of β-lg A and B variants with α-la. The complexes between β-lg and α-la associate with the casein micelles on prolonged heating (Anema and Li, 2003). However, according Kessler et al. (1986) and Anema and Li (2003), β-lg molecules are primarily involved in the reaction of aggregation, rather than association. Upon heating at temperature T < 85 °C, only a small percentage of κ-casein dissociates, so the deposit mainly consists of serum proteins, strongly suggesting that whey protein denaturation and aggregation is involved in the fouling reaction (Jeurnink and de Kruif, 1995). By contrast, at a heating temperature ranging between 90 °C and 130 °C, around 50 % of the β-lg is associated with the casein micelle (Oldfield et al., 1998). Furthermore, at temperatures of 85 °C to 95 °C, around 1 % of β-lg interacts with denatured milk fat globule membrane proteins, also forming aggregates (Walstra, 1990).

At higher temperatures (130 – 140 °C), the residual native or reformed secondary structure after unfolding at 80 °C of the β-lg molecule is completely destroyed by the chemical breakdown of disulfide bonds, leading to irreversible denaturation (Tolkach and Kulozik, 2007; de Wit, 2009) (Pathway XI). Severe heat treatment of milk (130 °C/several minutes) also cause the aggregation of casein micelles (Considine et al., 2007).

Apart from caseins, components such as lactose, calcium or citrate ions present in milk are responsible for the higher thermostabilities of β-lg in milk at 90 – 120 °C, compared to the thermostabilities of β-lg in whey or buffer solutions (Anema and McKenna, 1996). In general, increasing the ionic strength leads to two opposite effects (Unterhaslberger et al., 2006): first, an increase of the aggregation rate due to charge shielding and decreasing of intermolecular repulsion forces; and second, the protein structure stabilizes and the tendency of protein unfolding is reduced due to the reduction of intramolecular repulsion forces. The thermal stability of purified 5 % m/v BSA, α-la and β-lg was studied by Paulsson et al. (1985) in simulated milk ultrafiltrate (SMUF) and compared to the behavior in water in the pH range 3 – 10. At a neutral pH value (close to pH of the experiments in this work, pH 6.7), the denaturation temperature of BSA in SMUF (~ 60 °C) was 10 K higher than in water, while the denaturation temperature of α-la (~ 60 °C) and β-lg (~ 68 °C) was similar in water and SMUF. However, the transition enthalpy of α-la and β-lg in water was much lower than in SMUF (ΔH in SMUF at pH 7 = 640 kJ mol^{-1}, 249 kJ mol^{-1} and 285 kJ mol^{-1}, for BSA, α-la and β-lg, respectively). This suggests a conformation stabilizing effect of citrate or calcium on the proteins (Rüegg et al., 1977).

Rüegg et al. (1977) found for purified 8 % w/w BSA, 6.2 % w/w α-la and 6.2 % w/w β-lg in SMUF at pH of 6.7 denaturation temperature of T = 62.2 °C, 65.2 °C and 72.8 °C and enthalpy of ΔH = 939 kJ mol^{-1}, 318 kJ mol^{-1} and 227 kJ mol^{-1}, respectively. Furthermore, the authors also showed the dependence of the unfolding temperature on the heating rate.

O'Kennedy and Mounsey (2009) investigated the effect of pH of heating on the denaturation/aggregation of 1 % w/w β-lg dissolved in different proportion of SMUF. The solutions were heated at 78 °C for 10 min in capped glass vials containing 1 mL of sample in a water bath. They showed that the formation of sedimentable and soluble β-lg aggregates was affected by the solution ionic strength and calcium concentration (SMUF or 2 x SMUF), and thus concluded that the effect of Ca^{2+}, at the level as it occurs in milk serum, has little resemblance to the effect of Ca^{2+} in simple model systems. Generally, the major effect of

SMUF on the denaturation/aggregation of β-lg was apparently controlled by the solution ionic strength (O'Kennedy and Mounsey, 2009).

Fat is present in milk in the form of fat globules, which are composed of a triglyceride core and are surrounded by a biological membrane that is a complex mixture of proteins, triglycerides, phospholipids and other minor components. The fat has a minor effect on the fouling process (Visser and Jeurnink, 1997a; Chen and Bansal, 2006) (see Table 2.2). It appears that the fat present in deposit is entrained by other materials, e g. coagulated protein (Lyster, 1965; Skudder et al., 1986). However, if fat is heated, the composition, structure and functional properties of the fat globule membrane change (Fink and Kessler, 1985; Corredig and Dalgleish, 1998; Lee and Sherbon, 2002; Michalski et al., 2004). With sufficient heating, β-lg mainly becomes a new component to the fat membrane, forming new lipoprotein complexes. Through homogenization, the fat fouling increases due to the reactions of the activated serum proteins present at the fat globules' surface (Jeurnink et al., 1996a).

2.2.4 Calcium phosphate

A second major contribution to fouling by heating of milk is mineral, due to the inverse relationship of calcium phosphate solubility with temperature. Fig. 2.8 depicts solubility phase diagrams of calcium phosphate compounds.

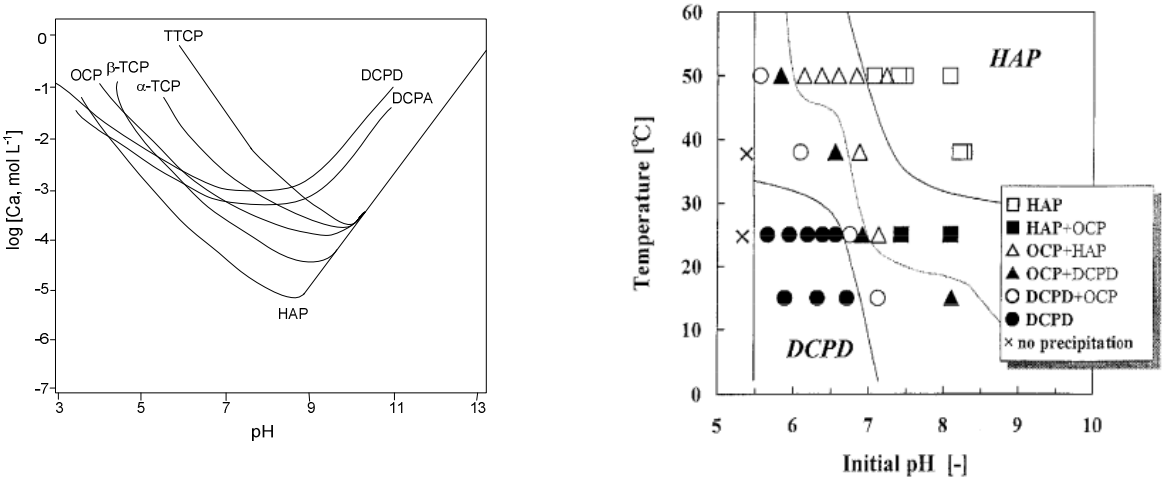

(a) (b)

Fig. 2.8. (a) Solubility isotherms for the system $Ca(OH)_2$–H_3PO_4–H_2O at 37 °C (Tung, 1998); (b) Effect of temperature on precipitations' diagram of the system K_2HPO_4-KH_2PO_4-$Ca(NO_3)_2$ (Tsuge et al., 2002). DCPA: dicalcium phosphate anhydrous, DCPD: dicalcium phosphate dihydrate, HAP: hydroxyapatite; OCP: octacalcium phosphate, TCP: tricalcium phosphate

Upon heating, the formation of prenucleation clusters of amorphous calcium phosphate (ACP) in the saturated or near saturated solution starts (Dey et al., 2010). Stable clusters are subsequently formed in a process called nucleation, which occurs either in the bulk liquid (homogenous nucleation) or at the surface of a foreign material (heterogeneous

nucleation) (Mullin, 1997), promoting the growth of the ACP clusters and the development of crystallinity in a subsequent step (Christoffersen et al., 1989). A schematic representation of the different stages of calcium phosphate crystallization on a surface is shown in Fig. 2.9. The presence of a foreign material, i.e. the metal surface, mostly diminishes the activation energy for the nucleation process (Mullin, 1997), in order that this nucleation type prevails and becomes the basis for building up a fouling layer.

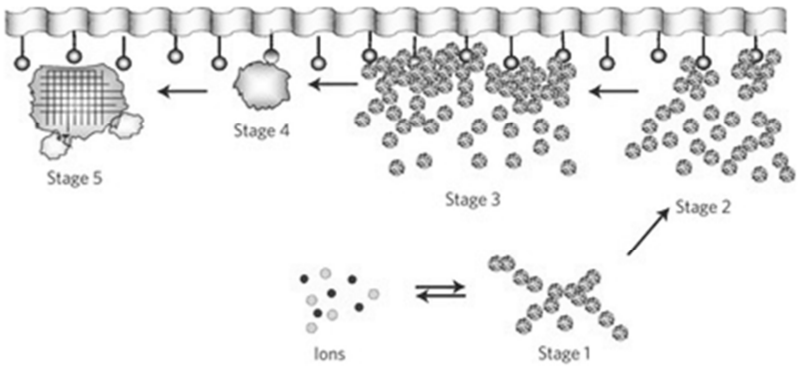

Fig. 2.9. Crystallization of calcium phosphate from simulated body fluid at 37 °C (Dey et al., 2010). Stage 1: loose aggregation of prenucleation clusters with ions in solution, Stage 2: prenucleation clusters adhered to the surface, Stage 3: aggregation leads to densification near the monolayer, Stage 4: nucleation of amorphous spherical particles, Stage 5: development of crystallinity

In the ternary system $Ca(OH)_2$–H_3PO_4–H_2O, there are eleven species with molar Ca/P ratio varying from 0.5 to 2 (Tung, 1998) for purely inorganic solutions. In complex inorganic solutions (e.g. with addition of citrates: Andritsos et al., 2002) and complex organic systems (e.g. in the presence of whey proteins: Tsuge et al., 2002), it is very difficult to predict which calcium salt will precipitate (Daufin and Labbé, 1998). The calcium phosphate species in milk are listed in Fig. 2.10. The products of calcium and phosphate precipitation are dictated by the stoichiometry of the equilibrium in the calcium phosphate phase (Anema, 2009) and the interaction of the precursor ions with other ions or molecules present in the aqueous solution. The stability of calcium phosphates is closely related to their structures, compositions and solubilities (Tung, 1998).

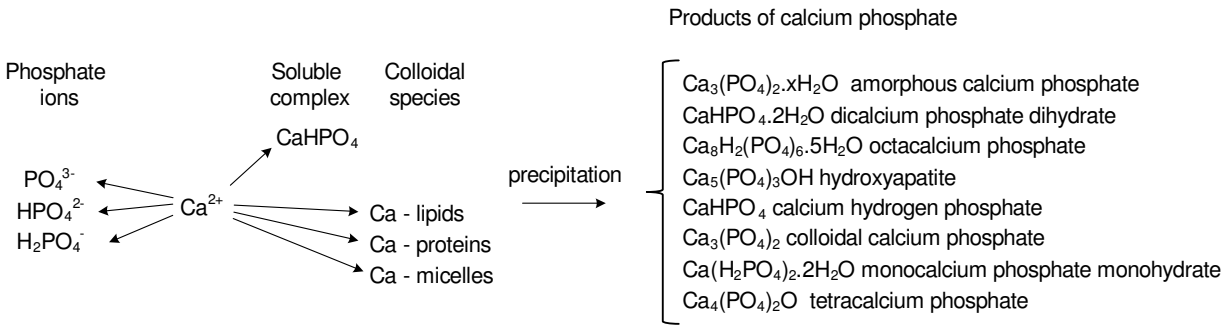

Fig. 2.10. Calcium and phosphate species in milk (modified from Daufin and Labbé, 1998)

During the heating of milk, part of the soluble calcium and phosphate precipitates as a calcium phosphate salt in solution or on the surface of the processing equipment, or associates with milk proteins. Moreover, the precipitate formed in bulk solution can attach to the surface, while it can also be removed from it, which makes the crystallization fouling complex. Calcium phosphate constitutes more than 80 % of the mineral fraction of milk deposits (Lyster, 1965; Skudder et al., 1981; Lalande et al., 1984). The analysis of milk deposits has shown that the calcium phosphate deposited is a mixture of tricalcium phosphate (ACP, Ca/P ratio = 1.5), dicalcium phosphate dihydrate (DCPD, Ca/P ratio = 1.0) and octacalcium phosphate (OCP, Ca/P ratio = 1.33) which, under prolonged heating, is eventually converted into the least soluble calcium phosphate compound, hydroxyapatite (HAP) (Visser et al., 1997; Herrmann et al., 2004), having a molar Ca/P ratio of 1.67. At a pH of 6.7, OCP is spherulitic, whereas at a pH of 5 – 6, it is either structureless amorphous calcium phosphate (ACP) or has a typical thin platelet crystalline structure characteristic for brushite DCPD (Visser and Jeurnink, 1997a). Upon cooling, the OCP dissolves again, but when the heating temperature is sufficiently high, the microcrystalline HAP is formed (Visser and Jeurnink, 1997a). The process of ACP-OCP-HAP formation in moderate supersaturated calcium phosphate solutions is strongly dependent on the overall composition of the system and is affected by various additives. Magnesium and citrate ions, α-la, β-lg and small quantity of casein inhibit the crystal growth of OCP and hence the formation of HAP is retarded (Visser and Jeurnink, 1997a; Rosmaninho and Melo, 2006a).

The deposition mechanism of calcium phosphate in milk not only depends on temperature gradients, but is also influenced by the interaction of Ca^{2+} and PO_4^- with milk constitutes especially proteins, as well as by the formation of proteinaceous deposits. It is known that calcium phosphate hardly forms particulates in milk under middle heating conditions (temperature below 90 °C) (Bell, 1925; Jeurnink et al., 1996a; Anema, 2009), but associates with the proteins (Visser and Jeurnink, 1997a). It is noteworthy that the amount of calcium associated with the casein micelles is 70 – 77 % and the amount of inorganic phosphate is around 53 %, either bound directly to the casein or as solid calcium phosphate within the micelle structure (colloidal calcium phosphate, CCP), while 23 – 30 % of calcium and 47 % of phosphate occurs in the serum (soluble) phase (Robbins et al., 1999; Lucey and Horne, 2009; O'Kennedy and Mounsey, 2009). Increasing the temperature of milk from 20 °C to 80 °C results in the transfer of the soluble calcium and soluble inorganic phosphate to the casein micelle, with a concomitant decrease in pH within the first few minutes of heating, yet little further change at longer heating or holding times (Anema, 2009). The change in pH can also be due to other processes, such as the reaction of lactose with formation of organic acids and the removal of carbon dioxide (Belmar-Beiny and Fryer, 1993). The calcium sensitive caseins, α_{s1}–, α_{s2}– and β–casein, beyond sequestering amorphous calcium phosphate to form thermodynamically stable complexes called calcium phosphate nanoclusters (Smyth et al., 2004), can also bind to the surface of calcium phosphate crystals (van Kemenade and de Bruyn, 1989). Tsuge et al. (2002) showed that the crystal shape of calcium phosphate was changed by the presence of whey protein in the solution, retarding the beginning of the precipitation. This effect was stronger on calcium than phosphate ions (Tsuge et al., 2002). Calcium ions also bind to β-lg molecules via carboxyl groups of amino acids. Thereby, calcium favors the formation of bridges between adsorbed proteins and unfolded or aggregated whey proteins in the bulk or of bonds between proteins and precipitated minerals,

thus collaborating to the fouling layer growth. Increasing the concentration of calcium in milk would lead to higher numbers of bindings, resulting in more stabilization of protein aggregates, as interpreted by Bramaud and Aimar (1997). Furthermore, the formation of a narrow network is promoted by high calcium concentration, in which other ions present in the solution are embedded (Guérin et al., 2007), thus reinforcing the deposit cohesion forces.

Another effect of calcium on the deposit formation is the induction of β-lg conformational changes, facilitating the protein denaturation and increasing the kinetic of protein aggregation. Thus, a small change in the calcium concentration has an important impact upon the deposit formation (Guérin et al., 2007) (see also Table 2.4), given that β-lg is one the major contributors to milk fouling. Three effects, or a combination of them, are responsible for the enhancement of the heat-induced denaturation and aggregation of β-lg and fouling due to calcium (Belmar-Beiny and Fryer, 1993; Simons et al., 2002; O'Kennedy and Mounsey, 2009):

(i) intermolecular cross-linking of adjacent negatively charged or carboxylic groups by the formation of protein-Ca^{2+}-protein complexes;
(ii) intramolecular electrostatic shielding of negative charges on the protein;
(iii) ion-induced conformational changes, which lead to altered hydrophobic interactions and aggregation at elevated temperatures; and
(iv) the formation of bridges between adsorbed protein on the surface and protein aggregates formed in the bulk.

However, an excess of calcium ion can exhibit an inhibitory effect on protein aggregation (O'Kennedy and Mounsey, 2009).

To investigate the role of the milk mineral components on the overall milk fouling, a model solution (simulated milk ultrafiltrate, SMUF) has been used (Wu et al., 1997; Andritsos et al., 2002; Rosmaninho and Melo, 2006a). This solution contains calcium and phosphate, as well as some interfering ions and organic ligands such as magnesium or citrate (also present in milk) and is devoid of lactose. Therefore, the solubility isotherms as in Fig. 2.8 can only be used as an approximation to predict the phase starting point and the forming species. The formation of the different phases depends on thermodynamic and kinetic factors, solubility effects, as well as solution composition, pH and ionic strength. Some works concerning the influence of magnesium, citrate, acetate and whey protein as well as pH on calcium phosphate precipitation from SMUF have been reported in the literature (Tsuge et al., 2002; Rosmaninho and Melo, 2006a; Gao et al., 2010).

While the SMUF solution approximates the milk serum salt composition, the absence of micellar casein leads to destabilization of calcium phosphate on heating at relatively low temperatures (~ 40 °C) (Parker and Horne, 1980), once SMUF is supersaturated with respect to various calcium phosphate compounds (Lyster, 1979; Gao et al., 2010). The precipitation of calcium phosphate in the pH range of 6 – 7 starts at 40 – 44°C (Visser and Jeurnink, 1997a). At this temperature, the turbidity in the freshly prepared SMUF solution increases over time, which is related to the initiation of particle formation and maximum deposition (Visser, 1998; Andritsos et al., 2002; Rosmaninho and Melo, 2006a). Daufin et al. (1987) showed, by fouling at 72 °C of various model fluids, that inorganic simple solutions gave an OCP deposit, whereas poorly crystallized HAP was observed with SMUF. The HAP structure

was found for SMUF deposition at pH 6.8 by Rosmaninho and Melo (2006a) and Spanos et al. (2007) preceded by ACP.

Whey protein (WPI or WPC) has been added to the SMUF solution to give a milk simulator solution. Thus, SMUF plus whey protein (WPI or WPC) solution has recently been tested as a model system for milk fouling (Morison and Tie, 2002; Rosmaninho and Melo, 2008), because it contains both main foulant components (calcium phosphate and protein).

Very few studies have been conducted concerning the deposition/precipitation of calcium phosphate on modified surfaces of heat exchangers (at T_{bulk} = 70 °C and ΔT = 1.5 K: Rosmaninho and Melo, 2006b; at T_{bulk} = 44 °C and 70 °C and ΔT = 1 K: Rosmaninho et al., 2007b), with most existing works having related its behavior on non-heated surfaces and used simple model systems (without the addition of interfering substances) (Wu et al., 1997; Wu and Nancollas, 1998; Andritsos et al., 2002; Boxler et al., 2011).

2.2.5 Driving forces for the start of fouling

The investigation of the interfacial physicochemical interactions governing the adsorption and further adhesion of foulants to solid surfaces is essential to understanding fouling mechanisms and proposing anti-fouling approaches. Various physicochemical forces between the fouling component and the metallic surface, which result in diverse interactions, will establish the attachment to the substrate and initiate the building up of a fouling layer.

Long-range attractive forces such as van der Waals and electrostatic forces are responsible for “bringing” the particles to the surface. Hydrophobic interactions are of polar origin and may be much larger than the Lifhitz-van der Waals or electrostatic forces. Once intimate contact between the particle and the surface has been attained through the combination of long-range and bridging effects, it is possible for short-range forces to take effect, including chemical and hydrogen bonding. (Bott, 1995) Fig. 2.11 provides an overview of the molecular interaction forces that may influence the process of adhesion.

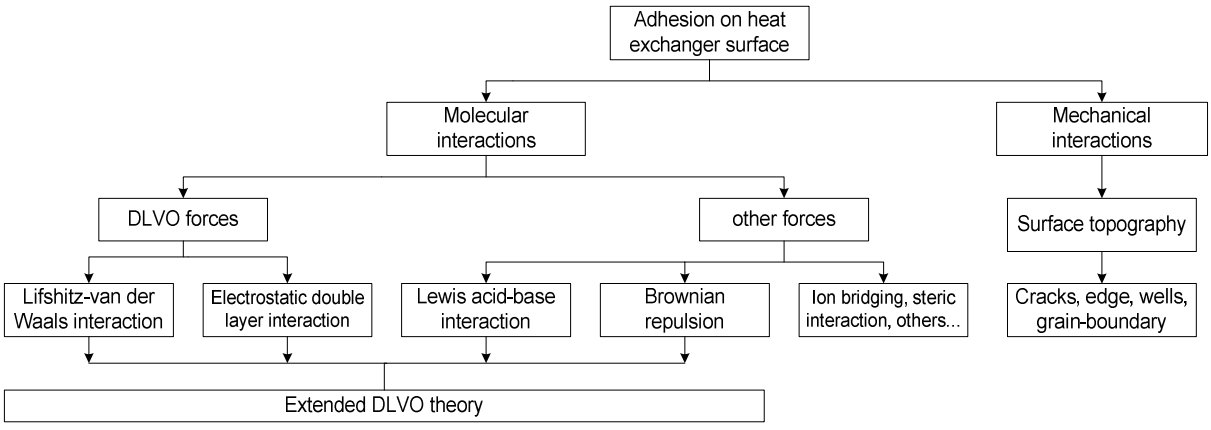

Fig. 2.11. Interfacial interactions influencing adhesion

The theory developed by Derjauin and Landau (1941) and Verwey and Overbeck (1948) has been used to explain the attachment of small solid and colloidal particles, as well as microorganisms on surfaces. It gives the resulting energy between objects (the particle and the substrate) as a function of distance. According to the DLVO theory, the principal interaction energies are determined by the balance between the attractive Lifshitz-van der Waals energy, which essentially depends on the geometry and the physical/chemical properties of the interacting bodies, and the repulsive double layer energy due to the tendency of particular materials to acquire an electrical charge when immersed in an aqueous medium (Oliveira, 1997). Van Oss (1995) extended the classical DLVO theory by including the hydrophilic repulsion and hydrophobic attraction, i.e. the Lewis acid/base interaction energy. In addition to these interaction energies, polymer molecules or crystals may adhere to a surface due to the effect of Brownian motion, which brings the precursor materials into contact with the solid surface (Al-Janabi et al., 2010). The total adhesive interaction is composed of the electrostatic, Lifshitz-van der Waals and the short-range interactions:

$$\Delta G^{TOT}_{s,l,foulant} = \Delta G^{EL}_{s,l,foulant} + \Delta G^{LW}_{s,l,foulant} + \Delta G^{AB}_{s,l,foulant} + \Delta G^{Br}_{s,l,foulant} \quad (2.13)$$

The balance of the possible interactions between a deposit and a metal surface determines whether or not a system will foul, i.e. if adhesion or fouling takes place under those conditions where ΔG^{TOT}_{132} is negative (Al-Janabi et al., 2010; Fowkes, 1964). Theoretical considerations indicate that the main driving forces for the adhesion of particles to a surface upon heating are the Lifshitz-van der Waals and the Lewis acid/base forces of attraction, whereas the electrostatic double layer forces (see also section 2.2.2.3 – surface charge) of repulsion and the repulsive forces caused by Brownian motion are too small to compensate for these attractive forces (Fowkes, 1964; van Oss et al., 1987).

The adhesion of macromolecules, such as proteins or polysaccharides, on surfaces is a more complex phenomenon compared to the adhesion of small solids or colloidal particles to the surface (Lund and Sandu, 1981). Due to the great variety of protein molecules and surfaces, it is difficult to arrive at one general theory that covers all situations (Lund and Sandu, 1981), including heat, mass and momentum transfer conditions during fouling. The process of protein adsorption is affected by the properties of the surface, such as surface free energy, roughness and electrochemical/electrostatic potential, as well as the solution conditions, including composition and ionic strength. Moreover, three characteristics of the macromolecules need to be taken into account in describing their adhesion behavior (Lund and Sandu, 1981): the molecule flexibility, the large number of active sites or groups on the molecule and the molecule orientation. Since proteins comprise different amino acids with varying reactive groups, they can interact with the surface in different manners, whereby microscopic or macroscopic attraction and repulsion are possible. Reactive groups of the protein molecules induce the adsorption of the protein on active sites of surfaces and the reaction with itself (crosslinking) or other compounds. At the same time, the active groups of proteins permit them to unfold and/or change their orientation (rearrange) on the surface. Besides, the proximity of the protein backbone to the surface can trigger other interactions previously hindered by steric or spatial constraints, in order that surface adsorption and conformational change may also occur simultaneously (Chandrasekaran et al., 2013). In turn,

the adhered (unfolded or denaturated) proteins expose reactive groups to fluid, enabling the adsorption of further protein molecules via non-covalent (electrostatic interations and hydrogen bonding) and covalent bonds (disulphide interchange reactions), thus leading to the formation of aggregates on the surface and a protein multilayer. The subject of protein adsorption onto surfaces is extremely broad, extending beyond the scope of this chapter. Useful and comprehensive reviews of protein adsorption have been given by by MacRitchie (1978), Wahlgren and Arnebrant (1991), Haynes and Norde (1994), Nakanishi et al. (2001) and Rabe et al. (2011). The adsorption of β-lactoglubulin has been investigated in detail by Arnebrant et al. (1987), Suttiprasit et al. (1992), Roscoe and Fuller (1993), Itoh et al. (1995), Kim and Lund (1997, 1998a, 1998b), Santos (2004) and Santos et al. (2006a, 2006b).

Before a protein molecule can adhere on a solid surface, it must arrive at the surface through transport by convection in the bulk phase and diffusion through the boundary layer. Under this condition, all the protein molecules in the immediate vicinity of the surface can interact with a surface and adsorb on almost any surface, on both high and low energy surfaces (van Oss, 2006). In terms of kinetic, for adsorption to occur, the energetic barrier of surface pressure as well as the electrical potential barrier needs to be exceeded by the protein molecule. The surface pressure barrier tends to reduce the effect of molecular diffusion, whereas the electrical potential barrier can either decrease or increase diffusion (Lund and Sandu, 1981).

The most important driving forces for protein adsorption are normally attributed to electrostatic and hydrophobic interactions, together with a gain in entropy due to protein conformational changes and dehydration of hydrophobic parts of the solid and protein surfaces (MacRitchie, 1978). Moreover, other forces such as Lifshitz-van der Waals contribute to the establishment of a final and stable interaction, leading to irreversible adsorption of the protein (Chandrasekaran et al., 2013). In thermodynamic terms, protein adsorption will occur spontaneously at $\Delta G_{ads} < 0$ J. However, due to microscopic attraction between electron-donor sites on peptide bonds and electron-acceptor sites in the surface, the attraction can prevail over the macroscopic repulsion and protein adsorb to some extent at $\Delta G_{ads} > 0$ J (and even $\Delta G^{EL} > 0$ J) (van Oss, 2006). Binding of small molecules to the protein (e.g. fatty acids or polysaccharides) might influence the thermodynamic of adsorption, as well as the amount of protein adsorbed. Once the protein is adsorbed on the surface, the protein can either desorb from the surface returning back in solution, if adsorption is fully reversible, or change its conformation, building an energetically more stable structure. The nature of the surface (high vs. low-energy surfaces) strongly influences the composition and recognizability of the adsorbed protein layer (van Oss, 2006; Vieira et al., 2009), which in turn affects the subsequent interactions, given that new regions of the protein with different amino acid compositions will be exposed (Castner and Ratner, 2002). Santos et al. (2006a) suggested more extensive conformational change of β-lactoglobulin after its adsorption on a DLC sputtered surface. Fig. 2.12 schematically illustrates the protein conformation changes on a surface.

The principle driving force in fouling of calcium phosphate particles seems to be the Lewis acid/base interaction due to its large negative contribution to the overall energy $\Delta G^{TOT}_{s,l,foulant}$ (Fowkes, 1964). The same applies for whey proteins in the presence of calcium ions, due to the hydrophobising effect of these ions on the protein and on the surface (Fowkes,

1964). The Lewis acid/base energy $\Delta G^{AB}_{s,l,foulant}$ is a function of the polar components of the surface free energy of the interacting bodies, i.e. of the electron donor and electron acceptor components (Oliveira, 1997; Al-Janabi et al., 2010). Therefore, the effect of the surface Lewis acid/base components on fouling of milk components have been extensively investigated in this work.

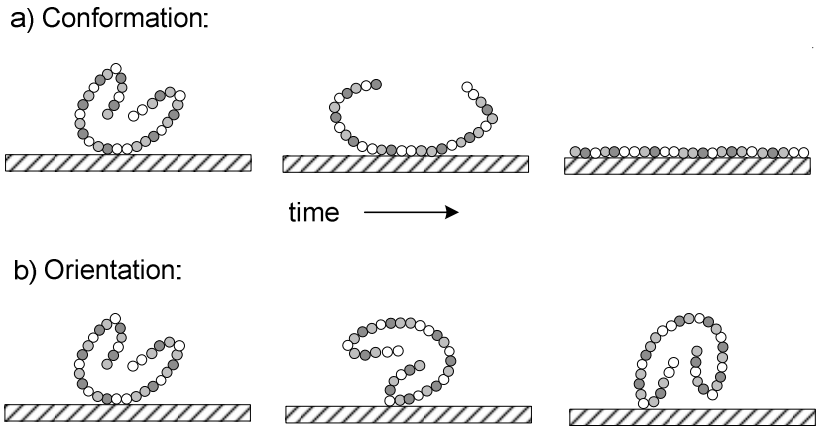

Fig. 2.12. The conformation and orientation of adsorbed proteins to a surface. (a) Protein denaturation with increasing adsorption time, (b) Protein adsorbing to the surface in different orientations (Castner and Ratner, 2002)

2.2.6 Influencing factors on milk fouling

Since the kinetic of protein denaturation and aggregation, as well as the formation of insoluble calcium phosphate and the adhesion of both milk constituents on a heat transfer surface are controlled by diverse factors, these factors thus also influence the initial fouling layer formation and growth. Table 2.4 provides an overview of the major factors and their effect on milk fouling, while Fig. 2.13 (see also Fig. 1.1) shows how some factors affect the deposit amount.

This work deals with the combined influence of more than one of the factors listed in Table 2.4, such as surface properties (γ^- and R_z), surface temperature and operation mode, on the crystallization plus particulate fouling, due to the heating of milk salts, and/or on the protein fouling, due to the heating of whey protein.

Table 2.4. Trends of the effect of various factors causing milk fouling

Influencing factor	Effect	Explanation	Reference
Electron donor component (γ^-) ↑	+	initial fouling rate and deposit formation ↑ γ^- = attractive interaction force	Wu et al. (1997), Wu and Nancollas (1998), Rosmaninho et al. (2007b, 2008)
	–	γ^- = repulsive interaction force	Visser (2001), Al-Janabi et al. (2010)
Whey protein concentration ↑	+++	a maximum was found at solids concentration of 25 % w/w. (see Fig. 2.13c)	Kessler et al. (1986), Jeurnink (1995a), Itoh et al. (1995), Jeurnink et al. (1996a), Visser et al. (1997)
Salts concentration (SMUF) ↑	– +	deposition of salts, formation of bridge between protein molecules, increase of solution ionic strength	Fryer and Slater (1986), Christian et al. (2002)
Ca concentration ↑	+++	either increasing or decreasing of Ca concentration lead to more fouling, due to induction of conformational changes of the β-lg, facilitating the protein denaturation and increasing the aggregate formation and the effect on the stability on the casein micelles (see Fig. 2.13c)	Jeurnink and de Kruif (1995), Jeurnink et al. (1996a), Visser et al. (1997), Christian et al. (2002), Guérin et al. (2007), Khaldi et al. (2015)
Ca concentration ↓	++		
Flow rate/flow velocity, Re ↑	– –	increase the wall shear stress and thus the removal, reduce the adhesion probability of foulant components on the surface due to shorther residence time	Gordon et al. (1968), Fryer and Slater (1984), Belmar-Beiny et al. (1993), Guérin et al. (2007)
	+	higher mass transfer coefficient, re-entrapment of aggregates in the deposit, formation of compact and adherent fouling layers	Fryer and Slater (1986), Santos et al. (2006b), Guérin et al. (2007)
Surface or processing temperature ↑	+++	enhancement of whey protein denaturation or calcium phosphate precipitation as well as effect on the protein adsorption rate (see Fig. 2.13a)	Burton (1968), Hegg et al. (1985), Dannenberg (1986), McGuire and Swartzel (1989), Visser and Jeurnink (1997a), Boxler et al. (2013b), Petit et al. (2013)
ΔT ↑	++	more protein denaturation and additional calcium phosphate precipitation	Gynning et al. (1958), Gordon et al. (1968), Daufin et al. (1987), Jeurnink et al. (1996b), Petit et al. (2013)
Processing or residence time ↑	++ / +	more time available for β-lg denaturation, aggregation, salts precipitation and fouling reactions	Dannenberg (1986), Fryer and Slater (1986), Kessler et al. (1986), Skudder et al. (1986), Daufin et al. (1987), McGuire and Swartzel (1989), Foster et al. (1989), Kessler and Beyer (1991), Petit et al. (2013)
pH ↑	– +	reduction of the milk salts solubility (see Fig. 2.8)	Gordon et al. (1968), Hegg et al. (1985), Kessler et al. (1986), Skudder et al. (1986), Foster et al. (1989), Kastanas et al. (1995), Jeurnink et al. (1996a), Visser et al. (1997)
pH ↓	+++	whey proteins tend to aggregate by their isoelectrical point (see Fig. 2.13b)	

Entrained air ↑	++	air bubbles cause super-saturation conditions at the triple interface	Gynning et al. (1958), Gordon et al. (1968), Jeurnink (1995b), Jeurnink et al. (1996a)
Surface roughness ↑	+	entrapment of soil in the crevices, greater surface area exposed in the rougher surface	Cucci (1954), Herreid and Le Luetscher (1963), Gordon et al. (1968), Dupeyrat et al. (1987)
	0		Britten et al. (1988): 0.05 – 2 µm, Yoon and Lund (1994): 0.08 – 0.6 µm
Milk aging ↑	++	aged milk causes more fouling due to the action of proteolytic enzymes or acid lactic produced by bacteria	Burton (1968), Jeurnink (1995b), Jeurnink et al. (1996a)
Pressure ↑	– –	degassing of milk	Jeurnink et al. (1996a), Jeurnink (1995b)
Composition, including seasonal variation and cattle diet	– +	variation of protein and minerals content resulting in different deposit composition	Lyster (1965), Burton (1966, 1968), Foster et al. (1989), Jeurnink and de Kruif (1995)
Fluid	– +	fresh > reconstituted or recombined milk; whey > whole milk > skim milk; acid whey > sweet whey; non-homogenized > homogenized milk; goat milk > cow milk WPC > milk WPC > β-lg	Bell and Sanders (1944), Hege (1984), Jeurnink et al. (1996a) Daufin et al. (1987), Jeurnink (1995b), Srichantra et al. (2006)* Kastanas et al. (1995) Spiro and Chong (1997) Kastanas et al. (1995) Robbins et al. (1999) Jeurnink et al. (1996b)

↑ = increasing parameter, ↓ = decreasing parameter, + = more fouling, – = less fouling, 0 = no influence; *differences in pre-treatment of raw milk, such as pre-heating, homogenization and drying conditions, can lead to more fouling of reconstituted milk

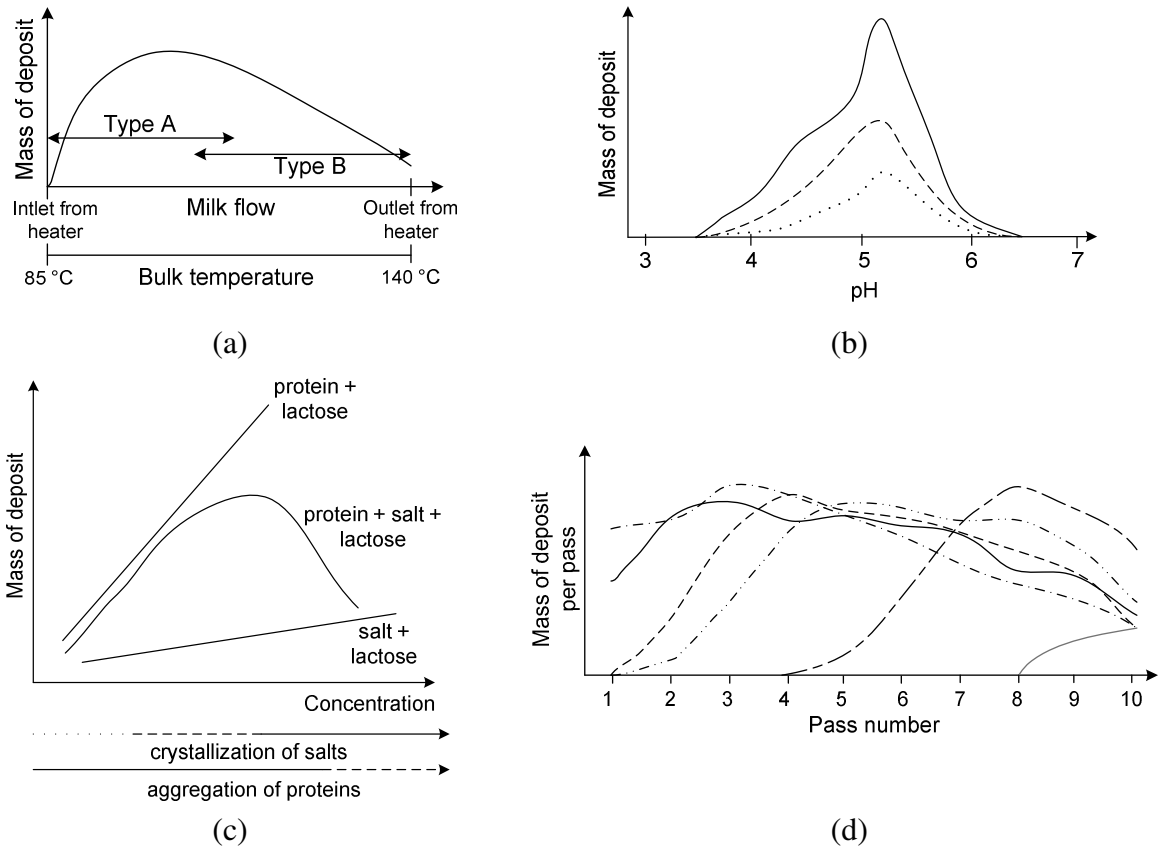

Fig. 2.13. Qualitative representation of the influence of (a) bulk temperature on milk fouling (Burton, 1968), (b) pH on salt-free β-lactoglobulin deposition* (Hegg et al., 1985), (c) concentration of individual components (Visser et al., 1997) on deposit formation and (d) outlet temperature on fouling distribuition in the passes of a PHE (Petit et al., 2013). Fig. 2.13b: ··· 70 °C, --- 80 °C, — 90 °C. Fig. 2.13d: — 70 °C, —·— 75 °C, —··— 80 °C, --- 85 °C, — 90 °C, —·— 95 °C.
*Deposition of milk is not possible below pH 5.5, because casein coagulates. The effect of pH on the deposit follows the same trend, see also (Kessler et al., 1986)

2.2.7 Milk fouling control/mitigation

The sequence of events/mechanisms that leads to the deposition influences the method of control that is adopted. Antifouling methods mainly involve the following (Sandu and Lund, 1985; Bott, 1995; Panchal and Knudsen, 1998):

i. chemical treatments such as softening (chemical precipitation), demineralization (desalting), acidification and sequestering (chelating) to remove or reduce fouling compounds. The most frequent used fouling inhibitors are inorganic polyphosphates, organophosphorus compounds, organic polymers and biocides;
ii. physical treatments or devices such as settling, filtration, centrifugation, abruptly changing of the flow direction (pulsation), oxygen/air stripping of feedstocks, the use

of a wire matrix insert, magnetic treatment, etc. (for further information, see Table IV by Lieske et al., 1997).

iii. technical: heat exchanger selection (construction material, mechanical and energetic surface properties, equipment sizing, possibility of forced convection generation and thus to have a induced turbulence in the exchanger, mechanically agitated thin-film heat exchanger) and heat exchanger design (design features required to reduce fouling and improve equipment cleanability); and

iv. operational: process parameters such as pH, pressure, temperature, ΔT, residence time, flow regime, continuous or batch mode.

Given that the end product temperature and holding time by the heat processing of milk and dairy products are predetermined (Regulation EU No. 605/2010, 2010), as well as the addition of antifouling chemicals such as Ca^{2+}-binders and pH adjustment (phosphates (Burdett, 1974; Skudder et al., 1981; Jeurnink et al., 1996a), KI (Mottar and Moermans, 1988) or hydroxypropylcellulose (Cash et al., 2006) being prohibited, restricted or potentially affecting product quality, the mitigation of milk fouling essentially depends on the heat exchanger proper design and operation.

In industrial applications, the milk follows an axial dispersion and a range of temperatures may exist at any given cross-section, as well as throughout the entire process (Adams et al., 1984). The amount of fouling is proportional to the volume of fluid that is hot enough to react (Paterson and Fryer, 1988). As soon as the denaturation temperature on the wall or the in laminar boundary layer near to the wall has been reached, protein denaturation and further deposition on the surface as well as aggregation in bulk can occur. As long the 'bulk', viz. the core flow reaches the denaturation temperature, fouling can be caused by both denatured and aggregated proteins and is influenced by the presence of the denatured proteins in the bulk. In addition, if the laminar boundary layer is reduced (e.g. by turbulence or by superimposed pulsed flow) by improving the heat transfer and the mixing in the bulk, the protein aggregates in the bulk rather than at the wall (Visser et al., 1997). The flow velocity is low in PHE around the contact points between the plates, as well as in the stagnation zones, resulting in higher wall temperatures, lower removal rates (Bansal and Müller-Steinhagen, 1993) and thus more deposition.

There are a number of technological approaches regarding heat exchanger design and operation to avoid or mitigate the effects of milk fouling and include:

i. lower temperature gradient (Gynning et al., 1958; Kessler et al., 1986);

ii. higher flow velocity (Leeder, 1956; Gordon et al., 1968; Belmar-Beiny et al., 1993) or use of superimposed pulsed flow (Bradley and Fryer, 1992; Boxler et al., 2014b). However, in plate heat exchangers, the operation at high velocities is limited, due to pressure drop considerations;

iii. pre-heating of milk (Bell and Sanders, 1944; Leeder, 1956; Burton, 1968; Kessler et al., 1986; Patil and Reuter, 1986; Mottar and Moermans, 1988; Foster et al., 1989; Kessler and Beyer, 1991; Jeurnink et al., 1996a; Delplace et al., 1997), permitting the protein denaturation and formation of protein aggregates. Srichantra et al. (2006)

recommended the homogenization of the milk before its pre-heating at a temperature higher than 75 °C;

iv. installation of an additional holding section (Burton, 1968; de Jong et al., 1992);

v. direct heating by steam injection or steam infusion (Jeurnink et al., 1996a; de Jong, 1997);

vi. higher operational pressures to degas the milk (Jeurnink, 1995b; Jeurnink et al., 1996a);

vii. cleaning of the stainless steel using cationic surfactants such as oxidizing acid solution, to improve the passive layer and achieve a high positive surface charge (Nassauer and Kessler, 1986);

viii. new geometry or alteration of the heat exchanger geometry, such as scraped heat exchangers (Blel et al., 2013), the application of electrical current (Leeder, 1956) or the insertion of turbulence promoters or static mixers in the heat exchangers; and

ix. novel technologies for food processing/preservation, such as high pressure processing (Toepfl et al., 2006), pulsed electric fields (Toepfl et al., 2006; Walkling-Ribeiro et al., 2011), ultrasound (Lin and Chen, 2007; Cárcel et al., 2012) and ohmic heating (Fillaudeau et al., 2006; Ayadi et al., 2008; Stancl and Zitny, 2010).

Although a reduction of deposit building up can be achieved using the above techniques, fouling takes place and requires frequent cleaning of equipment to minimize the risk potential with respect to hygiene safety. The modification of one or more heat transfer surface properties seems to be a promising anti-fouling strategy, given that the adhesion and detachment properties of the surface can be changed, thus altering the deposits' formation, composition and structure. Surface properties such as surface composition or chemistry, roughness and/or texture, charge, charge density and energy have been found to be important parameters influencing the fouling process. However, the precise role of each of the surface property is not yet known. Early attempts to prevent or reduce the formation of milk fouling using alternatives to metal surfaces have been published since the mid 1950s (Cucci, 1954; Masurovsky and Jordan, 1958). In the food industry, standard heat treatment equipments are made of stainless steel, owing to its good resistance to corrosion due to the formation of a passive layer of chromium oxide. 2R (cold rolled, bright annealed) and 2B (cold rolled, heat treated, pickled and skinpassed) are the most common finishes (Council of Europe Guideline, 2002). The DIN EN 1672-2 (2009) and the European Hygienic Engineering and Design Group (Hauser et al., 2004) recommend that surfaces in contact with products in the food industry should have a roughness R_a lower than 0.8 µm. Additional changes in stainless steel properties can be obtained by further surface treatment or coating. Several studies have been conducted concerning the effect of surface modification on fouling caused by milk-based products (for a review see section 2.4.1). The present study highlights and investigates the influence of topographic, energetic and electrokinetic surface properties of stainless steel modified by PECVD technique on the fouling of different milk components.

2.3 Cleaning

The adhesion of particles to surfaces is unavoidable in food processing facilities (Bobe et al., 2007) and thus the clean-up is one the most critical stages in the quality control of food processing operations (Kulkarni et al., 1975). Cleaning starts with the formation of the initial fouling layer, since the composition, structure and adhesion strength of the first adsorbed layer will influence how easy the deposit can be cleaned, as well as the cleaning patterns. The problem of milk deposits' cleaning was first described in 1940s (Johnson and Roland, 1940a, 1940b). In the 1950s, CIP (Cleaning-In-Place) was developed, initially as a manual process, for the hygienic cleaning of plant surfaces (Davey et al., 2013). Today, CIP is the standard technique for cleaning in the food industry (Belmar-Beiny and Fryer, 1993; Wilson, 2005) and is used firstly, to restore pressure drop and heat transfer efficiency by the removal of fouled deposits, and secondly, to ensure microbiological hygiene by disinfection of equipment's surface. CIP technique involves the circulation of cleaning agents through processing units without dismantling the process equipment. CIP systems are highly developed and automated, yet are rarely, if ever, optimized (Fryer and Christian, 2005). Most CIP systems are operated on a semi-empirical basis, i.e. cleaning schedules are often fixed irrespective of the deposit type and amount. The advantages of CIP over mechanical methods, including minimization of downtime, reduced cleaning times and costs, are discussed by Müller-Steinhagen (2000). To guarantee product quality requirements in the dairy industry, it is necessary to carry out CIP every 6 – 20 hours. The number of cleaning steps and the process conditions depend on the nature of deposit (Table 2.5) (Jeurnink and Brinkman, 1994). Heterogeneous deposits built up in alternating layers of e.g. protein and minerals are more difficult to clean than homogenous ones, as the cleaning solution has to be multipurpose.

Table 2.5. Nature of food deposits and cleaning method (Kessler, 1996; Graßhoff, 1997)

Component deposited	Cleaning method	Ease of removal	Change upon heating (aging)
Sugar	by water	easy	caramelization: more difficult to clean
Fat	by hot water with surfactants or alkaline solution	difficult, especially polymerized fat	polymerization: more difficult to clean
Protein	is water insoluble and slightly acid soluble, clean by alkaline solution	very difficult	denaturation/gelatinization: more difficult to clean
Mineral	has variable water solubility, removable mostly with acidic solution	easy to difficulty	interactions with other constituents: generally easier to clean. Burnt-precipitate with protein: very difficult to clean
Remaining microorganisms	are largely removable by alkaline solution and killed by sterilization	difficult (biofilm)	

In general, a complete CIP process involves the following steps, arranged in a series (Fryer and Christian, 2005):

1. Pre-rinse: pumping of hot or cold water to remove large, loosely bound substances from the surface;
2. Detergent cycle: circulation of cleaning chemical (alkali or acid; alkali and acid with an intermediate rinsing with the change of the solution) to release the deposit from the surface;
3. Intermediate rinsing: removal of cleaning chemicals and traces of deposit, as well as neutralization by the circulation of water;
4. Sanitization: disinfection and surface conditioning; and
5. Final rinsing (optional): removal of sanitizers and traces of CIP solutions, as well as the circulation of water prior to product processing.

Two cleaning processes are commonly used to remove milk deposits, namely a single-stage process and a two-stage process (Timperley and Smeulders, 1987) with or without detergent re-use. In single-stage cleaning, the deposit is removed by a highly acidic or alkaline solution or formulated detergents, which contain surface active agents and chelating agents. In the two-stage process, the proteins and fats are removed with an alkaline solvent (e.g. NaOH), while the mineral deposits are removed by an acidic solution (e.g. HNO_3 or H_3PO_4).

The various factors affecting the cleaning process have been reviewed by Jennings (1965), Kulkarni et al. (1975), Bird (1995), Graßhoff (1997), Gillham et al. (1999), Fryer and Christian (2005) and Fryer et al. (2006). Sinner (1960) arranged the main factors – temperature, chemicals (or cleaning agents), cleaning time or duration and fluid mechanical action (wall shear stress) – visually in a circle. In Fig. 2.14, Sinner's representation has been extended by two influencing parameters – (*i*) deposit, i.e. type, state, age, composition and quantity of deposit to be removed, and (*ii*) surface, i.e. design/geometry, material and properties of the surface to be cleaned. The process parameters jointly affect the cleaning result, influencing each other. The lesser efficiency of one of the factors must be balanced by an intensification of any or all of the remaining factors. Beyond these factors, the switching sequence of the alkaline and acidic solutions might also influence the cleaning process (Jeurnink and Brinkman, 1994), as well as the concentration of suspensed and soluble solids of re-used cleaning solutions (Irwin et al., 2006; Alvarez et al., 2007).

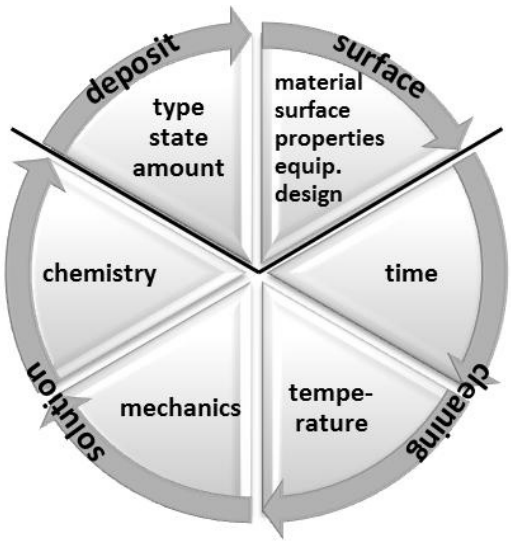

Fig. 2.14. Extended Sinner's circle (Graßhoff, 1998)

2.3.1 Cleaning mechanism and modelling

Like fouling, cleaning is a multistage process. Any of the following steps can be involved in the removal of food deposits (Plett, 1985):

i. transport of the cleaning chemical through the boundary layer to the surface;
ii. transport into the deposit layer: diffusion of chemical components into the deposit is dependent on the deposit structure. Reactions zones appear at the deposit/fluid interface;
iii. reactions between deposit and cleaning chemicals, including melting, mechanical break-up, wetting, soaking, swelling, desorption, emulsification, solubilisation, hydrolysis, saponification and dispersion. These reactions contribute to overcoming the cohesion and adhesion forces;
iv. transport to the interface: reaction products formed in the reaction zone will diffuse through the fouling layer due to concentration gradients; and
v. transport to the bulk: concentration gradients and hydrodynamic conditions allow the transport of the reaction products into the bulk.

The overall removal process is governed by a combination of mass transfer, diffusion and reaction process (Bird and Fryer, 1991), whereby any of these steps might be the controlling step. Jeurnink and Brinkman (1994) concluded that the cleaning process of a spongy protein matrix cannot be diffusion controlled, as the diffusion coefficient is small and the process would take hours; however, it only takes a matter of minutes.

Visualization and monitoring of the cleaning of milk and whey protein deposits have shown the non-uniform behavior of deposit removal (Bird and Fryer, 1991), in which deposit is removed in large chunks. Fig. 2.15 depicts typical cleaning curves for protein removal (Gallot-LaVallée et al., 1982, Gallot- La Vallée and Lalande, 1985; Fryer and Bird, 1994, Gillham et al., 1999).

Three stages can be identified in the cleaning rate curve (Fig. 2.15a):

I. Swelling: solution swells up the deposit, which forms a matrix of high void fraction, the deposit softens and breaks up, increasing the cleaning rate;
II. Erosion: uniform removal of deposit by shear stress forces at maximum cleaning rate. The removal depends on the deposit amount and the concentration and temperature of chemicals; and
III. Decay: despite removal of the majority of deposit, isolated islands or patches are detached by shear stress and mass transport. The cleaning rate slowly declines to zero.

The duration and efficiency of the three cleaning stages have proven sensitive to different combinations of solution chemistry and operating conditions (Bird and Fryer, 1991; Gillham et al., 1999; Tuladhar et al., 2002; Xin et al., 2004).

The thermal resistance curve (Fig. 2.15b) can also be split into three discrete regions. It is noteworthy that the thermal removal or heat recovery does not occur in the same way as mass removal during cleaning. The uniform and decay stages are earlier in the thermal resistance curve, while the length of the decay stage is shorter than the corresponding stage in the mass removal curve. One possible reason for this discrepancy/difference between dR_f/dt and dx_f/dt is due to the change in deposit voidage, rather than thickness. However, this change in deposit structure (swelling) followed by mass removal results in no change in the thermal resistance due to the simultaneous variation of the deposit thermal conductivity (Gillham et al., 1999; Tuladhar et al., 2002).

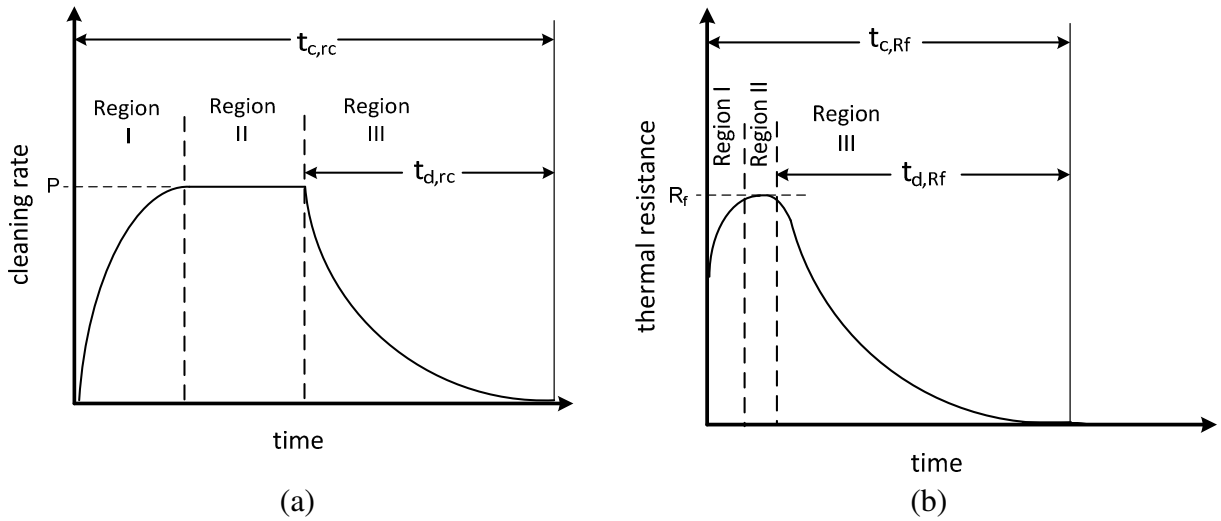

Fig. 2.15. Characteristic cleaning curves for protein removal (Gillham et al., 1999): (a) cleaning rate with time; (b) fouling resistance progress. Region I: chemical reaction and swelling; Region II: uniform removal; Region III: decay period. $t_{c,rc}$ and $t_{c,Rf}$ are the time required for complete cleaning in the cleaning rate curve and in the thermal resistance curve, respectively, and $t_{d,rc}$ and $t_{d,Rf}$ the length of the decay phase in the cleaning rate curve and in the thermal resistance curve, respectively

Studies concerning kinetic of removal or reentrainment of deposits are much less numerous than those on fouling, with few works having focused on the dynamics of the cleaning of heterogeneous deposits, such as those from heating of milk (Leclercq-Perlat and Lalande, 1991), especially at high wall temperatures (T > 100 °C). Table 2.6 provides a review of cleaning models for the removal of food soils from solid surfaces. The kinetics of cleaning has been described using 0^{th} or 1^{st} order reaction models based on chemical reaction and mass transfer controlled mechanisms. Due to the food deposits' heterogeneity and the complexity of mechanisms involved in each removal stage, most models are empirical or semi-empirical (LeClerq-Perlat and Lalande, 1991; Dürr, 2002). Nonetheless, Gallot-La Vallée and Lalande (1985) and Xin et al. (2004) proposed a more theoretical approach. Gallot-La Vallée and Lalande (1985) suggested that the cleaning rate was proportional to the diffusion of cleaning solution into soil and mass transfer of intermediate reaction products into the solution.

The model by Xin et al. (2004) is based on polymer dissolution and assumes that the detachment of protein molecules from the swollen gel-solution interface and the mass transfer of these detached molecules back into the cleaning solution is the rate-limiting step (Boxler et al., 2013a). In cleaning studies, it is the first time that a polymer dissolution concept was used to describe and predict complex protein cleaning process (Xin et al., 2004). The model includes two stages, the swelling plus uniform stage and the decay stage, which is different from other dissolution models.

The cleaning rate (r_c) is given in the swelling and uniform stage by (Xin et al., 2004):

$$r_c = \frac{r_{c,m} \exp[\xi(t - t_r)]}{\Psi + \exp[\xi(t - t_r)]} \tag{2.14}$$

where $r_{c,\,m}$ is the constant cleaning rate during the uniform stage, ξ the detachment kinetic constant, t_r the reputation time when the first protein chains disengage the gel-solution interface and ψ a dimensionless parameter which is related to the volume fractions' change of the protein chains.

And during the decay stage r_c is expressed as:

$$r_c = r_{c,m} \exp[-k_a(t - t_{su})] \tag{2.15}$$

where k_a is the first order rate constant for surface area reduction and t_{su} is the total cleaning time during the swelling and uniform stages.

Table 2.6. Modelling of cleaning from milk deposits

Operational parameters	Model	Reference
Cleaning solution concentration	$dC_x/dt = -kC_x C_{OH}$	Jennings (1959, 1965)
	$dN_x/dt = -\frac{D_{app} A}{x_{bound}} (C_w - C_b)$	Harper (1972)
	$C_x = C_0\{1-\exp[-(D_{app}At)/(xV)]\}$	Schlüssler (1976)
	$dt/dC_x = 1/[k_1(C_b - C_b^0)] + k_2/k_1$	Lenges (1982)
	$t_1 = (m_x(t=0))/k_1$, before t_1: $dC_x/dt = k_1[1-\exp(k_2 t)]$, after t_1: $dC_x/dt = k_1[\exp(k_2 t)-1]\exp(-k_2 t)$	Gallot-La Vallée et al. (1982)
	$dC_x/dt = k\ m_x(t=0)t\exp(kt)$, with $\ln k = a + bC_{OH} - cC_{OH}^2$	Gallot-La Vallée et al. (1984)
Temperature	$-d\log C_x/dt = 1.3412 - \frac{0.149}{T}$	Jennings (1959)
	$C_x = C_0\left\{1-\exp\left[-\exp\left(-\frac{a}{T}+b\right)t\right]\right\}$	Schlüssler (1970, 1976)
	$dC_x/dt = -kC_x$, with $\ln k = a - b/T$	Hoffmann and Reuter (1984)
	$k_1 = k_{75}\exp\left\{\left[\frac{1}{348} - \frac{1}{(273+T)}\right]E_r/2\right\}$, with k_{75} = 6.4 10^{-1} s^{-1}, E_r = 138.2 kJ mol^{-1}	Gallot-La Vallée and Lalande (1985)
Mechanical action	$\frac{C_{x,10\,min}}{C_x} = \exp[-0.1(10-t)]$	Jennings et al. (1957)
	$C_x = a\,\dot{v}^b$	Jackson and Low (1982)
	$dC_x/dt = -kC_x$, with $\ln k = a - b\tau_w$	Hoffmann and Reuter (1984)
	$F = Y\,L_x\,x_s + \kappa_s\,L_x$	Liu el al. (2006b)
Kinetic of cleaning	$dm/Adt = (C_s - C_b)k_c$	Gallot- La Vallée and Lalande (1985)
	$m(t)/m(30s) = \exp[av^{0.70}(t-30)]$	Grant et al. (1996)
	$C_x = 1-\exp\left[\left(\frac{t}{T}\right)^R\right]$	Weibull distribution (Dürr and Graßhoff, 1999; Dürr, 2002)
	Eqs. 2.14 – 2.15	Xin et al. (2002, 2004)
	$t_c = \left[1.1024 - 0.06082\left(\left(\tilde{A}-5800\right)/4700\right)^2\right]$, for stead and pulsed flow and ΔT = 1 K	Föste et al. (2013)
Combined/ complex models	$r_C = k_1\exp[aC_{clean\_solution} + (b/273+T)]$, with k_1 = 10,763; a = 0.1420 and b = -3047.72	Schüßler (1970)

A large number of studies have underlined the importance of improving CIP procedures (Bird, 1994; van Asselt et al., 2002; Alvarez et al., 2010) and deposit detachment kinetics have been modelled in relation to chemicals concentration, temperature and time of treatment, as well as hydrodynamics (see Table 2.6). The influence of the surface material on removal of deposits is evident and several experimental studies have shown the correlation between the surface cleanability and contact angle or surface energy (Nassauer, 1985; Wildbrett and Sauerer, 1989; Dürr, 2007; Mauermann et al., 2009; Ashokkumar et al., 2012). Conversely, there is no model correlating the cleaning kinetics of food deposits from solid surfaces with surface free energy, while little work has examined the combined effect of more than one surface property on cleaning behavior.

Boulangé-Petermann et al. (2006) assessed the effect of surface energy in the cleaning of oil droplets on two coated stainless steel surfaces, although no correlation between the cleaning performance (oil removal after 10 s and 30 s) and the surface energetic property was proposed. Ashokkumar et al. (2012) attempted to correlate the cleaning rate of oil after frying with turkey meat at 200 °C with the contact angle of diverse coated surfaces. Dürr (2007) analyzed the database and results of three other works with respect to such a combined influence of surface roughness and wettability on bacteria adhesion, removal and inactivation. The author found for the following expression the time needed to reach 63.2 % soil removal, $t_{c,63.2\,\%}$:

$$t_{c,63.2\%} = t_{c,0} + a\,R_a + b\cos\theta \qquad (2.16)$$

with $t_{c,0}$ = 20.1 min and the constants a = 42.4 min μm^{-1} and b = 24.4 min.

This study investigated the cleaning behavior of milk deposits on surfaces with different energetic properties, fitted the cleaning rate profiles to the polymer dissolution–based cleaning model of Xin et al. (2002, 2004) and showed the influence of the electron donor component onto the maximal cleaning rates.

2.4 Fouling and cleaning of milk deposits on modified surfaces

The next sections address the influence of surface properties, such as coating, roughness and charge as well as surface coating aging, on fouling and cleaning of milk deposits.

2.4.1 Influence of surface coating

There is a wide variety of processes for the coating of substrates, including electrochemical deposition, thermal spraying, contact welding, plating, ion implantation or sputtering, physical and/or chemical deposition, hybrid methods. All these methods differ in their deposition options (coating equipments, coating materials and precursors, coating rate), film properties (tribological and energetic properties, thickness and surface topography) and costs (equipment purchase and maintenance price, power consumption, space and personnel requirements). An important application of coatings is to reduce fouling, given that the modification of a heat transfer surface affects the interaction between the surface and the process fluid and thus the attachment, adhesion, retention, type and amount of fouling formed, as well as the removal of

foulant components on the surface and the resistance of the surface to corrosion fouling. A prolonged induction period would improve the plant operating efficiency, while less effort for cleaning would increase the plant productivity and save natural resources.

Extensive research on coated surfaces for the use in heat exchangers in dairy industry has been conducted in the last years, principally up the 1990s. Table 2.7 summarizes the published works on the fouling of milk and milk components on modified surfaces. Contradictory results can be found related to the effect of surface properties on milk, whey protein or calcium phosphate initial and multilayer deposition. Some authors have suggested that the fouling mechanism on coated surfaces may differ from standard stainless steel (Britten et al., 1988; Karlsson et al., 1996; Ramachandra et al., 2005; Premathilaka et al. 2006; Rosmaninho and Melo, 2006b) and that protein groups arrange differently on the surfaces (Premathilaka et al., 2006). However, as the deposit amount increases, the influence from the surface seems to decrease. Hence, some investigations based on deposit chemical analysis or weighing showed no effect of the surface properties on deposition (Dupeyrat et al., 1987; Britten et al., 1988; Yoon and Lund, 1994; Andritsos et al., 2002; Beuf et al., 2003) as well as final deposit composition (Yoon and Lund, 1989) or its superficial structure (Britten et al., 1988). By contrast, other works using more sophisticated analysis and ex or in situ monitoring methods, such as SEM, XPS, quartz crystal microbalance or ellipsometry, have shown an influence of the surface coating on both the initial and succeeding stages of the build-up (Gordon et al., 1968; McGuire and Swartzel, 1989; Karlsson et al., 1996; Murray and Cros, 1998; Ramachandra et al., 2005; Premathilaka et al., 2006; Santos et al., 2006a; Rosmaninho and Melo, 2006b, 2008; Rosmaninho et al., 2008; Balasubramanian and Puri, 2009; Boxler et al., 2011; Rungraeng et al., 2012). Therefore, further investigation on the fouling behavior on coated surfaces is required to understand the process in its entirety. Nonetheless, there seems to be a consensus among authors that surface coating has a stronger effect on cleaning than fouling (Britten et al., 1988; Beuf et al., 2003; Santos et al., 2004).

Table 2.7. Review on milk, whey protein or calcium phosphate fouling on coated surfaces (in chronological order).

Authors	Fluid	Surfaces	R_a [µm]	γ^{TOT}, γ^{polar} or γ^- [mN m^{-1}]	Experimental conditions	Monitoring method	Conclusion
Gordon et al. (1968)	Raw milk	SS Teflon® coating	320, 180 and 120 grit, pickle finish --	--	Cont. operation, with recirculation, milk was heated from 1-3°C to 82°C, $T_{heating}$ = 100°C, 0.7-8 m^3 h^{-1}	Weighing of deposit	More deposit formed on Teflon® coated surface than on SS.
Dupeyrat et al. (1987)	Whey	standard and polished 304 L SS, glass, Teflon® and polished Teflon®, polyethylene as well as silicone and fluorine resins applied to Al (6080)	--	144[a] 146[a] 144[a] 142[a] 146[a] --	Cont. operation, T_{bulk}= 72°C, (ΔT= 0 K), 20 min, v= 0.096 and 0.11 m s^{-1}	Weighing of deposit, infrared spectroscopy	Deposit amount and composition were almost the same whatever the surface (high dispersion of the masses which varied between 20 and 70 µg cm^{-2}).
Britten et al. (1988)	Raw whole milk pH 6.5	standard and polished 316 SS and nylon, polymethyl-methacrylate, polystyrene, cellulose 2.5/3.0 acetate and agarose coatings	0.8 0.05 2.0 0.2 0.1 0.2 / 0.6 0.3	-- -- 67.7[a], 19.3[b] 49.9[a], 19.3[b] 43.1[a], 17.1[b] 52.6[a], 29.5[b] 49.3[a], 25.1[b] 72.1[a], 50.5[b]	Batch operation (magnetic stirrer at 200 rpm), T_{bulk}= 60°C, $T_{heating}$= 100°C, 60 min	Chemical analysis (Kjeldahl, colorimetric method), weighing of deposit, SEM	Although similar deposit amount was formed on most of surfaces, the deposits showed very different adhesion. Polar contribution was the main factor influencing adhesion.

McGuire and Swartzel (1989)	Whole milk	standard and polished 304 SS and Teflon®, alumino-silicate coatings	0.4 0.04 1.9 2.3	51.4[a] 46.4[a] 22.1[a] 38.6[a]	Cont. operation, milk was heated from room temp. to 100°C, 134°C or 154°C, 1-30 min	Ex situ ellipsometry, infrared spectroscopy, weighing of deposit	Deposition rate depended on the surface properties. Different fouling layers' refractive indexes were obtained, indicating variation on the deposit density.
Kirtley and McGuire (1989)	β–Lg in phosphate buffer, 0.1 g L^{-1}, pH 7	304 SS as well as PTFE, polypropylene, polyethylene, nylon, glass	--	38.3[b] 0[b] 29.7[b] 12 - 22[b] 47.5[b] 127[b]	Batch operation, T_{bulk}= 30°C, 360 min	Weighing of deposit	A critical surface tension was found, in which protein adsorption was minimal.
Wahlgren and Arnebrant (1990)	β–Lg in phosphate buffer	silica and methylated silica surfaces as well as polysulfone coating	 --	-- 27[a] --	Batch operation, T_{bulk}= 25°C, 60 min	In situ ellipsometry	Different protein amount adsorbed on the surfaces. A surface-induced re-arrangement is suggested.
Yoon and Lund (1994)	Raw whole milk pH 6.7	Ti, standard and electropolished SS, Teflon® and polysiloxane coatings	0.19 0.13 0.08 0.60 0.10	-- more hydrophobic	Milk was heated from 41-45°C to 86-90°C in a PHE, v= 0.42 m s^{-1}, 72-82 min	Overall heat transfer coefficient, chemical analysis, weighing of deposit	Once a few layers were adsorbed, the surface type did not seem to affect the deposit composition
Jeurnink et al. (1996b)	0.25 % w/w WPC, 0.15 % w/w β–lg in water, pH 7.1	chromium oxide	--	--	Cont. operation, T_{bulk}= 25, 75 – 90 °C, holding time = 150 s	Reflectometry of the holding section	The protein denaturation near the surface is a prerequisite for continued deposition.
Karlsson et al. (1996)	β–Lg in PBS buffer, pH 6.0, 1.1 mg/ml	304 SS and chromium oxide (coated on silicon wafer) and methylated silica	< 0.1 -- --	 --	Batch operation (stirring: 325 rpm), T_{bulk}= 25, 60, 73, 77 and 80°C (ΔT= 0 K), 5-30 min	In situ null ellipsometry	As the protein amount increased, the influence from the surface seemed to decrease. Protein structural re-arrangement has been suggested.

Murray and Cros (1998)	β-casein and β-lg in immidazole buffer, pH 7.0, 10^{-3} % w/w	gold and gold treated with octadecyl-mercaptan	-- --	-- hydrophobic	Cont. operation, T_{bulk}= 25°C (ΔT= 0 K), 6 x10^{-4} m^3 h^{-1}, 180 min	Quartz crystal micro-balance	Rearrangement of the protein structure and changes in protein layer thickness has been supposed.
Wu et al. (1997); Wu and Nancollas (1998)	Calcium phosphate	PMMA, RFDG-PMMA, FEP, RFDG-FEP, silicone, RFDG-silicone as well as mica, anatase and rutile particles	--	12.0[c] 24.7[c] 1.2[c] 38.4[c] 1.8[c] 8.8[c] 50.9[c] -12.1[a],47.7[c] 11.1[a],15.6[c]	Batch operation, T_{bulk}= 37°C, 1140 min	Constant composition measurement, XRD, SEM	Heterogeneous nucleation depends on the surface properties.
Beuf et al. (2003)	Model fluid: whey protein, whole milk, sugar and xanthan gum	V2 SS as well as DLC, SiO_x, silica, Ni-P-PTFE, Excalibur®, Xylan®, SiF^+ and MoS_2 coatings	0.04 0.1 0.15 -- 0.25 1.77 1.81 0.2 0.15	41[a], 14.5[b] 36[a], 9[b] 40[a], 13.5[b] -- 20.2[a], 5.5[b] 21.7[a], 0.9[b] 21.5[a], 0.95[b] 45[a], 8[b] 40[a], 12[b]	Fluid was heated from 15°C to 102°C in a PHE, no recirculation, v= 1.42 m s^{-1} (Re=120)	Overall heat transfer coefficient, pressure drop, weighing of deposit	Difference between the reference SS and the coated surfaces could be found during fouling and cleaning experiments.
Wei et al. (2003)	β–Lg in PBS buffer, pH 7.4, 1 g L^{-1}	316 SS as well as polyethylene glycol, polyethylenimine	--	--	Batch operation, T_{bulk}= 25°C, 60 min	XPS and ToF-SIMS analysis	Surface with highest graft density was capable of preventing protein adsorption.
Premathilaka et al. (2006, (2007)	WPI in water, 6 g L^{-1}	304 SS as well as DLC and Si-DLC (prepared by CVD), TiN	0.25 --	--	Cont. operation, no recirculation T_{bulk}= 55°C T_{wall}= 70°C, 3 min	Ex situ XPS and angle resolved XPS	Different fouling mechanisms and protein groups' arrangement depending on the surface are suggested.

Rosmaninho and Melo (2006b)	SMUF	316 SS MoS_2, SiF_3^+, SiO_x, Ni-P-PTFE	0.02 – 0.06	51.9[a], 39.0[c] 45.7[a], 20.4[c] 49.4[a], 36.8[c] 55.5[a], 50.6[c] 15.5[a], 0.2[c]	Batch operation (rotational speed = 150 rpm, Re= 4.6 x 10^4), T_{bulk}= 44°C, 5 and 120 min	Deposit weighing, SEM	Distribuition, number and size of the aggregates on its first deposited layer was responsible for the build-up of final different deposit structures.
Santos et al. (2006a)	WPI in PBS buffer 5.4 g L^{-1} pH 6.7	SS as well as SiF_3, MoS_2 and TiC ion implanted, DLC sputtered, DLC and Si-O-DLC prepared by CVD and silica sol-gel coatings	30 24 25 20 30 28 27 35	--	Cont. operation, no recirculation, T_{bulk}= 72 and 85°C (ΔT= 0 K), V = 0.13, 0.39 and 0.59 m s^{-1} (Re= 3,800; 11,300; 17,100), 20 min	In situ ellipsometry and ex situ particle size determination	The adsorption rate constants for mono-layer and multilayer formation were found to be dependent on the surface coverage.
Parbhu et al. (2006)	Raw milk	SS as well as chromium oxide and silicate treated chromium oxide	--	--	Cont. operation (PHE), $T_{pasteurization}$ = 80 °C	Pressure drop	Adhesion of phosphate anion was lower on silicate treated surface, which induces less fouling.
Rosmaninho and Melo (2007)	WPI in SMUF	SS as well as TiN 1, TiN 25 and TiN 3	--	-- 55.3[c] 23.0[c] 46.2[c]	Cont. operation (v=0.2 m s^{-1}, Re= 6256), T_{bulk}= 48°C, T_{oil}= 70°C (ΔT= 1.5 K), 1080 – 1800 min	Overall heat transfer coefficient, deposit weighing, SEM	Deposition rate, final deposit amount and resistance to removal were influenced by surface properties.
Rosmaninho and Melo (2008)	WPI in SMUF	316 SS as well as SiO_x, silica, Si-O-DLC (prepared by PECVD), MoS_2 and Ni-P-PTFE coatings	--	24.3 - 39[c] 50.6 - 53.8[c] 12.4 - 15.3[c] 15 - 15.6[c] 20.4[c] 0.2 – 10[c]	Batch operation (rotational speed = 150 rpm, Re= 4.6 x 10^4), T_{bulk}= 50 and 85°C (ΔT= 0 K), 10 and 120 min	Deposit weighing, SEM	Number and size of the aggregates initially attached to the surface could be related to the amount of final deposit since they seemed to control the final deposit structure.

Rosmaninho et al. (2008)	SMUF	SS as well as TiN 1 (8.7% Ti) TiN 3 (8.7% Ti) TiN 2 (8.1% Ti) TiN 4 (8.1% Ti) TiN 5 (10.4% Ti) coatings	--	39.0[c] 55.3[c] 46.2[c] 23.0[c] 18.4[c] 26.0[c]	Cont. operation (v=0.2 m s^{-1}, Re= 6256), T_{bulk}= 48°C, T_{oil}= 70°C (ΔT= 1.6 K), 8400 min	Deposit weighing, SEM	Deposition rate and final deposit amount were influenced by surface properties.
Balasubra-manian and Puri (2008, 2009)	Skim milk	316 SS as well as Ni-P-PTFE, Lectrofluor™ and AMC148-18 coatings	--	--	Fluid was heated from 15°C to 72°C in a PHE, 162 $m^3 h^{-1}$channel^{-1}, 360 min	Deposit weighing	The coatings could reduce fouling by about 85 to 95% compared to SS surface.
Mauermann et al. (2009)	WPI in water, 5 % w/w	304 SS as well as FEP, PEEK + fluoro-polymer, Si-O-DLC (prepared by PECVD), Ti-DLC (prepared by PVD) and nanocomposite coatings	0.15 0.3 2 0.2 0.2 0.07 – 0.6	38.3[a], 6.6[b] 19.8[a], 1.5[b] 13.4[a], 0.1[b] 29.9[a], 2[b] 41.8[a], 0.4[b] 23.6[a], 2.4[b] 29.8[a], 7.1[b]	Batch operation, solution was heated from 60°C to 80°C (ΔT= 20 K)	Deposit weighing	The surface modifications showed different behavior regarding the amount and structure of deposit.
Kananeh et al. (2010)	WPC in water, pH 6.0, 10 % w/w	standard and electropolished SS as well as epoxy-resin based, polyurethane based and PTFE	0.15 0.17 0.92-1.14, 0.06-0.23 (R_a values of the sheets)	--	Cont. operation, with recirculation in a flow cell, v= 0.2 m s^{-1}, T_{bulk}= 45°C, T_{wall}= 96.5°C, 17 min and in a PHE, without recirculation in which solution was heated up to 85°C at 0.015 $m^3 h^{-1}$, 240 min	Deposit weighing	In general coated surfaces showed reduced deposition, however on PTFE more deposit build-up.

Boxler et al. (2011)	SMUF	304 SS as well as DLC, Si-DLC and Si-O-DLC coatings (prepared by PECVD)	0.2 0.13 0.125 0.125	40.5[a], 8.4[c] 44.7[a], 13.1[c] 39.4[a], 6.4[c] 34.5[a], 7.2[c]	Cont. operation, with recirculation T_{bulk}= 50 °C (ΔT= 0 K), v= 0.25 m/s; Re = 8600, 900 min	Vibration sensor, microscopy	The surface affected initial attachment of calcium phosphate as well as its subsequent adhesion and removal from the surface.
Rungraeng et al. (2012)	Pasteurized milk	316 SS as well as PTFE and CNT-PTFE coatings	-- --	32[a] 5[a] 1[a]	Past. milk was heated from 20°C to 60°C (ΔT= 12 K), in single channel PHE, with recirculation, 0.0054 m s^{-1} (Re= 171), 60, 120 and 300 min	Deposit weighing, SEM	The mass of deposit was reduced by 43 and 70% for the PTFE and CNT-PTFE respectively.
Barish and Goddard (2013)	Raw milk	316 SS as well as Ni-P-PTFE	0.32 0.17	41.4[a] 24.7[a]	Fluid was heated from 18°C to 85°C in a PHE, 480 min	Deposit weighing	The mass of deposit was reduced by 30 times on the coated surface.
Keshani et al. (2013)	Whole milk, skim milk and whey protein	SS as well as PTFE	0.08 0.04	40.1[a] 23.6[a]	Products were dried in a co-current spray dryer. Liquid feed = 23 and 28 ml/min and $T_{air\ inlet}$= 140 and 180 °C	Deposit weighing	Deposition, viz. adhesion and cohesion of particles depends on the liquid composition.
Patel et al. (2013)	Whole milk, skim milk and WPI	SS as well as doped DLC: DLC1 DLC2 DLC3	0.17 0.12 0.15 0.13	50.8[a], 30.2[c] 48 [a], 21.8[c] 43.5[a], 21.2[c] 41.3[a], 35.2[c]	Batch and cont. operation. Milk was heated to 84°C in a PHE, at 2.77 x 10^{-5} m^3s^{-1} (Re = 1100)	Deposit weighing, overall heat transfer coefficient	Modified surfaces showed no benefit in fouling mitigation as well as in ease of removal of the deposits.

CNT: carbon nanotubes, CVD: chemical vapor deposition, PVD: physical vapor deposition, RFGD: radio frequency glow discharge treated surfaces. Superscript a for γ^{TOT}, b for γ^{polar} and c for γ^{-}.

Surfaces have been modified by coating mainly to reduce the surface free energy. However, the optimal surface energy, in which deposition and adhesion are minimal, is not necessaryly a low value. In general, the adhesion of a hydrophilic particle or macromolecule as protein is favorable on low energy surfaces (hydrophobic surfaces) (van Oss, 2006; Purwanti et al., 2009). However, hydrophilic proteins can adsorb onto high energy surfaces (hydrophilic surfaces) through attraction between electron-donor sites on peptide-bends and electron-donor sites disseminated in the surface (Santos et al., 2006b; van Oss, 2006). Santos et al. (2006b) concluded that the formation of protein multilayers on the surface is dependent on the nature of the first layer, which can be altered by surface modification. Karlsson et al. (1996) and Marsh et al. (2002) showed that β-lg conformational changes are larger on hydrophobic than hydrophilic surfaces. The surface can influence: (*i*) the amount of protein adsorbed/desorbed; (*ii*) the protein unfolding and the denaturation mechanism on the surface; (*iii*) the binding force of protein molecules in close contact with the surface and in contact with adsorbed sublayers; and (*iv*) the formation of layers, which can be structurally different. Moreover, in the presence of Ca^{++}, the protein adhesion and consequent deposition can be enhanced, as reported by Guérin et al. (2007). Ca^{++} not only provides electrostatic crosslinking between two hydrophilic, negatively charged proteins, as discussed in section 2.2.4, but also serves as an electron-acceptor, which neutralizes electron-donors on the surface and thus renders the surface more hydrophobic (van Oss, 2006). The hypothesis that the fouling resistance and/or the deposit amount follow a quadratic relationship to surface free energy or to a surface energy contribution term is related to the findings in literature. Optimal surface free energy ranging from of 20 to 30 mN m^{-1} at which bacteria, food and mineral adhesion/deposition are minimal, have been determined experimentally and/or estimated by extended DVLO theory by Baier (1980), McGuire and Swartzel (1989), Zhao et al. (2004a, 2005a, 2005b, 2007), Zettler et al. (2005), Liu et al. (2006a), Rosmaninho et al. (2008) and Keijbets et al. (2009).

While no straightforward correlation between total surface energy and fouling behavior could be found for crystallization fouling by Förster et al. (1999), Zettler et al. (2005), Geddert et al. (2011b), a correlation between polar and/or apolar contributions of the surface free energy or one of their components for bacteria adhesion, protein and mineral fouling has been reported. Britten et al. (1988) found that the polar binding potential of coated surfaces was the main factor affecting the deposits' adhesion strength. Liu and Zhao (2011) correlated the bacteria adhesion with the ratio between the Lifshitz–van der Waals (γ^{LW}) to the electron donor (γ^-) surface energy components. Rosmaninho and Melo (2008) and Al-Janabi et al. (2010) found optimal values of the surface electron donor component, which seems to be most significant component of the polar contribution of the surface tension affecting fouling, with $\gamma^- = 10 - 55$ mN m^{-1}.

Rosmaninho and Melo (2008) and McGuire and Swartzel (1989) proposed a schematic representation of the mechanism and a model relating the deposition of milk or milk constituents to the surface free energy, respectively. The proposed mechanism for multilayer deposition of whey protein (WPI) in the presence of calcium phosphate (SMUF) on different coated surfaces is shown in Fig. 2.16. Rosmaninho and Melo (2008) suggested that the number and size of the aggregates initially attached to the surface will depend on γ^- and can be related to the amount of final deposit formed on each system, since they seem to control the final structure of the deposit.

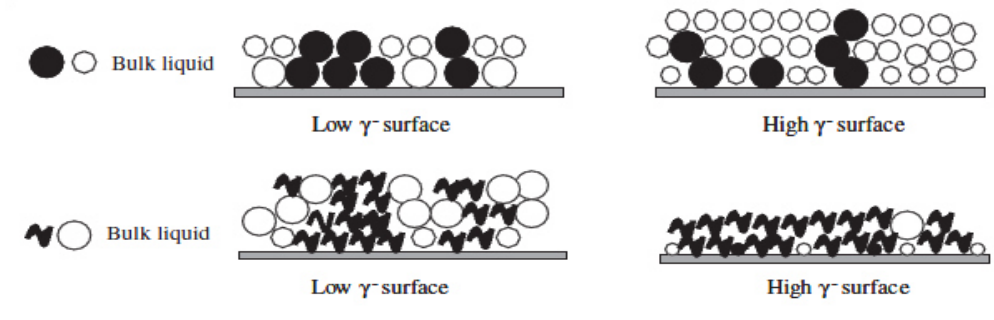

Fig. 2.16. Mechanism of whey protein-SMUF deposition (a) at low temperature (50 °C) and (b) at high temperature (85 °C) on different coated surfaces (Rosmaninho and Melo, 2008). native protein denatured protein calcium phosphate

The application of a large range of coated surfaces to improve cleaning efficiency has also been investigated and reviewed by Detry et al. (2010). Gordon et al. (1968) observed that dry milk deposits could easily be removed from PTFE. By contrast, Masurovsky and Jordan (1958) and Yoon and Lund (1994) found no reduction of the cleaning time on PTFE-coated plates fouled with milk heated up to 86 - 90 °C and contaminated with bacteria, respectively. Leclercq-Perlat and Lalande (1994) compared the removal of yoghurt contaminated with spores of *Bacillus stearothermophilus* from stainless steel with other materials used in food production equipments, including borosilicate glass, PMMA and PVDF, finding that the polymer materials are easier to clean than stainless steel and glass. The cleaning of β-lg deposits from stainless steel, chromium oxide coated on silicon and methylated silica surfaces showed significant difference between hydrophilic and hydrophobic surfaces (Karlsson et al., 1996). Beuf et al. (2003) analyzed different surface modifications, such as coatings (DLC, Silica, SiO_X, Ni-P-PTFE, Excalibur®, Xylan®) and ion implantation (SiF+, MoS_2), finding no significant difference between unmodified and the most modified stainless steel on the cleaning of deposit from a milk based model fluid. However, the cleaning efficiency of plates coated with Ni-P-PTFE increased considerably. Experimental results of Liu et al. (2006a) and Liu and Zhao (2011) also showed that Ni-P-PTFE coating significantly reduced the adhesion of food and bacterial deposits. Mauermann et al. (2009) studied different surface treatments, including two DLC-coated surfaces, on the cleaning of potato starch and whey protein deposits. Studies were carried out by means of spray cleaning, simulating the cleaning of open surfaces. a-C:H:O:Si (SICON®) and a-C:H:Ti (prepared by a reactive magnetron sputtering process) showed a better cleanability compared to the reference stainless steel. Kananeh et al. (2010) performed soiling and cleaning experiments using a whey protein solution, which was heated up to 85 °C on modified surfaces. A CIP time reduction was observed for the tested surfaces, namely PTFE, nano-composites and electro-polished stainless steel. Ashokkumar et al. (2012) investigated the cleanability of PTFE, silicone, quasicrystalline (Al, Fe, Cr) and ceramic coatings (ZrO_2, ZrN, and TiAlN). The authors found that polymer surfaces (PTFE and silicone) have lower cleaning ratings after frying turkey meat with oil at 200 °C than the other surfaces. No reports have been published on cleaning of milk deposits formed at temperatures over 110 °C on coated surfaces. Such soils are mineral rich, hard (Burton, 1968),

difficult to remove (Jeurnink and Brinkman, 1994), and many challenges still exist in describing the removal of these heterogeneous deposits.

The cleanability of a surface is directly related with the deposit adhesion force, i.e. the resulting Lifshitz-van der Waals (attractive) and electrostatic force (attractive or repulsive) forces between the surface and the deposit, which depends on the surface free energy and other surface properties, including roughness. Fryer et al. (2006) and Saikhwan et al. (2006) showed that the deposits of tomato paste, milk and egg proteins have a lower adhesion force on low energy surfaces than higher energy surfaces. However, Beck et al. (2005) found low separation forces by the deattachment of single round test particles and microorganisms on the highest energy surfaces (Enamel and SiO_2, whose γ^{TOT} was around 65 mN m^{-1}).

Contradictory results regarding the influence of surface free energy and surface energy components on fouling and cleaning can be explained by diverse surface characteristics and treatments also playing an important role in the both processes, which have not been considered, defined and discussed in published works. Thus, a comparison of the different studies is difficult. Some of these aspects are listed below:

i. surface aging, as well as its influence on fouling;
ii. surfaces with markedly difference in chemistry, charge and charge distribution, surface roughness or surface energy components;
iii. deposits with different microstructure, density and thermal conductivity and thus different mass, thermal resistance and deposit aging; and
iv. mechanical integrity after repeated fouling and cleaning cycles.

Other surface properties such as surface roughness and charge should additionally be taken into account in the choice of the most efficient surface and will be briefly discussed in the next sections.

2.4.2 Influence of surface roughness

Cracks and edges provide nucleation and anchorage points that might promote fouling. In general, the roughness that occurs on the surfaces of the metal, created by its manufacturing process, is larger than the size of individual microorganisms, ions and molecules, such as protein. Consequently, crystals, protein molecules or cells are able to “hide” within the roughness and will be protected from the flow removal forces (Bott, 2011). Surface roughness also influences the nucleation site density of air bubbles at the surface that induce fouling (Palethorpe and Bridgwater, 1988), as well as the local flow and heat transfer conditions. As the compact sublayer builds up, the original surface becomes rougher due to the formation of aggregates or granules of protein and agglomerates of crystals. Such heterogeneities, protuberances or voids will subsequently affect the overall heat transfer coefficient, thus influencing the fouling process (Albert et al., 2011) and the deposits’ final structure. An enlargement of the surface area relative to a smooth wall and an increase in near wall turbulence enhance the heat transfer (Albert et al., 2011) and apparent negative fouling resistances are determined by considering a constant overall heat transfer coefficient.

Owing to the microscopically surface structure and randomness in fouling layer growth, a porous deposit will be formed (Sandu, 1989). Besides, with increasing fouling layer

amount and density, protein will crosslink in deposit, building up a rough and spongy matrix in which further fouling constituents (e.g. fat) might be entrapped. In the case of crystallization, ions can diffuse in deeper regions of the crystalline rough fouling layer and crystallize there, forming a very compact deposit (Höfling, 2004).

Pflug et al. (1961), Herreid and Le Luetscher (1963) and Gordon et al. (1968) reported that roughness of the metal heating surface increased very slight the rate of deposition and retention of milk soil. Yoon and Lund (1994) observed no significant effect of surface roughness on milk fouling in the roughness range of 0.08 – 0.60 µm, concluding that deposit formation is generally a weaker function of surface roughness as it is to the substrate material. Liu et al. (2011), Kazi et al. (2012) and Jimenez et al. (2013) found that by increasing surface roughness, the $CaCO_3$ deposition increases, due to favorable trapping of crystals on grain boundaries and thus fouling anchoring on the surface.

The cleanability of various stainless steel finishes has been reviewed by Milledge and Jowitt (1980) and recently updated by the same author (Milledge, 2010). Detry et al. (2010) reviewed the relation between stainless steel grade, surface composition, finish, roughness and energy and the cleanability. The influence of surface roughness on cleaning behavior is controversial in various ranges of R_a values: while some works have revealed a good correlation between the surface roughness parameter R_a and cleanability, others found no direct relationship between these parameters. Furthermore, data on the effects of roughness tend to be empirical (Bott, 2011).

Note that R_a is only a measure of the average amplitude of the surface irregularities, rather than their frequency or shape (Milledge and Jowitt, 1980). Attempts have been made to relate other standardized roughness parameters, which are more adequate to describe surface topography to surface hygienic status than the usually mentioned R_a (Verran et al., 2000; Jullien et al., 2002).

According to Hoffmann and Reuter (1984) and Nassauer (1985), the cleaning behavior is significantly improved with a reduction of the roughness of a very rough surface with roughness values R_a ranging from 0.5 µm to 6.5 µm, whereas the influence of the roughness is lower on the cleanability of surfaces with a roughness R_a below than 2 µm. After cleaning, remaining soils are generally localized in surface defects, and sharp scratches are more difficult to clean than surface irregularities (Detry et al., 2010).

Britten et al. (1988) showed that the adhesion strength of milk deposits was not affected by the roughness ($0.05\ \mu m < R_a < 2\ \mu m$) of different coated surfaces, while Leclercq-Perlat and Lalande (1994) found that highly adhesive milk soil was more difficult to remove with increasing surface roughness ($0.11\ \mu m < R_a < 0.3\ \mu m$). Saikhwan et al. (2006) found no significant dependence of the cleaning result of the removal of tomato paste in a roughness R_a range of 0.072 µm to 0.8 µm. Investigation concerning the detachment of spherical single particles from stainless steels with different grindings and various coatings has also revealed that the roughness in the range of $0.1\ \mu m \leq R_a \leq 2\ \mu m$ had no influence on cleaning (Bobe and Wildbrett, 2006). In a study of surfaces with roughness R_a between 0.029 and 3.2 µm, the minimum adhesion was found at R_a of 0.8 µm, with both smoother and rougher surfaces having greater adhesion (Kouider et al., 2010).

Dupeyrat et al. (1987) explain apparently contradictory results regarding the influence of surface roughness on milk fouling through the phenomena of wetting hysteresis or differences in contact angles, i.e. the surface free energy. Dürr (2007) analyzed the database

and results of three manuscripts from other authors with respect to a combined or synergistic influence of surface roughness and surface hydrophobicity on microbial adhesion, cleaning and inactivation. Meanwhile, Leclercq-Perlat et al. (1994) reported that chemical polishing also changed the surfaces' chemical composition and its cleanability. These three works again emphasize the importance of considering the simultaneous effect of two or more surface properties on deposit build up and removal.

2.4.3 Influence of surface charge

Surfaces carry electrical charges, whose magnitude and sign depend on the surface material and pre-treatment, such as surface finishing or electrical and chemical treatment (electropolishing, surface conditioning, cleaning treatment), as well as the solution composition (Nassauer and Kessler, 1986; Schurz et al., 1990; Boulangé-Petermann et al., 1995; Bellmann et al., 1997; Cherepy et al., 2005). Surface charge affects the adsorption of foulant constituents and in turn the deposit formation (Nassauer, 1985; Bellmann et al., 1997; Altankov et al., 2003). The presence of a deposit could also modify the charge of the surface and its attraction and repulsion features. However, information about the influence of surface charge or zeta potential on fouling is rather limited in literature and the characterization of the interfacial electrostatic interactions due to surface charge of a flat substrate and the foulant remains delicate to measure and difficult to interpret (Boulangé-Petermann et al., 1995; Moulin and Roques, 2003). Hence, the difficulty of directly measuring the electrokinetic properties (in or on line or at process operating conditions) and the dynamic change of the electrostatic interactions during the deposition of successive fouling layers has restricted knowledge of ionic exchanges at the double layer or at the passive film interface of stainless steel surfaces. Furthermore, a correlation between surface charge or zeta potential, surface energy parameters and fouling has not yet been described.

The Gouy-Chapman-Stern model (Gouy, 1910; Chapman, 1913; Stern, 1924) or electrical double layer theory describes the structure of the electrostatic field surrounding a charged particle or surface in an electrolyte. According to this model, a charged surface of a solid, in an aqueous solution, attracts counterions, forming a compact layer of ions firmly adsorbed on the surface, called the inner layer or Stern layer. Surrounding the Stern layer there is a region where ions, which have the same signal charge as the surface, are less firmly attracted. This layer is called the diffuse or Gouy layer and, together with the Stern layer, forms the double layer. In some cases, the separation of the double layer into a charge-free Stern layer and a diffuse layer is insufficient to interpret experiments. The Stern layer is subsequently subdivided into an inner Helmholtz layer, bounded by the surface and the inner Helmholtz plane, and an outer Helmholtz layer, located between the inner Helmholtz layer and the outer Helmholtz plane (Müller et al., 1996; Delgado et al., 2007). This situation is displayed in Fig. 2.17.

If the solid or the liquid with respect to the other is moved, a shear stress of the ions layers occurs and an electrokinetic potential forms between the slipping or shearing plane at the outer boundary of the Stern layer (outer Helmholtz layer) and the medium, decaying with distance. The potential at the shear plane is known as zeta potential, reflecting the surface charge. The relation between the zeta potential and the surface potential is complex and under certain conditions both potentials can have different signs and the point of zero charge (PZC)

does not necessarily correspond to the isoelectric point (IEP) (Moulin and Roques, 2003). However, zeta potential has generally been used to characterize and study solid surface charges.

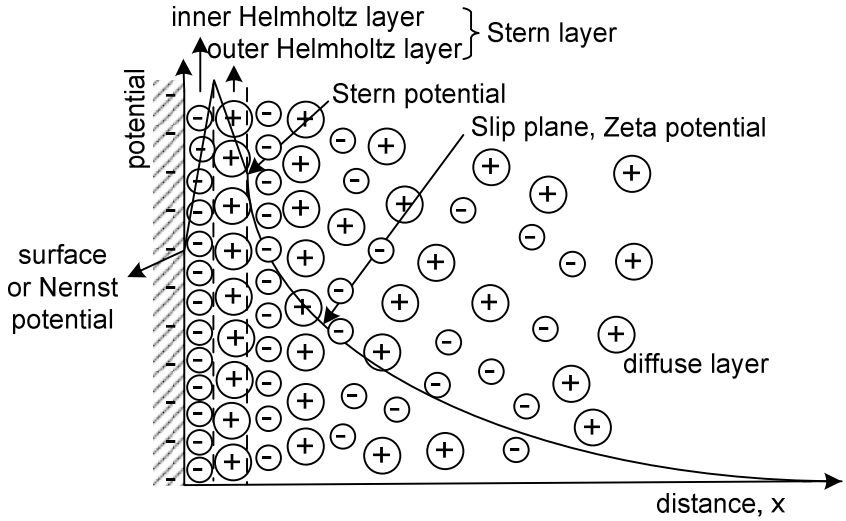

Fig. 2.17. Schematic representation of the charges and potential progress at a negative charged interface

Nassauer (1985) measured the Galvani potential difference by means of specific electrodes in a pipe system during milk proteins adsorption. The author showed an increase of the potential difference by the adsorption of native whey proteins (having a net negative charge) at neutral pH and decreasing by the adsorption of the proteins at basic or acid pHs, in which the protein structure is destabilized. Nassauer concluded that the denatured whey protein and caseins are mainly adhered to stainless steel by their hydrophobic groups. Furthermore, the adhesion of microorganisms and anionic or cationic surfactants on different materials in relation of their potential difference were compared (Nassauer, 1985; Nassauer and Kessler, 1986). Morrissey et al. (1976) investigated the relationship between the surface charge and protein-surface interactions, the adsorbed amount and the compactness of the protein layer, finding that additional adsorption took place above a certain potential and that the conformation of the proteins was changed by altering the surface potential. However, the results by Bos et al. (1994) suggested that protein adsorption is barely affected by external imposed interfacial potential due to variation of other properties of the system, which were not considered in their work. Bellmann et al. (2012) studied the adsorption of cationic and anionic starch on surfaces with different zeta potentials. The negative zeta potential surface adsorbed cationic starch, although the surface with positive potential adsorbed anionic as well as native and cationic starch molecules. Through the adsorption of charged inorganic particles (Al_2O_3 and SiO_2 particles) on the same surfaces, only oppositely charged particles attach to the surface. They hereby suggested that further properties of the corresponding adsorbate or foulant and interaction between their molecules might influence the adhesion mechanism and must also be considered (Bellmann et al., 2012). The adhesion of human fibroblasts was affected by the presence of specific functional groups on modified glass surfaces, which not only altered the surface contact angle, but also the surface zeta potential (Altankov et al.,

2003). Wu and Nancollas (1998) measured at pH value range of 7.3 – 7.5 for a high γ^- surface (γ^- = 48 mN m^{-1}, ζ = –47.5 mV) more negative zeta potential than for low γ^- surface (γ^- = 16 mN m^{-1}, ζ = –44.5 mV) and found that the nucleation of calcium phosphate phases was facilited in the high γ^- surface.

2.4.4 Coating aging and influence on fouling behavior

The durability, stability and cost effectiveness of the coatings has not often been reported in published works, with few systematic works on the effect of coating aging on fouling behavior. Some authors have pointed to alteration on coating properties such as adhesion to metal, color, hydrophobicity, or shown the difficulty of obtaining reproducible fouling experiments.

Beuf et al. (2003) observed significant difference between the first and the second processing runs in terms of fouling and cleaning, during heating a fouling model fluid constituting of whey proteins, whole milk, sugar and xanthan gum. Furthermore, they reported damaging of SiO_x, silica and DLC coatings. Al-Janabi et al. (2010) showed different fouling curves for $CaSO_4$ crystallization on Ni-P coating after the first fouling and cleaning cycles. Balasubramanian and Puri (2009) reported some discoloration of Ni-P-PTFE coating after use. Parbhu et al. (2006) showed variability of the fouling process within the trials for chromium oxide and silicate treated surfaces. Reused PMMA surfaces seemed more difficult to clean than new PMMA ones (Leclercq-Perlat and Lalande, 1994). However, EN-PTFE coating maintained its anti-fouling properties through ten independent experiments, showing non-significant differences in the milk deposit amount (Barish and Goddard, 2013).

Dupeyrat et al. (1987) emphasize the effect of cleaning agent on the surface free energy of coated surfaces, which can subsequently influence fouling. Rosmaninho et al. (2004) found different values for the contact angles of water, formamide and α-bromonaphtalene on new samples, after cleaning, as well as after being used for calcium phosphate deposition and cleaning again. They explained this difference by with to the entrapment of residual components in surfaces irregularities, which could not be removed by cleaning (alkali commercial detergent, 65 °C, 5 min). Mauermann et al. (2009) observed no quantitative change on surface roughness, yet drastic variation of the polar part of the surface free energy of stainless steel, as well as FEP, DLC and nanocomposite coatings after fouling and cleaning, with the exception of the PEEK + fluoropolymer coating. Moreover, the authors also detected the failure of some coatings. Saikhwan et al. (2006) measured differences on the surface free energy of DLC coatings after 10 - 12 fouling/cleaning cycles. Geddert et al. (2011a) also found a variation of the surface energy of DLC coatings, depending on the coating aging conditions, such as heat treatment (150 °C, 24 h) or chemical treatment in acid (6 % w/w HCl, 24 h) or in base (6% w/w NaOH, 24 h) solution. Secondary ion mass spectroscopy (SIMS) analysis of DLC and SICON® surfaces showed that hydrogen and silicon were replaced by oxygen bonds due to fouling and acid cleaning (Geddert et al., 2011). The inclusion of oxygen in the first atomic lattices thereby altered the coatings' surface free energy.

2.4.5 Surface coating by PECVD method

The application of a large range of coated surfaces for fouling mitigation or the improvement of cleaning efficiency has been investigated (see Section 2.4.1). However, most coatings have a poor thermal conductivity and/or are not resistant to the continuous thermal and mechanical stress (Mauermann et al., 2009; Al-Janabi et al., 2010; Kananeh et al., 2010), which thus inhibits their commercial use and application in food processing.

Hydrogenated amorphous carbon (a-C:H), also called diamond-like carbon (DLC) coatings, have attracted great interest due to their excellent properties such as thermal conductivity similar to metals, low friction coefficients with high hardness, extremely smooth surface and wear resistance, as well as their chemical inertness (Grill, 1993; Hieke, 2001; Robertson, 2002; Charitidis, 2010) (Table 2.8). Additionally, DLC is an excellent base coating to be alloyed with different elements (Hauert, 2003).

Table 2.8. Typical properties of the used a-C:H:X coatings and of Teflon® (Bewilogua et al., 2011)

Coating	Hardness [GPa]	μ vs. ball bearing steel	Abrasive wear [10^{-15} m^3 N^{-1} m^{-1}]	Water contact angle [°]	Surface free energy [mN m^{-1}]
a-C:H	25 – 35	0.15 – 0.2	0.5 – 1	65 – 75	40
a-C:H:Si	20	< 0.1	2 – 4	75 – 80	38
a-C:H:Si:O	8 – 10	0.4 – 0.6	10 – 15	95 – 105	24
Teflon®	< 0.5	0.1	>>	110 – 120	19

DLC-based coatings can be produced by diverse vacuum deposition methods: CVD, PVD (sputtering, ion assisted sputtering, ion beam or cathodic arc deposition, pulsed laser deposition) or PECVD (Grill, 1999; Robertson, 2002). The VDI 2840 guideline (Verein Deutscher Ingenieure, 2005) provides basic technological information about carbon films, coatings methods, film types and their properties. Through the plasma CVD or plasma enhanced CVD to modify or coat surfaces, the chemical reaction is initiated through the formation of plasma using hydrocarbon precursor gases. The plasma is usually induced through radio frequency (RF), microwaves or inductive coil. The growth and properties of DLC films are controlled by the substrate temperature and bias, gas pressure, composition and flow, RF power and geometric constraints (Grill, 1999). Deposition methods and mechanisms have been described by Grill (1999), Robertson (2002), Charitidis (2010). Essentially, a plasma is induced at a gas pressure of a few Pa and in consequence of the negative charging of the substrate, the ions are accelerated to the substrate surface. The surface is then cleaned by the plasma, which at the same time activates it, increasing the chemical affinity of the surface. The transition from plasma cleaning to deposition follows with the change of the precursor gas, which is injected in the vaccum chamber. Depending on the type of coating, different combinations of precursor gases are required: methane (CH_4) or acetylene (C_2H_2) for DLC coating, tetramethylsilane ($C_4H_{12}Si$), hexamethyldisiloxane ($C_6H_{18}OSi_2$) or tetrafluorethylene (C_2F_4) for doped DLC coatings. The voltage applied to the substrate ensures that the film formation process primarily takes place on the substrate surface.

Coatings properties compared to diamond or graphite can be achieved by varying the fraction of sp^2 and sp^3 bondings and hydrogen content, as shown in Fig. 2.18 (Robertson, 2002), as well as by build-in molecules in the carbon layer. The hydrogen concentration ranges from less than a few % at. to about 50 % at. (Donnet, 1998) and the amorphous nature of DLC permits introducing certain elements, such as Si, F, N, O, W, V, Co, Mo, Ti and their combinations, into the film, maintaining the amorphous phase of the coating. The mechanical and energetic properties of the DLC coatings can thus be varied and are a function of the film composition depicted in Fig. 2.19. A decrease in surface free energy is observed with the incorporation of Si or F in the DLC matrix, whereas the opposite behavior is obtained by the incorporation of O or N (Donnet, 1998). The effect of Si or F on the surface energy is attributed to the reduction of mainly the polar part of the surface energy, due to the loss of sp^2 carbon hybridization and dangling bonds (Donnet, 1998).

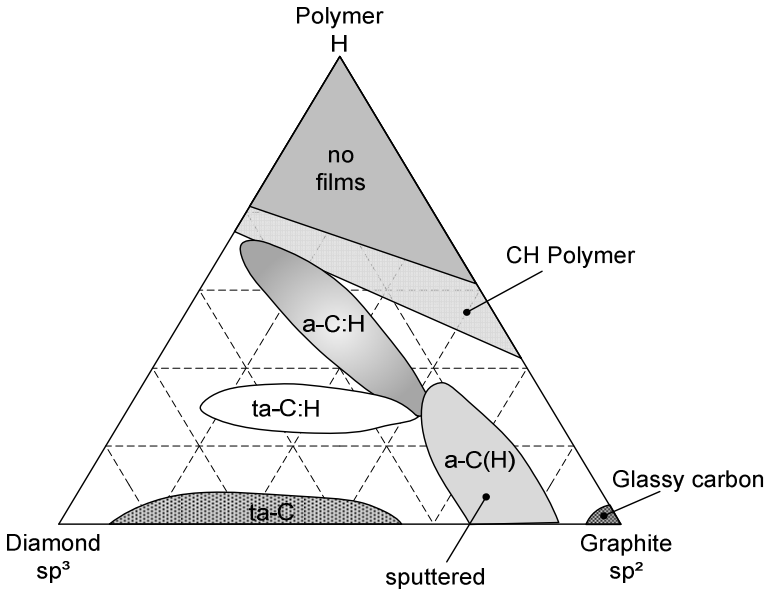

Fig. 2.18. Ternary phase diagram of bonding in amorphous carbon-hydrogen alloys

DLC films have a high elastic modulus, as well as high internal compressive stresses. The hydrogen content and the fraction of sp^2 and sp^3 carbon in the films (Robertson, 2002; Charitidis, 2010) and the incorporation of an interlayer prior to deposition (Azzi et al., 2010; Bewilogua et al., 2011) are associated with the internal compressive stress in the coating and its structure, defining its mechanical stability. By incorporating Si, N, B, F, O or metals in the films, a reduction in stresses can be observed, which is associated with a reduction in hardness and elastic modulus (Grill, 1999). Most DLC-based coatings are stable at temperatures up to 400 °C (Grill, 1999) and are thus suitable for ultra-high temperature processing in the food industry.

Since DLC coatings have shown non-cytotoxicity, viz. they have proven properties of bio- and haemocompatibility and are being applied on biomedical tools, such as coronary stents, heart valves, orthopedic implants (Grill, 2003; Hauert, 2003; Dearnaley and Arps, 2005; Hasebe et al., 2007; McLaughlin and Maguire, 2008). Rostagno and Cartasegna (2010) suggested that the corrosion and mitigation standards for food contact will be satisfied using

DLC coatings. DLC coatings have been approved as food safe contact substances (FDA, 2012) and some applications in the pharma and food industry have also been reported, such as tool for pressing Aspirin® tablets (Hieke, 2001), molding pasta (Schramm et al., 2004) and packaging beverages (Casiraghi et al., 2007; Hasebe et al., 2007). DLC and Si-O-DLC have proven to be suitable materials to mitigate deposition of calcium phosphate and calcium phosphate combined with whey protein batch-wise (Rosmaninho et al., 2007a; Rosmaninho and Melo, 2008). Mauermann et al. (2009) found more or no improvement on the deposition of whey protein and starch on Ti-DLC and Si-O-DLC coatings. Under continuous flow conditions without wall heating, Rosmaninho et al. (2007a) found no significant difference between DLC coated steel and the reference surface by the fouling of calcium phosphate. Beuf et al. (2003) obtained a similar result by heating a model milk based fluid up to 102 °C in a plate heat exchanger with DLC coated plates. Patel et al. (2013) also found no benefit in fouling mitigation by heating milk and whey protein in a batch and in PHE equipment, in which the stainless steel surface was DLC coated. The fouling of milk constituents on a range of doped DLC coated surfaces and cleaning of the formed deposits have not yet been systematically studied and thus will reflect the focus of this work.

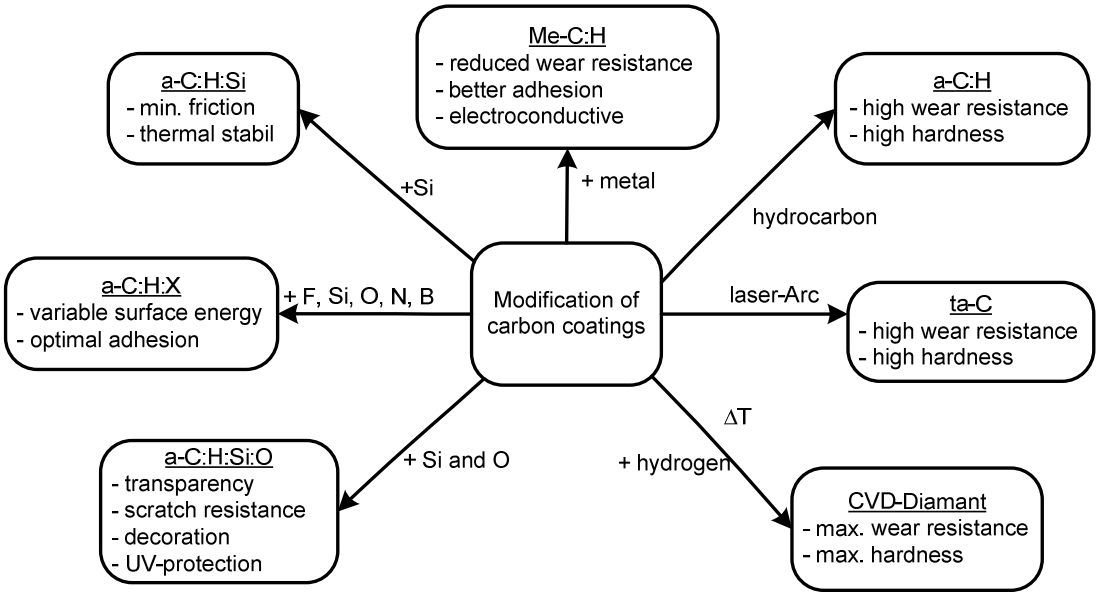

Fig. 2.19. Physical properties of modified DLC-based coatings (Hieke, 2001)

3 Material and Methods

In this chapter, the materials, the experimental devices and procedures as well as physical and chemical analysis are explained in detail.

3.1 Coated surfaces

Stainless steel is commonly the standard steel used in the food industry as it is durable, corrosion resistant and relatively easy to clean. Thus, stainless and electropolished stainless steel were chosen as substrate material for the heat transfer surfaces. For the sake of clarity, coupon refers to the plates used in batch-wise fouling experiments and plate refers to the PHE plates.

The coupons and plates were coated with DLC by plasma-enhanced chemical vapor deposition (PECVD) in a vacuum chamber (pressure of $< 10^{-3}$ Pa) at low temperature (< 200 °C). Before starting the DLC deposition, the substrates were cleaned by a sputtering process with argon ions. Then a silicon containing DLC (a-C:H:Si) interlayer (ca. 100 nm thick) was deposited to achieve a good final adhesion. Tetramethylsilane (TMS: $Si(CH_3)_4$) was used as precursor gas. In the next step the gas composition was changed to a pure hydrocarbon gas, for pure DLC films and in some cases TMS or hexamethyldisiloxane (HMDSO) was used additionally. DLC or amorphous hydrogen containing carbon coating (a-C:H:X) was modified by the incorporation of oxygen and silicon inside the carbon matrix. DLC (a-C:H), SICAN (a-C:H:Si) and SICON® (a-C:H:Si:O) coatings were generated by the Fraunhofer Institut for Surface Engineering and Thin Films, Braunschweig, Germany. The coating layer thickness was approximately 3 µm (Geddert et al., 2009) with a thermal conductivity of 0.3 – 1.3 W m^{-1} K^{-1} (Bullen et al., 2000). Therefore its influence on the heat transfer was negligible. A detailed description of the coating process, the fractional composition as well as the tribological properties of the DLC films are given in Bewilogua et al. (2011).

A total of 70 coupons for the fouling experiments in batch and for the cleaning behavior studies with dimensions of 80 mm x 20 mm x 2 mm were coated. Some of the stainless steel coupons were electropolished by Poligrat GmbH**,** München, Germany. The investigated surfaces are summarized in Table 3.1.

Table 3.1. Surfaces used in the experimental investigations (batch fouling runs and cleaning runs)

Surface	Denotation	Composition
Stainless steel	SS	X5CrNi18 10
Electropolished stainless steel	ESS	(1.4301, AISI 304)
DLC coating	DLC	a-C:H
ESS plus DLC coating	EDLC	(C 80-83, H 15-18, O 1-2)
SICAN coating	SICAN	a-C:H:Si
ESS plus SICAN coating	ESICAN	(C 63-65, H 21-24, Si 12-13)
SICON® coating	SICON	a-C:H:Si:O
ESS plus SICON® coating	ESICON	(C 41-43, H 22-23, Si 23-24, O 10-11)

Composition of stainless steel is given in % w/w and composition of coatings (Bewilogua et al., 2011) is given in % at.

For the fouling runs in the plate heat exchanger six pairs of plates (Varitherm VT04 PH K, GEA Ecoflex GmbH, Sarstedt, Germany) were coated with the same DLC coatings listed in Table 3.1. Table 3.2 and Fig. 3.1 give the plate characteristics and dimensions.

Table 3.2. Plate specification

Material	electropolished stainless steel 1.4401, AISI 316
Heat exchange area, A	0.046 m^2
Transversal area of the plate gap, $A_{plate\ gap}$	25 x 10^{-5} m^2
Corrugation depth or plate gap depth, â	2.45 mm
Hydraulic diameter of channel, d_h	4.9 mm
Chevron corrugation inclination angle, β	65 °
Corrugation wavelength, Λ	10.8 mm
Plate length, l	548 mm
Plate width	128 mm
Effective width, w	108 mm
Gasket material	NBR
Gasket fixing	glued using Bostik 1475 + Bosco-dur AF 8650 (Bostik GmbH, Wels, Austria)
Corrugation	herringbone H
Thickness, x_{plate}	0.60 mm

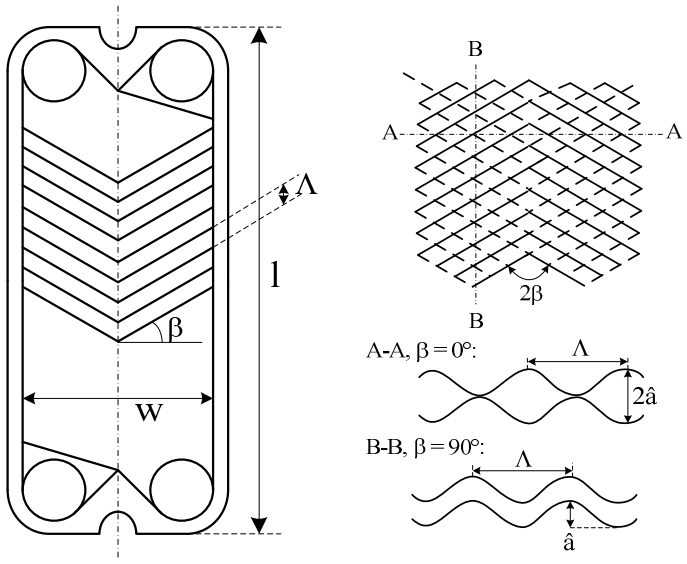

Fig. 3.1. Plate design

3.2 Process fluids

Whey protein isolate (WPI) and simulated milk ultrafiltrate (SMUF) were used to perform the deposition of (i) whey protein ('salt-free' solution), (ii) calcium phosphate and (iii) protein combined with calcium phosphate on the modified surfaces. Raw milk was used to compare the fouling behaviour of WPI plus SMUF on the coated surfaces.

3.2.1 Whey protein

Whey protein isolate powder (Lacprodan DI-9224) was provided by Arla Foods Ingredients Group P/S (Viby J, Denmark). The average composition is given in Table 3.3. WPI powder was dissolved in water or SMUF for the batch-wise experiments with only protein or with protein dissolved in calcium phosphate solution respectively, to a concentration of 5.5 g L^{-1}, corresponding to ca. 3.0 g L^{-1} of β-lactoglobulin (the β-lg concentration in milk is ranging from 3 to 4 g L^{-1} (Töpel, 2004)).

In order to guarantee a longer supply of native (or at least unfolded) β-lactoglobulin for the continuous experiments in the plate heat exchanger a solution with about 30 g L^{-1} β-lactoglobulin (concentration 10 x higher than the β-lactoglobulin content in milk) or 23 g L^{-1} of native β-lactoglobulin was used. For that 55 g L^{-1} WPI powder was dissolved in water at 60 °C followed by stirring for 60 min.

Table 3.3. WPI powder composition

Component	Value	Component	Value
Total protein [g g^{-1}]	0.88 – 0.92[a], 0.87[b], 0.88[c]	Fat [mg g^{-1}]	< 0.2[a]
β-lg [g g^{-1}]	0.55[c]		
Native β-lg [g g^{-1}]	0.42[b]	Mineral content [g g^{-1}]	< 0.04[a], 0.039[b]
α-la [g g^{-1}]	0.13 [c]	Ca [mg g^{-1}]	1[a], 0.74[b]
Immunoglobulin [g g^{-1}]	0.016[c]	P [mg g^{-1}]	2[a], 1.9[b]
Bovine serum albumin [g g^{-1}]	0.0070[c]	Na [mg g^{-1}]	5[a]
Glycomacropeptide [g g^{-1}]	0.18[c]	Cl [mg g^{-1}]	0.5[a]
Moisture [g g^{-1}]	< 0.06[a], 0.043[b]	K [mg g^{-1}]	13[a]
Lactose [mg g^{-1}]	< 0.2[a]	pH (5.5 g L^{-1} solution)	6.7 – 6.8[b]

[a]information from the manufacturer, [b]measured values, [c]Santos et al. (2006a)

3.2.2 SMUF

SMUF provides an aqueous salt mixture having a pH of 6.7 and 0.176 mol L^{-1} ionic strength that resembles the mineral composition of milk. Since SMUF contains no lactose, it is strictly a synthetic milk nanofiltrate. Three 200 ml stock solutions were prepared according to Jenness and Koops (1962) and kept overnight at 5 °C for stabilization before use. The final composition is shown in Table 3.4. The three solutions were then mixed together and filled up to the desired final volume. The solution was then heated to 40 °C for the batch-wise fouling experiments or to 60 °C for the continuous fouling experiments (PHE). Afterwards, the pH was adjusted to 6.7 using a KOH solution. The solution became turbid immediately after or during the addition of KOH due to the calcium phosphate precipitation, as also reported by (Spanos et al., 2007). Thus the solution was rapidly added into the product vessel to prevent subsequent heat dependent changes of the components and the fouling experiment was started immediately.

The salts were purchased from Merck KGaA (Darmstadt, Germany), Sigma-Aldrich Co. (St. Louis, USA) and Thermo Fisher Scientific (New Jersey, USA) and were of analytical

grade. Both SMUF and WPI solutions as well as the WPI plus SMUF solution were prepared using reverse osmosis (RO) water with a conductivity < 5 µS cm^{-1} (Berkefeld Midi RO 10-100 EP, VWS Deutschland GmbH, Celle, Germany).

Table 3.4. Composition of the SMUF solution

Stock solution	Reagents	Concentration [mmol L^{-1}]
1	KH_2PO_4	11.61
	$C_6H_5K_3O_7.H_2O$	3.70
	$C_6H_5Na_3O_7.2\ H_2O$	6.09
	K_2SO_4	1.03
2	$CaCl_2.2\ H_2O$	8.98
	$MgCl_2.6\ H_2O$	3.21
3	K_2CO_3	2.17
	KCl	8.05

3.2.3 Raw milk

Fresh, untreated raw milk from a local dairy farm (Klostergut Heiningen GmbH, Heiningen, Germany) was used in batch-wise fouling experiments. Table 3.5 shows the milk average composition and properties.

Table 3.5. Milk composition and properties

Component/property	Value	Component/property	Value
Total nitrogen [g g^{-1}]	0.005	Dry matter [g g^{-1}]	0.128 ± 0.01
Total protein [g g^{-1}]	0.032	Mineral content [g g^{-1}]	(7.3 ± 0.2) x 10^{-3}
Nitrogen non proteic [g g^{-1}]	0.001		
Fat [g g^{-1}]	0.037 ± 0.003	Density [g L^{-1}]	1.030
Lactose [g g^{-1}]	0.043 ± 0.003	pH [-]	6.8

3.2.4 Stainless steel and DLC coating particles

The zeta potential of stainless steel particles (steel no. 1.4404) with a diameter of 2 to 60 µm and d_{90} < 7 µm (UltraFine Powder Technology, Inc. Woonsocket, Rhode Island) was measured. For the zeta potential measurement in the Zeta Sizer Nano-ZS system (ZEN 3600 with a 633 nm He-Ne laser, Malvern Instruments Ltd., Grovewood Road, UK) the particles need to have a diameter less than 2.5 µm, otherwise, all particles sediment in the measurement cell or in the tubes. So the particles were suspended in water and filtered using a Whatman cellulose filter paper grade 42 with pore size of 2.5 µm (Whatman plc, Maidstone, UK).

Coating particles resulting from the coating process that sediment on bottom of the coating chamber were gently provided by Fraunhofer Institute IST, Braunschweig. The largest particles were also separated by a filtration using water as well as isopropyl alcohol as suspension media.

3.3 Fouling experiments

Fouling experiments were conducted batch-wise as well as in continuous mode. The goal of the batch-wise fouling deposition was to minimize the shear forces and therefore their influence on further fouling layer formation, allowing the generation of similar fouling (upper) layers and the comparison of the fouling on diverse surfaces. Continuous fouling experiments were carried out in a pilot scale plate heat exchanger to extend studies performed under batch conditions and trying to approach an industrial situation in thermal treatment.

3.3.1 Batch-wise fouling

Fouling experiments were carried out in a temperature controlled electropolished stainless steel double jacket vessel illustrated in Fig. 3.2a and whose dimensions are summarized in Table 3.6. The coated coupons were clamped on the two sides of the electrical heating element which was immersed in the test solution. The heating element (Fig. 3.2b) consisted of an electrical heater (type HLP, Türk Hillinger Elektrowärme GmbH, Tuttlingen, Germany) inside a rectangular stainless steel tube. To ensure good thermal conduction the space between heater and the cladding tube was filled with a thermal paste (Keratherm® Type GF 5000, Kerafol Keramische Folien GmbH, Eschenbach, Germany). The total heat transfer area is 0.0059 m^2 (Höfling, 2004). The untreated and coated coupons could be clamped with brackets on two opposite sides of the heating element. The initial surface temperature was adjusted using an enclosed transformer (type RTK, Ruhstrat GmbH, Bovenden, Germany). Under the coupons two calibrated type-K thermocouples (TMH GmbH, Maintal, Germany) were positioned in the middle of the heater rod to measure the surface temperature. The bulk fluid temperature was measured through another thermocouple placed inside the bulk solution. The calibration of all thermocouples (for the batch and the PHE set ups) was done by using a Quartz Thermometer (2804A, Hewlett Packard, Mountain View, USA) in which the quartz probe was immersed in a tempered oil bath (Thermostat HD-4, Julabo Labortechnik GmbH, Seelbach, Germany).

The solution was stirred (RW 20n, IKA®-Werke GmbH & Co. KG) by a 45° fourfold bladed pitched blade impeller (PBT), eccentrically located, whose speed was adjusted to 60 rpm, corresponding to an impeller Reynolds number of 12,360[2]. This speed gave turbulence but without surface vortex formation and gas entrainment. A calibrated pH-meter (GPRT 1400AN, Gresinger electronic GmbH, Regenstauf, Germany) registered the pH of the bulk solution. The measured data were recorded every 2 – 5 min by a data scan unit (Fluke 45, John Fluke MFG Co., Inc., Everett, USA). A thermostat (ThermoHaake K50, Thermo Electron GmbH, Karlsruhe, Germany) maintained the bulk temperature constant. The operating conditions are listed in Table 3.7. The bulk and initial surface temperature conditions were chosen depending on the precipitation or denaturation behavior of the foulant components, so that this should be avoided to occur in bulk during the batch-wise experiments. Furthermore, larger temperature differences (ΔT) between the bulk and surface

[2] The mean density and viscosity to determine the Reynolds number were calculated considering whey as fluid at temperature of 50 °C using the equations given by Kessler (1996). Density = 990.3 kg m^{-3} and dynamic viscosity = 0.801 x 10^{-3} kg $s^{-1}m^{-1}$.

were employed than used industrially in order to obtain a reasonable amount of deposit in a relatively short time (< 6 h) to characterize fouling behavior on the different coated surfaces.

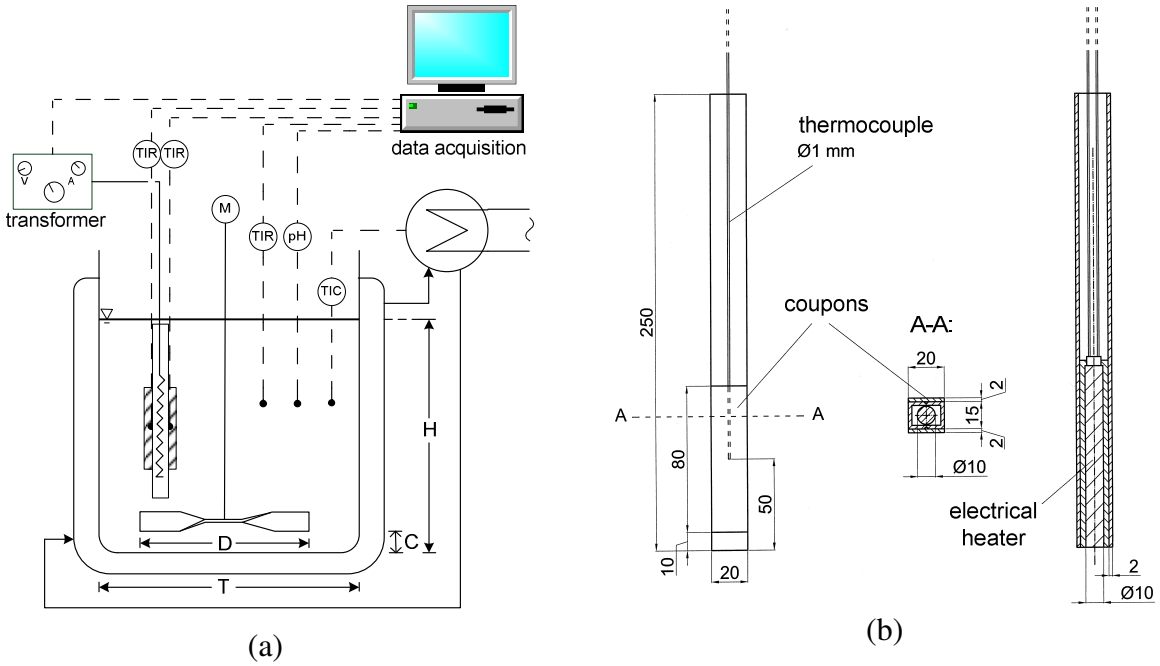

Fig. 3.2. (a) Experimental set-up of the batch-wise fouling test unit; (b) Schematic construction of the heating element

Table 3.6. System dimensions

Dimension	Value
Tank diameter, T	140 mm
Fluid depth, H	182 mm
Off-bottom clearance, C	10 mm
Impeller diameter, D	100 mm
Impeller height	15 mm
Blade width	20 mm

Table 3.7. Experimental conditions in batch-wise fouling experiments

Parameter	Value
Fluid	WPI SMUF WPI + SMUF
Surface conditioning	clean pre-fouled with SMUF
Bulk temperature	50 ± 1 °C or 40 ± 1 °C for SMUF only
Initial pH value	6.7 ± 0.1
Initial surface temperatures	80 ± 1 °C 120 ± 2 °C or 105 ± 2 °C for SMUF only
Specific heat flux	24 ± 2 kW m^{-2} or 31 ± 1 kW m^{-2} for SMUF only 58 ± 2 kW m^{-2}
Impeller Reynolds number	12,360

For the experiments with WPI the whey protein solution was heated up in the vessel to 50 °C. Then the heating element was immersed into the solution and the initial surface temperature T_0 was adjusted to 80 °C and 120 °C, which corresponds to the constant heat flux of 24 ± 2 kW m^{-2} and 58 ± 2 kW m^{-2} respectively, inducing the deposition. The heat flux was determined by:

$$\dot{q} = \frac{P}{A_t} \tag{3.1}$$

Calcium phosphate deposition was achieved using SMUF which was heated to 40 °C. Subsequently the pH value was adjusted to 6.7 using 1.5 mol L^{-1} KOH. The fouling runs were then started at this bulk temperature, since the precipitation of calcium hydrogen phosphate dihydrate ($CaHPO_4 \cdot 2H_2O$) and octacalcium phosphate ($Ca_8H_2(PO_4)_6 \cdot 5H_2O$) which act as precursor to the later-formed hydroxyapatite ($Ca_5OH(PO_4)_3$), begins at 44 to 45 °C (Andritsos et al. 2002; Daufin and Labbé, 1998; Tsuge et al., 2002). Similar to the WPI fouling experiments a heat flux of 31 ± 1 kW m^{-2} and 58 ± 2 kW m^{-2} was employed, corresponding to a T_0 = 80 °C and 105 °C, respectively.

For the experiments with WPI plus SMUF, primary SMUF was heated to 40 °C and the pH value was adjusted to 6.7. Thereafter, a known amount of concentrated whey protein solution was added to reach the desired initial concentration and then the foulant solution was heated up to 50 °C. After the temperature of 50 °C was reached, the heating element was immediately immersed into the test solution and the initial wall temperature T_0 was set up to 80 °C or 120 °C.

After 360 min or at a limit surface temperature of 230 °C the fouled coupons were gently lifted out of the solution and removed from the heating element. The fouled surfaces were then dried merely by keeping them at room temperature for 24 hours (Tissier and Lalande, 1986).

3.3.2 Fouling on conditioned surfaces

Additional experiments were performed to determine the influence of a mineral-containing first layer on the deposition of whey protein and whey protein plus SMUF and to investigate the effect of this initial layer as well as of the coating on the subsequent fouling. First, the surfaces were fouled with calcium phosphate for 30 min. Then, the heating element was gently lifted out of the SMUF solution and indulged in a WPI or WPI plus SMUF solution. The WPI or WPI plus SMUF were prepared as described in sections 3.2.1 and 3.2.2, so that the second deposition experiment could be started directly. After that similar procedures for the deposition runs, as described in the previous section, were conducted on the substrates SS and ESS as well as on the coated SS surfaces. At T_0 120 °C fouling experiments only with the substrates SS and ESS were performed. In this case the pre-conditioning with SMUF was conducted by a specific heat flux of 58 ± 2 kW m^{-2} and the further deposition (pure WPI or WPI plus SMUF) was performed at a specific heat flux of 40 ± 1 kW m^{-2}. The experiments were made in triplicate.

3.3.3 Monitoring of fouling

The thermal impact of fouling is often expressed in terms of the thermal fouling resistance (R_f) which is defined by the difference between the inverse of the fouled (U_f) and the clean (U_{clean}) overall heat transfer coefficient. Since the heat duty ($\dot{Q}$), the heat transfer area (A) were maintained constant and assuming a uniform and homogen fouling layer, the fouling resistance can be written from eq. (2.3) as:

$$R_f = \frac{1}{U_f} - \frac{1}{U_{clean}} = \left[\frac{T_{w,SS} - T_{PS}}{\dot{q}}\right]_{'f} - \left[\frac{T_{w,SS} - T_{PS}}{\dot{q}}\right]_{clean} \tag{3.2}$$

Since the bulk temperature (T_{PS}) was maintained constant, $R_f(t)$ can be calculated over time as:

$$R_f(t) = \frac{T_{w,SS}(t) - T_{w,SS,clean}}{\dot{q}} \tag{3.3}$$

3.3.4 Deposit recovery and analyses

In order to characterize the deposit, the fouled coupons were dried and the amount of deposit was determined by weighing (analytical balance A 200 S, Sartorius AG, Göttingen, Germany). The distribution and structure of the deposit over the heat transfer surface was observed by optical microscopy (Keyence VHX-100K, Keyence Deutschland GmbH, Neu-Isenburg) as well as by an environmental SEM and the composition of selected samples was assessed by X-ray microanalysis integrated in the SEM (see section 3.8.1).

In the literature normally milk deposit has been removed for chemical analysis by scraping the internal surface of a tube or the plates of a PHE. By this method the recovery is not efficient, particularly in the case of very hard deposits e.g. in case of wall temperatures above 120 °C. Therefore in this study the deposits were dissolved by alkali and acid treatment. The coupons were immersed in 2 % w/w NaOH and subsequently in 2 % w/w CH_3COOH at 50 °C separately for 30 – 60 min, to dissolve protein and mineral fouling respectively. The protein, the mineral content as well as total Ca and total P contents of the alkali and acid solutions were then determined (see section 3.7.3).

The coupons were rinsed with deionized water and dried. The cleaning effort of the surfaces was controlled by optical microscopy with a magnification up to 1000 times as well as by x-ray microanalysis of selected coupons. The batch-wise cleaning procedure was repeated until the surface was visually completely free from residuals.

3.3.5 Fouling in plate heat exchanger

Continuous fouling experiments were carried out in a pilot plant (Fig. 3.3) consisting of two insulated stirring tanks, that included the product vessel (T1) and the heating water vessel (T2) and two plate heat exchangers (VT04 CD-16, GEA Ecoflex, Sarstedt, Germany) connected to one heating unit (PHE1) and to a cooling unit (PHE2). Both PHE were operated

in countercurrent flow mode. PHE1 and PHE2 were composed of four plates with an effective heat exchange area of 0.092 m^2. In the middle channel the foulant fluid (one path per pass) and in the two outer channels the service fluid (two paths per pass) were circulated. PHE1 and PHE2 were insulated with rockwool (Klimarock, Mineralwoll GmbH & Co. OHG, Gladbeck, Germany), allowing for the determination of the product sides' as well as the service fluid sides' overall heat transfer coefficients through temperature measurements and energy balance.

PHE1 was brought to hydrodynamic and thermal steady state at the desired process temperatures and volumetric flow (Table 3.8) by circulating RO water for about 60 min. The temperature difference between product inlet and outlet temperature was 23 K with a heat flux of 27 ± 2 kW m^{-2}. Thereafter, the pump (multistage centrifugal pump, Movitec VF 2-4 B, KSB AG, Pegnitz, Germany) was turned off temporarily and concentrated pre-heated SMUF and WPI solutions were added into tank T1 to achieve the desired initial concentration. A rotating stirrer (RW20n, IKA®-Werke GmbH & Co. KG, Staufen, Germany) at 150 rpm eliminated temperature and concentration gradients in T1. The solution was recirculated in a closed loop for 120 min. This configuration was chosen to reduce the test solution required. The flow rate was monitored through a magnetic inductive flow meter (Ecoflux IFM 1010K/D6 with Altometer IFC 010 D transducer, Krohne Messtechnik GmbH, Duisburg, Germany) and was kept constant by an electrically controlled valve. All temperatures were measured by pre-calibrated type K thermocouples (TMH GmbH, Maintal, Germany) and the inlet and outlet pressure in PHE1 was recorded by pressure transmitters with an uncertainty of 0.1 % (PA-33X, KELLER AG, Winterthur, Switzerland). The measured data were collected every 5 s by a data logger (34970 A, Agilent Technologies Deutschland GmbH, Böblingen, Germany).

The supply unit provided heating water which was regulated and temperature was kept constant using an immersion heater (IST/6, 6 kW, ISA Heinrich Industrietechnik GmbH, Falkensee, Germany) in conjunction with PID automatic controller (TS 200-023, New Port Electronics GmbH, Deckenpfronn, Germany). The heating water was pumped (multistage centrifugal pump, Movitec VF 2-6, KSB AG, Pegnitz, Germany) at a constant flow rate adjusted by an electrically controlled valve. The flow rate was monitored through a magnetic inductive flow meter (Altoflux X-1000 with Altometer SC 100A transducer, Krohne Messtechnik GmbH, Duisburg, Germany). PHE2 was operated with cooling water and the product outlet temperature was maintained constant by controlling the cooling water flow.

Table 3.8. Operating conditions for PHE1

Parameter	Value
Product flow rate	0.085 ± 0.005 $m^3 h^{-1}$
Product mean velocity	0.1 m s^{-1} (Re = 870)
Product inlet temperature	62 ± 2 °C
Initial product outlet temperature	85 ± 1 °C
Specific heat flux	30 ± 2 kW m^{-2}
Heating fluid flow rate	1.7 ± 0.1 $m^3 h^{-1}$
Heating fluid mean velocity	0.95 m s^{-1} (Re = 15,000)
Heating fluid inlet temperature	87 ± 1°C
Heating fluid outlet temperature	85 ± 2°C
Volume of whey protein solution treated	0.02 m^3

Three experiments were performed for each surface after initial surface aging, of which two plates with the same coating were used in each trial. After each fouling cycle, PHE1 was gently dismantled and the plates were dried at room temperature overnight. The plates were photographed and the different patterns of deposition were observed. The plates were cleaned separately as described below. The plates were reintegrated in PHE1 and the pilot plant was cleaned using a 0.5 % w/w NaOH at 50 °C for 60 min (single stage cleaning). The equipment was then rinsed with water at 50 °C until a constant pH value was reached.

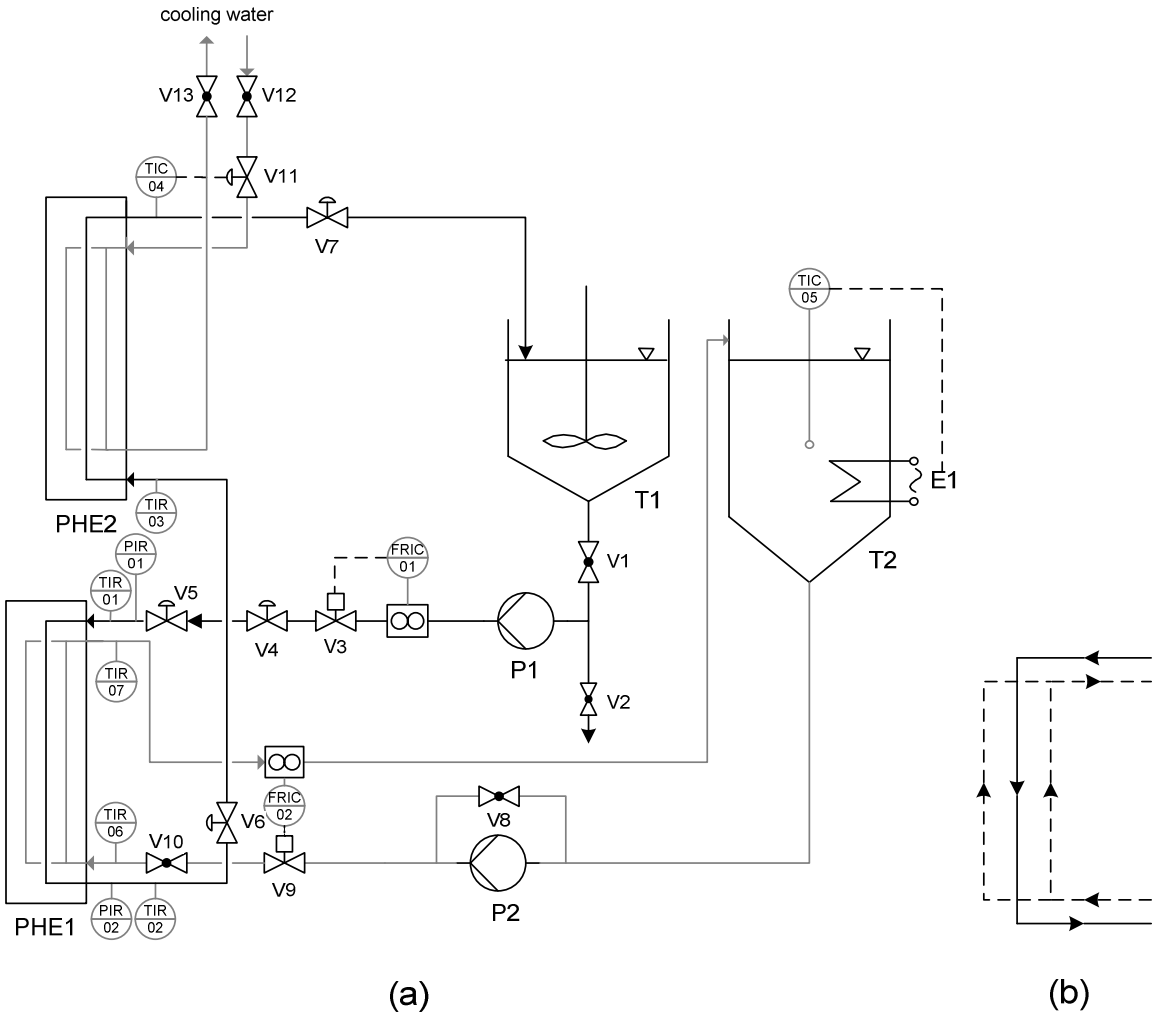

Fig. 3.3. (a) Experimental setup of the plate heat exchanger test rig. E1: electrical heater; P1, P2: centrifugal pump; PHE1: plate heat exchanger (heating unit); PHE2: plate heat exchanger (cooling unit); T1: product vessel; T2: heating fluid vessel; V1-V13: valves. (b) Flow arrangement in PHE1. — product fluid, - - service fluid

3.3.6 Determination of the fouling resistance

Since the plate heat exchanger PHE1 was insulated heat losses could be neglected and the heat duty can be written as:

$$\dot{Q} = \dot{Q}_{SS} = \dot{m}_{SS}\,\bar{c}_{p,SS}\Delta T_{SS} = \dot{Q}_{PS} = \dot{m}_{PS}\,\bar{c}_{p,PS}\Delta T_{PS} \qquad (3.4)$$

The mean heat capacities were calculated using thermal properties for whey (Kessler, 1996) and water (VDI-Wärmeatlas, 2006) (see appendix A1) at the average temperature of each fluid, e.g. for whey: $T_{m,PS} = \left(T_{P,in} + T_{P,out}\right) / 2$.

From the overall heat balance of the exchanger (siehe eqs. 2.1 – 2.3), the heat flux for parallel plates is given by:

$$\dot{Q} = UA_t\left(T_{SS} - T_{PS}\right) \tag{3.5}$$

As the temperature driving force across the heat exchanger usually varies along the length of the heat exchanger, the log mean temperature difference ΔT_m is used in Eq. (3.5):

$$\dot{Q} = UA_t\Delta T_m \tag{3.6}$$

$$\text{with } \Delta T_m = \frac{\left(T_{SS,out} - T_{PS,in}\right) - \left(T_{SS,in} - T_{PS,out}\right)}{\ln\left(\frac{\left(T_{SS,in} - T_{PS,out}\right)}{\left(T_{SS,out} - T_{PS,in}\right)}\right)} \tag{3.7}$$

Thus, the thermal fouling resistance is given integrally by the temperature measurements at a constant flow rate and at a constant inlet temperature of the heating medium and from the temporary change of the heat transfer coefficient U_f as:

$$R_f(t) = \frac{1}{U_f(t)} - \frac{1}{U_{clean}} = \frac{A_t\Delta T_{ln,f}(t)}{\dot{Q}_f(t)} - \frac{A_t\Delta T_{ln,clean}}{\dot{Q}_{clean}} \tag{3.8}$$

3.3.7 Deposit recovery and chemical analyses

In order to determine the protein and minerals content of the deposit, the plates were cleaned in batch and the acid and alkali solutions were analyzed. The plates were separately immersed in a 1 % w/w H_3PO_4 solution at 50 °C for 60 min to dissolve mineral residuals. Next, the plates were immersed in a 1 % w/w NaOH solution at 50 °C for 60 min to dissolve protein fouling, and then rinsed with deionized water. Total protein, mineral content and total Ca and total P contents were assessed as described in section 3.7.3.

3.4 Cleaning experiments

Before starting with the cleaning experiments the coupons were used in at least ten soiling and cleaning cycles. Therefore initial aging effects could be excluded.

In order to conduct cleaning experiments, reproducible protein deposits were generated as described in section 3.3.1. A foulant solution containing 5.5 g L^{-1} whey protein isolate dissolved in SMUF was used for the fouling experiments on the different surfaces, in

which the initial surface temperature were adjusted to 120 °C, corresponding to a constant heat flux of 58 ± 2 kW m^{-2}. The bulk temperature was kept constant at 50 °C. After 90 min the fouled coupons were gently lifted from the solution, removed from the heating element and kept in distilled water at 8 °C for up to 12 hours to retain the structure of the wet soils.

3.4.1 Cleaning in flow cell

To study the cleaning behaviour of the surfaces the fouled coupons were then attached to the test rig, schematically shown in Fig. 3.4a. The operating conditions for the cleaning experiments are listed in Table 3.9. A constant low heat flux was set on the electrical heating element (type HLP, Türk Hillinger Elektrowärme GmbH, Tuttlingen, Germany) underneath the flow channel (Fig. 3.4b) using an enclosed transformer (type RTK, Ruhstrat GmbH, Bovenden, Germany). The heat transfer area was determined as 0.00525 m^2. The temperature change was recorded by four type-K thermocouples (TMH GmbH, Maintal, Germany) located in the inlet and outlet of the flow channel and under the coupon. The cleaning solution (10 L) was preheated (Lauda RC20 CS, Lauda Dr. R. Wobser GmbH & CO. KG, Lauda-Königshofen, Germany) to 30 ± 1 °C and was recirculated using a centrifugal pump (Mag-Drive V-MD30, Verder Deutschland GmbH, Haan, Germany) through the bypass until steady state conditions were reached. The bypass valve was switched off and the NaOH solution was circulated in the channel. The flow rate was kept constant and monitored through a magnetically inductive flowmeter (Ecoflux IFM 1010K/D6 with a Altometer IFC 010D transducer, Krohne Messtechnik GmbH, Duisburg, Germany) installed at the outlet of the cleaning section. A rotating stirrer (RW20 DZM, IKA®-Werke GmbH & Co. KG, Staufen, Germany) at 60 rpm ensured the dissolution of deposits' pieces in T1. The measured data were collected every 30 s by a data logger (34970 A, Agilent Technologies Deutschland GmbH, Böblingen, Germany).

Table 3.9. Experimental conditions in cleaning experiments

Parameter	Value
Fluid	0.25 % w/w NaOH 0.5 % w/w NaOH
Bulk temperature	30 ± 1 °C
Initial pH value	12.5 ± 0.1 12.8 ± 0.1
Initial surface temperatures	40 ± 1 °C
Specific heat flux	18.0 ± 0.5 kW m^{-2}
Flow rate	0.15 $m^3 h^{-1}$
Flow velocity	1.5 m s^{-1}
Reynolds number	2,900

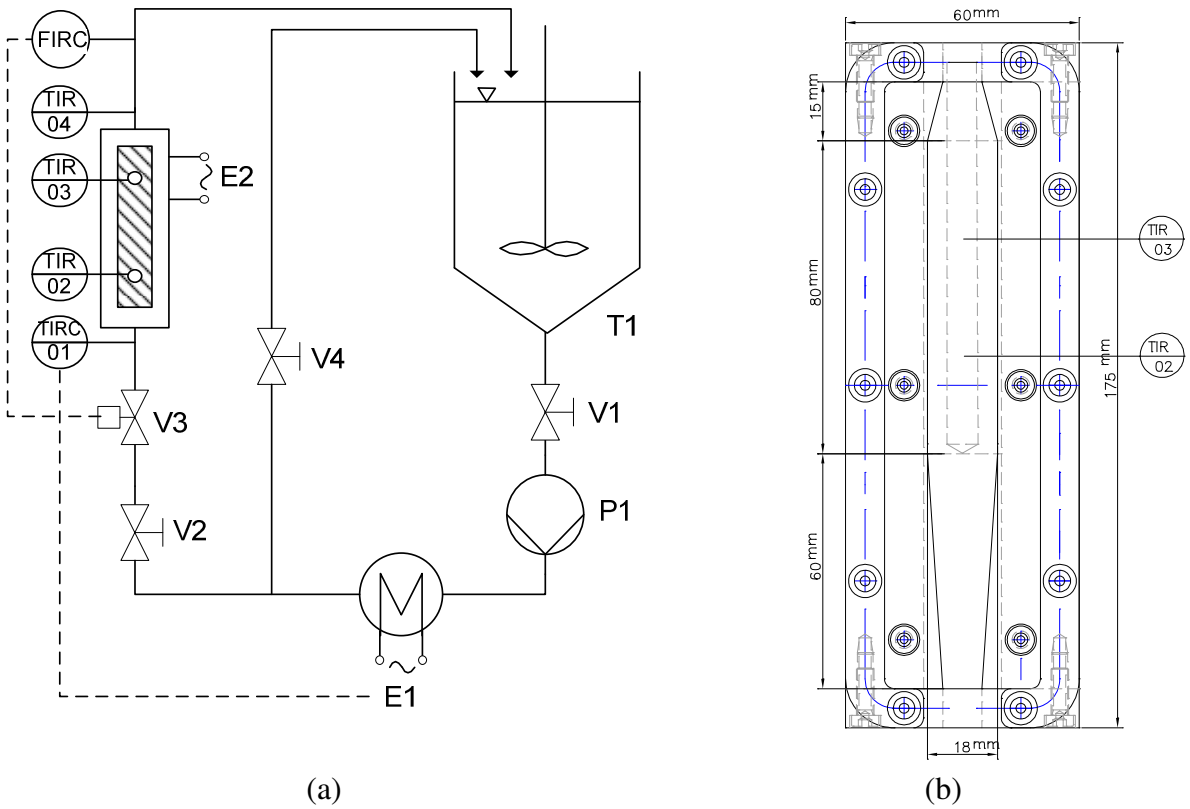

Fig. 3.4. Experimental set-up of (a) the cleaning test unit and of (b) the flow channel. E1: thermostat; E2: electrical heater; P1: centrifugal pump; T1: product vessel; V1 - V4: valves (Boxler et al., 2013a)

Temperature and flow velocity were adjusted, so that the steps of the swelling and removal of the fouling layer could be monitored. An optimal NaOH concentration of 0.5 % w/w was found for the cleaning of WPC and milk deposits at 50 °C (Bird and Fryer, 1991), hence this concentration as well as a lower concentration (0.25 % w/w) were used in the cleaning experiments. The CIP processes could be monitored visually by observing the removal of the fouling layer through the poly(methyl methacrylate) (PMMA) plate which covers the flow channel (Fig. 3.4b).

Samples of the cleaning solution were collected during the experiment and the protein concentration was measured using the TOC/TN_b analyzer whose method is described in section 3.7.1. Four trials were performed for each surface with two samples in each trial to assess the repeatability of the fouling and cleaning experiments and the reliability of the measuring method.

3.4.2 Full cleaning of the plates

After the cleaning experiments the surfaces were dismantled from the flow cell and immersed separately in a 1 % w/w HNO_3 solution at 50 °C for 60 min, to dissolve residual minerals, and then were rinsed with deionized water. Next the plates were immersed in a 1 % w/w NaOH solution at 50 °C for 60 min, rinsed and immersed in the acid solution again. The clean surface was controlled using a digital microscope.

3.4.3 Monitoring the cleaning progress

The cleaning progress was characterized by comparing the change of the overall thermal resistance of the clean and fouled surface and by monitoring the protein concentration in the cleaning solution. The clean overall heat transfer coefficient (U_{clean}) was obtained separately at the same experimental conditions as for the cleaning runs by measuring the wall temperature of cleaned surfaces. At $\dot{q}$ = constant, the thermal resistance R_f can be determined by:

$$R_f(t) = \frac{1}{U_f} - \frac{1}{U_{clean}} = \frac{\Delta T_{m,\,f} - \Delta T_{m,\,clean}}{\dot{q}} \tag{3.9}$$

A second indicator for the cleaning progress was the quantification of the protein concentration over time in the cleaning solution. Samples of the cleaning solution were collected during the cleaning experiments and the protein concentration in the samples was determined using the TOC/TN_b Analyzer, as described in section 3.7.1. The protein mass could be calculated by:

$$m_{protein} = c_{protein}.V \tag{3.10}$$

where V is the total cleaning solution volume, V = 10 L.

Then, the cleaning rate (r_c) was calculated from the protein mass and the coupon area A_{coupon}:

$$r_c(t) = \frac{\Delta m_{protein}}{A_{coupon}\,t} \tag{3.11}$$

3.5 Surface characterization

The surface properties have an influence on the fouling behavior, as discussed in Chapter 2. Thus, in order to understand the fouling behavior of the diverse studied systems on the modified stainless steel surfaces, the surface properties were characterized according to their chemical composition, roughness and surface free energy.

3.5.1 Surface roughness

Surface roughness was quantified using a contact profilometer (Perthometer Concept, Mahr GmbH, Göttingen, Germany), which includes a tracing arm (MFW 250) in combination with a PGK drive unit und the measuring stand PST-G. The perthometer was calibrated using a setting standard (PEN-10-1) with a 9.2 µm groove depth.

The coupons or plates were placed on the xy-table (PKT) and the surface inclination was adjusted manually (inclination should be lower than 0.1 µm). The measurements were made electromechanically by moving a tracing arm with a diamond stylus tip along the sample. The stylus tip radius was 5 µm/90°, the measuring force applied was at around

0.9 mN and the tracing length of 5.6 mm with an evaluating length of 250 µm was chosen. The captured and amplified electrical signal was then filtered (Gaussian filter) according to DIN 4760 (1982) by using the software Concept 5.0 that determined the roughness parameters from the roughness profile (p-profile).

Because of the finishing process, the samples can show an oriented texture. The roughness was then registered along two directions in the surface plane. For each coupon ten measurements in longitudinal and in transverse direction were performed and the average value for each surface was built. Since one surface finish parameter is incapable of reproducing different roughness structures and therefore of defining a surface adequately, two parameters R_a and R_z, which are the most common roughness parameters, were determined to complete the definition of a surface.

The mean roughness R_a is the arithmetic average of all absolute deviations 'z' of the roughness profile from the mean line within the reference range l_m (Fig. 3.5a) and is defined in DIN EN ISO 4287 (2010):

$$R_a = \frac{1}{l_m}\int_0^{l_m} |z(x)|dx \tag{3.12}$$

Applying the integration of the areas, individual profile outliers are ignored. R_a has the advantage or disadvantage that the measured values remain relatively constant by scanning the sample at different surface cutouts, especially compared to the characteristic R_{max} (roughness largest single) or to the R_z values (Sander, 1993).

The mean roughness depth R_z is the arithmetic mean value of the single roughness depths R_{zi} of five consecutive sampling lengths l_r, in which **s**ingle roughness depth R_{zi} is defined as the vertical distance between the highest peak and the deepest valley in each sampling length (R_{max}) (Fig. 3.5b). R_z provides information on the average vertical surface fissures. Single outliers are partly considered depending on their value (Sander, 1993).

The mean roughness depth is given by DIN EN ISO 4287 (2010):

$$R_z = \frac{1}{5}\sum_{i=1}^{5} R_{zi} \tag{3.13}$$

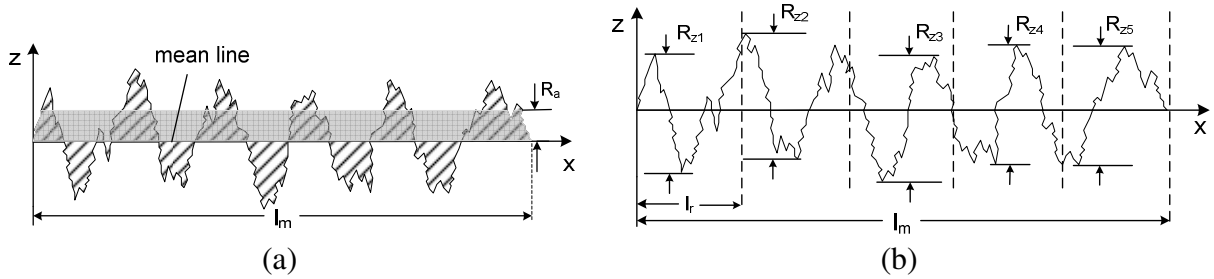

Fig. 3.5. (a) Mean roughness and (b) roughness depth

3.5.2 AFM topography measurements

The atomic force microscopy (Dual Scope™ with a C-21 controller and DS 95-50 scanner, Danish Micro Engineering A/S, Herlev, Denmark) was used to image the topography of the coupons and characterize their surface roughness. The AFM was operated in contact mode with constant height in air using a silicon cantilever (DME DS 95 DC Probe), whose dimensions are given in Table 3.10.

Table 3.10. Cantilever properties

Cantilever		**tip**	
geometry	rectangular	geometry	pyramid
length, width, thickness	445–455 µm, 45–55 µm, 1.5–2.5 µm	height	10 – 15 µm
force	0.07 – 0.40 N m^{-1}	radius	< 10 nm

The coupons were fixed on the measuring table. Once the surface to be scanned had been focused in the high resolution digital CCD camera, the cantilever was brought into close contact (one to several tens of nanometers) with the surface (DC mode). A laser beam was put with focus onto the back of the cantilever and was reflected onto a mirror and then onto a position sensitive photo detector (PSPD). The difference in light intensity when the cantilever dragged up and down with the surface was recorded by the detector and processed in a computer (SPM Program Version 1.4.06) providing the 3D topographical image of the surface.

The samples were scanned with a tracing speed of 100 µm s^{-1} in three positions, where the measuring area was 100 × 100 μm^2. The three dimensional roughness parameters S_y, S_a, S_z and S_{dr} were determined as given by DIN EN ISO 25178-2 (2008) and described below.

The maximum height of the surface S_y is defined as the height difference between the highest and lowest point in the image:

$$S_y = \max(\tau) - \min(\tau) \tag{3.14}$$

with

$$\tau(x,y) = \left\{ I(x,y) - \left\{ \frac{1}{P} \sum_{j=1}^{N} \sum_{i=1}^{M} I(i,j) \middle| (i,j) \in A_{3D} \right\} \middle| x = 1...M; y = 1...N; (x,y) \in A_{3D} \right\} \tag{3.15}$$

where P is the number of points in the area A_{3D}.

The arithmetic mean deviation of the surface S_a is given by:

$$S_a = \frac{1}{P} \sum_{j=1}^{N} \sum_{i=1}^{M} |\tau(i,j)| \tag{3.16}$$

Then point height S_z is defined as the average height of the five highest summits plus the average height of the five deepest valleys:

$$S_z = \frac{1}{5}\left(\sum_{i=1}^{5} |\tau_\pi| + \sum_{i=1}^{5} |\tau_{vi}| \right) \tag{3.17}$$

The surface area ratio S_{dr} expresses the increment of the interfacial surface area relative to the area of the projected ideal (flat) x-y plane and is given by Eq. (3.18). The S_{dr} parameter may further differentiate surfaces of similar arithmetic mean deviation (S_a), since S_{dr} will increase with the spatial intricacy texture whether or not S_a changes.

$$S_{dr} = \frac{\sum_{j=1}^{N-1} \sum_{i=1}^{M-1} A_{ij} - P'\Delta x\Delta y}{P'\Delta x\Delta y}.100\% \tag{3.18}$$

with

$$A_{ij} = \frac{1}{4}\left[\sqrt{\Delta y^2 + \left(\tau(i,j) - \tau(i,j+1)\right)^2} + \sqrt{\Delta y^2 + \left(\tau(i+1,j+1) - \tau(i+1,j)\right)^2} \right] \cdot \left[\sqrt{\Delta x^2 + \left(\tau(i,j) - \tau(i+1,j)\right)^2} + \sqrt{\Delta x^2 + \left(\tau(i,j+1) - \tau(i+1,j+1)\right)^2} \right] \tag{3.19}$$

where P´ is the number of $\Delta x\Delta y$ cells in the area A_{3D}.

3.5.3 Surface free energy

Surface free energy measurements were based on the sessile drop technique using the Drop Shape Analysis System DSA G10 (Krüss GmbH, Hamburg, Germany). At least three drops of each reference liquid were placed on the surface and the advancing contact angle at 20° (speed of the needle: ~ 1 µL s^{-1}) was recorded with a high speed video camera (60 fps). By this method the drop volume increased continuously and the ever-new contact angle was measured. Thereby up to 30 measurements were possible for one drop. The contact angle was calculated from the tangent at the intersection of the drop contour line with the solid surface. The drop profil/shape was fitted by a polynomial function (tangent method 2) (Krüss GmbH, 2004):

$$y = a + bx + cx^{0.5} + d/\ln(x) + ex^{-2} \tag{3.20}$$

The method is mathematically accurate, but is sensitive to distortions in the phase contact area caused by contaminants or surface irregularities at the sample surface (Krüss GmbH, 2004). From the adjusted parameters the slope on the contact point of the three phases at the baseline was first calculated and thereby the contact angle was determined.

Samples were cleaned with isopropyl alcohol (analytical grade, Fischer Scientific UK, Leicestershire, UK) before the measurement with each reference liquid, gently wiped, then rinsed with RO water to avoid any contamination. Next the samples were dried with compressed air and left for 10 - 15 minutes for stabilization. RO water, ethylene glycol,

formamide (Sigma-Aldrich Co., St. Louis, USA), 1-bromonaphtalene and diiodmethane (Merck Schuchardt OHG, Hohenbrunn, Germany) in p.a. grade were used as reference liquids. The surface tension data of the liquids used are shown in Table 3.11.

Table 3.11. Surface tension values of the reference liquids at 20 °C used in the different approaches

Approach	Liquid	Surface tension parameter [mN m^{-1}]					Reference
		γ_{13}	γ_{13}^{+}	γ_{13}^{-}	γ_{13}^{LW}, γ_{13}^{dis}	γ_{13}^{AB}, γ_{13}^{pol}	
Owens-Wendt-Rabel-Kaelble	water	72.8	–	–	21.8	51.0	(Ström et al., 1987)
	1-bromo-naphthalene	44.6	–	–	44.4	0.2	(Ström et al., 1987)
	formamide	59.0	–	–	39.4	19.6	(Rabel, 1971)
	diiodomethane	50.8	–	–	49.5	1.3	(Ström et al., 1987)
	ethylene glycol	47.7	–	–	30.9	16.8	(Ström et al., 1987)
van Oss-Chaudhury-Good	water	72.8	25.5	25.5	21.8	51.0	(van Oss et al., 1986)
	1-bromo-naphthalene	44.6	0	0	44.4	0.2	(Chen and Wakida, 1997)
	formamide	58.0	2.28	39.6	39.0	19.0	(van Oss et al., 1986)
	diiodomethane	50.8	0	0	49.5	1.3	(Ström et al., 1987)
	ethylene glycol	48.0	1.92	47.0	29.0	19.0	(van Oss, 1994)

In 1804 Thomas Young (Young, 1804) described the relation between the work of adhesion between the surface tension of a solid (γ_{23}) and a liquid (γ_{12}), the interfacial tension between the solid and the liquid (γ_{12}) and the contact angle of the liquid droplet wetted to a flat solid surface as:

$$\gamma_{13}\cos\theta_{12} = \gamma_{23} - \gamma_{12} \qquad (3.21)$$

Fig. 3.6 shows the contact angle as a force balance. cos θ is a measure of the equilibrium between the energies of cohesion between the molecules of the liquid and the force of adhesion between liquid and solid (van Oss, 2006).

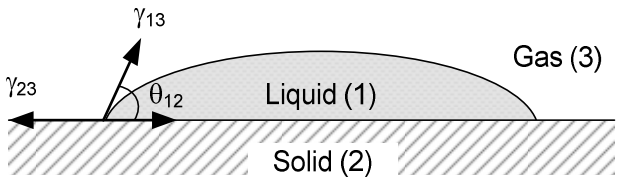

Fig. 3.6. Wetting equilibrium

Several models to extend Young's equation have been proposed (Good and Girifalco, 1960; Fowkes, 1964; Zisman, 1964; Driedger et al., 1965; Owens and Wendt, 1969; Wu, 1973; Schultz et al., 1977a, 1977b; van Oss et al., 1988; Li and Neumann, 1990). Two different approaches, the Owens-Wendt-Rabel-Kaelble approach (Owens and Wendt, 1969; Kaelble, 1970; Rabel, 1971) and the van Oss-Chaudhury-Good (van Oss et al., 1988) approach were used in this work. The Owens and Wendt approach (Owens and Wendt, 1969) is one of the most common methods for calculating the solid surface tension. However it is a semi-empirical model, while the van Oss-Chaudhury-Good method (van Oss et al., 1988) is based on the Lifschitz-van der Waals and on the acid-base theories.

The calculations according to the two models were performed using the software Drop Shape Analysis DSA1 v 1.90. The surface energy parameters (γ^{pol} and γ^{dis} as well as γ^{LW}, γ^{AB}, γ^{+} and γ^{-}) for at least four coupons or at least two plates were determined and then the mean and standard error of the parameters was built.

Owens and Wendt (1969) considered the total surface free energy (γ_{12}) as the sum of a dispersive component (γ^{dis}) and a non-dispersive, acid-base or polar component (γ^{pol}):

$$\gamma_{12} = \gamma_{13} + \gamma_{23} - 2\left(\sqrt{\gamma_{13}^{dis}\gamma_{23}^{dis}} + \sqrt{\gamma_{13}^{pol}\gamma_{23}^{pol}}\right) \tag{3.22}$$

Kaelble (1970) solved Eq. 3.22 for combinations of two liquids and calculated the mean values of the resulting values for the surface energy. Rabel (1971) calculated the polar and disperse fractions of the surface free energy with the aid of a single linear regression from the contact angle data of various liquids:

$$\frac{(1+\cos\theta_{12})\gamma_{13}}{2\sqrt{\gamma_{13}^{dis}}} = \sqrt{\gamma_{23}^{pol}}\sqrt{\frac{\gamma_{13}^{pol}}{\gamma_{13}^{dis}}} + \sqrt{\gamma_{23}^{dis}} \tag{3.23}$$

Eq. (3.23) (Owens-Wendt-Rabel-Kaelble approach) can be solved by a linear fit of the contact angles of different test liquids. The slope $\sqrt{\gamma_{23}^{pol}}$ reflects the polar component, and the intersection with the ordinate $\sqrt{\gamma_{23}^{dis}}$ the dispersive component.

The van Oss approach (van Oss et al., 1988) considers the total surface tension of a solid or a liquid (γ^{TOT}) as the sum of a nonpolar Lifshitz-van der Waals component (γ^{LW}) and an acid-base polar component (γ^{AB}):

$$\gamma^{TOT} = \gamma^{LW} + \gamma^{AB} \tag{3.24}$$

The Lifshitz-van der Waals interactions arise due to three distinct interactions: induction (Debye), orientation (Keesom) and dispersion (London), the last one being the most significant term (van Oss, 2006). The acid-base component consists of two non-additive parameters, one for the electron donor (γ^{-}) and one for the electron acceptor (γ^{+}) contribution:

$\gamma^{AB} = 2\sqrt{\gamma^{-}\gamma^{+}}$

The total interfacial tension between solid and liquid phases is expressed as:

$$\gamma_{12} = \gamma_{12}^{LW} + \gamma_{12}^{AB} = \left(\sqrt{\gamma_{13}^{LW}} + \sqrt{\gamma_{23}^{LW}}\right)^2 + 2\left(\sqrt{\gamma_{13}^{+}\gamma_{13}^{-}} + \sqrt{\gamma_{23}^{+}\gamma_{23}^{-}} - \sqrt{\gamma_{13}^{+}\gamma_{23}^{-}} - \sqrt{\gamma_{13}^{-}\gamma_{23}^{+}}\right) \quad (3.25)$$

Combining the Young's equation (Eq. 3.21) with the interfacial tension equation (Eq. 3.25), a relation between the measured contact angle of the probe liquid on the solid and the surface tension terms can be obtained:

$$(1+\cos\theta_{13}).\gamma_{12} = 2\left(\gamma_{13}^{LW}\gamma_{23}^{LW}\right)^{1/2} + 2\left(\gamma_{13}^{+}\gamma_{23}^{-}\right)^{1/2} + 2\left(\gamma_{13}^{-}\gamma_{23}^{+}\right)^{1/2} \quad (3.26)$$

The calculation of interfacial energies obtained by surface thermodynamics is based on the assumption of a chemically homogeneous, perfectly smooth surface. A review of the limitations and relative merits of these different approaches is given by Correia et al. (1997) and their thermodynamic consistency is discussed by Douillard (1997). The limitations of the approaches have been related principally to: firstly, the strong dependency on the choice of the reference liquids used for contact angle measurements, and/or, secondly, the hysteresis between advancing and receding contact angles (Adamson and Gast, 1997; van Oss, 2006).

To reduce the influence of reference liquid, five liquids were used for the contact angle measurements instead of three as recommended in the literature. The measurement points were plotted according to Eq. 3.21 for the Owens-Wendt-Rabel-Kaelble approach on a diagram (as exemplified in Fig. 3.7). The adequacy, either of the chosen liquids or of the measurement, could be controlled optically by the graphical presentation. A failed measurement caused by chemical reactions with the surface, impurities or inhomogeneity could be detected very easily and could be repeated or dropped. If a liquid did not fit the linear correlation (Fig. 3.7), it was not considered in the final surface free energy calculation.

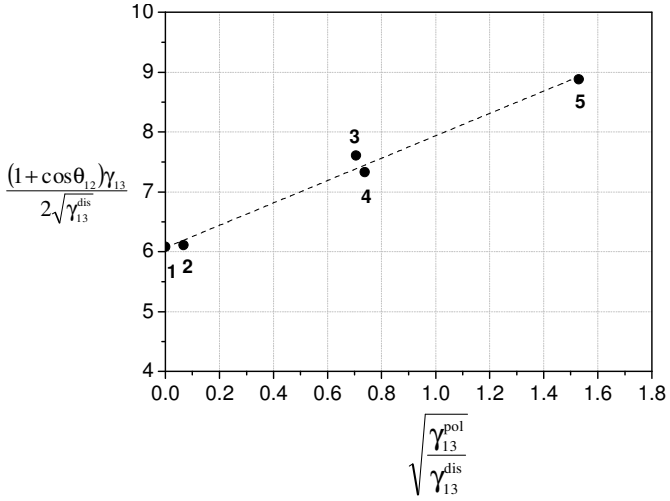

Fig. 3.7. Determination of surface free energy of a stainless steel coupon by regression of wetting equilibrium (Eq. 3.23). Reference liquids: 1 – diiodmethane, 2 – 1-bromonaphtalene, 3 – formamide, 4 – ethylene glycol and 5 – water

In general the contact angle hysteresis is attributed to surface roughness, chemical and structural surface heterogeneities, and solution impurities adsorbing on the surface, but also to liquid-surface interactions, such as swelling, rearrangement or alteration of the surface by the solvent (Adamson and Gast, 1997). All these factors impede the free movement of the contact line, thus causing the formation of metastable configurations in the three phase systems by the wetting equilibrium (Boinovich and Emelyanenko, 2011). The Gibbs energy of the system reaches a local minimum, which can be separated from other local minimum by a Gibbs energy barrier (Adamson and Gast, 1997).

Basic equations to predict the contact angle on rough surfaces were proposed by Wenzel (1936) (Eq. 3.27) and Cassie and Baxter (1944) (Eq. 3.28) for rough or heterogeneous surfaces and reviewed by Swain and Lipowsky (1998) and Whyman et al. (2008).

$$\cos\theta_{rough} = r\cos_{smooth} \tag{3.27}$$

$$\cos\theta_{heterogeneous} = f_1\cos_1 - f_2 \tag{3.28}$$

The establishement of a mathematical relationship which is generally valid for the description of the hysteresis effect from contact angle and roughness measurements has been unsuccessful, as pointed out by Palzer et al. (2001), Long and Chen (2006) and Chibowski (2007). Recently new models for calculating the contact angle hysteresis based on the Wenzel and Cassie and Baxter theories have been proposed by Zhang et al. (2012) and Vedantam and Panchagnula (2008). In this work the influence of surface roughness on the surface energy parameters was verified by analysis of variance (ANOVA).

The influence of temperature on surface wettability and consequently on surface free energy has also been related in the literature (Zhao et al., 2004b; Ashokkumar et al., 2012) and semi-empirical linear relationships have been given by McGuire et al. (1990) and Ashokkumar et al. (2012). Therefore, the contact angle for the reference liquids from Table 3.11 of SS and a coated surface was measured in the temperature range of 20 °C – 80 °C, which is far away from the boiling point of the reference liquids. The surfaces were placed in a tempering unit (tempering chamber G211, Krüss GmbH, Hamburg, Germany), which was heated by thermostat water. The surface temperature was measured with an infrared thermometer (IR 550-10S, Voltcraft®, Hirschau, Germany). The reference liquids in the syringe were not heated.

3.6 Zeta potential measurements

Particle size and particle electrophoretic mobility were measured with Zeta Sizer Nano-ZS (ZEN 3600 with a 633 nm He-Ne laser, Malvern Instruments Ltd., Grovewood Road, UK), which enables to measure particles in a size range from 0.6 nm to 6 µm (size distribution determination) and in a size range from 5 nm to 10 µm (zeta potential measurement). The measuring instrument (Zeta Sizer) was calibrated with polystyrene nanosphere™ size standard (Duke Scientific Corporation, Palo Alto, US), with a mean diameter of 200 ± 6 nm, and with a standard carboxyl modified polystyrene latex solution provided by Malvern Instruments, with a zeta potential of –55 mV.

The size measurement technique is based on dynamic light scattering (NBS®): the sample containing the particles or molecules is illuminated by a light source (He-Ne laser beam) and the intensity of the light backscattered by the particles is detected. The dynamic light scattering measurements permit to obtain the size distribution expressed as the frequency of particle volume versus size.

The hydrodynamic diameter or Stokes diameter[3] was determined using a fixed scattering angle of 173°, thus reducing an effect known as multiple scattering. The data were converted into a particle size distribution using the non-negative least-squares modeling routine (Malvern, 2004) whose parameters are defined in the ISO 22412 (2008). The autocorrelation function was calculated taking the fluctuation of the scattered intensity over time. From the polynomial fit of the logarithm of the correlation function, the diffusion coefficient of the molecules was calculated and hence the hydrodynamic diameter (d_h) was determined using the Stokes–Einstein equation:

$$d_h = \frac{k_B T}{3\pi\mu D_{app}} \tag{3.29}$$

Zeta potential is measured using laser Doppler electrophoresis. Thereby the electrophoretic mobility, i.e. average velocity of charged macromolecules, micelles and colloidal particles on an applied electric field, is detected by laser Doppler velocimetry. Zeta Sizer use the M3 - PALS® technique that, other than the detection of the Doppler frequency shift, determines the phase change (Malvern, 2004). The spectrum of the scattered light detected at an angle of 17° is obtained by a digital signal processor. Then the phase shift is measured by comparing the phase of the light scattered by the particles with the phase of the incident (reference) beam. Using additionally the M3® method (Mixed Mode Measurement) the effect of the electroosmosis is avoided due to the periodical reverse of the applied field. The M3® method consists of two measurements for each zeta potential measurement. One with the applied field being reversed slowly (SFR) and a second with a rapidly reversing (FFR) applied field (Malvern, 2004). The electroosmotic flow is determined by subtracting the zeta potentials calculated from the FFR and SFR measurements. Thus, the true electrophoretic velocity of the particle without superimposition of the electroosmotic flow can be obtained. Furthermore, an attenuator was used to set automatically the intensity of the laser and hence set the intensity of the scattering that depends on the size and concentration (sample turbidity) of the particles.

The particle velocity is dependent on the strength of the electric field or voltage gradient, the dielectric constant and viscosity of the medium, and its zeta potential (Müller et al., 1996). The particle velocity in an electric field is referred to as its electrophoretic mobility, which can be expressed by measuring the Doppler shifts of scattered laser light as (Tscharnuter, 2001):

$$\Phi = \langle A \rangle \int_0^{te} \vec{q}\left(v_E \vec{E} \right) dt \tag{3.30}$$

[3] Diameter of a sphere that has the same translational diffusion coefficient as the particle being measured, assuming a hydration layer surrounding the particle or molecule.

with

$$\vec{q} = \frac{4\pi n}{\lambda_0} \sin\left(\theta_s / 2\right) \tag{3.31}$$

Electrophoretic mobility is converted to zeta potential using a model. The selection of the model depends on two parameters, the particle size and the double layer thickness. Typically, the Helmholtz-Smoluchowski model is appropriate for aqueous solutions and the Hückel model for non-aqueous (Müller et al., 1996).

Then, the zeta potential (ζ) can be calculated from the Helmholtz-Smoluchowski equation:

$$\zeta = \frac{v_E 4\pi\eta}{\varepsilon} \tag{3.32}$$

Smoluchowski's theory is valid for any shape of particle, if the curvature radius *a* largely exceeds the Debye length κ^{-1}, i.e. $\kappa a \gg 1$ (Delgado et al., 2007). For the calculation, depending on particle size and on electrolyte concentration, the Debye-Hückel or Henry equations are applied (Müller et al., 1996). For a nonconducting sphere, with a diameter ranging from 1 nm to 18 µm and dispersed in aqueous electrolytes containing 10^{-3} mol L^{-1} salt, $0.1 < \kappa a < 100$ and $\zeta < 50$ mV (in such conditions, surface conductivity and concentration polarization are negligible) the following expression was derived (Henry, 1931):

$$\zeta = v_E \frac{3\eta}{2\varepsilon f(\kappa a)} \tag{3.33}$$

3.6.1 Zeta potential of whey protein and stainless steel particles

In order to investigate the thermal bulk aggregation of the whey proteins throughout the batch-wise fouling experiments (for the standard stainless steel surface) undiluted samples were taken every 30 min and the hydrodynamic diameter was measured immediately at 50 °C, i.e. the same bulk temperature, in a spectroscopic glass cuvette (PCS1115).

WPI and stainless steel particles were dispersed in diverse solutions, as listed in Table 3.12. The protein denaturation was performed batch-wise in a glass vessel by heating the WPI solution or the WPI plus stainless steel particles suspension at 80° C for 30 min (at pH = 6.7) in a water bath before the zeta potential measurements. Then the solution was immediately cooled in another water bath to 25 °C. The electrophoretic mobility was measured at working voltage on the electrodes of 40 V (for size) and 100 V (for zeta potential) and at 25 °C or 50 °C using a green disposable folded capillary cell (DTS1060). The pH value was adjusted by means of an automated titrator (MPT-2, Malvern Instruments Ltd.) in which 0.25 mol L^{-1} NaOH or 0.25 mol L^{-1} HCl were used for pH setting. Thereby, the samples were allowed to stabilize for 1 min on Zeta Sizer and three measurements were conducted at each individual pH value. Additional measurements to identify the hysteresis on zeta potential in a range of pH 3 to 9 and pH 9 to 3 were also conducted. The refractive index of protein (1.45) and water

(1.330) were taken as applicable. The viscosity and dielectric constant of water at 25 °C were 0.89 mPa s^{-1} and 78.5, respectively, and at 50 °C were 0.55 mPa s^{-1} and 70.2, respectively.

Since the stainless steel particles adhered to the wall of the plastic tubes and connections, an intensive cleaning was necessary after the titration measurements. The device was rinsed with RO water, isopropanol (at least 10 cycles) and afterwards with RO water (at least 30 cycles) again and before any new measurement rinsed again with the electrolyte solution (10 cycles).

Table 3.12. Composition and concentration of the solutions and suspensions for zeta potential measurement

Product	Solvents	Concentration [g L^{-1}]	T [°C]	pH range [-]
WPI	water and SMUF	0.55	25 and 50	3 to 9; 9 to 3
WPI	10^{-3} mol L^{-1} KCL	0.55	25	9 to 3
denatured WPI	water and 10^{-3} mol L^{-1} KCL	0.55	25	9 to 3
SS particles	10^{-3} mol L^{-1} KCL	1	25	9 to 3
denatured WPI in SS particles	10^{-3} mol L^{-1} KCL	WPI: 0.55; SS particles: 1	25	9 to 3

3.6.2 Zeta potential of the coated surfaces

The coatings are not available as a powder or other particulate system and a milling or galling of the surface could lead to tribological charge and cause false values of the zeta potential. Coating particles provided by the Fraunhofer Institute showed by far no spherical surface. Furthermore, they agglomerated in the aqueous electrolyte and therefore measurements of the zeta potential could not be realized using the Zeta Sizer.

A series of preliminary electrokinetic tests could be carried out on a streaming potential measuring device SurPASS (Anton Paar GmbH, Graz, Austria). The zeta potential determination is based on the detection of streaming potential or streaming current. The planar surfaces were assembled in the campling cell and an electrolyte was circulated through the measuring cell in a well-defined gap. Due to the pressure difference or to the flow, a movement of the charges in the double layer occurs and gives rise to the streaming potential. A symmetric configuration with two identical surfaces was used. Measurements were limited to the temperature range of the instrument from 10 °C to 40 °C. The measurements were conducted at 28 ± 1°C using 10^{-3} mol L^{-1} KCl and at 40 ± 1 °C for pH 6.7 using 5.5 g L^{-1} WPI, SMUF or SMUF-rich WPI solution. The pH titration of the electrolyte solution was set by automatic dosage of 0.1 mol L^{-1} HCl or 0.1 mol L^{-1} NaOH.

3.7 Chemical Analysis

3.7.1 Determination of protein content

Thermally denatured, insoluble proteins, either in solution or bound at a solid surface, cannot be quantified directly by dye binding methods. These assays will under-estimate protein content, if the protein is incompletely dissolved in solution. Lengthy techniques such as the

Kjeldahl method or techniques based on measurement of residual native protein in solution such as chromatography (HPLC) or gel electrophoresis (PAGE) are required. In order to quantify the total protein content by colorimetric or spectrophotometric techniques, it is first necessary to dissolve the protein entrapped on deposit or agglomerated in solution. Gotham et al. (1988) described a resolubilization protocol by heating the protein solution in urea and 2-mercaptoethanol and then measuring the protein content using the Bradford assay (Bradford, 1976). Still, in the presence of complex foods, interferences due to non-protein constituents can occur (van Morr et al., 1985; Compton and Jones, 1985; Gotham et al., 1988; Sapan et al., 1999), leading to protein over- or underestimation by the dye binding methods. The Dumas method (Dumas, 1870) is an alternative method to Kjedahl, chromatographically or dye binding methods and has been used for rapid routine N determination in milk based products according to DIN EN ISO 14891 (2002).

Evaluation of the cleaning process of hard protein deposits by a rapid and sensitive method for protein determination has not been described in the literature. Because of low quantities of protein in a large volume, Rasmussen and Maxcy (1979) evaluated various methods, such as drying, condensing and precipitation, to concentrate the cleaning solution before further analysis. The only apparent workable procedure was the precipitation of the protein, which could be separated by centrifugation and filtration, and determined at last by the colorimetric method of Bramhall with certain adaptations (Rasmussen and Maxcy, 1979).

In this work a CHNX elemental analysis device, whose working principle and method is described below, was employed for protein quantification, since the protein concentration was very low (< 50 mg L^{-1}), such as in the cleaning solution.

Total protein was found from TN_b (total bound nitrogen) by a TOC/TN_b analyzer (varioTOCcube, Elementar GmbH, Germany). The method consists of the oxidation of bound nitrogen (TN_b) by means of high temperature combustion (850 °C) in the presence of oxygen, which guarantees the complete break of protein bonds even for insoluble deposit pieces. This leads to the release of CO_2, H_2O and N_2 and NO_x, which refers to NO and NO_2. As carrier gas synthetic air (UN1956, Westfalen AG, Münster, Germany. Specification: 0.205 m^3 m^{-3} O_2, $\leq 0.1 \times 10^{-6}$ m^3 m^{-3} NO + N_2 and $\leq 0.1 \times 10^{-6}$ m^3 m^{-3} C_nH_n) with a flow rate of 0.012 m^3 h^{-1} was used. In the catalytic post combustion platinium catalyst (W.C. Heraeus GmbH, Hanau, Germany) NO_x was reduced to N_2. H_2O was removed by passing the gasses through a halogen absorber (silver wool) with a subsequent 3-step gas drying system including a magnesium perchlorate absorption column. The nitrogen content was then quantified by a nondispersive infrared (NDIR) detector and converted by a factor of 6.38 (DIN EN ISO 14891, 2002) to total protein.

The protein content of the deposits could thus be calculated as:

$$m_{protein} = \frac{6.38}{A}\left\{\left[\left([TN_b]_{sample} - [TN_b]_{blanc}\right)V\right]_{alkali\ \ solution} + \left[\left([TN_b]_{sample} - [TN_b]_{blanc}\right)V\right]_{acid\ \ solution}\right\} \tag{3.34}$$

where A is the coupon area (A_{coupon} = 0.0016 m^2) or the PHE plate area (A = 0.046 m^2).

The instrument was calibrated by analyzing a standard solution with a wide range of known nitrogen concentration. Thus, the signal from the NDIR sensor could be converted into nitrogen content. Potassium hydrogen phthalate ($C_8H_5KO_4$) was used as TOC standard, and

sodium nitrate ($NaNO_3$) and ammonium chloride (NH_4Cl) were used as TN_b standard. All chemicals had p.a. grade and were purchased from Merck Schuchardt OHG (Hohenbrunn, Germany). Ultrapure water (Purelab^{TM} UHQ, Elga Berkefeld GmbH, Celle, Germany) was taken to prepare the stock and standard solutions (0.5 – 25 TN_b mg L^{-1}) as well as for cleaning the auto-sampler syringe.

3.7.2 Determination of mineral content

The carbonaceous residue was reduced to ash by heating in a muffle furnace (MR170, Heraeus GmbH, Hanau, Germany) at 550 ± 25 ^{o}C for 36 hours, then cooled and weighed (Method 945.46) (AOAC, 2005). The quartz ash crucible were placed in the muffle furnace at about 550 ^{o}C for a minimum of six hours, then cooled in a desiccator before use.

3.7.3 Determination of calcium and phosphate contents

The Ca and P contents were determined by inductively coupled plasma optical emission spectroscopy ICP-OES (radial Vista MPX, Varian Deutschland GmbH, Darmstadt, Germany). The method is based on the circumstance that excited atoms or ions emit a characteristic electromagnetic radiation and thus provide information on the composition of the sample. The samples were directly injected into the plasma by a sea spray atomizer (atomization pressure 240 kPa). The excitation of the atoms and ions was carried out via inductively coupled plasma, where argon was used as plasma at a flow rate of 0.9 m^3 h^{-1} and as carrier gas at a flow rate of 0.09 m^3 h^{-1}. The emitted radiation was decomposed by means of a polychromator, and then read on the MPX Megapixel CCD Detector.

The characteristic wavelengths used to compare to previously measured intensities were for ion Ca: 315.89 nm, 317.93 nm, 373.69 nm, 393.37 nm and 396.85 nm, and for atom P: 177.43 nm, 178.22 nm, 185.88 nm, 213.62 nm and 214.91 nm. The wavelength for Ar 470.07 nm was used as internal reference line. The Ca and P contents were determined by external calibration. The calibration series included several calibration standards (0 - 200 mg L^{-1}). The calibration standards were prepared by dilution of single element stock solutions of concentration 10.000 mg L^{-1} with ultrapure water (Specpure®, Alfa Aesar, Karlsruhe, Germany). The measurements were carried out three times and the Ca or P content could be calculated by:

$$m_{Ca} = \frac{6.38}{A}\left\{\left[\left([Ca]_{b,sample} - [Ca]_{b,blanc}\right)V\right]_{alkali\ \ solution} + \left[\left([Ca]_{b,sample} - [Ca]_{b,blanc}\right)V\right]_{acid\ \ solution}\right\} \quad (3.35)$$

where A is the coupon area (A_{coupon} = 0.0016 m^2) or the PHE plate area (A = 0.046 m^2).

3.8 Deposit visualization

The structure of the fouling layers was examined in a scanning electron microscopy (SEM) (Jeol JSM 6400, JEOL Ltd.,Tokyo, Japan) equipped with an WDS/EDS measuring device (Genesis 4000, EDAX Inc., Mahwah, USA). Some samples were coated (gold sputtering) for SEM viewing, because non-conductive specimens tend to charge when scanned by the

electron beam at high vacuum. The microscopy was operated at 6 x 10^{-3} Pa and at an electron beam accelerating voltage of 15 kV.

Alternatively, the deposits were examined in an environmental scanning electron microscopy (ESEM) (EVO® LS25, Carl Zeiss SMT GmbH, Oberkochen, Germany) in which X-ray microanalysis on uncoated non-conductive specimens could be performed. The acceleration voltage of the electron beam was adjusted to 8 kV and the pressure in the sample chamber was reduced to 60 Pa. The measurement at low pressure instead of vacuum was required to avoid problems due to charging of the non-conductive samples. Because of the measurement in low pressure the VPSE detector (Variable Pressure Secondary Electron) was selected.

3.8.1 X-Ray microanalysis

Following the optical examination of the fouling layers with the SEM, the chemical composition was determined by energy dispersive X-ray microanalysis (EDS). X-ray microanalysis is a semi-quantitative surface characterization technique which provides a good indication of the relative amounts of each element on the surface. This analysis exploits the fact that the atoms in the upper layers of sample are excited by the high-energy electrons from an electron beam, causing the ejection of an electron in an inner shell and creating thus an free space where the electron was. This electron hole is immediately filled by an electron from a higher shell, which has a higher energy level. During the transition of the electron from an outer, higher-energy shell to an inner, lower-energy shell, the difference in energy may be released in form of X-ray, light or heat radiation. The emitted X-ray radiation is characteristic for each chemical element, so with using an X-ray detector, the elemental composition of the sample can be determined.

The EDS system QUANTAX (Bruker AXS Inc., Madison, USA) was used to determine the sample chemical composition. The corresponding X-ray detector (type XFlash® 5030/300) is integrated into the sample chamber of the ESEM. The detector is a so-called SDD (silicon drift detector) which allows fast and high-resolution measurement. In addition, to protect the detector a light element window (HT 2.2 polymer) was used, by which also elements with low atomic number or low emission energy level, such as carbon, nitrogen and oxygen, could be measured (QUANTAX Manual, 2008). The measurements were carried out with unchanged setting of the electron microscope ESEM, viz. at 8 kV accelerating voltage and a sample chamber pressure of 60 Pa.

For evaluating the measured X-ray spectra, the ESPRIT software (Bruker AXS Inc., Madison, USA) was used. Here, the so-called real standard less analysis was selected, the chemical composition of the sample was calculated from a comparison of the overall spectrum and the spectrum contained in the radiation and software databases. Thus, no calibration of the system was necessary. The selection of the elements to be measured was made automatically, since the consideration of elements that were not present in the sample can lead in misinterpretations of the spectrum and thus falsified results.

The information depth is about 1 – 2 µm (QUANTAX Manual, 2008; Barkshire et al., 2000) and depends on material composition and density. It corresponds to the maximum depth of the characteristic X-ray radiation that has been emitted from the local sample atoms to leave the sample and thus can be detected. The emitted X-ray radiations from deeper atoms

get absorbed on their way through the sample material and thus cannot be detected. It means that the results give information about the upper fouling layers' composition, results of total protein, Ca and P contents of the whole deposit were determined by other methods (sections 3.7.1 and 3.7.3).

Quantitative microanalysis was performed at least at three different positions in more than two unmodified and modified coupons and the average composition was recorded. The results are given by normalizing the peak intensities of the main constituents (C, N, O, Cr, Fe, Ni and Si, for the surfaces and additionally Na, Mg, P, Cl, K, Ca for calcium phosphate or WPI plus SMUF deposits) to 100 %.

3.9 Error and statistical analysis

At least three experiments at identical conditions were performed for each surface to assess repeatability, of which two plates with the same coating were used in each fouling trial. For the fouling experiments on PHE as well as for the cleaning experiments on flow cell results for the surfaces after initial aging are presented. As shown in detail for the coupons (section 4.1.5) the coated surfaces have reached a stable state relatively quickly (after three fouling and cleaning cycles). Therefore, initial aging effects on deposition in the next fouling as well as cleaning could be excluded.

Vertical bars on the diagrams indicate standard error from the mean and results in the tables are presented as mean ± standard error (Eq. 3.37). In the fouling resistance progress diagrams lines are fits and do not represent modelling results. The final fouling resistance $R_{f,\,end}$, determined as a mean of the R_f values for the last 15 min experiment, and the average fouling resistance rate in the first hour $(dR_f/dt)_{1h}$ or in the first 30 min $(dR_f/dt)_{0.5h}$ were used to compare fouling on the different surfaces.

The standard error of the mean is defined as (DIN ISO 3534-1, 2009):

$$SE = \frac{s}{\sqrt{n_{sample}}} \tag{3.36}$$

The Statgraphics package (version Plus 5.0, Statpoint Technologies, Inc., Warrenton, USA) was used for the statistical analysis. The differences between means were detected by the Fisher multiple comparison test. Treatment means were considered significantly different at $p \leq 0.05$, i.e. at a 95 % of confidence.

An analysis of variance (ANOVA) (Montgomery, 1997) was conducted to establish the separate as well as simultaneous effect of the following factors and improved the overall process understanding:

(i) initial surface temperature (T_0), fluid (WPI, SMUF or WPI plus SMUF), surface roughness (R_z) and electron donor component (γ^-) on final fouling resistance ($R_{f,\,end}$), initial fouling rate $(dR_f/dt)_{1h}$, deposit mass and deposit chemical composition in the batch-wise fouling experiments;

(ii) roughness and γ^- on $R_{f,\,end}$, $(dR_f/dt)_{0.5h}$ and deposit chemical composition in the continuous fouling experiments on PHE;

(iii) roughness and γ^- on the cleaning rate ($r_{c,m}$) and ($R_{f,\,cleaning,\,30\,min}/R_{f,fouling,end}$) in the cleaning experiments.

Furthermore, the effects of the variables T_0, γ^-, fluid and R_z on $R_{f,\,end}$ as well as deposit amount and composition in the fouling experiments were studied using a multilevel factorial design (Montgomery, 1997). The design considered three levels of T_0, three levels of fluid and eight levels of γ^- and R_z (Table 3.13) for the batch-wise fouling experiments and four levels of γ^- and R_z for the continuous fouling experiments (Table 3.14). Because the surface free energy of the aged coupons or plates as well as their roughness are not adjustable, a orthogonal array design is difficult to implement. Therefore the level of γ^- and R_z were linearly coded later. The experimental data were adjusted to a second order polynomial model (Eq. (3.38)) by multiple regression analysis. Insignificant terms ($p > 0.10$) were eliminated through step-wise regression.

$$y = c_1 (T_0)^2 + c_2 (\gamma^-)^2 + c_3 (R_z)^2 + c_4 (T_0 \times \gamma^-) + c_5 (T_0 \times \text{fluid}) + c_6 (T_0 \times R_z) + c_7 (R_z \times \text{fluid}) + c_8 (T_0) + c_9 (\gamma^-) + c_{10} (R_z) + \text{const.} \quad (3.37)$$

A t-test is used to test the significance of each individual term in the model (Motgomery, 1997). The T-Statistic value is given as:

$$T - \text{Statistic} = \frac{c_i}{SE(c_i)} \quad (3.38)$$

The relationship between the variables and the response parameters could be graphically represented by a three-dimensional response plot.

Table 3.13. Uncoded and corresponding coded values of the independent variables for the multilevel factorial design of the batch-wise fouling experiments

Actual (uncoded) variables					Coded variables			
Fluid	**T_0 [°C]**	**γ^- [mN m^{-1}]**	**R_z [µm]**	**Surface**	**Fluid_cod**	**T_0_cod**	**γ^-_cod**	**R_z_cod**
WPI	80	8.4	1.87	SS	-1	-1	-1	1
SMUF	105	13	1.7	DLC	0	0.25	-0.41	0.69
WPI+SMUF	120	15.5	1.69	SICAN	1	1	-0.089	0.67
		22	1.67	SICON®			0.58	0.63
		15.1	0.78	ESS			-0.141	-1
		11	0.87	EDLC			-0.667	-0.83
		14	0.97	ESICAN			-0.282	-0.65
		24	0.89	ESICON®			1	-0.8

Table 3.14. Uncoded and corresponding coded values of the independent variables for the multilevel factorial design of the continuous fouling experiments (PHE)

Actual (uncoded) variables			Coded variables	
γ^- [mN m^{-1}]	**R_z [µm]**	**Surface**	**γ^-_cod**	**R_z_cod**
4.6	1.19	SS	-1	-1
9.2	1.38	DLC	0.070	-0.0656
8.7	1.6	SICAN	-0.046	1
13.2	1.2	SICON®	1	-0.944

4 Results and Discussion

4.1 Surface characterization

In the following, the mechanical and energetic (measured) variables that characterized the heat transfer surfaces and influenced the adhesion and build-up of fouling layers will be presented and discussed.

4.1.1 Surface roughness and topography

The two-dimensional roughness parameters for the different surfaces and samples, viz. coupons and plates from PHE, are presented in Tables 4.1 and 4.3. The coating by PECVD generates a 3 µm thick layer (Bewilogua et al., 2011) on the stainless steel substrate, which slightly decreased the mean roughness depth of the surface for stainless steel (Table 4.1) and slightly increased the mean roughness depth of the surface for electropolished stainless steel (Tables 4.1 and 4.3). The mean roughness (R_a) decreased by 0.06 µm for the substrate SS and increased by 0.01 - 0.04 µm for the substrate ESS, while the roughness depth (R_z) decreased by 0.2 µm and increased by 0.2 – 0.4 µm for SS and ESS, respectively.

In addition to the stylus-based parameters, the surfaces have been studied with respect to their topographical characteristic values (Table 4.2). The three-dimensional roughness parameters S_a and S_z showed a similar tendency compared to the two-dimensional roughness parameters R_a and R_z, although the values were slightly lower. Fig. 4.1 shows the comparison of profilometer and AFM data. The stylus tip radius of AFM is smaller than that of the profilometer and therefore AFM measurement is expected to be more accurate, given that the original profile is not distorted. Furthermore, the AFM has a better spatial resolution than the profilometer. The S_{dr} data (Table 4.2) show that the interfacial area of a surface over the sampling area for the unpolished stainless steel substrate decreased due to coating, while it increased for the electropolished substrate. The data is also supported by the AFM images. Thus, both the measurement and visualization of the topographic surface features can potentially relate to fouling and cleanability.

Table 4.1. 2D-Roughness of the unmodified and modified coupons

Surface	R_a [µm]	R_z [µm]
SS	0.18 ± 0.03	1.87 ± 0.02
DLC	0.13 ± 0.01^{a}	1.70 ± 0.02^{ij}
SICAN	0.12 ± 0.02^{abc}	1.69 ± 0.02^{ik}
SICON®	0.12 ± 0.02^{bd}	1.67 ± 0.02^{jk}
ESS	0.10 ± 0.05^{e}	0.78 ± 0.01^{lmn}
EDLC	0.10 ± 0.01^{fg}	0.87 ± 0.03^{lop}
ESICAN	0.11 ± 0.01^{cdfh}	0.97 ± 0.02^{moq}
ESICON®	0.11 ± 0.01^{egh}	0.89 ± 0.02^{npq}

Results are presented as mean ± standard error. Superscript letters indicate statistically identical values for R_a and R_z ($p < 0.05$).

Table 4.2. 3D-Roughness of the unmodified and modified coupons

Surface	S_y [µm]	S_a [µm]	S_z [µm]	S_{dr} [%]
SS	2.5 ± 0.5	0.15 ± 0.03	2.1 ± 0.5^{a}	1.0 ± 0.2
DLC	2.32 ± 0.06^{ab}	0.110 ± 0.002^{a}	2.2 ± 0.4^{a}	0.71 ± 0.01^{ab}
SICAN	2.18 ± 0.07^{a}	0.0857 ± 0.009^{a}	1.6 ± 0.1^{b}	0.57 ± 0.01^{ac}
SICON®	1.6 ± 0.1^{b}	0.069 ± 0.003^{bcdef}	1.3 ± 0.1^{b}	0.44 ± 0.01^{bc}
ESS	0.57 ± 0.05^{cde}	0.052 ± 0.001^{beghi}	0.39 ± 0.01^{cde}	0.030 ± 0.004^{def}
EDLC	0.59 ± 0.06^{cfg}	0.056 ± 0.003^{gfjk}	0.52 ± 0.06^{cfg}	0.108 ± 0.006^{dgh}
ESICAN	0.55 ± 0.08^{dfh}	0.050 ± 0.004^{chjl}	0.444 ± 0.07^{dfh}	0.058 ± 0.01^{egi}
ESICON®	0.8 ± 0.1^{egh}	0.062 ± 0.008^{dikl}	0.564 ± 0.07^{egh}	0.039 ± 0.006^{fhi}

Results are presented as mean ± standard error. Superscript letters indicate statistically identical values for S_y, S_a, S_z and S_{dr} ($p < 0.05$).

Table 4.3. Surface roughness of the modified and unmodified plates (PHE)

Surface	Roughness [µm]	
	R_a	R_z
Stainless steel	0.17 ± 0.01^{ab}	1.19 ± 0.05^{e}
DLC	0.21 ± 0.01^{ac}	1.38 ± 0.08
SICAN	0.23 ± 0.02^{bd}	1.6 ± 0.1^{ef}
SICON®	0.17 ± 0.04^{cd}	1.2 ± 0.3^{f}

Letters *a to f* refer to statistically different roughness ($p < 0.05$). Results are presented as mean ± standard error.

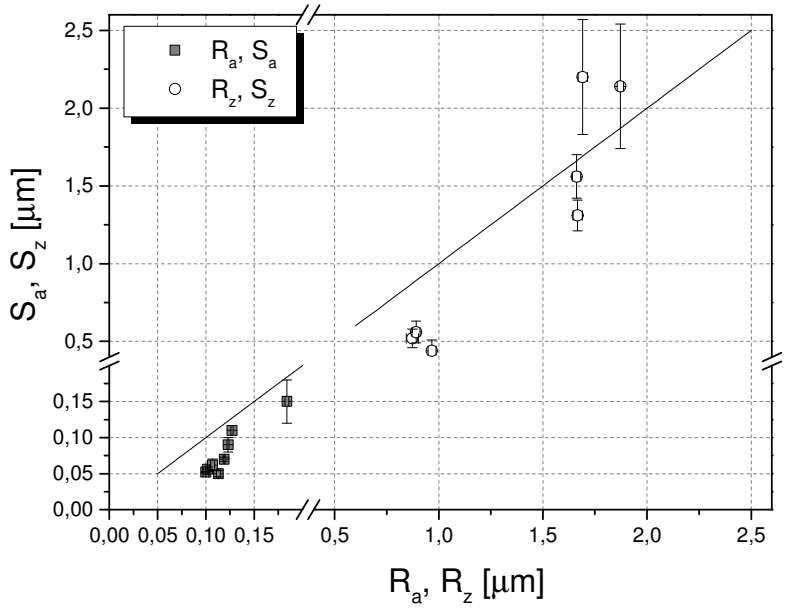

Fig. 4.1. Roughness measurements obtained using two different devices: profilometer (R_a, R_z) and AFM (S_a, S_z)

AFM images (Fig. 4.2) of the unmodified and modified surfaces show that the PECVD process combined with the thin coating layer ensures a near-surface coating where the original topography is not altered. The stainless steel coupons revealed grain boundaries (Fig. 4.2a) that appear as cracks, edges and valleys. This heterogeneous grainy surface structure results from the finishing method. According to supplier information (Frank + Warnecke Industriebedarf GmbH, Braunschweig, Germany), the SS finish was probably C2(IIa), i.e. hot mechanical rolled, pickled finish (annealed and passivated). By electropolishing, the SS is submitted to an electrochemical treatment creating a smooth surface structure (Fig. 4.2c). A smoothing of grain boundary structure of the SS substrate on the coated SS could be identified, resulting from the a-C:H:X layer formation (Fig. 4.2b). On the other hand, on ESS substrate, the thin coating layer roughened the surface (Fig. 4.2d). Thereby, there was an increase of roughness parameters for the coupons (Tables 4.1 and 4.2), as well as for the plates (PHE) (Table 4.3).

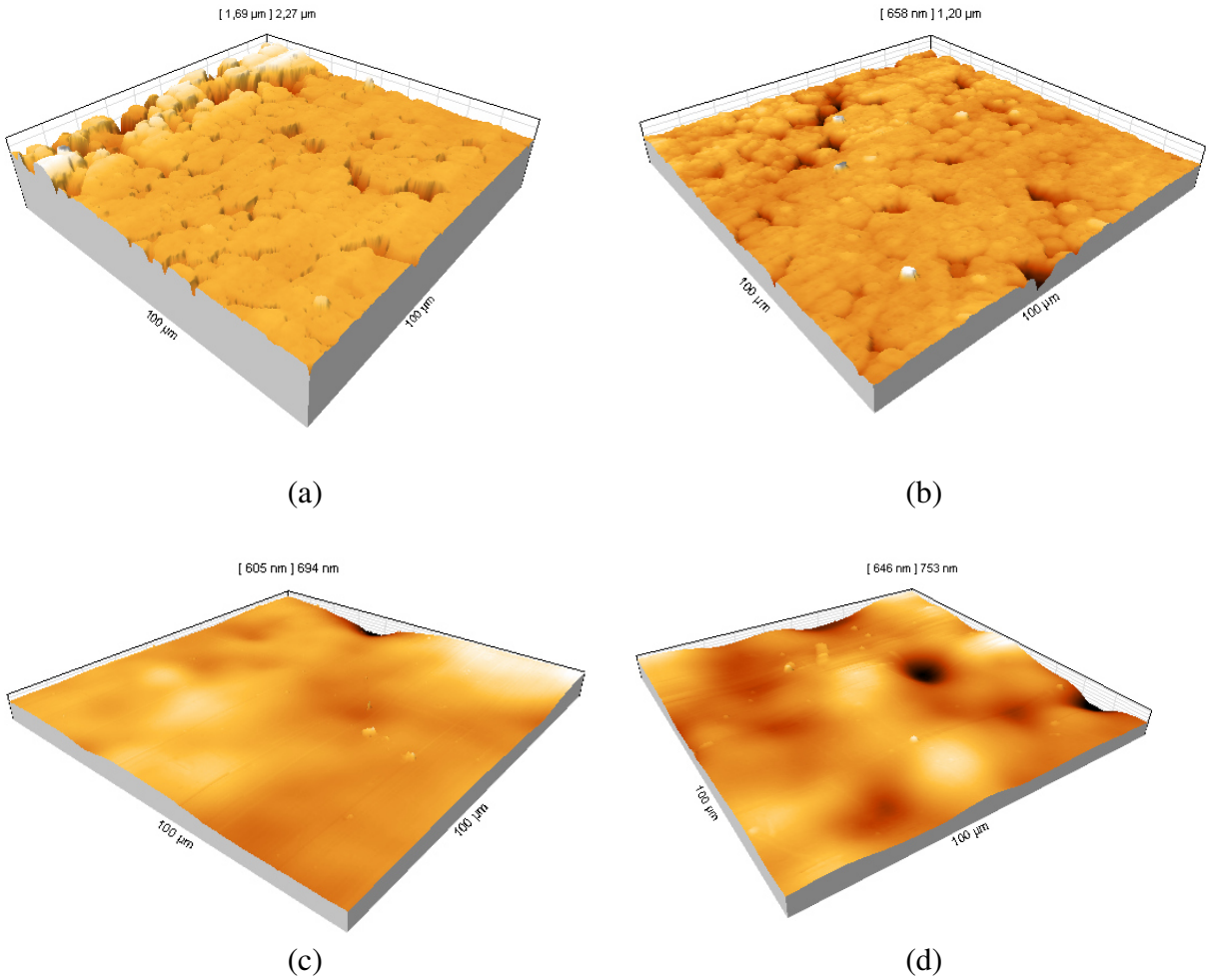

Fig. 4.2. Topography of (a) SS, (b) SICAN, (c) ESS, (d) ESICAN surfaces (100 x 100 μm^2)

4.1.2 Surface free energy

The energy components according to the van Oss approach as well as the dispersive and the polar part of the surface free energy according the Owens-Wendt-Rabel-Kaelble (OWRK) approach for new and used surfaces are shown in Tables 4.4 – 4.6 for the coupons and in Tables 4.7 – 4.9 for the PHE plates. Twenty SS coupons, six samples from ESS, as well as twelve coated SS coupons, two coated ESS coupons and two coated PHE plates for each coating were characterized. Contact angles of used coupons were measured after the fifth soiling/cleaning cycle and contact angles of used PHE plates were measured consecutively after a minimum of three fouling/cleaning cycles.

Table 4.4. Surface free energy components of new coupons according to van Oss approach

Surface	Surface free energy [mN m^{-1}]				
	γ^{LW}	γ^{AB}	γ^{+}	γ^{-}	γ^{TOT}
SS	37.7 ± 0.7^{a}	1.7 ± 0.3^{d}	0.28 ± 0.05	6 ± 1^{k}	39.4 ± 0.8
DLC	39.2 ± 0.7^{a}	2.5 ± 0.4^{d}	0.5 ± 0.1^{fghi}	5.3 ± 0.4^{kl}	41 ± 1
SICAN	36.2 ± 0.4^{b}	0.7 ± 0.1^{e}	0.05 ± 0.01^{f}	4.1 ± 0.4^{l}	36.4 ± 0.4
SICON®	28.8 ± 0.8^{c}	0.47 ± 0.06^{e}	0.05 ± 0.01^{g}	1.5 ± 0.1^{m}	29.4 ± 0.7
ESS	36.2 ± 1^{b}	0.7 ± 0.2^{e}	0.06 ± 0.04^{h}	6 ± 1^{k}	37 ± 1
EDLC	42.8 ± 0.8^{a}	3.0 ± 0.4^{d}	0.32 ± 0.06	7.2 ± 0.4^{k}	45.8 ± 0.4
ESICAN	37.3 ± 0.1^{ab}	1.2 ± 0.1^{de}	0.13 ± 0.01^{i}	2.8 ± 0.5	38.5 ± 0.1
ESICON®	27.7 ± 0.4^{c}	1.0 ± 0.1^{de}	0.14 ± 0.05^{j}	1.9 ± 0.2^{m}	28.7 ± 0.5

Superscript letters indicate statistically identical values for γ^{LW}, γ^{AB} and γ^{-} and statistically different values for γ^{+} ($p < 0.05$).

Table 4.5. Surface free energy components of used coupons according to van Oss approach

Surface	Surface free energy [mN m^{-1}]				
	γ^{LW}	γ^{AB}	γ^{+}	γ^{-}	γ^{TOT}
SS	38.5 ± 0.1	4.3 ± 0.2	0.6 ± 0.06^{d}	8.4 ± 0.4	42 ± 1
DLC	39.6 ± 0.3^{a}	6.3 ± 0.3^{bc}	0.75 ± 0.07^{d}	13 ± 1	45.2 ± 0.6
SICAN	39.7 ± 0.2^{a}	6.0 ± 0.2^{b}	0.6 ± 0.04^{d}	15.5 ± 0.9^{e}	45.2 ± 0.6
SICON®	40.0 ± 0.3^{a}	7.9 ± 0.2	0.75 ± 0.06^{d}	22 ± 1^{f}	47.9 ± 0.9
ESS	39.8 ± 0.3^{a}	5.7 ± 0.4^{bc}	0.54 ± 0.08^{d}	15.1 ± 0.9^{e}	46 ± 1
EDLC	40.4 ± 0.2^{a}	6.7 ± 0.4^{bc}	1.1 ± 0.2^{d}	11 ± 1	47.6 ± 0.6
ESICAN	39.9 ± 0.4^{a}	11.4 ± 0.4	2.3 ± 0.2	14 ± 1	52.3 ± 0.3
ESICON®	40.8 ± 0.5^{a}	13.3 ± 0.4	1.9 ± 0.2	24 ± 2^{f}	55.1 ± 0.6

Superscript letters indicate statistically identical values for γ^{LW}, γ^{AB}, γ^{+} and γ^{-} ($p < 0.05$).

Table 4.6. Surface free energy components of used coupons according to OWRK approach

Surface	Surface free energy [mN m^{-1}]		
	γ^{dis}	γ^{polar}	γ^{TOT}
SS	35.4 ± 0.3^{a}	4.5 ± 0.3^{af}	39.8 ± 0.4
DLC	36.7 ± 0.3^{b}	9.2 ± 0.3^{g}	45.8 ± 0.3^{h}
SICAN	36.1 ± 0.4^{abc}	8.9 ± 0.3^{g}	46.7 ± 0.4^{hj}
SICON®	36.3 ± 0.3^{bc}	10.1 ± 0.5^{g}	47.8 ± 0.4^{ij}
ESS	38.0 ± 0.4^{d}	5.2 ± 0.4^{f}	46 ± 1^{h}
EDLC	39.0 ± 0.3^{d}	9.5 ± 0.4^{g}	46.8 ± 0.8^{hi}
ESICAN	38.6 ± 0.4^{de}	12.4 ± 0.7	52.1 ± 0.9^{k}
ESICON®	38.0 ± 0.6^{bde}	18 ± 1	55 ± 1^{k}

Superscript letters indicate statistically identical values for γ^{dis}, γ^{polar} and γ^{TOT} ($p < 0.05$).

Table 4.7. Surface free energy components of new PHE plates according to van Oss approach

Surface	Surface free energy [mN m^{-1}]				
	γ^{LW}	γ^{AB}	γ^{+}	γ^{-}	γ^{TOT}
SS	36 ± 1	4.1 ± 0.4^{c}	0.4 ± 0.1^{fg}	9 ± 1^{jkl}	40.5 ± 0.7
DLC	37.3 ± 0.4^{a}	10.0 ± 0.4^{cde}	2.0 ± 0.05^{fh}	13 ± 0.1^{jmn}	47.3 ± 0.1
SICAN	38.1 ± 0.6^{b}	3.6 ± 0.1^{d}	1.8 ± 0.2^{gi}	1.7 ± 0.5^{km}	41.7 ± 0.7
SICON®	33 ± 1^{ab}	2.6 ± 0.9^{e}	1.1 ± 0.2^{hi}	1.6 ± 0.4^{ln}	36 ± 2

Superscript letters indicate statistically different values for γ^{LW}, γ^{AB}, γ^{+} and γ^{-} ($p < 0.05$).

Table 4.8. Surface free energy components of used PHE plates according to van Oss approach

Surface	Surface free energy [mN m^{-1}]				
	γ^{LW}	γ^{AB}	γ^{+}	γ^{-}	γ^{TOT}
SS	40.1 ± 0.1	3.5 ± 0.2^{abc}	0.66 ± 0.08^{f}	4.6 ± 0.2^{ijk}	43.5 ± 0.1^{opq}
DLC	40.8 ± 0.2	6.7 ± 0.2^{ad}	1.22 ± 0.08^{fgh}	9.2 ± 0.2^{ilm}	47.5 ± 0.1^{o}
SICAN	41.7 ± 0.1	5.5 ± 0.1^{bde}	0.87 ± 0.01^{ng}	8.7 ± 0.1^{jln}	47.2 ± 0.2^{p}
SICON®	40 ± 1	6.5 ± 0.6^{ce}	0.8 ± 0.1^{h}	13.2 ± 0.1^{kmn}	46.8 ± 0.5^{q}

Superscript letters refer to statistically different surface energy components ($p < 0.05$).

Table 4.9. Surface free energy components of used PHE plates according to OWRK approach

Surface	Surface free energy [mN m^{-1}]		
	γ^{dis}	γ^{polar}	γ^{TOT}
SS	38.7 ± 0.1^{a}	4.4 ± 0.1^{def}	43.1 ± 0.1^{jkl}
DLC	38.9 ± 0.1^{b}	8.7 ± 0.1^{dhg}	47.6 ± 0.1^{j}
SICAN	39.4 ± 0.1^{c}	7.7 ± 0.1^{egi}	47.0 ± 0.2^{k}
SICON®	37.1 ± 0.9^{abc}	10.3 ± 0.4^{fhi}	47.3 ± 0.5^{l}

Superscript letters refer to statistically different surface energy components ($p < 0.05$).

A total surface free energy γ^{TOT} for stainless steel (new or used SS and ESS) of 40 – 46 mN m^{-1} was obtained, as was expected for oxide-covered metals (Saikhwan et al., 2006; Bargir et al., 2009, Geddert et al., 2011b). Due to the coating process, the interfacial energies of the stainless steel substrates change. Prior to the initial aging process, a notable difference in all surface free energy contributions could be identified, including the total surface free energy between the surfaces (Table 4.4 for the new coupons and Table 4.7 for the new plates), confirming the low value of the surface free energy of silicon doped DLC coatings from the literature (Bewilogua et al., 2011; Grischke et al., 1995). Furthermore, the results indicate that the Lifshitz-van der Waals component γ^{LW} or the dispersive part γ^{dis} contributed more significantly to γ^{TOT} than the acid-base component γ^{AB} or the polar part γ^{polar}. According to Bargir et al. (2009), Lewis basic contributions are dominated by amorphous carbon coatings due to the high density of carbon-based groups and dangling bonds on the carbon backbone.

A variation of the surface free energy with use of the coatings in fouling and cleaning experiments was evident, resulting in an increase of the γ^{AB} as well as of the γ^{LW} components and of γ^{TOT}. A detailed discussion regarding the influence of coating aging in the surface properties is given in section 4.1.5. The used coatings show then a total surface free energy similar to stainless steel (± 5 mN m^{-1}), with the exception of ESICAN and ESICON®, although a different fouling behavior could be observed, as shown in this work and by Geddert et al. (2009) for the induction period of $CaSO_4$ crystallization on DLC coated SS substrate. It emphasizes the importance of comparing the components of the surface energy (acid-base/polar, electron acceptor and donor components) separately.

The used surfaces (Tables 4.5 and 4.6 for the used coupons and Tables 4.8 and 4.9 for the used PHE plates) gave similar dispersive components (γ^{LW} values ranging from 39 to 41 mN m^{-1} and γ^{dis} values ranging from 35 to 39 mN m^{-1}) and and very low values for the electron-acceptor component γ+ (between 0.6 and 2.3 mN m^{-1}). However, significantly different polar part (γ^{AB} values ranging from 4.3 to 13 mN m^{-1} and γ^{polar} values ranging from 4.5 to 18 mN m^{-1}) and different and higher γ^- (between 8.4 and 24 mN m^{-1}) were determined. Related to the untreated stainless steel surfaces, the coating tends to advance the polar part of the surface energy. A combination of silicon (SICAN) or silicon and oxygen (SICON®) inside the coating also leads to an increase of the γ^-, showing the sequence: SS < DLC < EDLC = SICAN = ESS < ESICAN < SICON® = ESICON®. According to Grischke et al. (1995) and Trojan et al. (1994), the addition of oxygen to an acetylene plasma increases the wettability and the surface energy of the resulting doped DLC coating, which is mainly affected by the increase in the polar part. While the addition of silicon reduces the surface energy, resulting in a surface with a low wetting, a well-defined addition of oxygen and a silicon-containing hydrocarbon will further reduce the surface free energy (Grischke et al., 1995, Trojan et al., 1994). Regarding the carbon groups, the greater density of sp^3 bonding possibly renders the surface more susceptible to oxidation into C–OH (sp^3 bonding), C(O)OH (sp^2 bonding), ether and other centers for adsorption, thus increasing the surface hydrophobicity (Bargir et al., 2005).

The γ^- component has been used to correlate the formation of deposits on diverse surfaces (calcium sulphate: Al-Janabi et al., 2010; calcium carbonate: Bargir et al., 2009; whey protein and calcium phosphate: Rosmaninho and Melo, 2008; calcium phosphate: Wu and Nancollas, 1998), as well as demonstrating the influence of the surface energetic

characteristics on the removal kinetics of bacteria (Jullien et al., 2002; Boulangé-Petermann et al., 2004) or food soils (Boulangé-Petermann et al. 2002; Mauermann et al., 2009; Detry et al., 2010) and on adhesion of chocolate (Keijbets et al., 2009). For the investigated DLC coatings, the variation on the term γ^- of the polar contribution was considerably higher than on the term γ^+. The literature also relates to an absence of the electron accepting values for many materials, including DLC coatings (Santos et al., 2004; Bargir et al., 2009). Therefore, γ^- was used in this work to compare the deposition formation on the different coated surfaces as well as comparing their cleanability.

The comparison of surface energy parameters calculated by the van Oss and the OWRK approaches (Tables 4.5 and 4.6) showed that the polar part by van Oss (γ^{AB}) was generally lower, while the LW contribution (γ^{LW}) and the total surface free energy (γ^{TOT}) were higher than the equivalent surface energy terms of the OWRK approach (viz. γ^{polar}, γ^{dis} and γ^{TOT}, respectively). Similar results were found by Hejda et al. (2010). The surface energy depends on the liquids used for measuring the contact angle (Correia et al., 1997) and the acid-base theory (van Oss approach) seems to be more sensitive to the selection of liquids compared to other methods (Hejda et al., 2010). Depending of the assumptions in the development of the approach models, some liquids can be more appropriate than others, thus resulting in different values of surface energy parameters for each approach.

The difference of the surface free energy contributions between the coupons and the plates (new surfaces: Tables 4.4 and 4.7 (van Oss approach), used surfaces: Tables 4.5 and 4.8 (van Oss approach)) can be due to the pre-treatment of the surfaces undergone before the PECVD deposition, chemical composition (coupons: SS 1.4301; plates: SS 1.4401), or cleaning of the surfaces using different acid agents (coupons were rinsed in 1 % w/w HNO_3 or 2 % w/w CH_3COOH while the plates were rinsed in 1 % w/w H_3PO_4).

4.1.3 Zeta Potential

The surfaces were characterized according to their electrokinetic properties. Fig. 4.3 compares the zeta potential of coated coupons with the reference substrate. The contribution of the surface conductivity due to the electrochemical double layer could not be excluded with certainty. For this reason, further measurements (varying the electrolyte and electrolyte concentration) were required. Hence, it will be assumed that the effect of surface conductivity is lower than the observed zeta potential difference between the diverse surfaces.

The surfaces exhibit a positive zeta potential up to a pH value of 3.5 – 4, with respect to the surrounding electrolyte, while they had a negative zeta potential in the light acid, neutral and alkali media. The values of zeta potential of the surfaces vary from +20 mV to –35 mV for the pH range of 2 to 9. From pH of 3 to 6, the ζ values of stainless steel, DLC and SICAN slightly differ, indicating that the surface charge behavior is very similar in this pH range. However, SICON® showed higher values of ζ. Above to a pH value of 6, SICON® behaved similar to SICAN, whereas SS and DLC showed different ζ progressions.

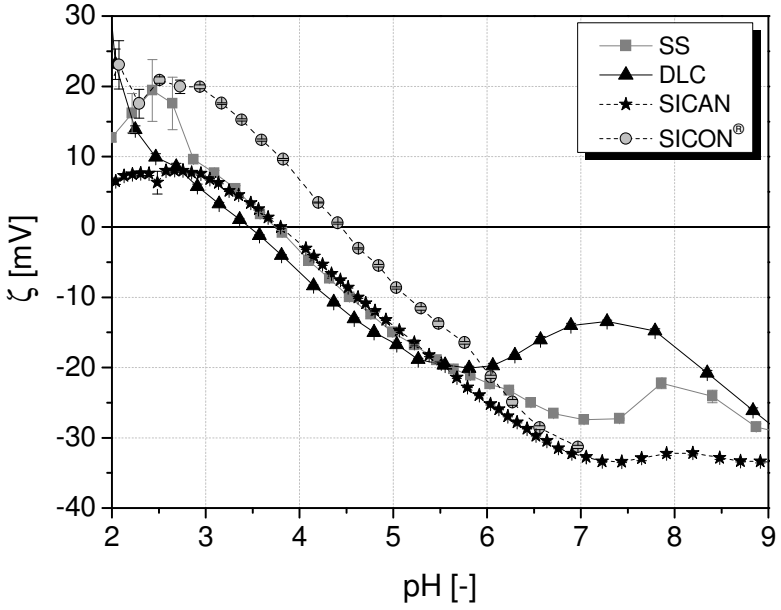

Fig. 4.3. Zeta potential of new coupons in 10^{-3} mol L^{-1} KCl

At the initial pH value of the fouling experiments (pH = 6.7), the surfaces were differently negatively charged. However, note that the zeta potential measurement was conducted at a temperature of 28 ± 1 °C using a KCl solution, which is a reference electrolyte used to compare surfaces. (For results at a higher temperature (at 40 °C, which is the limit of the measuring device) using WPI and SMUF-rich WPI solutions, in which the experimental conditions approximate, consult section 4.1.5 and Table A2 in appendix.) During the WPI and WPI plus SMUF fouling, the pH remained constant, while with the SMUF fouling the pH decreased significantly, reaching values of 6.4 or 6.2 after 360 min at T_0 = 80 °C or 105 °C, respectively (see Fig. 4.33, which will be discussed later). However, the zeta potential of the surfaces on the following stages of the build-up is not the same as the zeta potential of the primary surface, given that the surface is already covered by a multi fouling layer.

Based on severe simplifications, the surface free energy can be considered as a measurement of the van der Waals and Lewis acid/base forces, while the zeta potential reflects the electrostatic forces (Boulangé-Petermann et al., 1995). The resulting forces arise from a summation of the van der Waals and the electrostatic forces (extended DLVO theory - van Oss, 1995). On the isoelectric point act especially van der Waals forces, because these forces are more attractive and higher than the electrostatic forces. From the zeta potential curves with the pH, the isoelectric points (IEP = pH with $\zeta = 0$) of the surfaces could be derived (Table 4.10). The IEP of stainless steel is very similar to the IEP of stainless steel particles (IEP 3.8 in 10^{-3} mol L^{-1} KCl, Fig. 4.23, which will be discussed in section 4.2.3) and in accordance with literature data (IEP = 3 – 4.8 in 10^{-3} mol L^{-1} KNO_3, Boulangé-Petermann et al. (1995) and Fukuzaki et al. (1995); IEP = 3 – 4, Chandrasekaran et al. (2013)). SS and SICAN surfaces showed identical IEP (Table 4.10) as well as identical LW contributions γ^{LW} (Table 4.4) and similar values of IEP, as well as similar γ^{LW} to DLC, while the IEP and the γ^{LW} of SICON® was significantly different from the other surfaces.

Since the fouling experiments were conducted at a pH value above the surface IEPs, the van der Waals as well as electrostatic forces play an important role in the deposition of whey protein and calcium phosphate. Therefore, the effect of the electrokinetic surface properties on fouling cannot be excluded.

Table 4.10. Isoelectric points of coated and reference new surfaces obtained in 10^{-3} mol L^{-1} KCl

Surface	IEP [-]
SS	3.8
DLC	3.5
SICAN	3.8
SICON®	4.5

4.1.4 Influence of roughness and temperature on surface free energy

Roughness

The R_a values (0.1 µm < R_a < 0.2 µm, for the coupons and R_a ~ 0.2 µm, for the plates) as well as the R_z values (0.9 µm < R_z < 1.9 µm, for the coupons and 1.2 µm < R_z < 1.6 µm, for the plates) were statistically different for some surfaces, although the difference was not so large. Therefore, to ensure that the roughness does not influence the energetic surface parameters (especially γ^-), the ANOVA was run to verify the effect of roughness on the electron donor component γ^-.

No statistically significant correlation between the roughness parameters R_z or R_a for the investigated interval roughness and γ^- could be found ($p > 0.05$). The low roughness values could explain the non systematic dependence of surface roughness on contact angles. Hence, the surface free energy can be used as a principal parameter to compare the studied surfaces.

Temperature

The contact angle formed by the solid–liquid interface and the liquid–vapor interface for diverse reference liquids at SS and SICON® with the surface temperature was measured. Fig. 4.4 details the relation between cos θ and temperature. In general, the slopes exhibited a slightly linear increase of cos θ with temperature. The liquids were not heated, but a rise in temperature in contact with the surface could cause a lower viscosity and lower surface tension of the liquids making them spread better on the surface and building up a lower contact angle. SICON® showed a different wetting behavior when compared to SS, given that the surface was better wetted. Both surfaces were not wetted completely with water. Despite this temperature effect on the wetting equilibrium, this effect can be considered minor for the studied surfaces (crystalline and quasicrystalline) when comparing to other coated surfaces, such as ceramic or polymeric (Ashokkumar et al., 2012) and thus will be neglected. Zhao et al. (2004b) reported a significant decrease of γ^- for ta-C coatings in the temperature range of

20 to 95 °C, while for SS and DLC coating the decrease was minor, as shown for SS and SICON® in Figs. 4.4a and 4.4b, respectively.

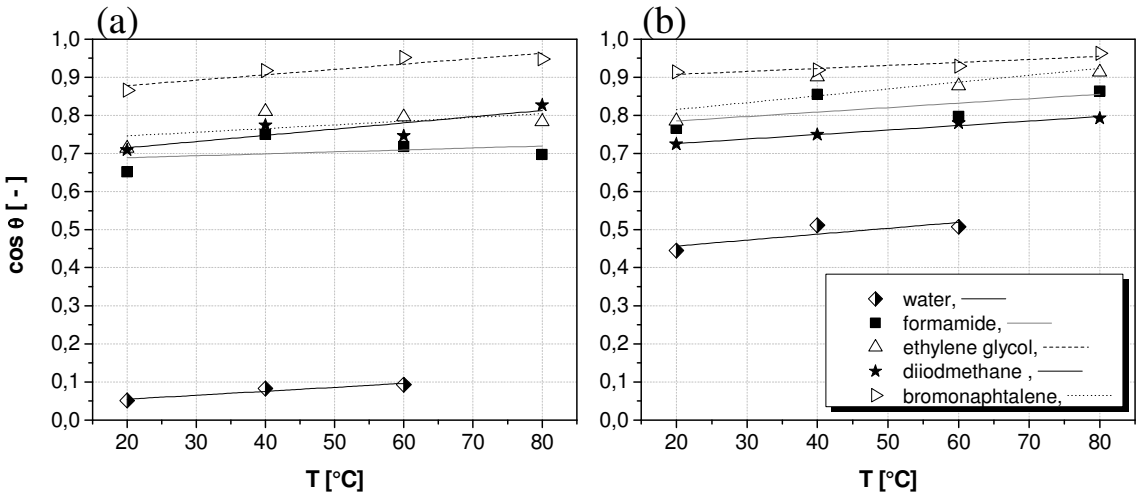

Fig. 4.4. Variation of cos θ with temperature for (a) SS and (b) SICON®

4.1.5 Coating aging: influence on roughness, surface free energy, composition and zeta potential

Roughness

The difference in the roughness induced by coating aging due to fouling/cleaning cycles and handling the coupons (Table 4.11) was statically significant for SS, ESS and SICAN ($p < 0.05$). It should be noted that the SS and ESS substrates as well as the coated coupons came from different charges, expecting a slight variation in their topography. Coated electropolished stainless steel was not tested.

Table 4.11. Influence of surface aging on surface roughness (value after ≥ 9 soiling/cleaning cycles – new surface value)

Surface	$R_{a,used} - R_{a,new}$ [µm]	$R_{z,used} - R_{z,new}$ [µm]
SS	0.02	0.1
DLC	0.003	0.02
SICAN	0.007	0.1
SICON®	0.003	0.02
ESS	0.02	0.1

Surface free energy

Variations in the surface free energy due to fouling and cleaning processes could be observed. The nonpolar and the polar contribution of the surface energy of new and used coatings are compared for the coupons in Fig. 4.5 and for the plates in Fig. 4.6. For the coupons, the nonpolar and the polar parts, and thus also the overall surface free energy, significantly increased, except for SS and EDLC. For the plates, a reduction on the polar part for the SS

and DLC was measured. This probably results from different fouling and therefore cleaning conditions used in the experiments with the coupons and the PHE plates. Fig. 4.7 depicts the influence of fouling and cleaning cycles on the electron donor component γ^- of coupons. A drastic increase of this term can be observed up to 4 cycles (up to 7 cycles for ESICON®), after which the value is nearly constant. The same behavior was observed for the polar part and consequently for the total surface free energy (Figs. 4.8 – 4.9). These results permit to conclude that although the surface energy components changed with use, a stable state was reached relatively quickly. Thus, additional aging effects on deposition in further fouling cycles could be excluded.

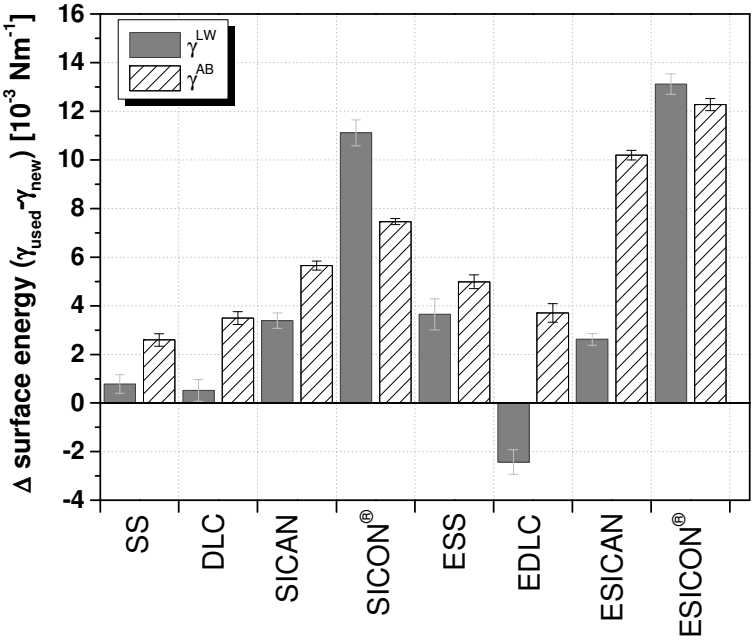

Fig. 4.5. Influence of surface aging on surface free energy properties of the coupons (mean value after ≥ 5 soiling/cleaning cycles – value new surface)

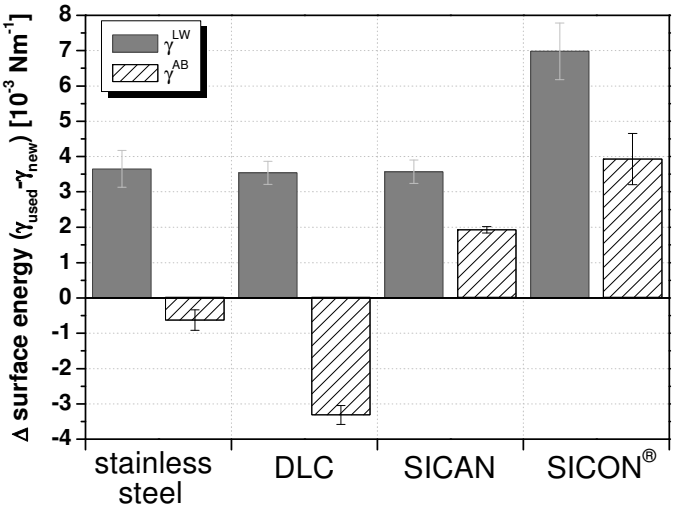

Fig. 4.6. Influence of surface aging on surface free energy properties of the PHE plates (mean value after ≥ 3 soiling/cleaning cycles – value new surface)

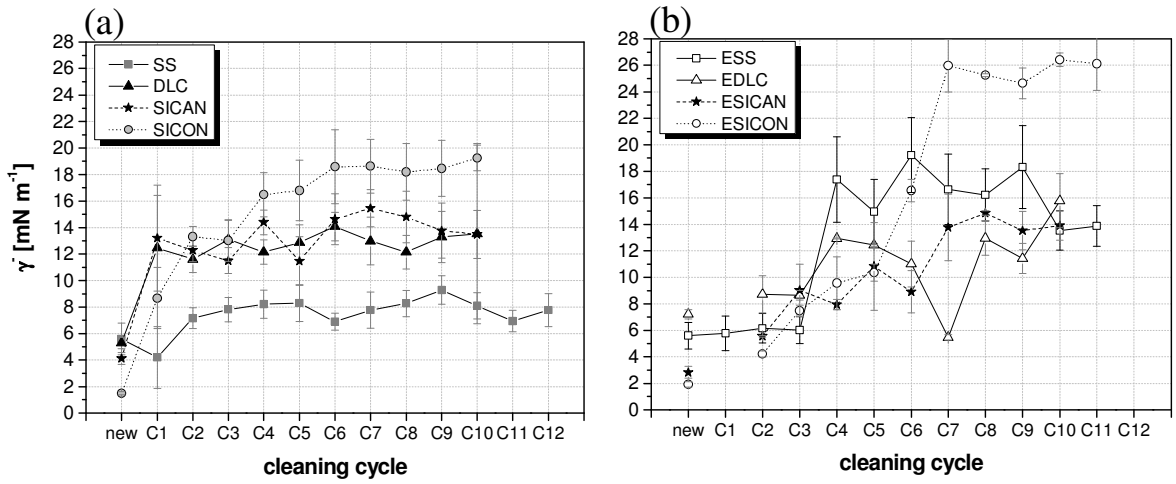

Fig. 4.7. Influence of fouling and cleaning cycles on the electron donor component γ^- of (a) coated SS surfaces and (b) coated electropolished SS surfaces

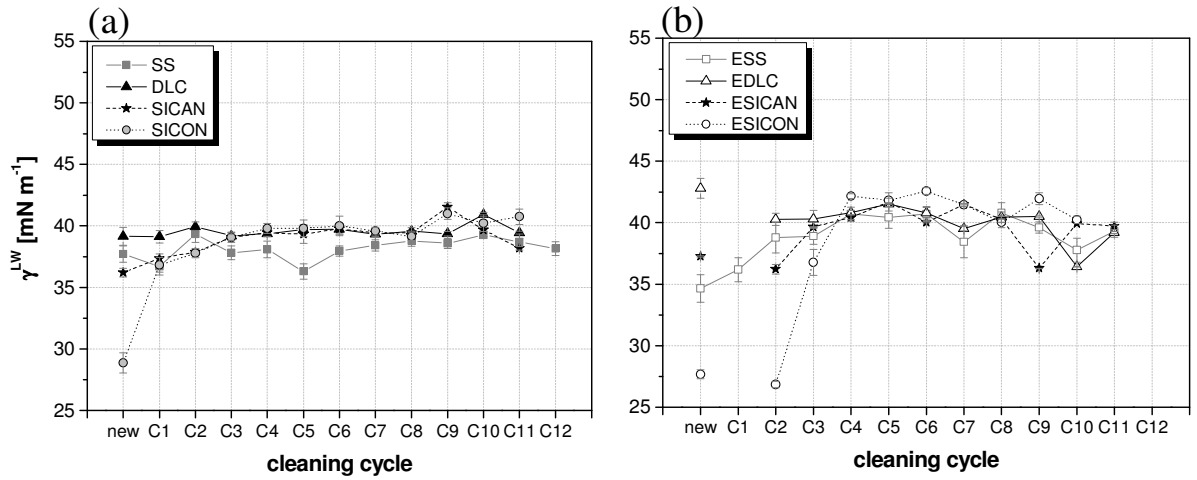

Fig. 4.8. Variation of the LW contribution (van Oss approach) with cleaning cycles for (a) coated unpolished SS surfaces and (b) coated electropolished SS surfaces

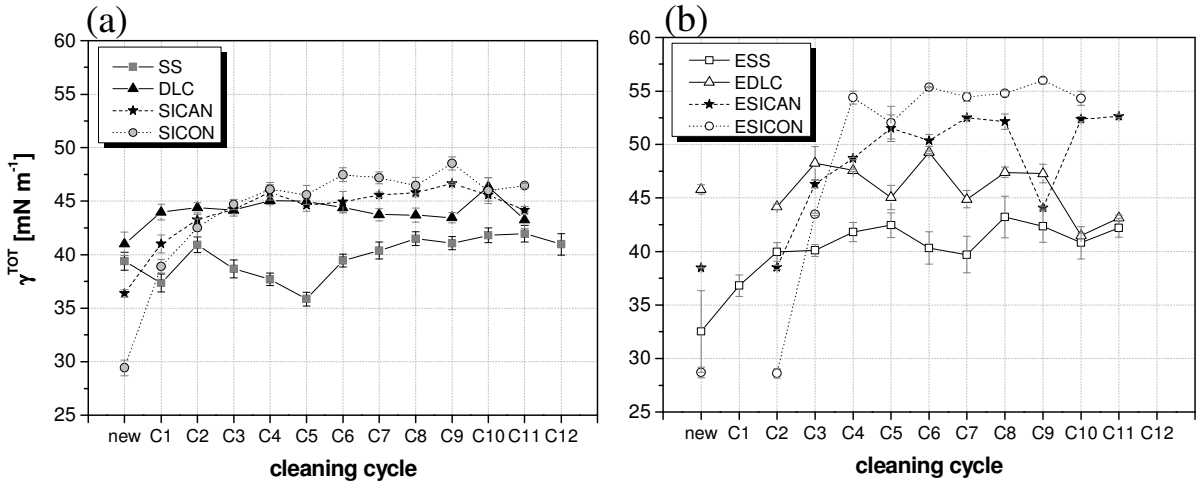

Fig. 4.9. Variation of the total surface free energy (van Oss approach) with cleaning cycles for (a) coated unpolished SS surfaces and (b) coated electropolished SS surfaces

Surface composition

In order to explain the variation on the energetic surface properties, the surface composition was assessed via X-ray microanalysis. Table 4.9 shows the composition of the new and used stainless steel, given in % w/w, while Table 4.10 summarizes the results of the element analysis of the unmodifed and coated coupons, given in % at..

Table 4.9. Composition of new and used stainless steel coupons, given in % w/w

Element	new SS	used SS
C	0.67 ± 0.02	0.68 ± 0.03
N	2.06 ± 0.05	1.98 ± 0.05
O	0.70 ± 0.01	0.72 ± 0.01
Cr	17.35 ± 0.07	18.05 ± 0.07
Fe	62.0 ± 0.2	60.3 ± 0.1
Ni	15.36 ± 0.03	16.3 ± 0.1

The determined chromium content suited the required content of 17.0 to 19.5 % w/w for SS 1.4301 (DIN EN 10027, 2005), while the measured nickel content was above the specified for the type of steel used. For steel, denoted by the number 1.4301, a Ni content from 8.0 to 10.5 % w/w is expected (DIN EN 10027, 2005). The carbon and nitrogen content were also higher than that found in the literature (Boulangé-Petermann et al., 2004; DIN EN 10027, 2005; Informationsstelle Edelstahl Rostfrei, 2006), which values are C ≤ 0.07 % w/w and N ≤ 0.11 % w/w. A difference in the composition between the two coupons is also observed. The used coupon contains 2 % w/w less Fe and about 1 % w/w more Cr or Ni compared to the new one.

By contact with air a passive layer form in chromium-nickel steels. This layer is rich in iron oxide and chromium oxide and is mainly responsible for the corrosion resistance of the respective steels. To enhance the natural resistance to corrosion, surfaces in the food industry are frequently passivated prior to their first use, using an oxidizing acid (e.g. nitric acid) (Maller, 2007). Jin and Atrens (1987) found that the concentration of chromium oxide increases when increasing the duration of passivation, while the concentration of iron oxide decreases. This is partly due to the higher affinity of chromium to oxygen. Furthermore, the authors, as well as Brüesch et al. (1985), observed that chromium molecules diffused during the passivation process from deeper layers to the top, whereby the chromium content reached a maximum followed by a minimum. The resulting spaces were filled, preferably with nickel, in order that a third layer, which is low in chromium but rich in nickel, is formed subsequent to the oxide layer. Moreover, a low oxygen content was detected, confirming that the oxide layer is thin, reaching 1 – 3 nm thick according to Jin and Atrens (1987), compared to the depth of the electron beam penetration, which is about 0.5 – 5 µm (QUANTAX Manual, 2008).

Table 4.10. Composition of new and used stainless steel and coated stainless steel coupons, given in % at.

Element	new coupons				used coupons			
	SS	**DLC**	**SICAN**	**SICON®**	**SS**	**DLC**	**SICAN**	**SICON®**
C	2.8 ± 0.1	89 ± 2	39 ± 1	27.9 ± 0.6	3.4 ± 0.5	89 ± 1	42 ± 1	26.3 ± 0.6
N	7.3 ± 0.2	7 ± 1	1.5 ± 0.2	2.7 ± 0.1	6.2 ± 0.4	5.9 ± 0.7	1.9 ± 0.1	1.8 ± 0.06
O	2.2 ± 0.1	2.1 ± 0.4	0.9 ± 0.1	27.1 ± 0.4	2.6 ± 0.3	2.6 ± 0.2	1.2 ± 0.1	27.8 ± 0.9
Si	--	--	56 ± 1	40 ± 1	--	--	54 ± 1	41 ± 1
Cr	16.5 ± 0.1	1.5 ± 0.4	0.50 ± 0.07	0.74 ± 0.02	16.7 ± 0.4	1.6 ± 0.2	0.49 ± 0.05	1.23 ± 0.04
Fe	55.0 ± 0.3	0.10 ± 0.01	0.38 ± 0.03	0.38 ± 0.04	54.7 ± 0.9	0.09 ± 0.03	0.31 ± 0.04	0.34 ± 0.04
Ni	13.0 ± 0.1	0.15 ± 0.01	0.55 ± 0.04	0.50 ± 0.02	13.7 ± 0.4	0.16 ± 0.04	0.51 ± 0.04	0.51 ± 0.03

Comparing the coating composition of Table 3.1, given by Bewilogua et al. (2011), with the results of Table 4.10, a higher C content was detected for DLC, a higher Si content was measured for SICAN and SICON®, while a higher O content was also detected for SICON via x-ray microanalysis. This is due to the fact that hydrogen, whose concentration is around 15 - 24 % at. on these coatings, cannot be quantitatively detected by this type of analysis, but for example by secondary ion mass spectroscopy (SIMS), which on the other hand is a destructive analysis, disabling the use of coupons in subsequent experiments.

The coating composition was changing in use. SS and SICAN revealed a higher C content, while the N content decreased and the O content increased on all surfaces. Si, Cr and Fe contents were similar for all surfaces after several fouling/cleaning cycles, with the exception of SICON® (higher Cr and lower Fe contents) due to coating damaging/cohesion failure.

To evaluate the measured X-ray spectra, the automatic feature recognition was used. The evaluation by this software decomposed the total measured spectrum into individual peaks. Corresponding to the energy levels, the corresponding elements were assigned. Due to the very similar energy levels of carbon and nitrogen (C: 286 eV and N: 392 eV, QUANTAX Manual, 2008), the two partially overlapping peaks cannot be clearly separated, and thus a reciprocal influence of the measurement results for these two elements must be assumed. Furthermore, the energy level of oxygen emitted radiation is only marginally higher than that of nitrogen, which can result in higher concentrations of these two elements at peak overlap and thus can result in possible measurement error. Another possible source of error in the evaluation of the measured power spectra is known as pile-up peaks, which can occur at twice the energy amount of a main peak and arise from the fact that two very quick successive x-ray quanta with equal energy levels are not processed as separate signals, but rather are taken as one signal. This effect is largely suppressed by a special hardware component (pile-up suppression in backscattering spectrometry), but it cannot be completely avoided in the case of a main peak with a high intensity (QUANTAX Manual, 2008). Therefore, these potential sources of error can explain the C and N contents in new SS coupon and N content in new DLC surface.

The Ca and P composition that could remain on the surfaces or in the grain boundaries after cleaning and could therefore affect the energetic surface properties was measured. The concentration of Ca and P on the new and used surfaces was very low: Ca = 0.08 – 0.14 % at.

and 0.1 – 0.4 % at., respectively, and P = 0.04 – 0.3 % at. and 0.05 – 0.2 % at., respectively. No difference between new and used surfaces could be detected ($p > 0.05$), indicating that the batch-wise cleaning procedure was effective for recovering the fouling layer.

Zeta Potential

The surface aging could also be monitored by zeta potential ζ measurements. Whereas the zeta potential of stainless steel was nearly unchanged in the three model solutions, the zeta potential of the coatings varied. In general, ζ of DLC decreased, except for the surface in contact with WPI (Fig. 4.10). While the ζ of SICAN and SICON® in the model solutions increased after use, indicating thus an alteration of the electrostatic forces between the surface and the fluid.

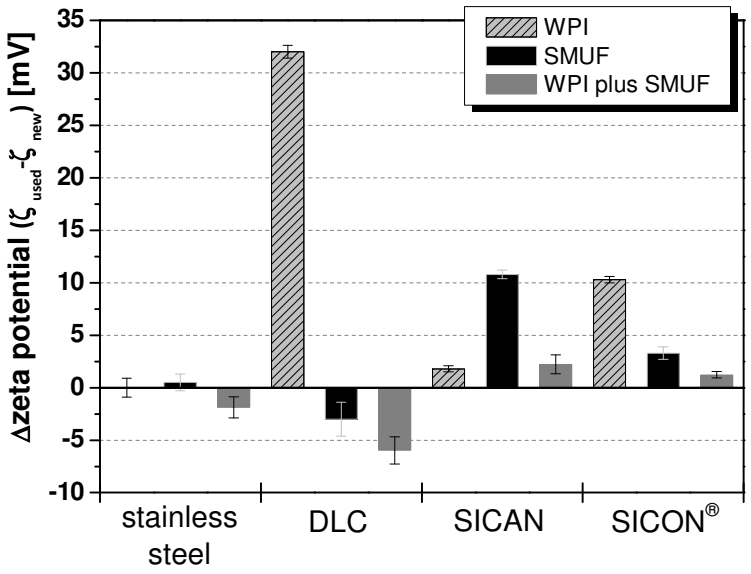

Fig. 4.10. Influence of surface aging on zeta potential of the coupons (mean value after ≥ 5 soiling/cleaning cycles – value new surface) in diverse solutions

The zeta potential of the surfaces in KCl or WPI ranged at the pH of 6.7 negatively from –9 mV to –50 mV, contrariwise the ζ using SMUF or SMUF-rich WPI solution ranged positively from +12 mV to +28 mV (Table A2 in appendix). The magnitude of the surface charge is the result of preferencial adsorption of anions or cations (Altankov et al., 2003). However, according to Hunter (1981), specifically chemically or physically adsorbed ions into the inner or compact part of the double layer can reverse the sign of ζ. This observation can explain the difference of the surface zeta potential sign in the diverse electrolytes (KCl, water or SMUF). Moreover, calcium phosphate starts precipitating at 40 °C at a pH 6.7 (Visser, 1998; Andritsos et al., 2002), and may also have affected the value of the zeta potential. When a particle is sedimenting through a liquid, a continuous flow of ions occurs from the bulk solution into the lower half of the particle double layer. The ions flow around the particle surface and return to the bulk from its upper surface, with the net effect that the sedimenting particles constitute a current in one direction, while the ion flow is a current in the opposite direction (Hunter, 1981).

Coating damage

The damage of the coatings was not expected, because the DLC coatings are referred to as hard and wear resistant (Grill, 1999; Hieke, 2001; Robertson, 2002; Guideline VDI 2840, 2005; see also Table 2.8), as well as corrosion resistant (Maguire et al., 2005; Wang et al., 2008). Moreover, the tribological properties of low surface energy a-C:H:X coatings are still excellent (Grischke et al., 1995). However, structural punctual defects of the coatings could partially be observed in this work, resulting from damaging through chemical cleaning or coating cohesion failure. Despite the surface chemical cleaning before the coating and sputtering with argon, dirt particles from the coating chamber might also be responsible for defects/points of low coating cohesion. Fig. 4.11 shows optical micrographs of new and used SICON® coated SS coupons, whereby the rough coupons proved less resistant to the cleaning procedures, although weaker conditions (concentration and temperature) were used than at the industrial CIP cleaning. Damaged coupons were not used any further. Defects of the coating on the coated electropolished SS coupons and on the coated PHE plates could not be observed.

The preventive characteristic of stainless steel regarding corrosion using DLC-coatings have been widely investigated (Feng et al., 2003; Maguire et al., 2005; Wang et al., 2008; Nam et al., 2009; Azzi et al., 2010). Results have shown that DLC-coatings can improve the corrosion resistance of steel. While DLC itself cannot be corroded, some coating cracks could be observed. Due to the amorphous nature of DLC, the formation of microscale features such as grain boundaries, pinholes or nanopores (ca. 0.5 nm) are unavoidable (Zeng et al. 2002; Maguire et al., 2005). Moreover, DLC coatings produced by physical vapor deposition (PVD) processes are subject to defects including voids, scratches, flaking, cracks and macroparticles in the coating, both at and below the surface. Usually, the corrosion initiated at these microscopic features or defects that lead to the exposure of the metals to the environment and, subsequently, to deterioration in interface adhesion (Zeng et al. 2002; Maguire et al., 2005). To avoid the presence of such features, multilayers are deposited on the substrate (Bewilogua et al., 2011).

No detailed investigation of the variation of the coating properties, such as surface free energy or composition with lifetime (aging), due to chemical and mechanical stress under industrial conditions, has yet been carried out. Hence, the long-term stability of the a-C:H:X coatings on heat exchangers exposure to industrial fouling and CIP cleaning conditions requires further investigation.

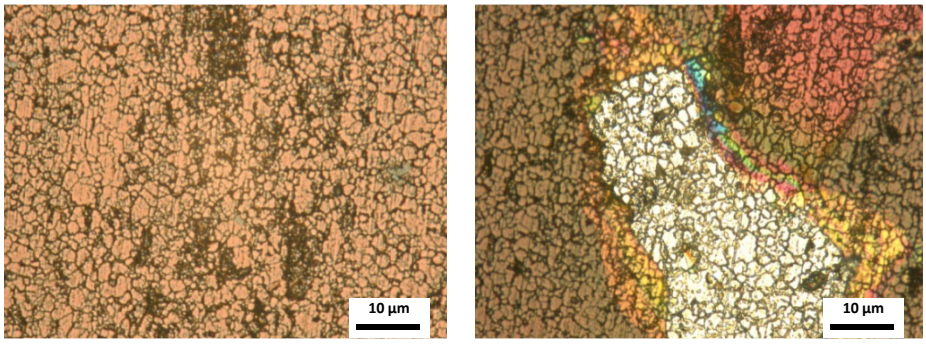

(a) (b)

Fig. 4.11. Micrographs (magnification x 1000) of (a) new and (b) used SICON® coupons

4.2 Fouling of milk components – Initial considerations

This section initially addresses the effect of the model solution and initial surface temperature on the fouling mechanisms in the batch-wise and continuous deposition on stainless steel. Subsequently, the influence of the energetic and topographic surface modifications on batch and continuous fouling and cleaning processes is shown and discussed in further sections.

4.2.1 Batch-wise fouling

The fouling behavior in a batch-wise mode differs from that of a continuous flow in heat exchangers. The flow patterns of four bladed PTB impellers in unbaffled and baffled tanks, as those used for the batch-wise fouling runs in this work (see Fig. 3.2a), have been analyzed using flow visualization techniques complemented with CFD simulation (Kresta and Wood, 1993; Schafer et al., 1998; Derksen, 2001; Kuncewicz and Pietrzykowski, 2001; Chapple et al., 2002; Roy et al., 2010; Roy and Acharya, 2012). Various aspects of mixing in stirred tanks have also been presented in Paul et al. (2004). Accordingly, the fluid dynamics regarding mass and heat transfer in such geometry is well known. Although the impeller Reynolds number ($Re = 1.2 \times 10^4$) in the batch apparatus was in the lower turbulent flow range for stirred tanks ($Re > 1 \times 10^4$) some deposit removal could be observed during the fouling. This phenomenon was particularly observed for the SMUF deposition (which will be discussed later, in section 4.3.2). This occurs when the fluiddynamic forces, tending to disrupt the deposit, are higher than the adhesive and cohesive forces of deposit. In other words, adhesive bonds of the fouling deposit to the heat transfer surface or its internal cohesiveness were sufficiently weak that particles of deposit could be swept away by the turbulent burst/shear forces.

Since the bulk temperature was maintained at 50 °C, i.e. below the denaturation temperature of β-lg (ranging from 70 °C to 74°C), it was expected that no β-lg aggregates form in the bulk. However, the solution nearby the heated surface can reach the temperature required for denaturation. Thus, the protein can unfold and/or denatures in the boundary layer and either adsorbs on the surface or adsorbs on the surface and denatures there. According to Foster et al. (1989) and Foster and Green (1990), who studied the fouling behavior of milk in a batch apparatus, insoluble material could only be generated directly on to the heated surface and almost all of this insoluble material adhered to the surface. Fig. 4.12 depicts the possible pathways of the adsorption of β-lg on the heat transfer surface. According to Itoh et al. (1995) and Blanpain-Avet et al. (2012), although the aggregation of β-lg molecules can occur near the surface, these aggregated molecules hardly adsorbed on the surface. The adsorption of β-lg in batch at an elevated temperature occurs preferentially by aggregation of denatured protein at the surface (Itoh et al., 1995).

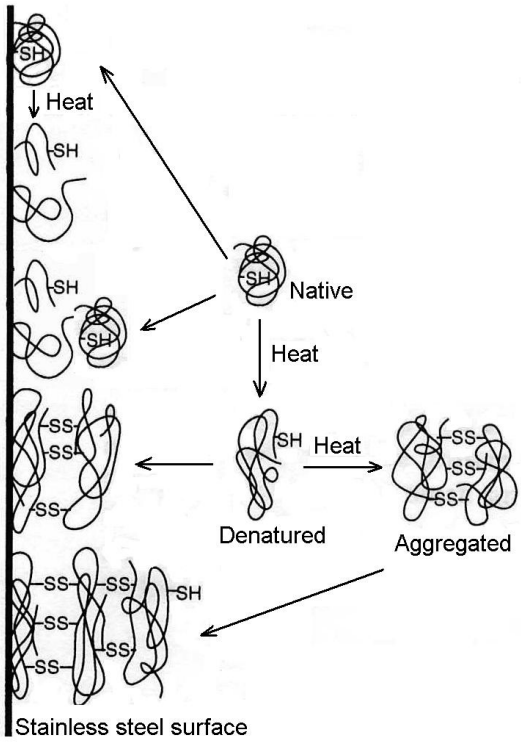

Fig. 4.12. Schematic illustration of β-lg adsorption in the batch apparatus (adapted from Itoh et al., 1995)

Calcium phosphate starts precipitating from a SMUF solution at a pH 6.7 and at a bulk temperature of 44 °C (Rosmaninho and Melo, 2006a). Hence, once the three SMUF stock solutions were mixed together, the pH value was adjusted and the initial surface temperature reached 80 °C, calcium phosphate can precipitate on the heated surface, promoting fouling or in bulk (in the boundary layer). Since the particles precipitated in bulk were not removed, calcium phosphate fouled as result of a local supersaturation, as well as due to the attachment of particles to the surface. Fig. 4.13 shows calcium phosphate structure formed on stainless steel after 360 min deposition, which resembles the thermodynamically more stable phase hydroxyapatite.

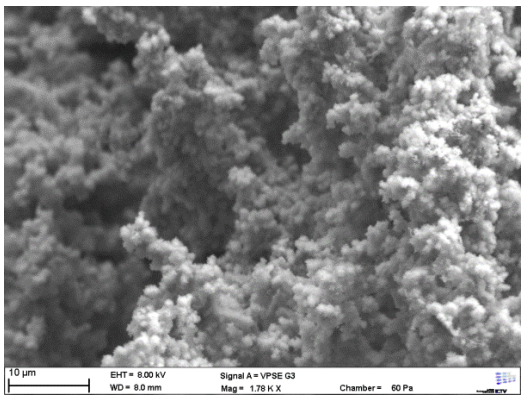

Fig. 4.13. Hydroxyapatite structure on stainless steel

Insoluble material in bulk (aggregated protein or calcium phosphate particulate) can also build up directly on to the surface by re-entrapment into the fouling layer. Therefore, the fouling mechanism primarily depends on the protein denaturation and the calcium phosphate crystallization kinetics during heating, as well as the thermodynamics of the intermolecular interactions. In the batch apparatus, the fouling progress is dominated by reaction of the fouling constituents in the boundary layer. Subsequent adhesion and deposition to the surface occurs due to thiol/disulphide intermolecular interactions, van-der-Waals or electrostatic interactions of the fouling constituents with the surface or already deposited protein or calcium phosphate. The absence of milk salts or whey protein was responsible for the formation of deposits with completely different morphology and deposit amount, as shown in Fig. 4.14. While the whey protein deposit seemed transparent (at T_0 = 80 °C) or opaque (at T_0 = 120 °C) and was firmly adhered to the surface, the deposit of SMUF was white, porously and powdery/pulverous. The deposit from the SMUF-rich whey protein solution was a mixture of both deposit types, namely proteinaceous and crystalline. The effect of the surface temperature on the fouling process was a crucial parameter (cp. Fig. 4.14 a-b, Fig. 4.14 c-d and Fig.4.14 e-f as well as Figs. 4.15 a-b) and was more distinctive when milk mineral components were present.

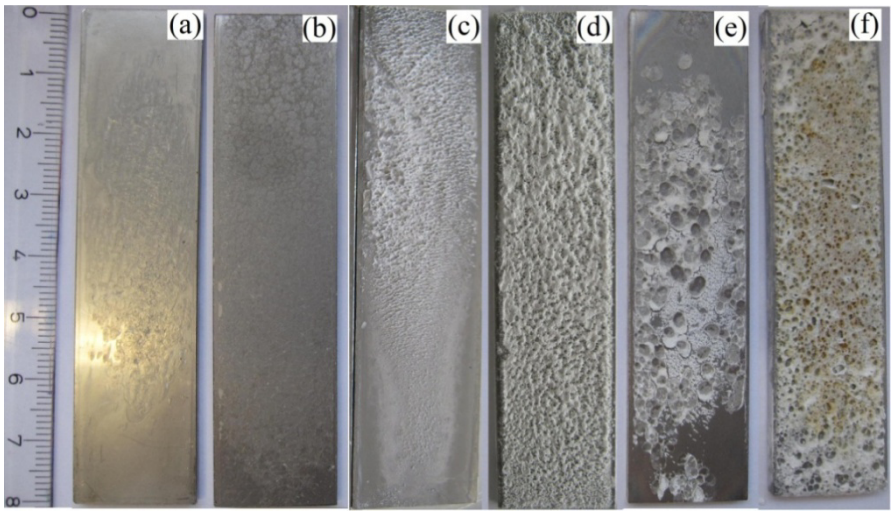

Fig. 4.14. Typically dry deposit on stainless steel formed from (a) WPI at T_0 = 80 °C, (b) WPI at T_0 = 120 °C, (c) SMUF at T_0 = 80 °C, (d) SMUF at T_0 = 105 °C, (e) WPI plus SMUF at T_0 = 80 °C and (f) WPI plus SMUF at T_0 = 120 °C

The presence of bubble-like structures was characteristic for the whey protein and the WPI plus SMUF deposits at initial surface temperature T_0 = 120 °C. Given that the stirred tank was operated at atmospheric pressure, there was the formation of the vapor phase at the heat transfer surface due to the superheating. Surface temperatures of 150 – 172 °C and 195 – 230 °C were achieved by the deposition of WPI after 360 min and by the deposition of WPI plus SMUF after 90 min, respectively. Furthermore, the temperature difference between the heat transfer surface and the liquid was very high (ΔT ranged from 30 K to 80 K), corresponding to a high heat transfer coefficient that favors the bubble formation/boiling. The

interface solid-liquid-gas and the bubbles dynamic (formation, growth and released of the vapor phase by boiling) have a profound effect on deposit morphology (Bott, 1995) and can influence fouling in unexpected ways (Lund and Sandu, 1981). Fryer and Slater (1984), Jeurnink (1995b) and Jeurnink et al. (1996a) reported that milk fouling is enhanced by the nucleation of air/vapor bubbles at the heating surface of heat exchangers or evaporators, due to local increase in milk protein concentration.

Adsorption of protein and ions to the surface starts immediately, including at low temperature (25 °C), although further deposition depends on the protein denaturation and the presence or absence of calcium and phosphate ions (compare fouling curves for WPI and WPI pus SMUF in Fig. 4.15; interactions with lactose or fat can be neglected since the content of both components in WPI is lower than 0.2 mg g^{-1}). The concentration of native, denatured and aggregated protein in the bulk will change over time, particularly for the wall temperature T_0 = 120 °C (ΔT = 70 K) in which the formation of aggregates could be measured (Figs. 4.14a and A1b for WPI and Figs. 4.14b and A2b for WPI+SMUF). As previously discussed, the bulk temperature was maintained constant at 50 °C and at this temperature the native β-lg (precursor of the unfolded β-lg) is thermally stable. Therefore, protein denaturation could only take place in the thermal boundary layer.

However, at relatively high temperature difference between wall and bulk (ΔT = 30 K), no formation of additional large aggregates could be detected for the experiments at T_0 = 80 °C (Figs. 4.14a and A1a for WPI and Figs. 4.14b and A2a for WPI+SMUF). In the absence of calcium phosphate, no fouling growth could be observed at this initial wall temperature and the fouling resistance was around zero (Fig. 4.15a). The same behavior was observed for the WPI deposition on pre-conditioned surfaces (which will be discussed later, Fig. 4.36). This confirmed that the fouling rate in batch-wise experiments was mainly dependent on the boundary layer and surface reactions.

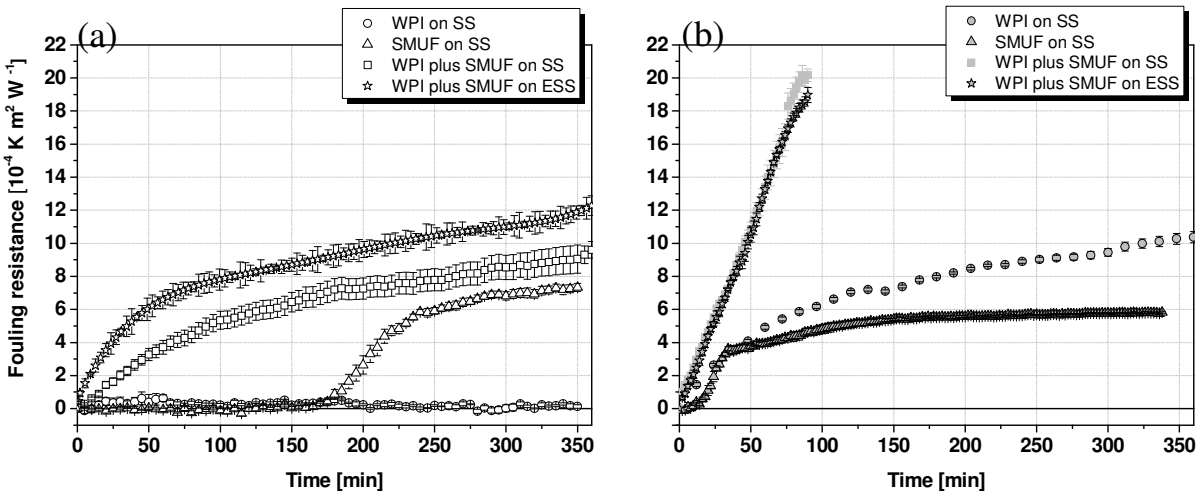

Fig. 4.15. Fouling resistance for WPI, SMUF and WPI plus SMUF at (a) T_0 = 80 °C, (b) T_0 = 120 °C (105 °C for SMUF)

In order to understand the deposition mechanisms, samples of the bulk solution were taken over time and protein content and particle size were determined. In the 2.5 L bulk solution, there were 33.6 g of solids (protein + salts, viz. WPI + SMUF), ~ 0.32 g deposited on the two plates (at T_0 = 120 °C, ~ 200 g m^{-2} mass, see Table 4.21), i.e. 1 % of solids attached to the surface. Therefore, the change of the composition and concentration was negligibly low. This result is in accordance with findings in the literature showing that the mass of β-lg in deposits was very low compared to the overall mass of β-lg in the fouling solution (Petit et al., 2013). The total protein concentration in bulk was almost constant during the fouling experiments, as shown in Fig. 4.16. However, a reduction in particle size was observed at T_0= 80 °C, possibly due to the reassociation of the protein in dimeric or monomeric form. Moreover, at T_0 = 120 °C a slight increase in particle size due to the formation of protein aggregates was detected, particularly for the SMUF-rich WPI solution (Fig. 4.16b). This means that the protein structure/conformation changed in the solution, although the solution did not deplete on protein due to the deposition. Furthermore, the results indicated that the salts in SMUF were responsible for inducing detectable protein aggregation in bulk, as observed by Mounsey and O'Kennedy (2009), at least at T_0 = 120 °C and that protein aggregates formed on thermal boundary layer were almost attached to surface, as also suggested by Foster and Green (1990) in a batch-wise apparatus. Denaturation/aggregation levels of 70 and 50 % were evident in batch-wise heating (78 °C/10 min) of β-lg in SMUF and 2 x SMUF, respectively, at constant pH of 6.7 (O'Kennedy and Mounsey, 2009), although not or less detected at SMUF solutions without pH adjustment, as in this study.

Tolkach and Kulozik (2007) discourage the use of on-line monitoring of whey protein denaturation reaction by particle measurement, since the existing techniques can only assess the aggregation, yet cannot distinguish between native and partially unfolded states of β-lg molecules. Blanpain-Avet et al. (2012) could not detect aggregates on whey protein deposits. The observations of above works could further explain why the formation of protein aggregates was not measured in the batch-wise experiments.

The composition of minerals in the solution (especially Ca and P) was not recorded.

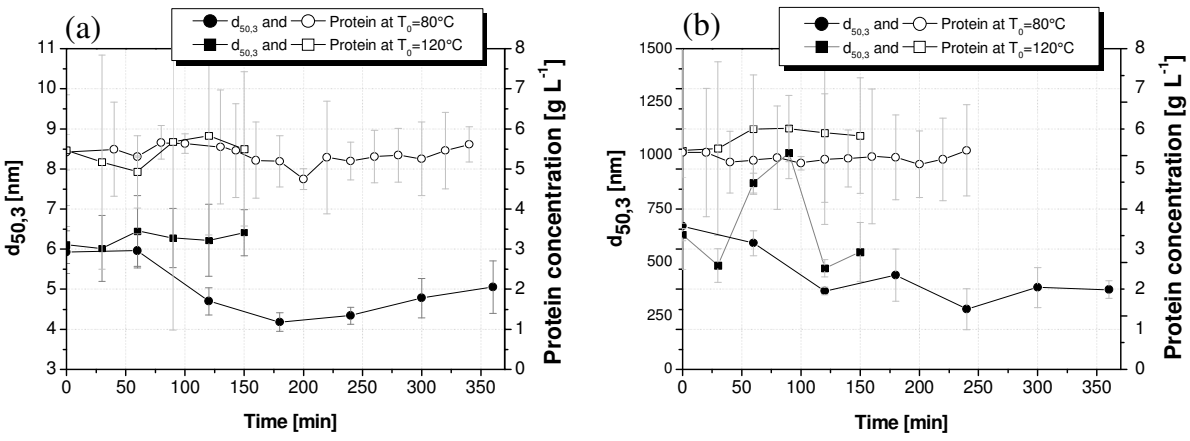

Fig. 4.16. Particle size and protein concentration of bulk solution for fouling at a wall temperature of T_0 = 80 and T_0 = 120 °C of (a) WPI and (b) WPI plus SMUF

Figs. 4.17 and 4.18 compare deposits of SMUF, whey protein, whey protein on surfaces pre-conditioned with SMUF (WPI/SMUF), as well as whey protein plus SMUF on unpolished and electropolished stainless steel at initial surface temperatures of 80 °C (Fig. 4.17) and 120 °C (Fig. 4.18) after 30 min deposition. Fouled coupons shown in Figs. 4.17 and 4.18 were dried as described in section 3.3.1 and sputtered with gold for high resolution at SEM. Further information about the deposition mechanisms on the coated surfaces will be discussed in the next sections.

At T_0 = 80 °C, small spherical calcium phosphate crystals (1 - 5 µm in size), grape of particles and agglomerates of amorphous calcium phosphate could be observed. The crystals seem to be uniformly distributed on the surface in the SMUF and the WPI/SMUF deposits on SS, as well as the WPI plus SMUF deposits on SS and ESS (Figs. 4.17 a, c, d, h). In contrast to the SMUF and WPI/SMUF deposits formed on the ESS, calcium phosphate crystals were found as discrete clumps non-uniformly spread throughout the surface (Figs. 4.17 e, g). On both stainless steels, a thin transparent protein layer located in particular areas (Figs. 4.17 b, f) was formed. On the surface soiled with salts (WPI/SMUF), the protein adhered to this first layer (slight increase of the fouling resistance, see Fig. 4.38), although the layers did not grow further. Moreover for the SMUF rich-whey protein model solution, calcium ions form bridges between the adsorbed proteins and native proteins in bulk or unfolded proteins near to the wall and therefore the deposit builts up further. On the ESS, the spherical crystals were again clearly noticeable, while on SS they failed first on the grain boundary and were thus less visible (Figs. 4.17 d, h).

The roughness projections provide additional sites for nucleation, adsorption and chemical surface activity, while the grooves provide regions for deposition that are sheltered from the bulk velocity (Epstein, 1981; Bott, 1995). Comparing the surface area ratio of SS and ESS, S_{dr} = 1.0 % and S_{dr} = 0.03 %, respectively, it is clear that a rougher surface has more interfacial area available for the attachment. Surface roughness also reduces the thickness of the viscous sublayer and hence increases eddy transport to the wall (Epstein, 1981; Bott, 1995). However, whey protein aggregates (size: 5 – 30 µm, Petit et al., 2013 and Ndoye et al., 2013; size: 40 – 100 nm, Zúñiga et al., 2010) and calcium phosphate agglomerates (size: 0.1 – 0.25 µm, Rosmaninho et al., 2003; size: 40 – 80 nm, Dey et al., 2010) must diffuse into the grains before adhering therein, as schematically shown in Fig. 4.19. Therefore, the attachment of protein aggregates and calcium phosphate particles and agglomerates is probably more prone on a smooth than on a rough SS surface. On the other hand, native (size: 1 nm – 10 nm, Table 2.1) and unfolded protein clusters (size: 50 – 60 nm, Jimenez et al., 2013) and Ca and P ions or clusters (size ~ 1 nm, Table 2.1) can easily attach to a rough surface because of their size and they will firstly deposit in grain or grain-boundary (for SS surfaces: S_z ~ 1.5 – 2 µm and S_a ~ 130 – 190 nm, for ESS surfaces: S_z ~ 0.5 – 1 µm and S_a ~ 40 – 50 nm). These observations can explain the distribution of particles or agglomerates of calcium phosphate on the SS and ESS surfaces as well as the higher fouling resistance on SS than on ESS (see Fig. 4.15b and Fig. 4.36 for WPI after 30 min in SMUF, which will be discussed later).

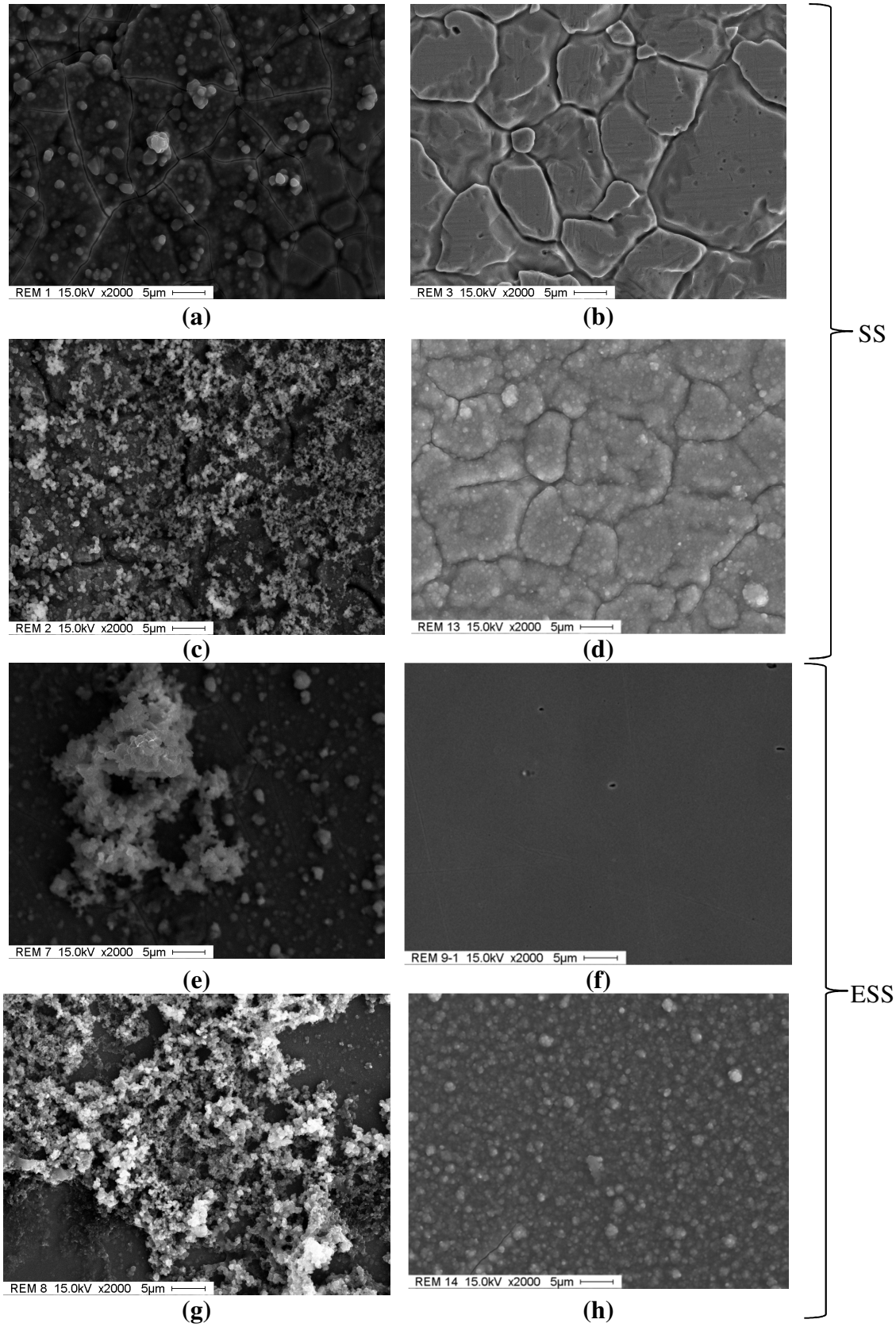

Fig. 4.17. Scanning electron micrographs of (a) SMUF, (b) WPI, (c) WPI after 30 min in SMUF and (d) WPI plus SMUF deposits on unpolished stainless steel at T_0 = 80 °C as well as (e) SMUF, (f) WPI, (g) WPI after 30 min in SMUF and (h) WPI plus SMUF deposits on electropolished stainless steel at T_0 = 80 °C.

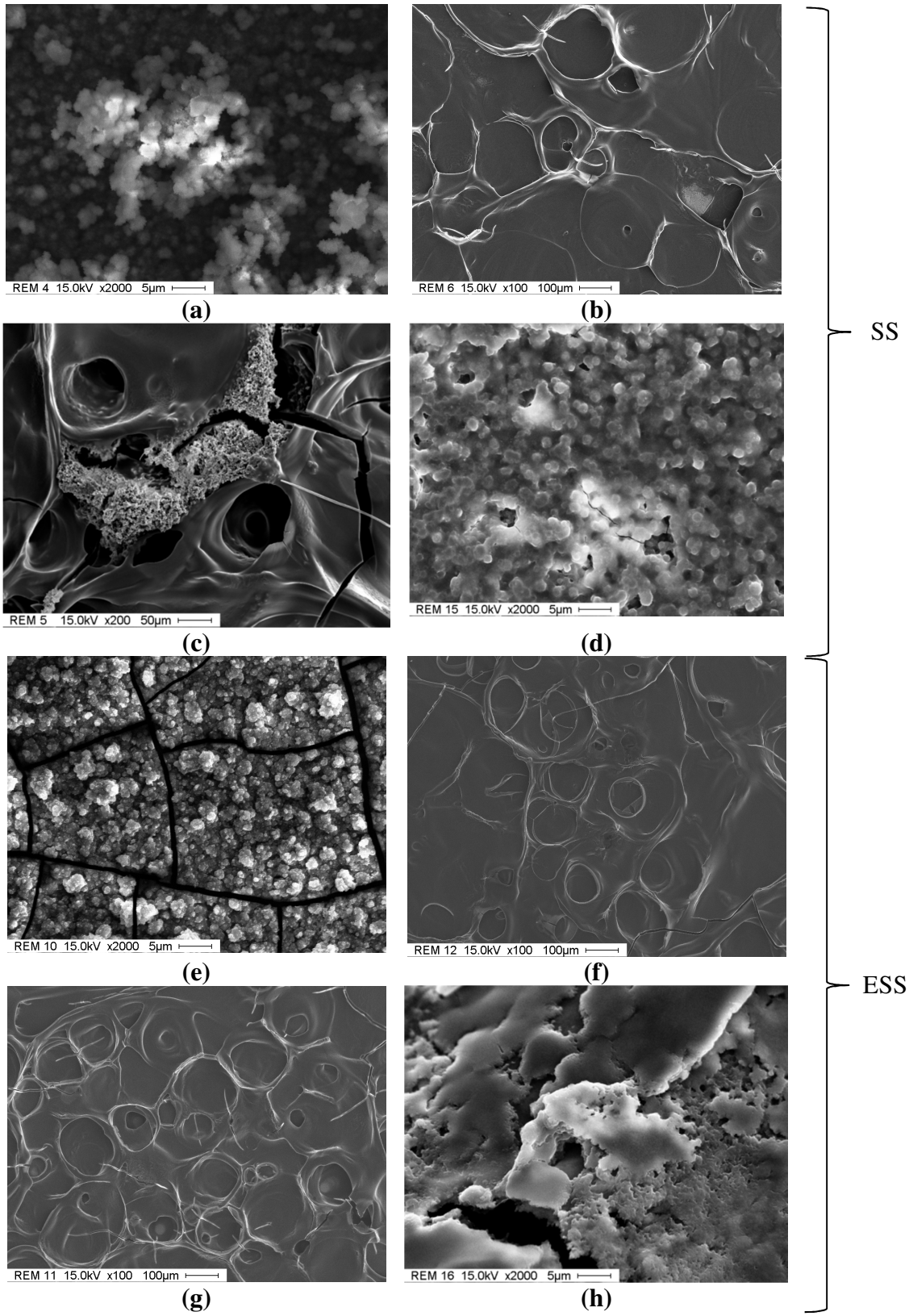

Fig. 4.18. Scanning electron micrographs of (a) SMUF, (b) WPI, (c) WPI after 30 min in SMUF and (d) WPI plus SMUF deposits on unpolished stainless steel at T_0 = 120 °C as well as (e) SMUF, (f) WPI, (g) WPI after 30 min in SMUF and (h) WPI plus SMUF deposits on electropolished stainless steel at T_0 = 120 °C

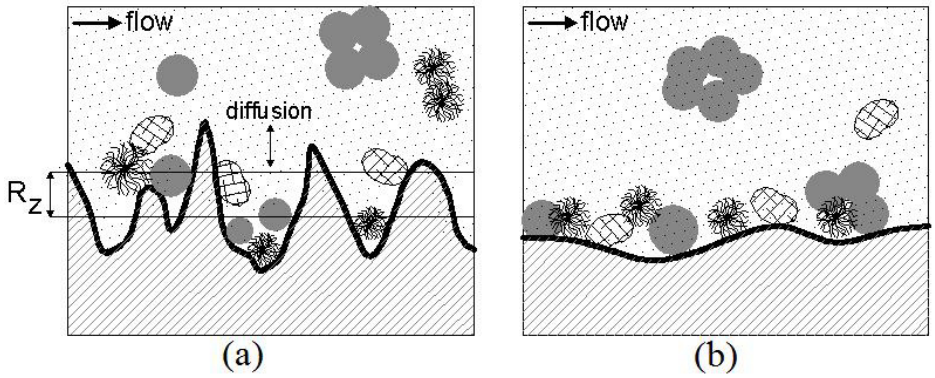

Fig. 4.19. Initial stages of deposition of a calcium phosphate-rich whey protein solution on (a) unpolished and (b) electropolished surface. ● native and ✺ denatured β-lg, · calcium phosphate ions, ⊗ calcium phosphate aglomerates

At T_0 = 120 °C, a compact fouling layer with no discernible aggregates was formed for all model solutions, covering the surface uniformly. For this reason, the micrographs for WPI und WPI/SMUF (Figs. 4.18 b, c, f, g) are shown at a lower magnification (scale: 50 – 100 µm). A significant difference of the deposit morphology can be seen at this wall temperature. On SS, agglomerates of calcium phosphate were present, while on ESS the deposit was broken away from the surface. For WPI, the polymerizing of the protein occurred on the surfaces due to the high wall temperature (Figs. 4.18 b, f). The WPI/SMUF and WPI plus SMUF deposits on SS showed a similar structure to that at T_0 = 80 °C, in which mineral fouling is entrapped in the protein matrix (Figs. 4.18 c, d). However, the WPI/SMUF and WPI plus SMUF deposit on ESS (Figs. 4.18 g, h) seemed to be more proteinaceous, as confirmed by chemical analyses (see Table 4.21).

4.2.2 Fouling at continuous flow conditions

For the fouling under continuous flow conditions, the fouling was controlled by mass transport of foulants from bulk to the heat transfer surface, as well as their adhesion or re-entrapment into the fouling layer (deposition) and erosion of deposited protein or minerals from fouling layer back into the bulk (removal) (Boxler et al., 2014a).

Fouling experiments were performed in recirculation mode through the plate heat exchanger PHE1 in a closed loop for 120 min, while continuous processing is performed without recirculation in the dairy industry. Without recirculation with a continuous feeding at the PHE inlet, there is a constant supply of fluid entering the PHE, unlike in the recirculation mode, for which the concentration of native β-lactoglobulin in the bulk fluid gradually decreases over time. Therefore, the fouling mechanism and the fouling layer build-up (involving unfolded or aggregated protein) are likely to differ in the presence or absence of product recirculation. With a recirculation, the formation of β-lactoglobulin aggregating in the bulk fluid is promoted due to the higher residence time in the closed loop, which promotes a fouling layer involving primarily denatured and aggregated β-lactoglobulin. However, without recirculation, native, unfolded, denatured, as well as aggregated β-lactoglobulin can

form fouling. If the bulk and the boundary layer temperature are sufficiently high for protein unfolding, denaturation and aggregation, all these protein stages might contribute to deposit formation.

According to Petit et al. (2011), 90 % of β-lactoglobulin from a solution containing 53.3 g L^{-1} of β-lactoglobulin and 264 mg L^{-1} of Ca denature at a bulk temperature of 80 °C – 90 °C in 2 – 5 min, while at 70 °C the process take more than 30 min. By heating the same foulant solution in a plate heat exchanger from the temperature of 60 °C – 70 °C to 85 °C – 95 °C with a residence time ranging between 37 s and 76 s and different heating rates (heat effectiveness, defined as $(T_{P,out} - T_{P,in})/(T_{SS,in} - T_{P,in})$, of 75 – 98 %), Petit et al. (2013) found a β-lg denaturation level of 80 – 100 % after the heat exchanger. The holder (residence time of 102 to 210 s) allowed completing the protein denaturation and enhancing aggregate growth (50 – 60 % of the final aggregate size) (Petit et al., 2013). In this work, the model solution, which contained 30 g L^{-1} β-lactoglobulin and 400 mg L^{-1} Ca, was heated with a heat effectiveness of 92 % from 62 °C to 85 °C along the PHE1 patterns in 4.8 s, see Fig. 3.3. Since the residence time was lower than in the works of Petit et al. (2013), yet the proportion of Ca to protein in the solution was higher (Petit et al. (2013): Ca/β-lg = 0.5 % w/w; this work: Ca/β-lg = 1.3 % w/w), it is difficult to say by comparison of the operation conditions whether an almost complete protein denaturation in PHE1 took place. Note that the higher the residence time, the higher the level of protein denaturation (Petit et al., 2013), while the effect of the Ca concentration on β-lg denaturation depends on the type of calcium salt added to the solution (Petit et al. (2013): $CaCl_2$; this work: SMUF) and on the final ionic strength (O'Kennedy and Mounsey, 2009).

The average residence time of the fuild between exit of PHE1 and re-entrance to the supply tank T1 was about 8 s. Within this time the fluid is cooled from exit temperature of PHE1 of 85 °C to 62 °C. At this temperature level (between 60 °C to 70 °C), β-lg unfolds reversibly and forms the "molten globule" state (Tolkach and Kulozik, 2007). Hence, it can be supposed that β-lg in unfolded, "molten globule", denatured and aggregated states in different concentrations contributed to the formation of the fouling layer in PHE1.

In relation to crystallization fouling, calcium phosphate particulates would already be present in the bulk solution, which became turbid at the PHE1 entrance temperature (= 62 °C). Therefore, calcium phosphate fouls as a result of local supersaturation, as well as due to the attachment and removal of particles from the surface or fouling layer.

4.2.3 Zeta Potential of whey protein in WPI and SMUF-rich WPI solutions and adsorption of WPI on stainless steel particles

The zeta potential of WPI and denatured WPI, SMUF-rich WPI solution and WPI denatured in a stainless steel particles suspension is discussed in the following.

For the SMUF-rich WPI solution, no hysteresis on zeta potential from pH 3 to 9 and pH 9 to 3 could be identified (Fig. 4.20). However, for WPI in water, the zeta potential progress depended on the direction of pH adjustment, such that the difference was slight, an average of zeta potential was built and the mean zeta potential for whey protein and SMUF-rich whey protein solutions at 25 °C and 50 °C and the corresponding particle size are given in Figs. 4.21 and 4.22, respectively. O'Kennedy and Mounsey (2009) observed a larger difference on zeta potential profile of combined β-lg and α-la dissolved in water and in a

$CaCl_2$ + KH_2PO_4 solution by titration from pH 5 to 7, and vice versa. According to the authors, a mechanism to explain this difference is unknown. However, the effect of pH in the range 5 – 7 on the zeta potential of the combined β-lg and α-la dissolved in water and in the $CaCl_2$ + KH_2PO_4 solution, which varied from +1 mV to –20 mV and from +1 mV to –10 mV (O'Kennedy and Mounsey, 2009), respectively, was very similar to the data shown in Fig. 4.20a or Fig. 4.21. The zeta potential curves are also consistent with the results from Ly et al. (2008) for WPI dissolved in water. The shape of the ζ – pH plot (Fig. 4.21) clearly indicates the significance of the H^+ and OH^- ions and the ionic strength in determining the state of the whey protein surface charge and protein stability. The zeta potential varied from –30 mV to +25 mV in the pH range 3 to 9. From pH 3 to the isoelectric point (IEP), higher zeta potentials were measured at lower temperatures. Up to a pH value of 4, the influence of the temperature was only slight. At higher ionic strength, the shielding of the charge becomes strong and the double layer more compressed (Application Note MRK379-01, 2005), thus reducing the electrostatic repulsion between two molecules. Therefore, the zeta potential of SMUF-rich WPI solution was lower than WPI. The results are consistent with those of Mounsey and O'Kennedy (2009), who verified an increase in zeta potential as well as particle size (Fig. 4.22, which will be discussed below) when pure β-lg was dissolved in water and SMUF.

The magnitude of the zeta potential at pH 6.7 and temperature of 50 °C (pH and bulk temperature used by the fouling experiments) indicates the stability of the dispersion. The zeta potential of WPI was reduced in negative charge from a value of –26 mV in water to a value of –10 mV in SMUF (Fig. 4.21). Indeed, similar values were obtained by Mounsey and O'Kennedy (2009).

Close to the isoelectric point (ζ = 0 mV), which was pH = 4.6 for WPI and pH = 4.8 for WPI plus SMUF (IEP of whey proteins = 4 – 5, Walstra et al., 1999), the system is more instable and thus larger particle size was measured due to protein aggregation (Fig. 4.22). Furthermore, larger particles were detected at 25 °C compared to 50 °C.

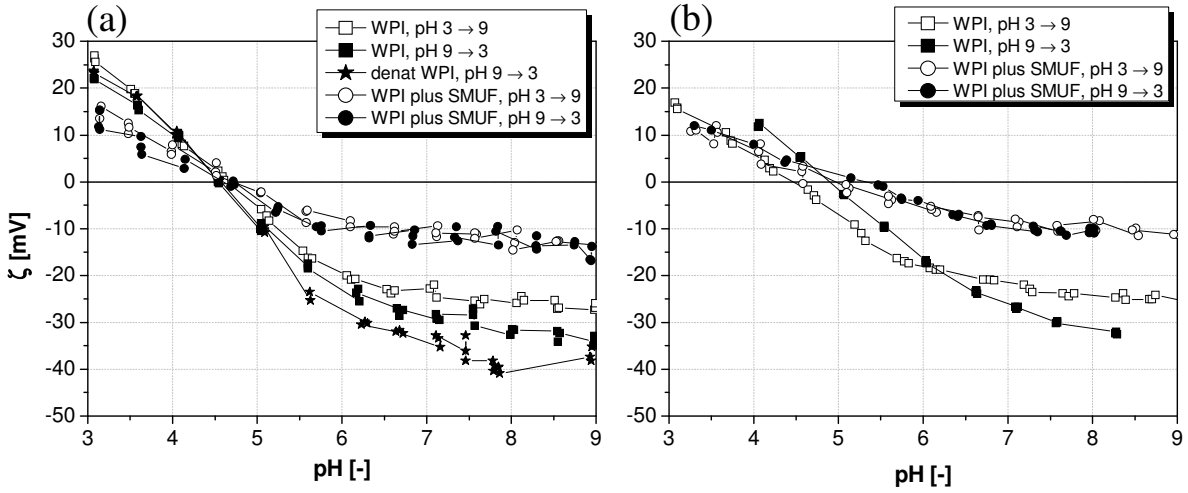

Fig. 4.20. Zeta potential of WPI dissolved in water or in SMUF at (a) 25 °C and (b) 50 °C

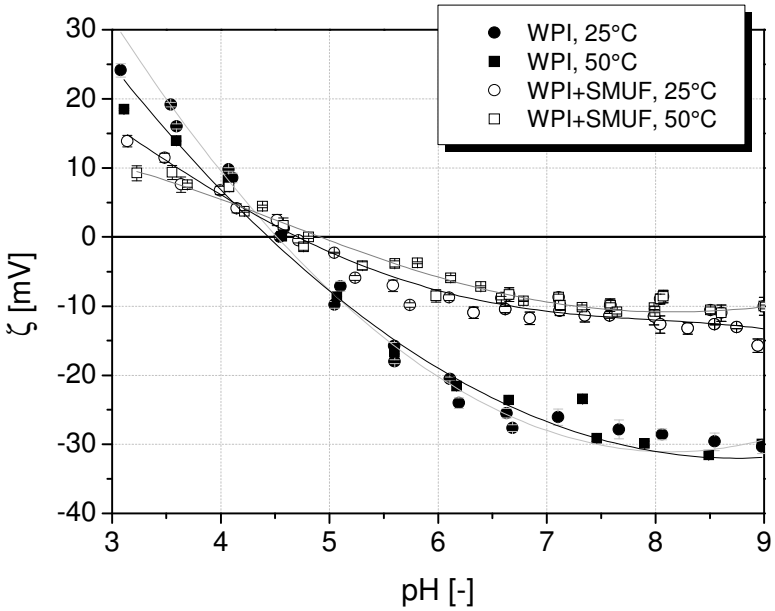

Fig. 4.21. Zeta potential of WPI in water and WPI plus SMUF at 25 °C and 50 °C

WPI had an average hydrodynamic diameter of 4.7 ± 0.1 nm for pH between 6.0 and 7.0, which is coherent with data in the literature. Martínez et al. (2009) obtained a particle size of 6 nm for native β-lg and Zúniga et al. (2010) an average diameter of 6.7 nm for native β-lg, as well as an average size of 42 – 92 nm for β-lg aggregates at pH 6.0 to 6.8. The average hydrodynamic diameter of WPI increased to 275 ± 45 nm for pH between 6.0 and 7.0 when dispersed in SMUF, which is indicative of protein molecules' association under increased ionic strength.

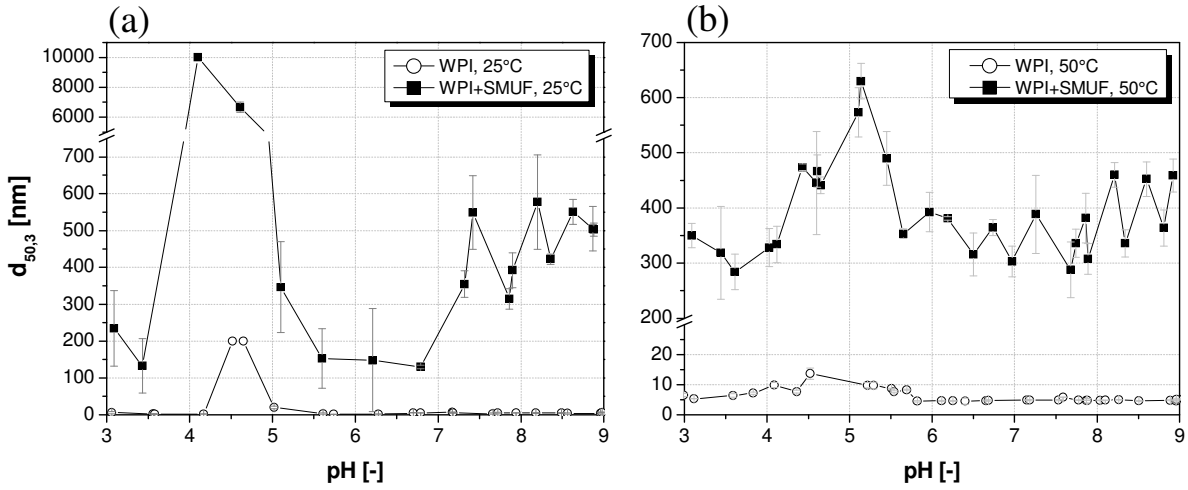

Fig. 4.22. Average hydrodynamic diameter with pH at (a) 25 °C and (b) 50 °C

Fig. 4.23 shows the zeta potential of WPI, denatured whey protein, stainless steel particles and denatured whey protein plus stainless steel particles in 10^{-3} mol L^{-1} KCl solution. (Lines are shown to guide the eye and do not represent modelling results). The zeta potential

of denatured and adsorbed protein in SS particles varied in the range of –50 mV to +30 mV, while the ζ of denatured protein was similar to the unheated WPI in water, ranging from –30 mV to +20 mV. For untreated WPI in KCl, the zeta potential changed only slightly with pH, particularly after the IEP. The likely explanation for this behavior can be found in the balance between the specific ionic binding to the protein surface and its preferential hydration by the solvent (Unterhaslberger et al., 2006), which in this case prevailed due to the low concentration of ions in the solution. The IEP of native or denatured whey protein with or without the SS particles in suspension was around 5, higher than the IEP in water, while the IEP of the SS particles was about 3.8. The IEP of the β-lg for the two variants, β-lg A and β-lg B, in 0.1 mol L^{-1} KCl is around 5.3 (O'Kennedy et al., 2006).

As seen in Fig. 4.23, the denatured whey protein in SS particles showed the higher ζ across the whole pH range. Indeed, at a pH of 6.7, the same as in the fouling experiments, the zeta potential was about – 40 mV, viz. the adsorption of whey protein onto stainless steel at this pH is very favorable and the protein will probably not desorb. This indicates that the denaturation and adsorption of whey protein in SS particles generated a suspension more stable than the suspension of SS particles or denatured WPI alone, and that protein fouling on SS was thus a favorable and irreversible process.

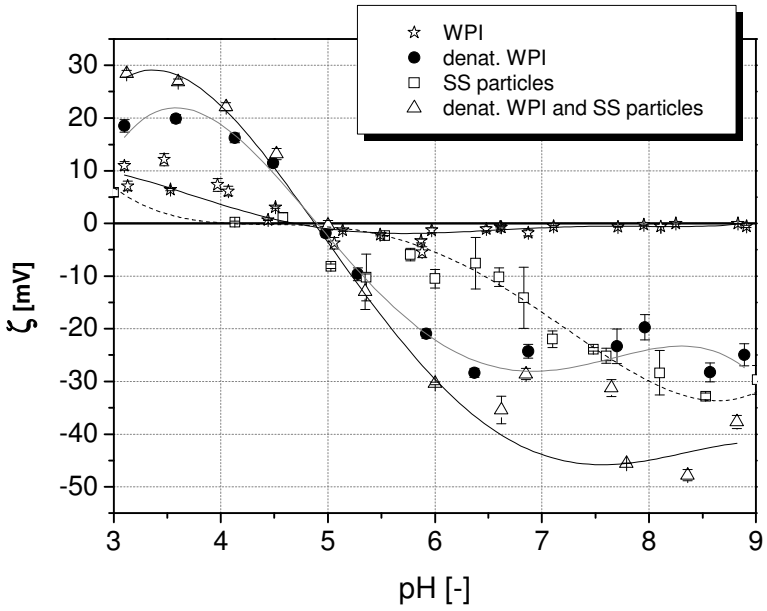

Fig. 4.23. Zeta potential of WPI, stainless steel particles and WPI plus stainless steel particles in 10^{-3} mol L^{-1} KCl at 25 °C

The SEM images of the stainless steel particles before and after protein adsorption under thermal treatment can be observed in Fig. 4.24. The particles seem to be recovered by a protein layer, in which some voids and heterogeneities are visible, while some particles seem to be connected to others by means of proteins stuck on the surfaces.

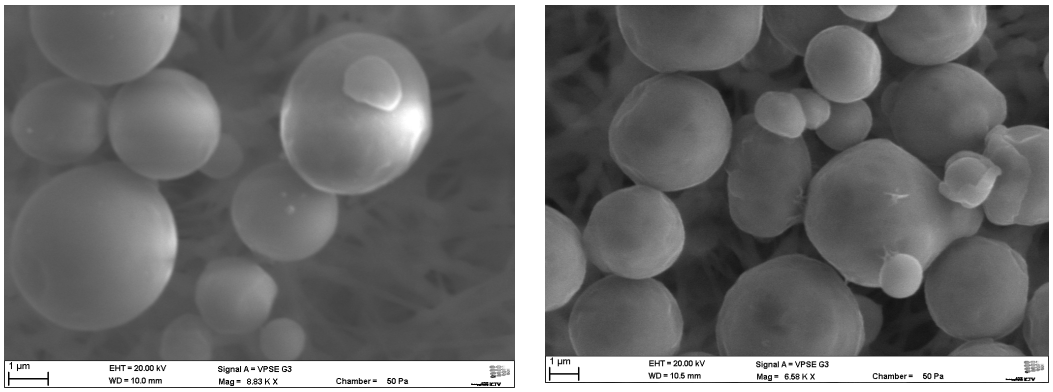

(a) (b)

Fig. 4.24. SEM micrographs of (a) SS particles and (b) SS particles after heating (at 80° C for 30 min and pH = 6.7) and adsorption of WPI. The particles were filtered using a cellulose nitrate filter (pore size: 1.2 µm) and washed with deionized water to remove interfacial and loosely bound protein

4.3 Influence of the surface coating and the initial surface temperature on the batch-wise deposit formation of various milk components

In the next sections, the deposition of whey protein, calcium phosphate and both combined on the DLC-based coated surfaces is compared with the reference of stainless steel.

4.3.1 Whey protein fouling

The fouling experiments with whey protein (WPI) without adding extra minerals showed that adsorption of proteins on the substrate as well as coated surfaces occurred at the heating surface temperature of 80 °C. Fig. 4.25 shows WPI deposits after an exposure time of 30 min and drying at room temperature. After 30 min fouling the entire coupons were covered by a very thin, transparent layer of protein, which only could be visualized by ESEM (Fig. 4.26b) or identified by X-ray microanalysis (Table 4.14), as well as by a drops-like layer (Fig. 4.26d, e), which was visible to the naked eye (Fig. 4.25). The deposition on SICON® seems to be most pronounced, while no obvious differences can be seen between the stainless steel and the other two coatings (cp. Fig. 4.25 a-d) by examination on digital or on scanning electron microscopy. The alignment of all the droplets on a surface was the same, with the tips pointing upward, that the drops were grown in the direction of gravity.

(a) (b) (c) (d)

Fig. 4.25. WPI deposit after 30 min at T_0 = 80°C on (a) SS, (b) DLC, (c) SICAN and (d) SICON®. Coupons dimensions are 20 x 80 x 2 mm^3

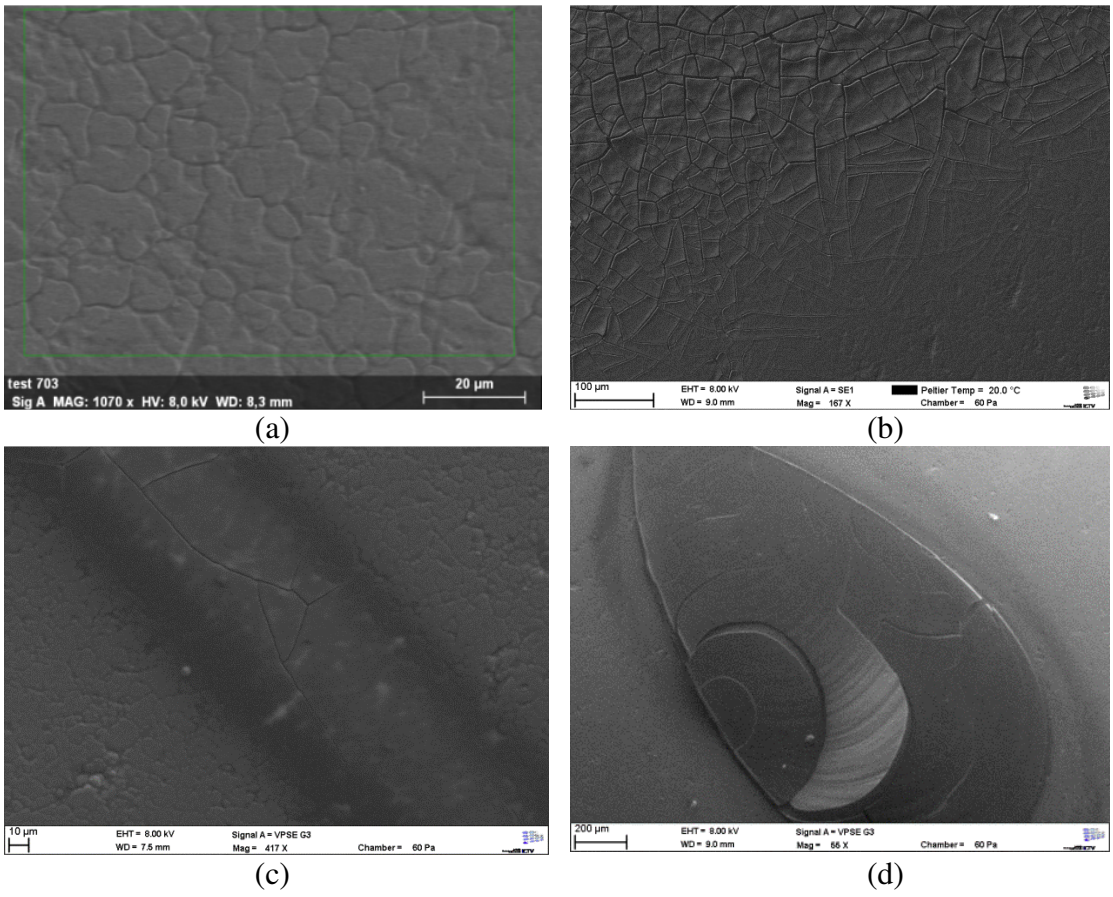

(a) (b)

(c) (d)

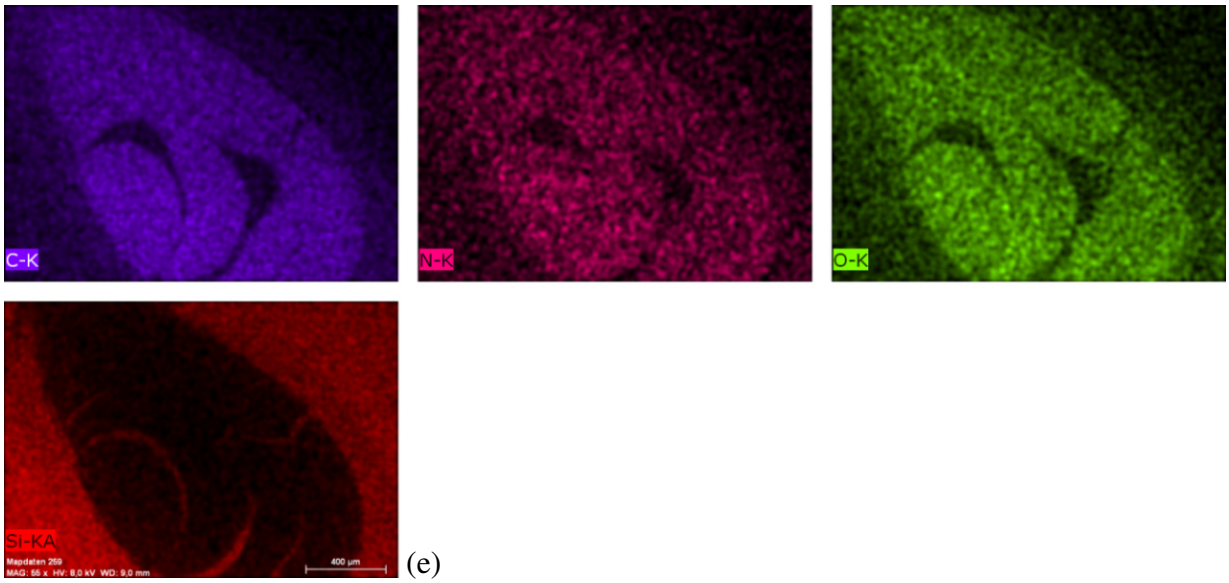

(e)

Fig. 4.26. WPI deposit on (a) SS (see also table 4.14), (b) DLC and (c) SICAN, (d) droped-shape WPI deposit on SICAN and (e) its mapping using X-ray microanalysis

Table 4.14. Composition of clean and with whey protein fouled stainless steel coupons (Fig. 4.26a), given in % at.

Element	clean stainless steel	fouled stainless steel
C	3.4 ± 0.5	18 ± 1
N	6.2 ± 0.4	14 ± 1
O	2.6 ± 0.3	6.5 ± 0.9
Cr	16.7 ± 0.4	12 ± 5
Fe	54.7 ± 0.9	41 ± 18
Ni	13.7 ± 0.4	9 ± 4

No further layer growth and no significant increase of the fouling resistance were measured (Fig. 4.27a). Furthermore, no formation of protein aggregates in bulk could be detected (Fig. 4.22a). Ellipsometry measurements have shown that β-lg adsorbs at a bulk temperature of 25 °C, viz. at conditions of no protein denaturation (Hegg and Larsson, 1981; Santos et al., 2006b). Substantial adsorption (> 10 mg m^{-2} h^{-1}, for stainless steel) including the build-up of multilayers takes place with increasing temperature (bulk at 80 °C) (Karlsson et al., 1996). Karlsson et al. (1996) also proposed that the surface can influence the structural rearrangement of adsorbed protein and, according to Premathilaka et al. (2006) and van Oss (2006), the protein rearrangement depends on the surface energy. In this work, the protein adsorbed preferentially on the SICON® coating (see deposit mass on Table 4.15). This is in agreement with results of others authors, who reported higher adsorbed amounts of β-lg on hydrophobic than hydrophilic surfaces at bulk temperatures below the denaturation temperature of β-lg (Kirtley and McGuire, 1989; Al-Malah et al., 1992; Karlsson et al., 1996). Santos et al. (2006a) found the same trend at a higher bulk temperature and not heated surface

(85 °C, ΔT = 0 K), namely a higher adsorbed β-lg amount on Si-doped DLC coating than undoped ones.

At a higher initial surface temperature (T_0 = 120 °C), the growth of the deposit started immediately and the fouling resistance increased rapidly during the first 150 min, to values of around 6.5 – 7.5 x 10^{-4} K m^2 W^{-1} (Fig. 4.27b). The fouling curves showed an almost linear increase in fouling with time for all coatings. This indicated that the deposit firmly adhered to the surfaces and that there was no significant removal of deposited material. Moreover, this also suggested that the reaction between unfolded proteins near to the wall and proteins already deposited on the surface was favored. Hence, protein multilayers could be formed at the interface. Up to 150 min, the fouling curves of the coated surfaces were almost identical, while R_f reached higher values for untreated stainless steel. After 150 min, the effect of the surface modification on fouling was significant. The coated surfaces showed lower R_f values, which trended to limiting and constant values during the last 20 min of the experiment. For stainless steel, no asymptotic trend of the fouling resistance could be observed, indicating that the deposit was still building up on this surface. (Boxler et al., 2013b)

The pH value was constant at both initial surface temperatures during the experiments.

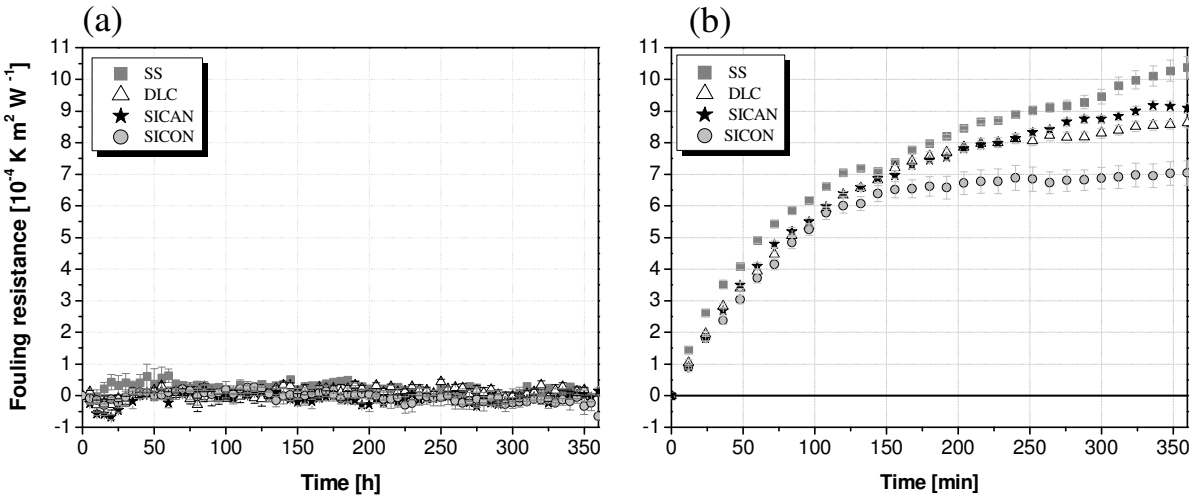

Fig. 4.27. Fouling resistance for whey protein at T_0 = (a) 80 °C and (b) 120 °C

Table 4.15. Final fouling resistance, deposit dry mass and T_{end} for whey protein deposition at initial surface temperatures T_0 = 80 °C and 120 °C

Surface	80 °C			120 °C		
	$R_{f,end}$ [10^{-4} m^2 K W^{-1}]	Mass [g m^{-2}]	T_{end} [°C]	$R_{f,end}$ [10^{-4} m^2 K W^{-1}]	Mass [g m^{-2}]	T_{end} [°C]
SS	0.15 ± 0.02^{ab}	1.0 ± 0.4	80.6 ± 0.8	10 ± 1^{c}	74 ± 6	172 ± 6
DLC	0.11 ± 0.08	0.8 ± 0.2	80.2 ± 0.8	8.6 ± 0.4^{de}	75 ± 4	166.0 ± 0.9
SICAN	0.03 ± 0.01^{a}	0.6 ± 0.1	80.7 ± 0.7	9.1 ± 0.5^{df}	78 ± 4	172 ± 6
SICON®	-0.15 ± 0.06^{b}	2.4 ± 0.4	83 ± 1	5.6 ± 0.4^{cef}	71 ± 4	150 ± 3

Results are presented as mean ± standard error. Superscript letters indicate statistically different values for $R_{f,end}$ and mass ($p < 0.05$).

The dry deposit aspect after 360 min is presented in Fig. 4.28. The deposit was uniformly distributed on the whole plates, although it showed a heterogeneous structure, with the deposit thickness varying from 150 to 200 µm. The deposited mass on the diverse surfaces were not statistically different ($p < 0.05$), ranging from 71 to 78 ± 4 g m^{-2}. However, the properties of the deposit changed with the surface: the deposits were denser on SICAN and SICON® compared to untreated stainless steel. Although a temperature of 150 – 170 °C on the surfaces was reached by the end, no color change due to scorch of protein sublayers could be observed. The adhesion of deposits, viz. the interaction deposit/substrate, was stronger compared to the fouled layers at lower wall temperature, which partially peeled off from the surfaces after drying. This is attributed to the formation of covalent disulphide bonds between the protein molecules at temperatures above the denaturation temperature of β-lg. (Boxler et al, 2013b)

As the deposit thickness increases, the effect of the surface properties should become less important, while the deposit composition (Dupeyrat et al. 1987; Yoon and Lund, 1994) and the amount of deposit formed (Britten et al., 1988) should not change. However, this hypothesis is not supported by the behavior observed in Fig. 4.27 (as well as in Figs. 4.29 for calcium phosphate deposition and in Fig. 4.34 for WPI plus SMUF fouling, which will be discussed later). During the first 150 min of experimental run, a dependency of the surface energy, particularly of the γ^- parameter, to fouling in the initial deposition stages, could not be detected by the thermal fouling resistance measurement (see Fig. 4.27b). After 150 min, the evolution of the R_f differed for the various surfaces. This is in accordance with Karlsson et al. (1996), who observed an influence of the surface on the following stages of the build-up. (Boxler et al., 2013b) Changes in protein configuration upon adsorption in dependence on the surface energy, as discussed in chapter 2.2.5, could explain the variation of $R_{f,end}$ of the different coated surfaces.

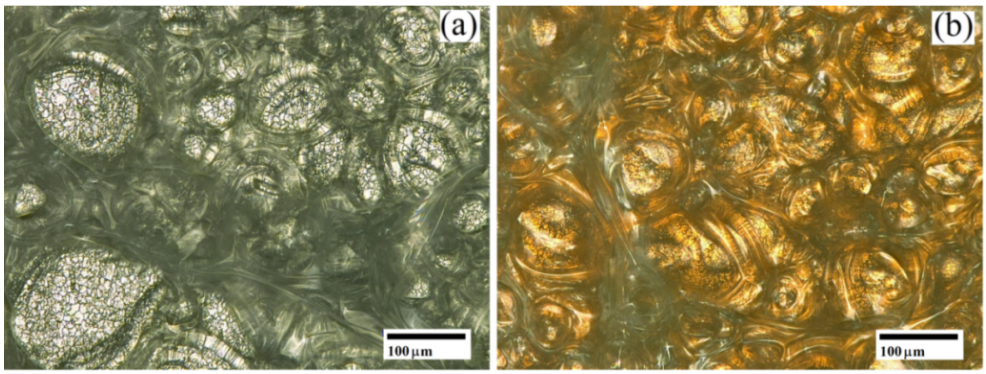

Fig. 4.28. Whey protein deposit on (a) SS and (b) SICON® generated at T_0 = 120 °C

4.3.2 Calcium phosphate fouling

Fig. 4.29 shows the deposition of SMUF on the DLC and Si doped DLC coated surfaces at initial surface temperatures of 80 and 105 °C. The fouling behavior of SMUF on the coated surfaces at T_0 = 80 °C differed entirely from the fouling on the unmodified stainless steel (Fig. 4.29a). An induction period of approximately 180 min for stainless steel, 80 – 90 min for DLC and SICAN, and 15 min for SICON®, in which R_f is negative or equal to zero, could be

identified. A shorter induction time for calcium phosphate nucleation on surface with higher γ^- (48 mN m^{-1}), as in the case of SICAN and SICON® (γ^- = 15.5 and 22 mN m^{-1} compared to 8.4 and 13 mN m^{-1} for SS and DLC, respectively), was also described by Wu and Nancolas (1998). The authors found for crystallization of calcium phosphate on anatase and rutile particles that an increase in the surface electron donor capacity can promote crystallization by reducing the energy barrier for nucleation. Geddert et al. (2011b) also reported a shorter induction time on SICON® than on DLC or SICAN coatings for $CaSO_4$ fouling, but similar to the induction time on stainless steel.

After the induction period, the fouling resistance increased very rapidly for the stainless steel, DLC and SICAN surfaces, with the fouling curves of DLC and SICAN showing similar R_f progress. Given that the fouling experiments were conducted in absence of high wall shear stress, it can be assumed that almost all deposited material at the heated surface adhered to it. However, deposit removal and repeated adhesion on the SICAN and SICON® coatings occurred, which corresponds to an abrupt decrease and continuing increase of R_f. Hence, the deposit/surface adhesive interaction on these surfaces was lower than the cohesive strengths of the soil. The same trend was found by Boxler et al. (2011) for SMUF deposition on DLC coated surfaces under continuous flow conditions. Different and approximately constant fouling resistance values were reached at the end of experiment at T_0 = 80 °C, varying from 4 to 7 x 10^{-4} K m^2 W^{-1} for SICON® and stainless steel, respectively. (Boxler et al., 2013b)

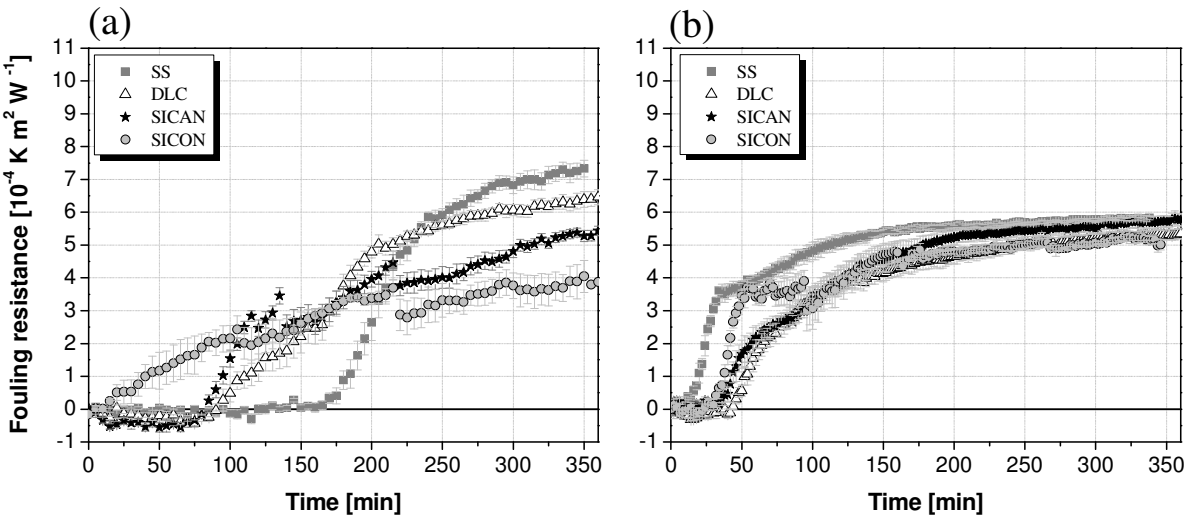

Fig. 4.29. Fouling resistance for calcium phosphate at T_0 = (a) 80 °C and (b) 105 °C

For all surfaces, a homogeneous white and opaque layer with amorphous structure built up on almost the entire substrate, who thickness varied from 120 to 200 µm. The amount of material deposited was higher on unmodified stainless steel than on the coated one. The deposit mass varied from 32 to 50 g m^{-2} for SICON® and stainless steel, respectively (Table 4.16).

Table 4.16. Final fouling resistance, deposit dry mass and T_{end} for calcium phosphate deposition at initial surface temperatures T_0 = 80 °C and 105 °C

Surface	80 °C			105 °C		
	$R_{f,end}$ [10^{-4} m^2 K W^{-1}]	Mass [g m^{-2}]	T_{end} [°C]	$R_{f,end}$ [10^{-4} m^2 K W^{-1}]	Mass [g m^{-2}]	T_{end} [°C]
SS	7.3 ± 0.3^{ab}	50 ± 3^{fgh}	99 ± 1	5.80 ± 0.04^{i}	99 ± 3^{k}	135.4 ± 0.6
DLC	6.4 ± 0.3^{cd}	36 ± 3^{f}	99 ± 1	5.3 ± 0.2	90 ± 3	135.6 ± 0.2
SICAN	5.3 ± 0.3^{ace}	38 ± 4^{g}	98.2 ± 0.6	5.8 ± 0.2^{j}	97 ± 4^{l}	140 ± 1
SICON®	3.8 ± 0.4^{bde}	32 ± 6^{h}	93.3 ± 0.3	5.1 ± 0.2^{ij}	74 ± 4^{kl}	135 ± 2

Results are presented as mean ± standard error. Superscript letters indicate statistically different values for $R_{f,end}$ and mass ($p < 0.05$).

The fouling layer after 30 min SMUF exposure consisted of a soft deposit of amorphous crystalline structure, which was irregularly distributed over the entire coupon (Fig. 4.30). The calcium phosphate deposit showed two different microstructures, which can be seen in the SEM micrographics (Fig. 4.31). First, the entire surface was covered by a thin layer, whose upper surface was uneven. Cracks in this thin fouling layer were formed, probably during drying, so that the layer broke into many pieces of different sizes. Some of these fragments could be almost completely or at least partially removed from the coupon, in order that the substrate surface became visible. On the continuous fouling layer, further "overgrowths" with an amorphous structure were formed in different sizes. Small crystal-like structures grew on stainless steel and on DLC spheroids, contributing to building a homogenous and more compact fouling layer, while on SICAN and SICON® larger and looser crystal aggregates spread randomly over the first fouling layers. This indicates that particulates formed in the bulk solution (bulk precipitation was evident from the increased solution turbidity) adhered to the nucleation sites and/or the developing crystal layer, promoting the deposit growth. This interpretation agrees with the findings by Daufin et al. (1987), who observed the insolubilization of a large amount of calcium phosphate from a synthetic milk ultrafiltrate and suggested that the particles deposited on the heat transfer surface had previously been precipitated in bulk.

For $CaSO_4$ fouling on the same DLC coatings, Geddert et al. (2011b) observed no defined initial nucleation points and smaller crystals on low energy surfaces such as SICON®, while fewer but longer crystals could be visualized on stainless steel. Rosmaninho et al. (2007b), comparing fouling on TiN coated surfaces (T_{bulk} = 70 °C, ΔT = 1 K), noticed that surfaces with higher γ^- were less susceptible to crystallization fouling caused by the direct deposition of calcium phosphate ions, but they were more prone to particulate fouling, caused by the adhesion of suspended particles from the bulk, such as observed on the SICAN and SICON® coatings in this work.

Mayer et al. (2012) measured the adhesion force of single $CaCO_3$ crystals on the same DLC and DLC doped coatings, reporting the lowest adhesion strength for SICON® and the highest for the DLC coating, which supports the behavior of the sawtooth fouling curves shown in Fig. 4.27. This indicates that the cohesive strength between deposit-deposit bonds was lower than the adhesive strength between deposit-surface, confirming the observations of Andritsos et al. (2002) and Hasson (1968) who argued that deposits from particulates adhere

less strongly on the substrate than crystalline deposits. Hence, the $R_{f,\,end}$ and the deposit mass at both initial temperature was the lowest on SICON® (higher γ^- surface, $\gamma^- = 22$ mN m^{-1}) and the highest on stainless steel ($\gamma^- = 8.4$ mN m^{-1}).

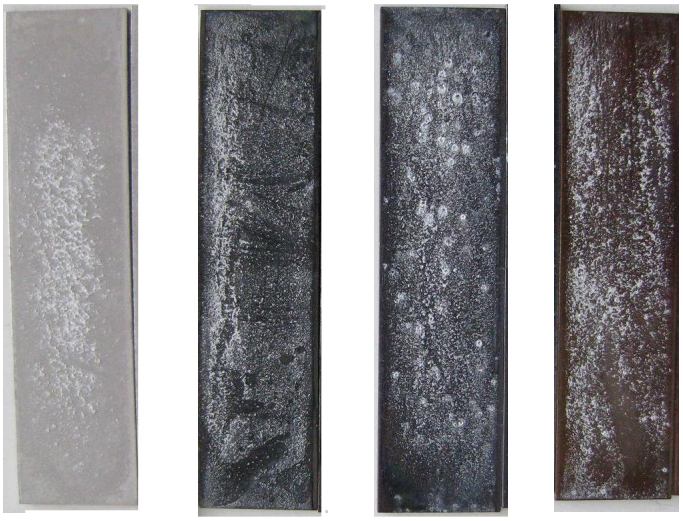

Fig. 4.30. SMUF deposit at $T_0 = 80$°C for a contact time of 30 min on (a) SS, (b) DLC, (c) SICAN and (d) SICON®

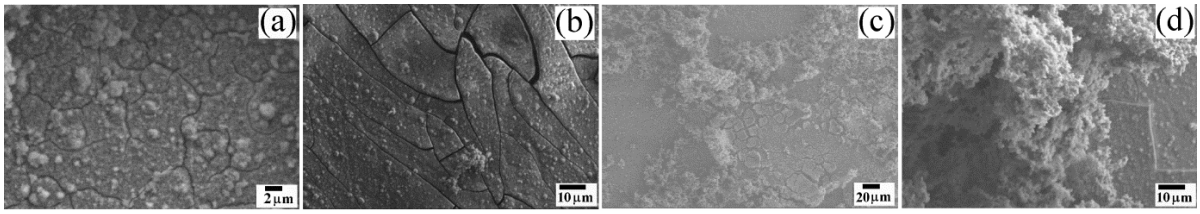

Fig. 4.31. Scanning electron micrographs of (a) SS, (b) DLC, (c) SICAN and (b) SICON® by exposure to SMUF at $T_0 = 80$ °C for 30 min.

An analysis of the fouling layer chemical composition by micro-X-ray revealed that the deposit primarily consisted of 22 – 30 % w/w calcium, about 10 % w/w phosphorous and about 50 % w/w oxygen. Moreover, even low concentrations of each C, Na, Mg, Cl and K from the SMUF salts, as well as Cr, Fe, Ni and Si from the stainless steel or from the coatings were detected (Table 4.17). The detection of these elements in the fouling layer can be expected as they were present in the initial solution. Tissier and Lalande (1986), Lalande et al. (1984) and Rosmaninho and Melo (2006a) also found small amounts of the elements Mg, as well as C, Na and K in milk and SMUF deposits. The Ca/P molar ratio varied from 1.6 (DLC) to 2.6 (SICAN).

Table 4.17. Composition of SMUF deposit at T_0 = 80 °C on different surfaces after 30 min fouling, given in % w/w.

Element	SS	DLC	SICAN	SICON®
C	3.5 ± 0.1	5.4 ± 0.1	4.4 ± 0.3	4.0 ± 0.4
O	43 ± 1	49.3 ± 0.8	46.5 ± 0.9	48 ± 1
Na	1.2 ± 0.1	2.1 ± 0.2	0.9 ± 0.1	0.7 ± 0.1
Mg	1.08 ± 0.04	1.13 ± 0.01	0.7 ± 0.1	0.80 ± 0.04
Si	--	--	7 ± 1	1.9 ± 0.5
P	12.3 ± 0.4	11.08 ± 0.02	9.5 ± 0.5	11.3 ± 0.7
Cl	1.8 ± 0.2	2.9 ± 0.8	1.6 ± 0.2	1.2 ± 0.1
K	3.7 ± 0.3	5 ± 1	2.9 ± 0.2	2.9 ± 0.2
Ca	30 ± 1	22.5 ± 0.3	26.5 ± 0.4	29 ± 1
Cr	2.4 ± 0.4	--	--	--
Fe	2.0 ± 0.4	--	--	--
Ni	0.8 ± 0.2	--	--	--

At the surface temperature T_0 = 105 °C, again different induction times were observed for the diverse surfaces (Fig. 4.29b), which were shorter than at the T_0 = 80 °C. An induction time of 10 min was measured for stainless steel, 45 min for DLC, 35 min for and SICAN and 25 min for SICON®. The fouling resistance increased during the first 75 min significantly and an asymptotic final value of the fouling resistance was reached earlier than for the runs at lower initial surface temperature. Again, the fouling curves of DLC and SICAN showed similar R_f progress. After 360 min, the fouling curves of all surfaces reached similar final fouling resistances, $R_{f,\,end}$, ranging from 5 to 6 x 10^{-4} K m^2 W^{-1}, which were on average not higher than the $R_{f,\,end}$ for SMUF deposition at T_0 = 80 °C (Fig. 4.29a). Such behavior might be attributed to the higher difficulty in incorporating large calcium phosphate particulates formed at a higher temperature (Rosmaninho et al, 2007b: T_{bulk} = 70 °C, ΔT = 1 K).

A uniform, fragile and compact deposit layer formed on all surfaces on the samples at T_0 = 105 °C, whose thickness ranged from 600 to 700 µm. On stainless steel and DLC, the layer was denser, while on SICAN and SICON® the deposit was fragile and easily broken. Some deposit fragments were completely or partially removed from the coupon (Fig. 4.32). However, even at these areas the surface was always covered with a thin layer of crystals. This suggests that the deposits' cohesive strength was lower than its adhesive strength. The deposit mass varied from 99 g m^{-2} to 74 g m^{-2} for stainless steel and SICON®, respectively (Table 4.16).

The upper loosest deposit layer could be washed off from the coupons by rinsing with water (which corresponds to the first step of a cleaning process), leaving an adhering initial layer on the substrate, which could only be removed by acid cleaning. Further results regarding the cleaning behavior will be discussed in section 4.4.

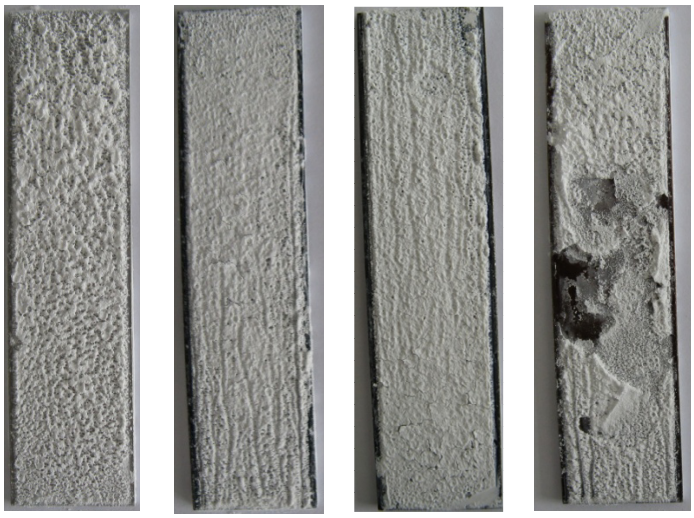

(a) (b) (c) (d)

Fig. 4.32. Dry calcium phosphate deposits at T_0 = 105 °C on (a) SS, (b) DLC, (c) SICAN and (d) SICON®

A negative relationship between the final fouling resistance (or the deposit mass) at T_0 = 80 °C and 105 °C (Table 4.16) and the electron donor component could be found. These results contradict the findings presented by Rosmaninho and Melo (2006b) and Rosmaninho et al. (2007b), who detected a positive relationship between the final amount of deposit and the surface γ^- component (on the first 15 min as well as after 120 or 240 min fouling). However, it should be noted that the authors investigated coated surfaces with higher γ^- (γ^- varying from 18.4 to 55.3 mN m^{-1} and as an exception Ni-P-PTFE with a γ^- of 0.2 mN m^{-1}) than the γ^- of the DLC studied coatings.

As evidenced by the whey protein fouling at T_0 = 120 °C, the effect of the energetic surface properties was not suppressed during the buildup of further fouling layers on the existing ones. The long-term effect of the surface on fouling layer growth rate and on structuring of the deposits was also observed by Zhao et al. (2005b) for Ni–Cu–P–PTFE coatings and Rosmaninho et al. (2007b) for TiN coatings.

A dissimilar pH evolution of the SMUF solution between the experiments at T_0 = 80 °C and 105 °C was observed, reflecting the fouling behavior of Fig. 4.28. During the induction time (fouling curves), the pH was almost constant for all surfaces at both initial surface temperatures. Subsequently, as soon as the pH value decreased, the fouling resistance increased (growth phase). At T_0 = 80 °C, the fouling progress and the reaction of precipitation of calcium phosphate in bulk proceeded differently on the diverse surfaces, whereas at T_0 = 105 °C they were similar for the different surfaces. After 150 min, the SMUF solution at T_0 = 105 °C reached the same pH as the SMUF solution at T_0 = 80 °C after having been in contact with the different surfaces for 360 min (pH = 6.4 – 6.5, with exception for SS: pH_{end} = 6.55). Up to 150 min, the fouling resistance progress at T_0 = 105 °C was almost asymptotic (despite the pH continued to decrease) for all surfaces, while at the T_0 = 80 °C the fouling behavior tended to be asymptotic only up to 300 min. Christoffersen et al. (1989) associated initial constant pH with the appearance of agglomerates of amorphous calcium phosphate (ACP) from the precursor ACP phase. Moreover, they also observed a slight initial increase on pH, which could not be explained. This phenomenon was detected in the

experiments for the unmodified stainless steel (Fig. 4.33a). Thereafter, as well as by the deposition at 105 °C, the pH decreased with time, mainly due to the removal of phosphate ions from the solution and liberation of H^+ by the crystallization of calcium phosphate (Belmar-Beiny and Fryer, 1993) ($Ca_2^+ + H2PO_4^- \rightarrow CaHPO_4 + H^+$). This further variation of pH is related to the transformation of ACP into other phases, such as brushite, octacalcium phosphate, hydroxyapatite or calcium-deficient apatite (Christoffersen et al., 1989; Mekmene et al., 2009).

The results showed that the formation of aggregates in the bulk at higher surface temperature was faster than at lower temperature, as has been reported by Spanos et al. (2007), and it affected the fouling layer formation. Moreover, different pH evolution associated with the formation of different calcium phosphate phases in bulk reflects the difference on the mechanisms of the deposition process steps, namely surface reaction and particle adhesion, for each coating. Calcium and phosphate ions might play an important role in the initial conditioning of the surface but do not control the overall deposition, within which the attachment of calcium phosphate particulates on the first/growing fouling layer seems to be a dominant factor in the fouling process.

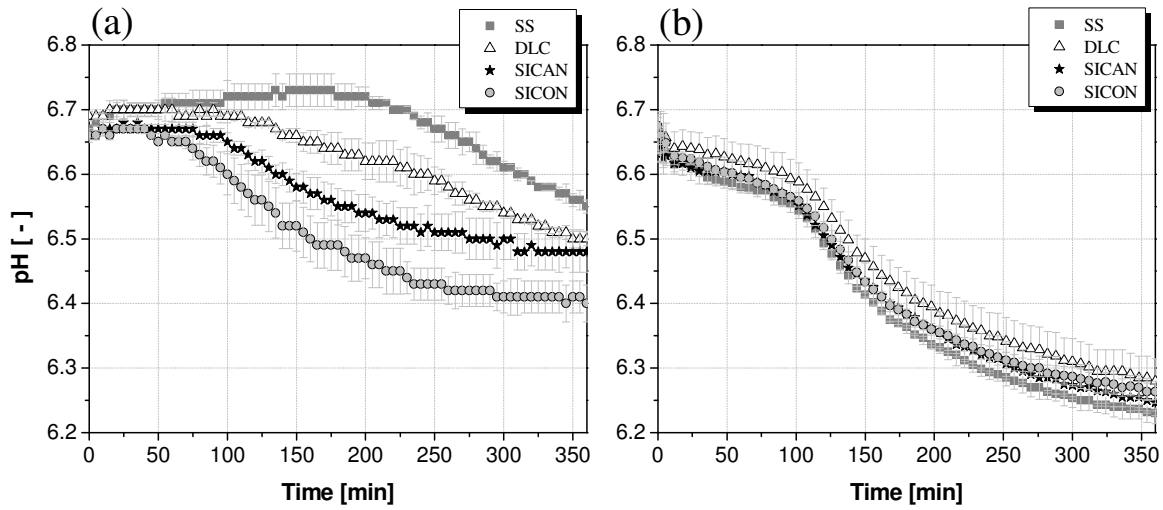

Fig. 4.33. pH evolution during calcium phosphate deposition at initial surface temperature T_0 = (a) 80 °C and (b) 105 °C.

4.3.3 Fouling of SMUF-rich whey protein solution

Fouling of whey protein in the presence and absence of milk salts is clearly different, as can be seen when comparing Figs. 4.27 and 4.34. Calcium ions affect the structure of deposits and increase the rate of deposit growth (Guérin et al., 2007). This is due to the fact that the electrostatic repulsion between the proteins is decreased and thermal denaturation and aggregation are favored in a solution with high ionic strength. In the presence of calcium ions, the deposition of proteins might also occur through the formation of non-covalent bonds (Jeurnink et al., 1996a). In addition, higher calcium concentrations reinforce adhesion forces between protein aggregates (Guérin et al., 2007). Conversely, crystallization fouling is

reduced through the presence of whey protein (Tsuge et al., 2002; Rosmaninho and Melo, 2008), due to the binding of calcium by proteins. (Boxler et al., 2013b)

Fig. 4.34 shows the fouling curves for the SMUF-rich whey protein solution on the uncoated, coated and electropolished plus coated surfaces at the initial surface temperatures T_0 = 80 °C and 120 °C. The deposition depended on the energetic and mechanical surface properties, principally at T_0 = 80 °C. An immediate and continuous increase of the fouling resistance was observed, with the exception of SICON® and ESICON® at T_0 = 80 °C, in which a short induction time of 25 min could be measured. The highest fouling resistance was detected on the uncoated stainless steel at both initial temperatures (Tables 4.18 and 4.19) and the R_f for the DLC coated surface was the lowest at the experiments' conclusion (Tables 4.18 and 4.19). The fouling resistance did not reach an asymptotic value, except for the coated surfaces at T_0 = 80 °C, in which R_f reached approximately constant values after 325 min. Therefore, the average fouling resistance rate in the first hour $(dR_f/dt)_{1h}$ was additionally used to compare fouling on the surfaces at both initial temperatures (see Tables 4.18 and 4.19). Tables 4.19 and 4.21 show the deposited masses. Considerably lower fouling rates $(dR_f/dt)_{1h}$ as well as lower deposit masses were measured on the coated surfaces at both initial temperatures than on uncoated stainless steels, with the exception of the $(dR_f/dt)_{1h}$ of EDLC at T_0 = 120 °C (Table 4.20).

As can be seen from Figs. 4.34a and 4.34b, the influence of surface roughness mainly affected the fouling resistance progress at T_0 = 80 °C on the electropolished stainless steel. Distinct initial fouling rates $(dR_f/dt)_{1h}$ and final fouling resistances $R_{f,end}$ yet similar deposited masses (comparable to the mass on SS) were measured on these surfaces, which differed from each other in terms of the total surface free energies, as well as the electron acceptor and donor components (γ^+ and γ^-, respectively). The unpolished plus coated surfaces had identical γ^{TOT} and γ^+ values, but distinct γ^- values. On the unpolished plus coated surfaces, the $(dR_f/dt)_{1h}$, $R_{f,\,end}$ and deposited masses for SICAN and SICON® were statistically identical. After 360 min the fouling resistance reached a value of (2 – 9) x 10^{-4} K m^2 W^{-1} for the unpolished surfaces and a value of (7 – 11) x 10^{-4} K m^2 W^{-1} for the electropolished surfaces, depending on the surface coating. The values of R_f for the unpolished surfaces were higher than those found for pure whey protein (0.1 x 10^{-4} K m^2 W^{-1}) or pure calcium phosphate (4 - 7 x 10^{-4} K m^2 W^{-1}) deposition.

Investigation of batch-wise $CaSO_4$ deposition on unpolished and electropolished stainless steel (R_a = 0.27 and 0.12 µm, respectively) coated with the same DLC films showed similar fouling resistance progress and a slightly different induction time (Geddert et al., 2009). Furthermore, the authors observed no enhancement in fouling mitigation through the substrate electropolishing. This confirms the results presented in Figs. 4.34 a-b and Figs. 4.34 c-d, as well as the correlated tables, since more fouling occurred on the electropolished plus coated surfaces than the coated unpolished surfaces. It is noteworthy that the surface roughness values R_a ranged from 0.1 to 0.18 µm and were significantly lower than the threshold values mentioned in recommendations and standards (R_a < 0.8 µm, DIN EN 1672-2, 2009). Therefore, appending from these results, the additional electrochemical pretreatment of the surface brought no advantage regarding fouling mitigation.

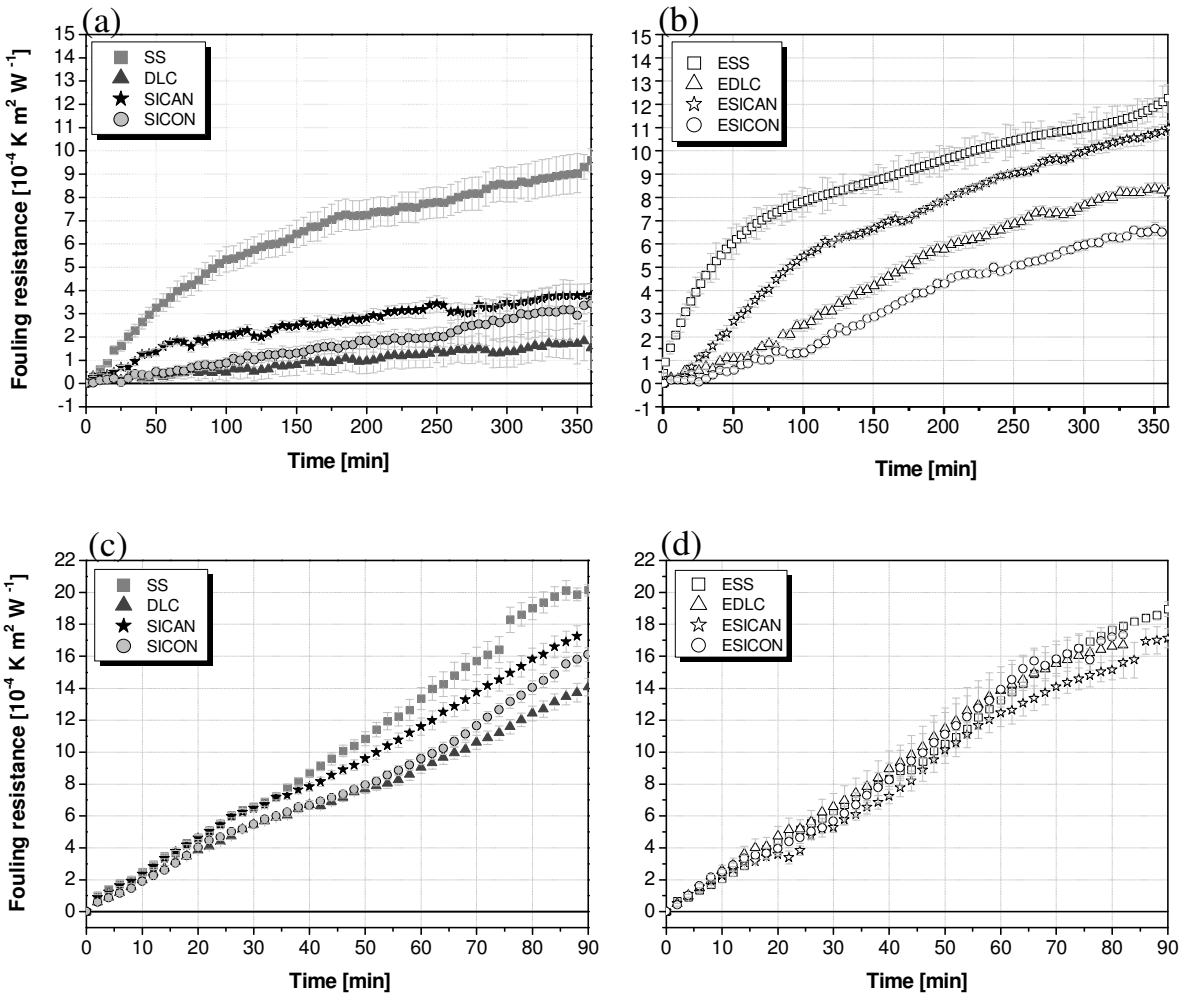

Fig. 4.34. Fouling resistance for WPI in SMUF at T_0 = 80 °C for (a) coated unpolished surfaces and for (b) coated electropolished surfaces as well as at T_0 = 120 °C for (c) coated unpolished surfaces and for (d) coated electropolished surfaces

Table 4.18. Fouling rate for the first hour $(dR_f/dt)_{1h}$, $R_{f,\,end}$ and T_{end} at initial surface temperature T_0 = 80 °C

Surface	Fouling rate [10^{-4} m^2 K W^{-1} h^{-1}]	$R_{f,\,end}$ [10^{-4} m^2 K W^{-1}]	T_{end} [°C]
SS	5.0 ± 0.3^{a}	9.0 ± 0.7^{abcd}	113 ± 3
DLC	0.58 ± 0.04^{bcde}	1.7 ± 0.4^{e}	83 ± 2
SICAN	1.3 ± 0.3^{bfgh}	3.7 ± 0.7^{f}	92 ± 3
SICON®	0.9 ± 0.2^{cfij}	3.0 ± 0.5^{ef}	92 ± 1
ESS	5.2 ± 0.6^{a}	10.4 ± 0.8^{ag}	107 ± 4
EDLC	1.5 ± 0.2^{dgik}	8.6 ± 0.6^{bh}	104 ± 2
ESICAN	3.4 ± 0.3	11.0 ± 0.4^{cg}	110 ± 2
ESICON®	2.0 ± 0.6^{ehjk}	7.2 ± 0.6^{dh}	101 ± 2

Superscript letters indicate statistically identical values ($p > 0.05$).

Table 4.19. Deposit dry mass, protein, Ca and P contents in deposit at initial surface temperature T_0 = 80 °C

Surface	Mass [g m^{-2}]	Protein [g g^{-1}]	Ca [g g^{-1}]	P [g g^{-1}]
SS	149 ± 5^{ab}	0.73 ± 0.05	0.038 ± 0.007	0.021 ± 0.001
DLC	23 ± 2^{cd}	0.69 ± 0.07	0.02 ± 0.01	0.013 ± 0.001
SICAN	34 ± 5^{ce}	0.70 ± 0.04	0.021 ± 0.003	0.017 ± 0.002
SICON®	32 ± 5de	0.62 ± 0.03^{ab}	0.024 ± 0.001	0.018 ± 0.001
ESS	131 ± 12^{afgh}	0.79 ± 0.09^{a}	0.017 ± 0.009	0.014 ± 0.006
EDLC	110 ± 14^{fij}	0.82 ± 0.04^{b}	0.02 ± 0.01	0.014 ± 0.007
ESICAN	125 ± 4^{bgik}	0.73 ± 0.01	0.013 ± 0.007	0.014 ± 0.003
ESICON®	112 ± 19^{hjk}	0.77 ± 0.02	0.02 ± 0.01	0.015 ± 0.006

Superscript letters denote statistically identical values for mass ($p > 0.5$) and statistically different values for protein, Ca and P ($p \leq 0.05$).

Table 4.20. Fouling rate for the first hour $(dR_f/dt)_{1h}$, final fouling resistance $R_{f,\,end}$ and T_{end} at initial surface temperature T_0 = 120 °C

Surface	Fouling rate [10^{-4} m^2 K W^{-1} h^{-1}]	$R_{f,\,end}$ [10^{-4} m^2 K W^{-1}]	T_{end} [°C]
SS	13.8 ± 0.6^{abcd}	18.9 ± 0.3^{a}	230 ± 4
DLC	8.2 ± 0.3^{e}	13.0 ± 0.5	224 ± 2
SICAN	10.9 ± 0.3	14.9 ± 0.5^{bce}	223 ± 2
SICON®	9.0 ± 0.2^{e}	15.2 ± 0.3^{bdf}	229 ± 2
ESS	13.1 ± 0.5^{afg}	18.3 ± 0.3^{ag}	224 ± 5
EDLC	15 ± 1^{bh}	16 ± 1^{cdhi}	195 ± 4
ESICAN	13 ± 1^{cfi}	16.3 ± 0.7^{efh}	218 ± 4
ESICON®	12 ± 1^{dghi}	17.2 ± 0.6^{gi}	210 ± 4

Superscript letters indicate statistically identical values for the fouling rate and $R_{f,\,end}$ ($p > 0.05$).

Table 4.21. Deposit dry mass, protein, Ca and P contents in deposit at initial surface temperature T_0 = 120 °C

Surface	Mass [g m^{-2}]	Protein [g g^{-1}]	Ca [g g^{-1}]	P [g g^{-1}]
SS	189 ± 7	0.56 ± 0.05^{a}	0.022 ± 0.001^{a}	0.020 ± 0.002^{abc}
DLC	193 ± 9	0.69 ± 0.06^{bcde}	0.048 ± 0.02^{abcde}	0.036 ± 0.003^{adefghi}
SICAN	193 ± 7	0.52 ± 0.06^{bf}	0.006 ± 0.002^{bf}	0.011 ± 0.002^{djk}
SICON®	213 ± 6^{a}	0.45 ± 0.05^{cgh}	0.010 ± 0.007^{c}	0.012 ± 0.001^{egl}
ESS	190 ± 18	0.73 ± 0.02^{afij}	0.032 ± 0.004^{f}	0.025 ± 0.002^{bfj}
EDLC	198 ± 32	0.66 ± 0.03^{hkl}	0.019 ± 0.002^{d}	0.016 ± 0.002^{g}
ESICAN	173 ± 17^{a}	0.51 ± 0.04^{dik}	0.019 ± 0.003^{e}	0.018 ± 0.001^{h}
ESICON®	193 ± 21	0.44 ± 0.02^{ejl}	0.026 ± 0.009	0.023 ± 0.007^{cikl}

Superscript letters refer to statistically different values for mass, protein, Ca and P ($p \leq 0.05$).

At elevated temperatures, the precipitation of calcium phosphate and the denaturation and aggregation of the protein were enhanced. Hence, the fouling resistance as well as the amount of deposit was higher at T_0 = 120 °C. The experiments were interrupted after 90 min, due to the surface becoming extremely hot (= 230 °C). For the coated unpolished surfaces, the evolution of the fouling resistance was almost identical in the earlier stages of fouling (first 30 min for unpolished plus coated surfaces and first 60 min for the electropolished and coated surfaces). Thereafter, the fouling curves slightly drifted apart for the coated unpolished surfaces, indicating that subsequent stages of deposition were affected by the surface properties and/or aging of the initial fouling layers. For the coated electropolished surfaces, the R_f remained very similar. The final fouling resistance reached a value of (13 – 19) x 10^{-4} K m^2 W^{-1} for the unpolished surfaces and a value of (16 – 18) x 10^{-4} K m^2 W^{-1} for the electropolished surfaces. These values of R_f were much higher than those found for whey protein (6 – 10) x 10^{-4} K m^2 W^{-1} or calcium phosphate (around 5.5 x 10^{-4} K m^2 W^{-1}) after 6 hours of experiment at T_0 = 120 and 105 °C, respectively.

Comparing the fouling rates $(dR_f/dt)_{1h}$ and the $R_{f,\,end}$ for the deposition at T_0 = 120 °C on all surfaces, no difference on fouling behavior between the electropolished plus coated surfaces could be found. In contrast, a difference among the coated surfaces and between the coated and the electropolished plus coated surfaces could be detected. No statistical difference could be measured in terms of deposit amount, except between the two extremes ESICAN and SICON®.

Comparing the final fouling resistance or the $(dR_f/dt)_{1h}$ and the deposit mass at T_0 = 80 °C and 120 °C (Tables 4.18 - 4.21, see also Fig. A3 in appendix), no linear relationship between these both parameters could be found ($p > 0.05$), as described by equation (2.6). The density and thermal conductivity of the fouling layer and thus its fouling resistance can be altered by: (*i*) deposits with different microstructure and/or composition on the modified surfaces; (*ii*) build-up of β-lg layers with different molecular structures throughout the fouling (Blanpain-Avet et al., 2012); (*iii*) changes on the deposit structure with time due to aging (Davies et al., 1997; Floris et al., 2008); or (*iv*) changes on the distribution of elements or composition with deposit depth due to diffusion of minerals through the protein matrix (Changani et al., 1997). Moreover, an inhomogeneous deposit distribution on the surfaces (principally at T_0 = 80 °C) or different deposit roughness can give differing film heat transfer coefficients (supposed to be constant), thus contributing to explain this discrepancy. Rosmaninho and Melo (2006b) verified a reverse relation between deposit mass and fouling layer thickness for calcium phosphate deposits on coated stainless steel surfaces (MoS_2, SiF_3^+, SiO_x and Ni-P-PTFE). They associate this inconsistency with the different deposit structures (compactness). Khaldi et al. (2015) related different evolution of fouling resistance with changes in deposit structure due to increasing the calcium concentration in a WPC solution.

The composition of the deposits is given in Tables 4.19 and 4.21. The deposits at T_0 = 80 °C resembled those of type 1 described by Lyster (1965) and type A of Burton (1968) for pasteurization temperatures, whereas deposits at T_0 = 120 °C were more proteinaceous than deposit type 2 (Lyster, 1965) and type B (Burton, 1968) (see Table 2.2). The results could also be confirmed by microscopic examination (Fig. 4.34) and are in line with those obtained for heating of milk at 120 - 140 °C without preheating and holding (Foster and Green, 1990). Note that at deposit type 2 or type B, the milk is submitted to a pre-heating or

pasteurization (to some extent including a subsequent pre-holding) treatment before the UHT heating (T = 135 - 150 °C for 2 - 3 s). In this work, different to industrial conditions, the protein solution was not previously pasteurized, viz. native β-lg remained susceptible to deposition to the heated surface, while the bulk temperature was maintained at a temperature of 50 °C. A modification of the stainless steel properties by coating directly affected the deposit composition. At T_0 = 80 °C, lower protein content of the deposit on SICON® and higher on ESS and EDLC were measured. At this temperature, the Ca and P contents of the deposits did no vary so strongly. Lower Ca and P contents on ESICAN and higher contents on SS were detected. At T_0 = 120 °C, lower protein contents of the deposit were again measured on SICON® and ESICON®, and again were higher on ESS, EDLC and DLC. The Ca and P contents of the deposits varied significantly and lower Ca and P contents were measured on SICAN and SICON® and higher ones on DLC. According to the deposition mechanisms proposed by Rosmaninho and Melo (2008) for SMUF plus native whey protein solution, calcium phosphate will preferably deposit on low γ^- surfaces, which are SS, DLC and EDLC surfaces in this work. The molar Ca/P ratio varied for the different surfaces. In agreement with the results of Lyster (1965) and Lalande et al. (1984), the molar Ca/P ratio was found to be close to 1.4 at the lower surface temperature for SS, DLC and DLC and this ratio was lower for the deposits on the other surfaces (Ca/P varied from 0.7 to 1). At higher temperature, the Ca/P ratio was lower than the values found in the literature, which ranged from 1.3 to 1.6 depending on the milk pre-treatment (Lyster, 1965; Lalande et al., 1984), ranging between 0.4 for SICAN and 1 for SS and DLC. These results hold great practical significance, showing that the composition of fouling layer can be altered with surface design and consequently the deposit's cohesive and adhesive strengths. The latter will certainly influence cleaning behavior, requiring an integrated approach with fouling and cleaning for surface tailoring (Boxler et al., 2013b).

Due to the buffer capacity of the whey protein, the pH was constant during the experiments, at both initial surface temperatures.

At an initial temperature T_0 = 80 °C, three different structures on deposit could be observed: (*i*) regions with separately crystalline or proteinaceous (= gelatinous-like structure) deposits (Fig. 4.35a), which promote an inhomogeneous fouling layer (see also Fig. 4.50, used surfaces); (*ii*) protein on the crystalline aggregates (Fig. 4.35b); and (*iii*) hydroxyapatite aggregates entrapped in the protein matrix (Fig. 4.35c). At T_0 = 120 °C, the deposits on the diverse coated surfaces were visually very similar (Fig. 4.36, see Fig. 4.63 for wet deposits) and completely covered the surface with a thickness varying from 200 to 250 µm. However, the deposit structure was heterogeneous and the upper layer was rough due to the formation of bubbles during deposition (Fig. 4.37). Regions characteristic to crystalline and/or proteinaceous deposits and slightly scorched material of the beneath fouling layer could be observed.

It is expected that the multilayer deposition is independent of the properties of the primary surface. However, the fouling curves in Fig. 4.35 show that the different aging processes took place at the initial fouling layers, influencing the subsequent deposit formation and hence the overall fouling process. Moreover, the influence of the surface on further fouling process steps of (*i*) WPI at wall temperature of T_0 = 120 °C after 150 min (Fig. 4.26b) and (*ii*) calcium phosphate at T_0 = 80 °C after 90 min and at T_0 = 105 °C after 80 min (Fig. 4.28), as well as the fouling layer structure and composition, was also observed.

However, this influence was lower in the case of deposition at higher surface temperature (compare Figs. 4.32 a-c, Figs. 4.32 b-d and Figs. 4.28 a-b), in which the chemical reaction rates in bulk (protein denaturation and agglomeration and calcium phosphate precipitation) were faster.

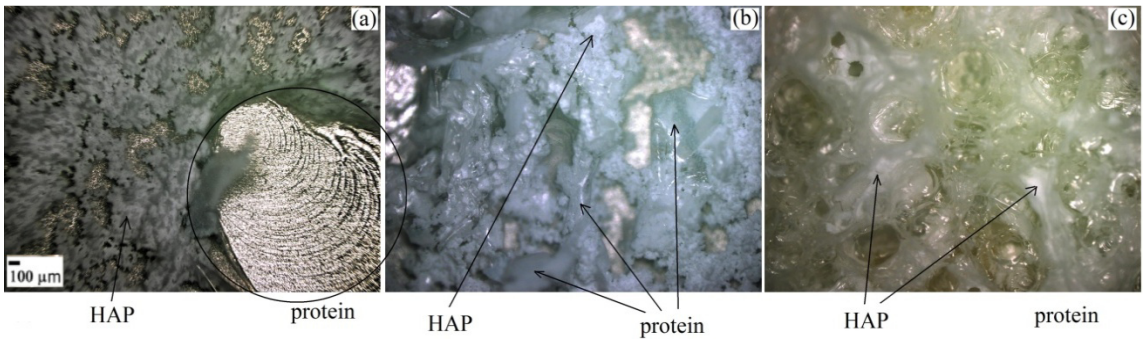

Fig. 4.35. Dry deposits of SMUF-rich whey protein solution at T_0 = 80 °C. HAP = hydroxyapatite

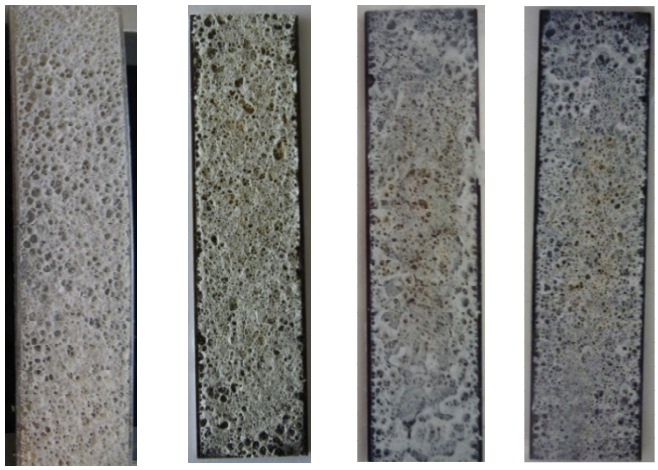

Fig. 4.36. WPI plus SMUF dry deposit at T_0 = 120°C after 90 min fouling on (a) SS, (b) DLC, (c) SICAN and (d) SICON®

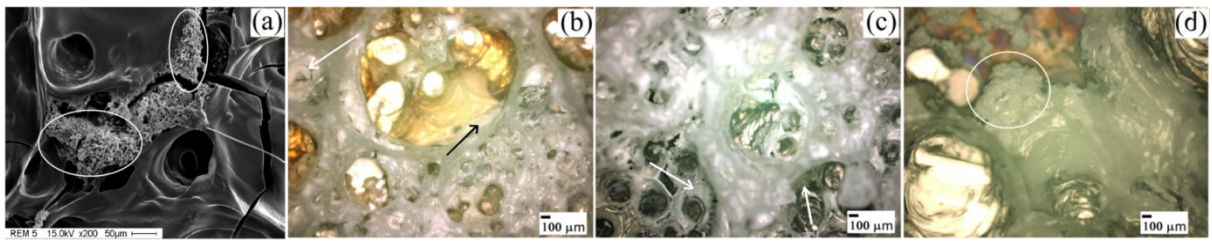

Fig. 4.37. Dry deposits of SMUF-rich whey protein solution formed on (a) ESS, (b) SS, (c) DLC and (d) SICON® at T_0 = 120 °C. Hydroxyapatite aggregates are marked on the images

At T_0 = 120 °C, the heat transfer surfaces reached a temperature of 150 °C – 190 °C after 30 min fouling, depending on the surface treatment. At high temperatures, the protein matrix will convert to a more carbonaceous form with a corresponding increase in thermal conductivity (Davies et al., 1997). Temperatures above 105 °C lead to the decomposition of hydrogen sulfide and methyl sulfide from cysteine residue and formation of dehydroalanine, which continues to react, forming lanthionine and lysioalanine (Töpel, 2004). At temperatures above 130 °C, carboxylgroups of glutamic and aspartic acid react with amino group of lysine and crosslink to different polypeptide chains (Töpel, 2004). Moreover, according to Foster and Green (1990) and Changani et al. (1997), calcium and phosphorus probably diffuse through the protein matrix to the deposit-surface interface and the deposit structure changes with time. This raises the hypothesis that the different initial fouling layers on the various surfaces as well as the impact of aging will not only affect the deposit amount, but also its properties (microstructure, density and thermal conductivity) and consequently the fouling resistance R_f (Boxler et al., 2013b).

4.3.5 Effect of surface conditioning with calcium phosphate on formation of deposit

To better understand which milk component deposits first during the induction phase and show the influence of the initially attached layer on the succeeding stages of deposition, the fouling behavior of whey protein and SMUF rich-whey protein solutions on pre-fouled surfaces with calcium phosphate were compared with fouling on clean surfaces (bare surfaces).

The deposition behavior of WPI on the conditioned surfaces is shown in Fig. 4.38a for T_0 = 80 °C and Fig. 4.39a for T_0 = 120 °C. At T_0 = 80 °C, the fouling resistance was nearly close to zero during the experiments, with the exception of ESS, on which the final R_f reached a value of 0.7 x 10^{-4} K m^2 W^{-1}. Some increasing and negative values of R_f can be related to: (*i*) deposit formation and removal; or (*ii*) improvement of the heat transfer due to roughness/turbulence (Albert et al., 2011). Around 1 to 3 g m^{-2} deposit built up on the diverse surfaces (Table 4.22). The growth of a thin protein layer after 360 min could be verified by means of SEM (Fig. 4.40) and X-ray microanalysis. The protein adsorbed in the mineral layer, but a progressive growth of the fouling layer did not take place in the absence of additional calcium ions and further protein denaturation. The peel off of the dried deposit was principally observed for those surfaces with high γ^- (Fig. 4.40b). Accordingly, the fouling was comparable to the WPI fouling on clean surfaces discussed at the beginning of section 4.3.1. (Boxler et al., 2013b) These results agree with those of Delsing and Hiddink (1983), who found that the presence of calcium ions in bulk solution is essential for the growth of protein fouling layers. Furthermore, steric hindrance by the pre-adsorbed β-lg could also inhibit further deposition of β-lg (Kim and Lund, 1998).

Fig. 4.39a shows the WPI deposition at T_0 = 120 °C on untreated and electropolished stainless steel conditioned with SMUF. As by the fouling of pure whey protein at higher initial temperature the buildup and growth of the fouling layer, measured as continuous increase of R_f, was observed on both surfaces. Again, similar $R_{f,\,end}$ and mass were obtained as in the deposition of pure whey protein at 120 °C (Table 4.22, see Table 4.15 for comparison).

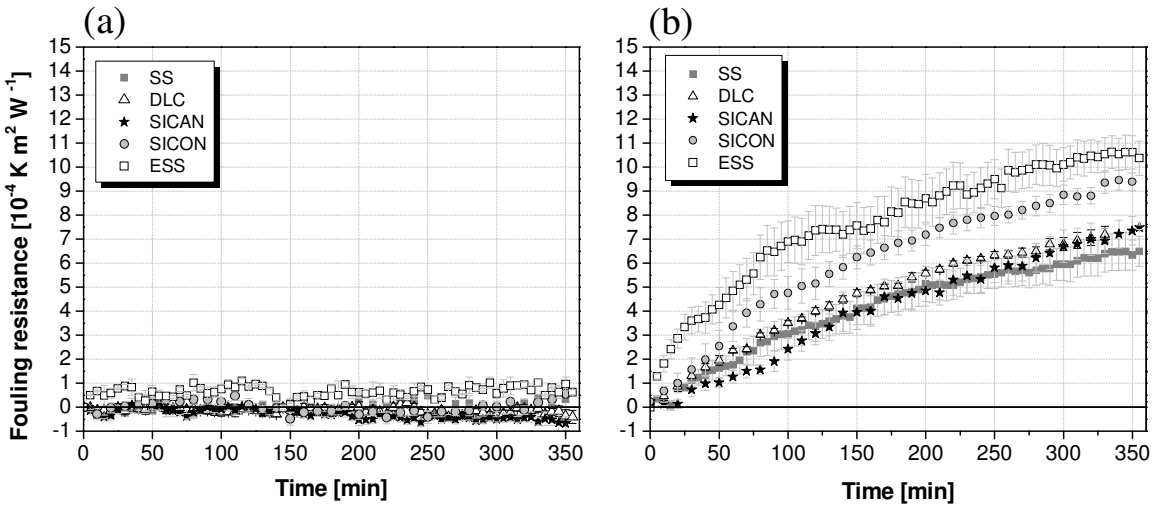

Fig. 4.38. Fouling resistance for (a) WPI and for (b) WPI plus SMUF at T_0 = 80 °C on surfaces pre-conditioned with SMUF

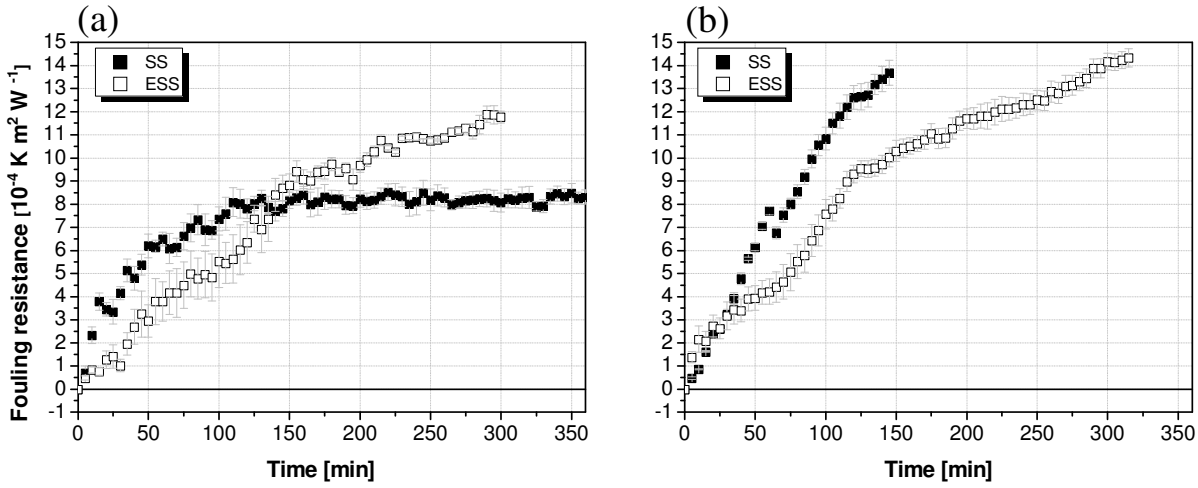

Fig. 4.39. Fouling resistance for (a) WPI and for (b) WPI plus SMUF at T_0 = 120 °C on surfaces pre-conditioned with SMUF

Figs. 4.38b and 4.39b depict the fouling curves of whey protein plus SMUF on the pre-conditioned surfaces at T_0 = 80 °C and 120 °C, respectively. The conditioning of the surface reduced the fouling formation T_0 = 80 °C on SS, whereas more deposit was built up on the coated surfaces and similar $R_{f, end}$ and similar deposit amount was measured on the ESS (Table 4.23).

At T_0 = 120 °C, the deposition of WPI plus SMUF on the conditioned surfaces (Table 4.23) was lower than on clean surfaces (see Tables 4.19 and 4.21 for comparison). After 90 min, namely the exposure time of the clean SS and ESS surfaces, a $R_{f, end}$ of around 19 x 10^{-4} K m^2 W^{-1} was reached, while after the same experiment time on the conditioned surfaces $R_{f, end}$ of 10 x 10^{-4} K m^2 W^{-1} and of 7 x 10^{-4} K m^2 W^{-1} were measured for the SS and ESS, respectively. However, this improvement might be due to the lower specific heat flux

used ($\dot{q}$ = 40 kW m^{-2} for the pre-conditioned surfaces, while $\dot{q}$ = 58 kW m^{-2} for the clean surfaces).

The results show that the influence of the surface properties on fouling was lower due to the first mineral layer, given that more similar fouling progress and masses were obtained than on the deposition on the clean surfaces. However, the fouling progress and the deposit mass were still affected by the surface properties. It is noteworthy that the different calcium phosphate deposit morphologies and structures on the different coated surfaces formed after 30 min (see Fig. 4.31 for T_0 = 80 °C).

Table 4.22. Fouling rate for the first hour $(dR_f/dt)_{1h}$, final fouling resistance and deposit dry mass of WPI on with SMUF conditioned surfaces

T_0 [°C]	Surface	Fouling rate [10^{-4} m^2 K W^{-1} h^{-1}]	$R_{f, end}$ [10^{-4} m^2 K W^{-1}]	Mass [g m^{-2}]
80	SS	0.02 ± 0.02	0.2 ± 0.1^{a}	1.9 ± 0.4^{f}
	DLC	0.1 ± 0.1	- 0.2 ± 0.1^{bc}	3.5 ± 0.6^{fgh}
	SICAN	- 0.1 ± 0.1	- 0.6 ± 0.2^{ade}	1.2 ± 0.3^{gi}
	SICON®	0.41 ± 0.01	0.3 ± 0.1^{be}	2.7 ± 0.2^{i}
	ESS	0.45 ± 0.05	0.7 ± 0.1^{cd}	1.0 ± 0.1^{h}
120	SS	5.3 ± 0.5	8.4 ± 0.2	87 ± 7
	ESS*	4 ± 1	11.6 ± 0.3	63 ± 12

Superscript letters indicate significant differences for the fouling rate, $R_{f, end}$ and mass at the two initial surface temperatures (80 °C and 120 °C) separately ($p < 0.05$). *The experiment was stopped after 300 min.

Table 4.23. Fouling rate for the first hour $(dR_f/dt)_{1h}$, final fouling resistance and deposit dry mass of WPI plus SMUF on with SMUF conditioned surfaces

T_0 [°C]	Surface	Fouling rate [10^{-4} m^2 K W^{-1} h^{-1}]	$R_{f, end}$ [10^{-4} m^2 K W^{-1}]	Mass [g m^{-2}]
80	SS	2.0 ± 0.2^{a}	7.5 ± 0.7^{ghi}	60 ± 5^{op}
	DLC	1.71 ± 0.07^{b}	4.3 ± 0.6^{gjk}	49 ± 5^{qr}
	SICAN	0.83 ± 0.05^{cd}	5.0 ± 0.3^{hlm}	53 ± 6st
	SICON®	2.6 ± 0.3^{ace}	7.2 ± 0.4^{bjln}	100 ± 8^{oqs}
	ESS	4 ± 1^{abde}	10.5 ± 0.5^{ikmn}	98 ± 15^{prt}
120	SS	7.8 ± 0.3^{f}	13.1 ± 0.4	187 ± 16
	ESS*	3.6 ± 0.4^{f}	14.1 ± 0.3	204 ± 18

Superscript letters indicate significant differences for the fouling rate, $R_{f, end}$ and mass at the two initial surface temperatures (80 °C and 120 °C) separately ($p < 0.05$). *The experiment was stopped after 150 min.

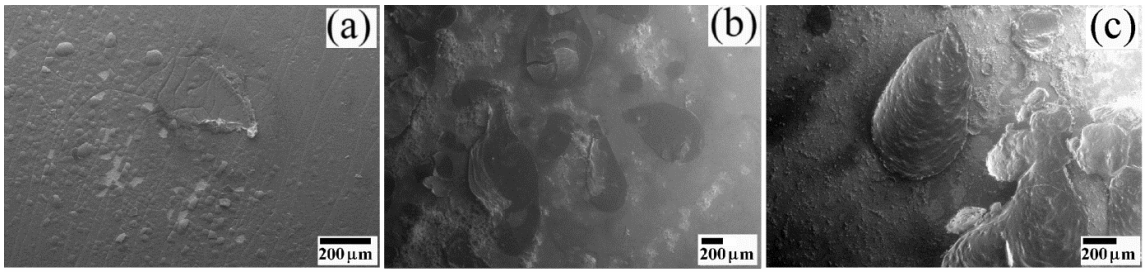

Fig. 4.40. Scanning electron micrographs of WPI deposit on (a) SS, (b) SICAN and (c) SICON® pre-conditioned with calcium phosphate at an initial surface temperature of 80 °C after 360 min.

Finally, summarizing the results of all experiments at T_0 = 80 °C and 105 °C or 120 °C and comparing the results from WPI and from WPI plus SMUF on clean surfaces and conditioned surfaces (Fig. 4.41), it is possible to conclude that the surface will not only affect the initial fouling layer but also the subsequent deposit build up. Furthermore, the results confirm that the first fouling layer is formed by salts and protein simultaneously, resulting in layers with different properties such as structure and composition on the diverse surfaces.

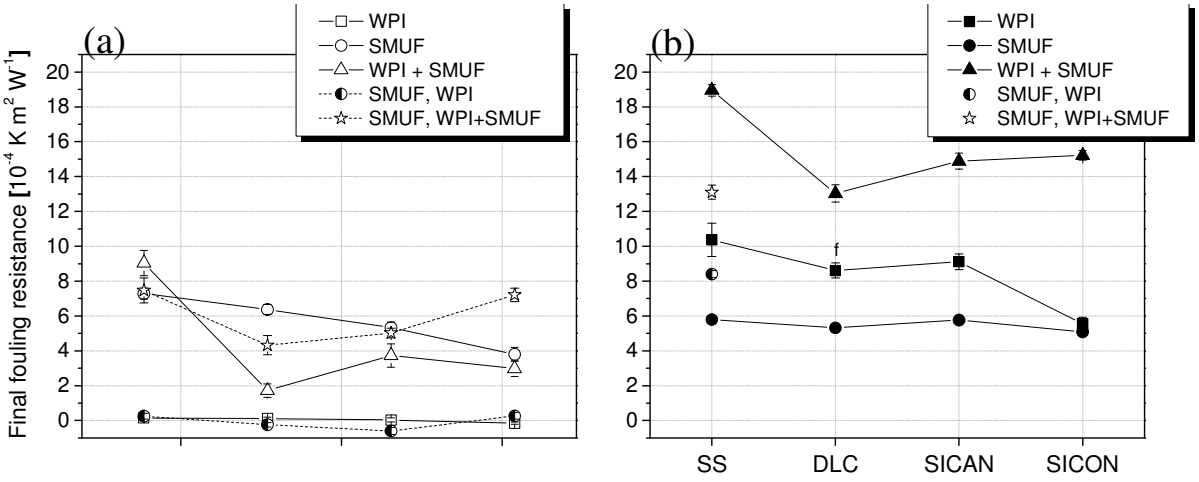

Fig. 4.41. Final fouling resistance of whey protein, calcium phosphate and SMUF-rich whey protein solution as function of the surface coating and surface conditioning at initial surface temperatures of (a) 80 °C and (b) 120 °C (105 °C for SMUF). Surfaces presented in increasing order of γ^- value.

As shown in sections 4.3.1, 4.3.2 and 4.3.3 for the deposition of the model solutions of whey protein, calcium phosphate and SMUF rich-whey protein solution, respectively, no linear relationship between the final thermal fouling resistance and the deposit mass could be found. Fig. 4.42 gives the $R_{f,\,end}$ as function of the resulting deposit mass for the deposition of all model solutions including milk (whose results will be discussed in section 4.3.6) on the studied surfaces. (Lines are shown to guide the eye and do not represent modelling results).

The thermal fouling resistance increases similarly linearly with the deposit mass up to a deposit mass of 100 g m^{-2} (viz. $R_{f,\,end}$ of 10 x 10^{-4} K m^2 W^{-1}). For further deposition, the linearity of the curve flattens out, viz. the influence of the deposit quantity on the fouling resistance was lower. This is probably due to deposit aging, as discussed in detail in section 4.3.3 for WPI plus SMUF fouling. At T_0 = 120 °C, raw milk deposited faster than the model solutions and scorched material of the under fouling layer could be observed, clearly showing the deposit aging. According to Epstein (1981), a hard nonporous deposit will typically have relatively high values of both density and thermal conductivity, while a soft porous deposit will have considerably lower values of ρ_f and λ_f. Thus, Eq. (2.6) can be written in differential form to allow the possible variation of ρ_f and λ_f (Epstein, 1981):

$$dR_f = \frac{dx_f}{\lambda_f} = \frac{dm_f}{\rho_f \lambda_f} \tag{4.1}$$

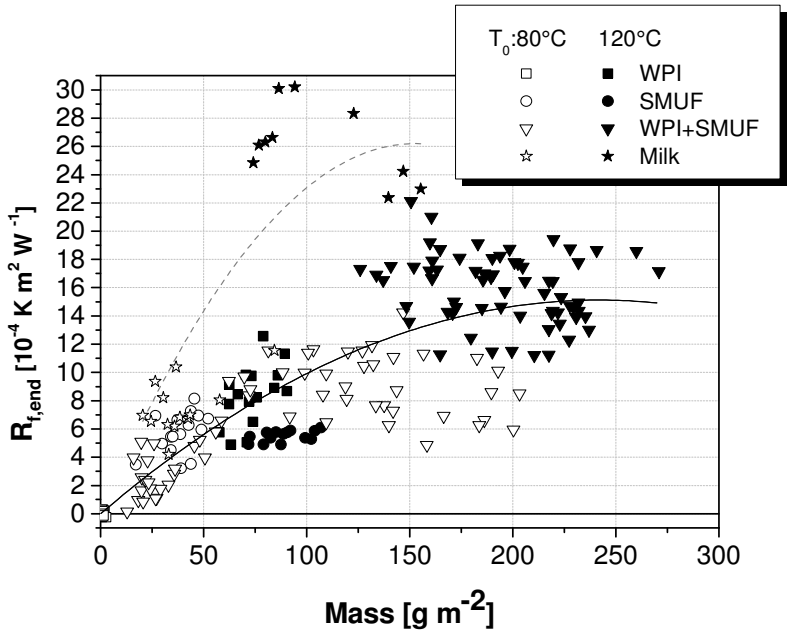

Fig. 4.42. Final fouling resistance for deposition of whey protein, SMUF, WPI plus SMUF and milk at initial temperatures of 80 °C and 120 °C (for SMUF, 105 °C) as a function of deposit mass. Full line: all model solutions, including milk at T_0 = 80 °C, dashed line: milk at T_0 = 80°C and 120 °C

4.3.6 Effect of surface coating on milk fouling

The fouling progress by raw milk deposition on the DLC coated surfaces is shown in Fig. 4.43. Despite the natural variations in the milk composition, a good reproducibility of the experiments in terms of fouling resistance was obtained, although a variation on the dry deposit mass up to 20 % for some surfaces was measured. The fouling growth phase began immediately without an induction period for all surfaces. At initial surface temperature T_0 = 80 °C the SICAN coating showed one slight fouling tendency due to the low buildup: low $R_{f,\,end}$ and low $(dR_f/dt)_{1h}$ (Table 4.24). The profile of the fouling curves for the stainless

steel, electropolished stainless steel and DLC were almost identical. At T_0 = 120 °C, no significant difference regarding fouling between the coated and uncoated stainless steel surfaces could be detected. No linear correlation between $R_{f, end}$ and deposit mass was found, suggesting, as for the WPI, SMUF and WPI plus SMUF fouling, that the deposit microstructure on the studied surfaces was different or that an aging process was taking place (principally at T_0 = 120 °C).

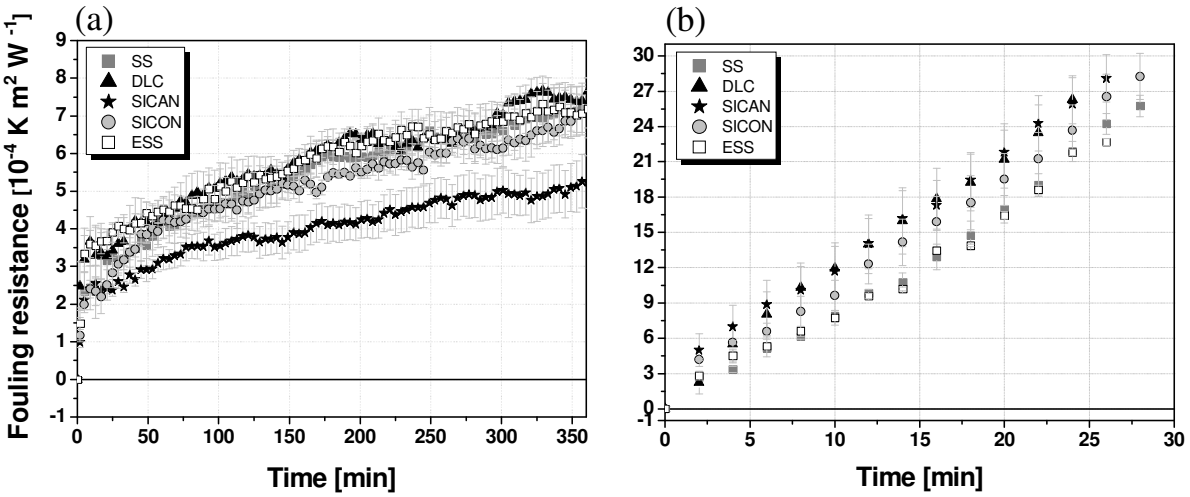

Fig. 4.43. Fouling resistance for raw milk at T_0 = (a) 80 °C and (b) 120 °C

Table 4.24. Fouling rate for the first hour $(dR_f/dt)_{1h}$, final fouling resistance and deposit dry mass of raw milk

T_0 [°C]	Surface	Fouling rate [10^{-4} m^2 K W^{-1} h^{-1}]	$R_{f, end}$ [10^{-4} m^2 K W^{-1}]	Mass [g m^{-2}]	T_{end} [°C]
80	SS	2.3 ± 0.5	7.2 ± 0.6^{a}	195 ± 9	109 ± 1
	DLC	1.9 ± 0.6	7.8 ± 0.3^{b}	86 ± 22	106 ± 2
	SICAN	1.6 ± 0.5	5.4 ± 0.9^{abcd}	116 ± 40	104 ± 2
	SICON®	2.9 ± 0.3	7.2 ± 0.3^{c}	185 ± 57	110.5 ± 0.7
	ESS	2.1 ± 0.3	7.2 ± 0.4^{d}	131 ± 52	107 ± 0.5
120	SS	54 ± 2	25.0 ± 0.6	290 ± 34^{g}	226 ± 3
	DLC	63 ± 4	25 ± 2	302 ± 89^{h}	229 ± 8
	SICAN	60 ± 3	27 ± 1^{e}	298 ± 64^{i}	230 ± 6
	SICON®	56 ± 6	27 ± 1^{f}	394 ± 53^{h}	232 ± 4
	ESS	50 ± 2	22.2 ± 0.3^{ef}	397 ± 58^{gi}	222 ± 2

Superscript letters indicate significant differences for the fouling rate, $R_{f, end}$ and mass at the two initial surface temperatures (80 °C and 120 °C) separately ($p < 0.05$).

The fouling behavior of milk on the coated surfaces at low and high initial surface temperatures distinguished from the SMUF-rich protein solution as follows:

- more mass built up by milk fouling than by WPI plus SMUF fouling (cp. Tables 4.24 and 4.19);

- the final fouling resistance by milk fouling was higher than by WPI plus SMUF fouling (cp. Tables 4.24 and 4.18);
- the deposition of milk at T_0 = 80 °C as well as at T_0 = 120 °C was faster, viz. the fouling rate for the first hour $(dR_f/dt)_{1h}$ was higher for milk than for the SMUF-rich WPI solution (cp. Tables 4.24, 4.18 and 4.20). At T_0 = 120 °C, the limit surface temperature of 230 °C was achieved after about 50 min for milk, while the deposition of SMUF-rich WPI solution took 90 min;
- milk dry deposit presented a bubble-like or spongy structure (Fig. 4.44) as the deposit of WPI plus SMUF at T_0 = 120 °C (Fig. 4.36). Accordingly, a heterogeneous spongy deposit has also been related in the literature (Tissier and Lalande, 1986) after the heat processing of milk. However, the milk deposit showed a yellowish color or seemed to be more turbid than the deposit of WPI plus SMUF eventually due to casein or fat. Furthermore, slightly scorched material of the lower fouling layer could be observed on the SS and DLC surfaces. At relatively moderate heating temperatures below 100 °C, the β-lg dominates the composition of the milk protein covering (Bansal and Chen, 2006). Nonetheless, according to McGuire and Swartzel (1989), the caseins (α_1, α_2, β and κ-caseins) which are organized into micellar structure, are extremely stable, but may become part of the fouled layer by entrapment. Exposing the milk to high temperatures for long periods of time, micellar components might also irreversibly adsorb. Additionally, fat globules may also entrap into the fouling layer and contribute to deposit growth. By heating at high temperatures (> 100 °C) the milk fat membrane damages, resulting in more fouling (Bansal and Chen, 2006), because lipoprotein complexes tend to migrate faster toward the heated surface (Visser and Jeurnink, 1997a). This can explain why fouling was more intense with milk than WPI plus SMUF, particularly at higher wall temperature; and
- little or no calcium phosphate agglomerates could be observed at T_0 = 80 °C by milk fouling comparing to the WPI plus SMUF deposits. Identical results were obtained by Robbins et al. (1999), who compared deposition of WPC and milk on stainless steel. Calcium phosphate crystals spread over the deposit, not being located in particular areas, as with the WPC plus SMUF deposit. In milk, calcium ions are partially associated with casein molecules, while in SMUF-rich WPI solution Ca^{2+} is free to precipitate with PO_4^- (as in pure SMUF solution), as well as binding to β-lg promoting its aggregation. Fig. 4.45 shows bubble-like and protuberance structures, as well as some agglomerates or microparticles of calcium phosphate, which could be identified by X-ray microanalysis (Fig. 4.46).

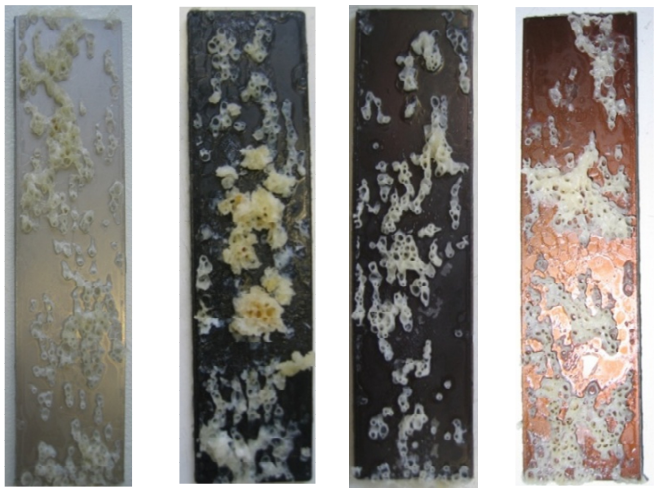

(a) (b) (c) (d)

Fig. 4.44. Milk deposit after 360 min at T_0 = 80°C on (a) SS, (b) DLC, (c) SICAN and (d) SICON®

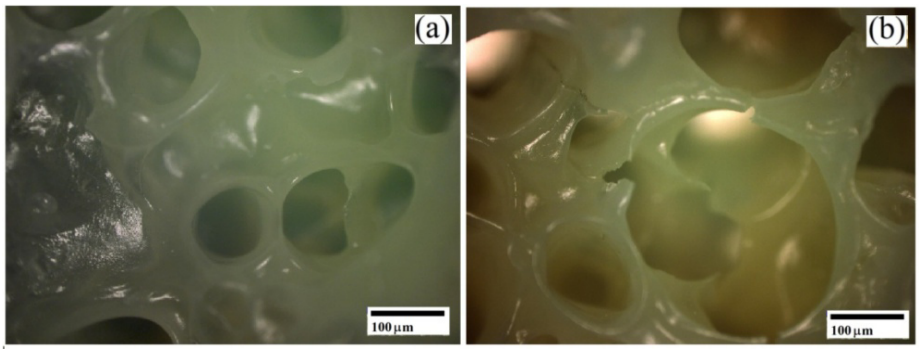

Fig. 4.45. Milk deposit on (a) SS and (b) SICON® surfaces generated at T_0 = 80 °C.

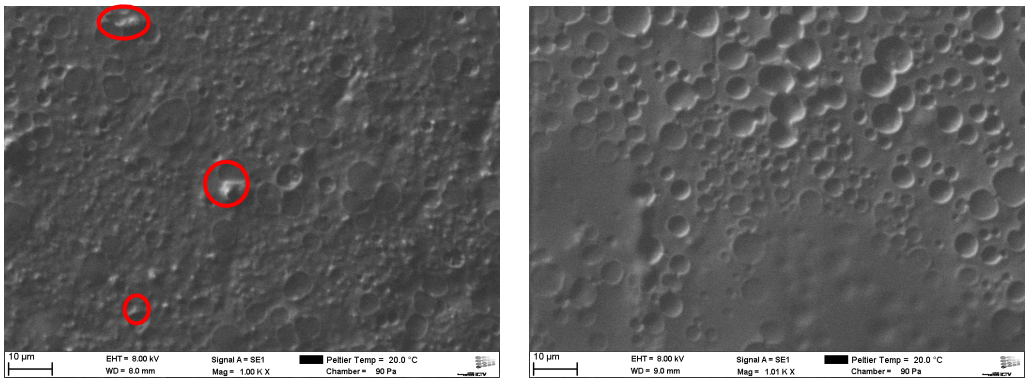

(a) (b)

Fig. 4.46. SEM micrographs of milk deposit on (a) DLC and (b) SICON® surfaces generated at T_0 = 80 °C. Calcium phosphate aglomerates are marked on the images.

The pH progress during deposition at both initial wall temperatures for all investigated surfaces is presented in Fig. 4.47. The difference between the pH evolutions in bulk for the diverse surfaces could be observed, as for calcium phosphate deposition, indicating that different mechanisms took place in the bulk solution. It should be noted that the pH of milk for the experiment with SICAN was lower, while the pH with ESS was higher than for the other surfaces.

Since milk becomes acid due to storage (1 - 3 days), it can explain the initial pH value of 6.40 ± 0.05. In the first 10 min, the pH decreased due to the conversion of soluble calcium and soluble inorganic phosphate to the colloidal phase (Anema, 2009). Otherwise, in the pH evolution of SMUF (Fig. 4.33), the pH increased during the course of the experiment achieving after 360 min up a value of 6.25 at T_0 = 80 °C and after 30 min up a value of 6.65 at T_0 120 °C. The observed pH change could have several reasons, such as:

• removal of carbon dioxide (Belmar-Beiny and Fryer, 1993);

• at pH values from 6.5 to 6.7, the association of β-lg with κ-casein the Ca^{2+} activity is stabilized (Kessler, 1996) and thus the precipitation of calcium phosphate is also stabilized;

• the unfolded proteins aggregate. In the aggregation reaction, ionic calcium from the serum is used to reduce calcium bridges between the molecules. The calcium subsequently does not take part in the crystallization reaction.

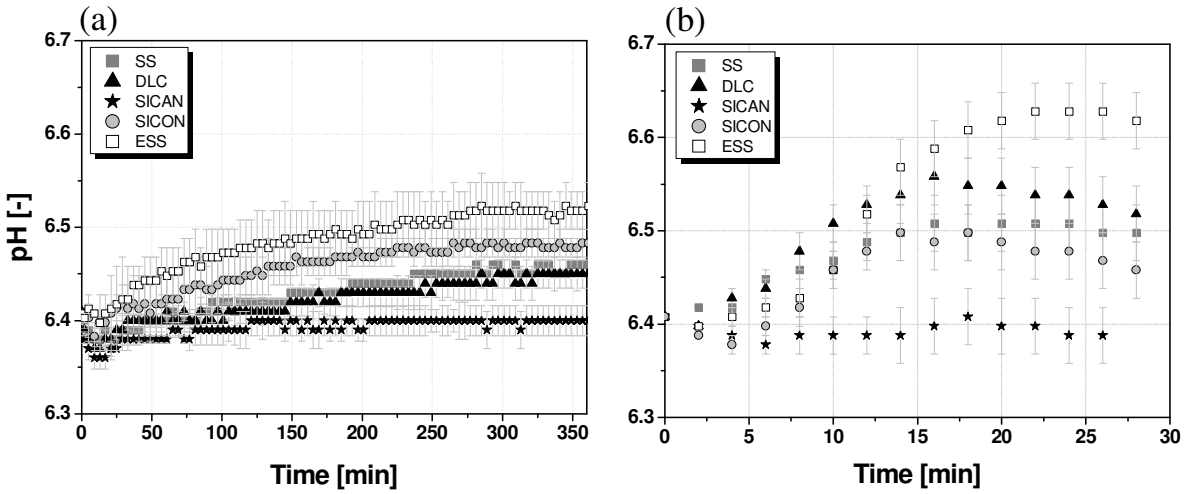

Fig. 4.47. pH evolution during milk deposition at T_0 = (a) 80 °C and (b) 120 °C

4.3.7 Influence of coating aging on fouling

Most of works provide no information about the history of the coating or do not discuss the reproducibility of deposition experiments after the use the coating several times. Section 4.1.5 showed that the chemical, topographic, energetic and electrokinetic surface properties of the studied DLC coatings changed after the fouling and cleaning processes. Therefore, the effect of the coating aging on deposition of the calcium phosphate-rich whey protein solution has been discussed in this section. The experiments were performed at T_0 = 80 °C, given that a greater difference between the fouling behaviors of the different DLC coated surfaces could be found at this temperature (see Fig. 4.34). Fig. 4.48 depicts the fouling curves on newly

coated surfaces, which can be compared to Fig. 4.34a for used surfaces under identical experimental conditions. The results of the repeated fouling runs at each coating separately are shown in Fig. 4.49.

The results indicate that the stainless steel and the newly coated surfaces demonstrate approximately similar fouling behavior (Fig. 4.48). However, the coating aging process affected the fouling behavior (Fig. 4.49). After contact with milk protein and salts or with cleaning agents, a significant difference in fouling and cleaning between the first, second and subsequent runs could be observed (siehe also section 4.5.1). Each trial represents the result of the deposition of two coupons. According to Jullien et al. (2002) and Boulangé-Peterman et al. (1995), any contact between stainless steel and food or detergents will alter the surface energy, consequently affecting the deposit formation. After an initial coating aging (about four fouling and cleaning runs), the reproducibility of the measurements was quite satisfactory. This result for thermal fouling resistance reflects the change in the surface energy, particularly concerning the electron donor component γ^- (see Fig. 4.7), which increased up to four fouling/cleaning cycles, thereafter remaining approximately constant. The final fouling resistance, the initial fouling growth rate and the deposit mass for the used coated surfaces were lower than for the new ones (Table 4.25). These results can be attributed to the variation on the energetic and electrokinetic surface properties for the coated coupons after several fouling/cleaning cycles.

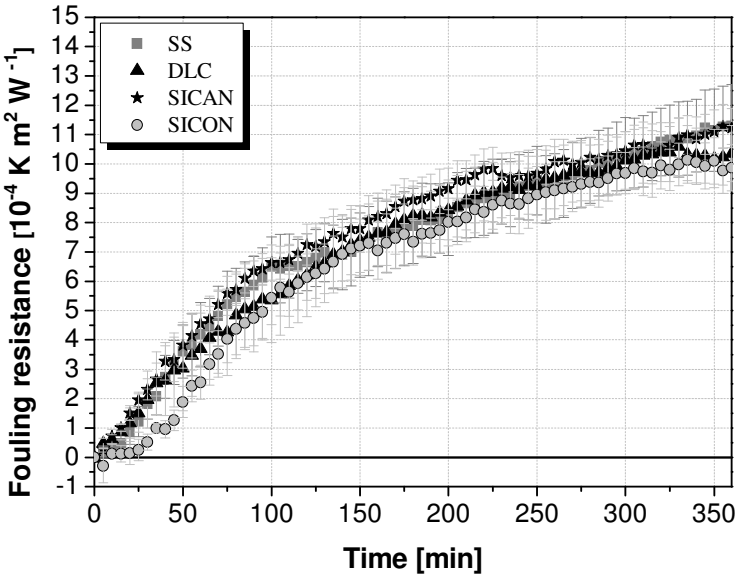

Fig. 4.48. Fouling resistance for WPI plus SMUF at T_0 = 80 °C on new (after one cleaning, no fouling run) surfaces

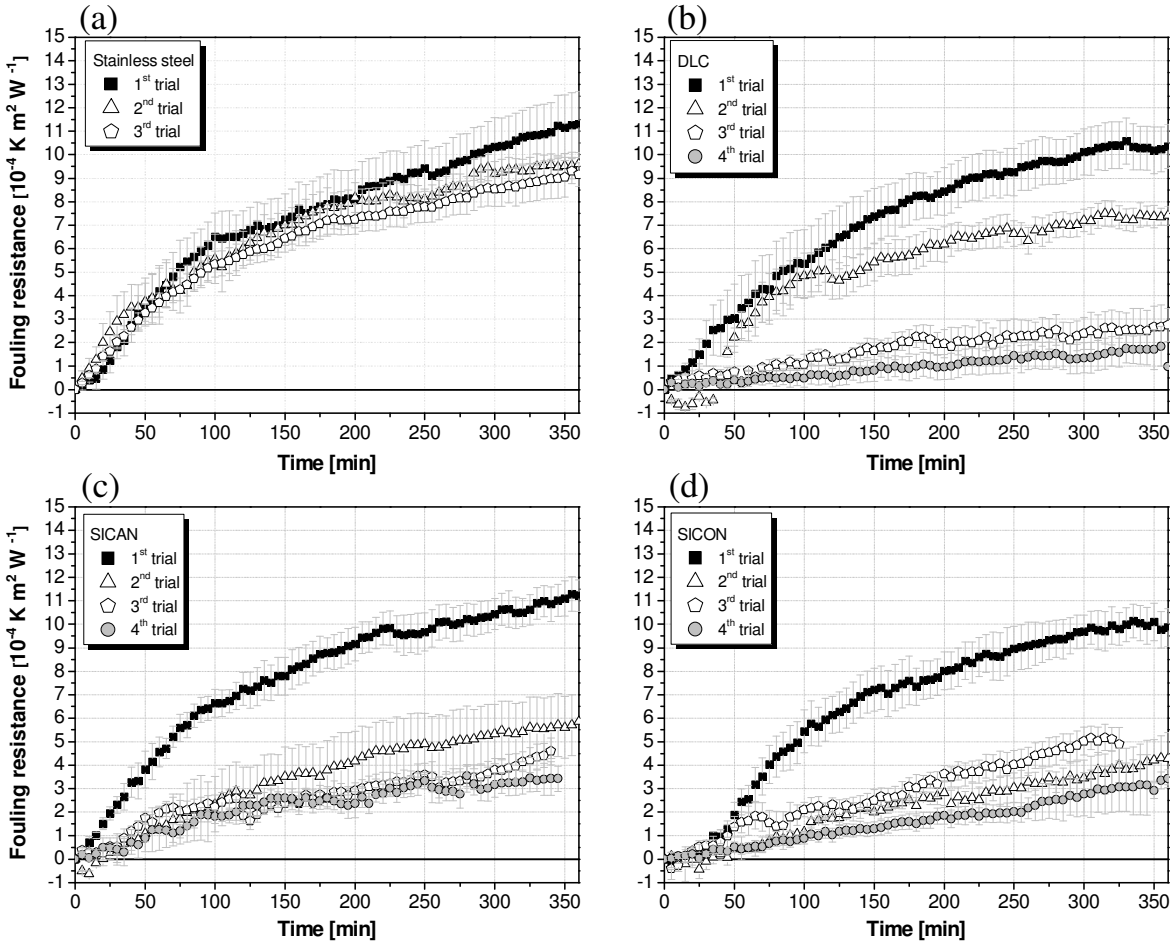

Fig. 4.49. Influence of the surface aging on the fouling resistance for WPI plus SMUF at T_0 = 80 °C on (a) SS, (b) DLC, (c) SICAN and (d) SICON®

Table 4.25. Fouling rate for the first hour $(dR_f/dt)_{1h}$ and deposit dry mass of SMUF rich-WPI deposition at T_0 = 80 °C

Surface	Fouling rate [10^{-4} m^2 K W^{-1} h^{-1}]		Mass [g m^{-2}]	
	new	used	new	used
SS	4.8 ± 0.6	5.0 ± 0.3	169 ± 10	149 ± 5
DLC	3.6 ± 0.7	0.58 ± 0.04	108 ± 22	23 ± 2
SICAN	4.6 ± 0.6	1.3 ± 0.3	164 ± 9	34 ± 5
SICON®	4.5 ± 0.6	0.9 ± 0.2	146 ± 6	32 ± 5

Fig. 4.50 compares typical deposits of SMUF rich-protein solution at T_0 = 80 °C after 360 min fouling on new (after first cleaning cycle) and used (after at least five fouling and cleaning cycles) surfaces.

The deposit on new coated surfaces seemed to be more proteinaceous than the deposit on used coupons due to the predominant gelatinous-like structure. On the stainless steel and on the used coatings both crystalline and proteinaceous deposits could be observed as well as hydroxyapatite aggregates entrapped in the protein matrix. The formation of bubbles or drop

shaped structure characterized the proteinaceous deposit. While on SS and DLC the dry deposit adhered strongly on the surface, on SICAN and SICON® the deposit peeled off in some regions indicating the low adhesion of the deposit in such surfaces.

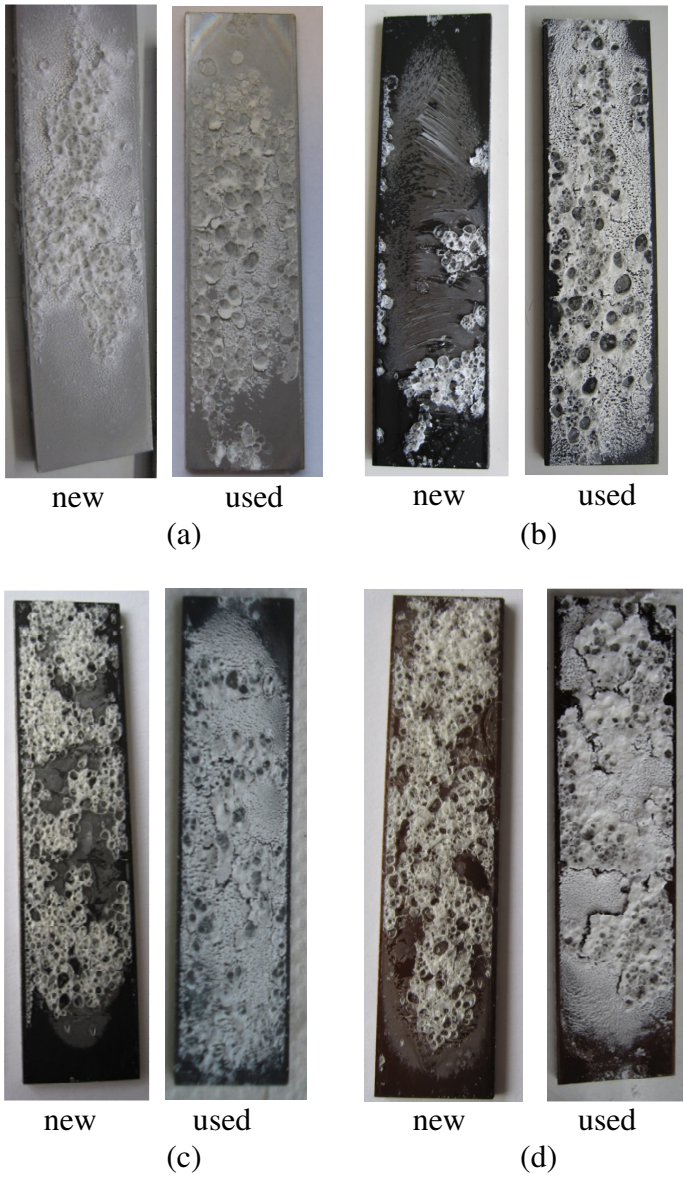

Fig. 4.50. Comparison of new and used surfaces fouled with WPI plus SMUF at T_0 = 80°C after 360 min fouling on (a) SS, (b) DLC, (c) SICAN and (d) SICON®

4.3.8 Continuous fouling of SMUF-rich whey protein (PHE)

Most deposition occurred in the top corner of the plates (inlet in Fig. 4.51), due to the low flow velocity and high temperature difference between product inlet and service fluid outlet (= 23 K) in this area. The plates' contact points or the stagnation zones, where the flow velocity is low, were also more prone to fouling. The deposition was strongly dependent on the energetic surface properties. On stainless steel and DLC, more deposit built up than on SICAN and SICON®. Fig. 4.52 compares the deposits formed on stainless steel, SICAN and SICON® in the plates' inlet upper third. Due to the low adhesion on SICAN, a peeling off of the deposit could be observed for the dry deposits (Fig. 4.52b), although no visible damage on the coatings could be detected during/after the experiments (Boxler et al., 2014a).

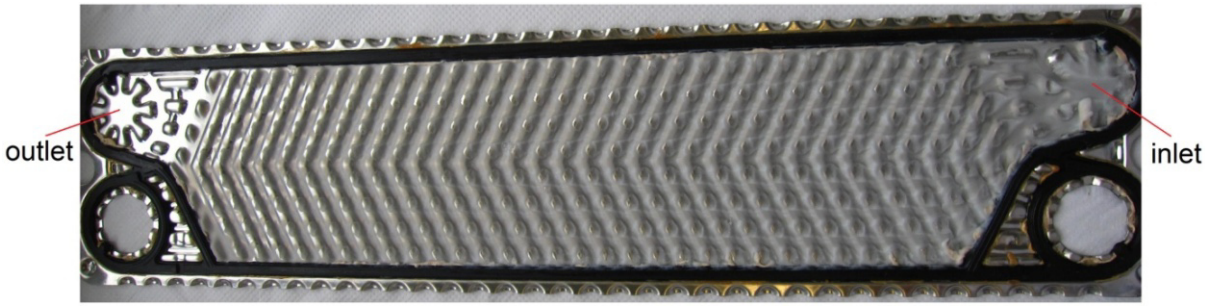

Fig. 4.51. Deposition pattern on stainless steel

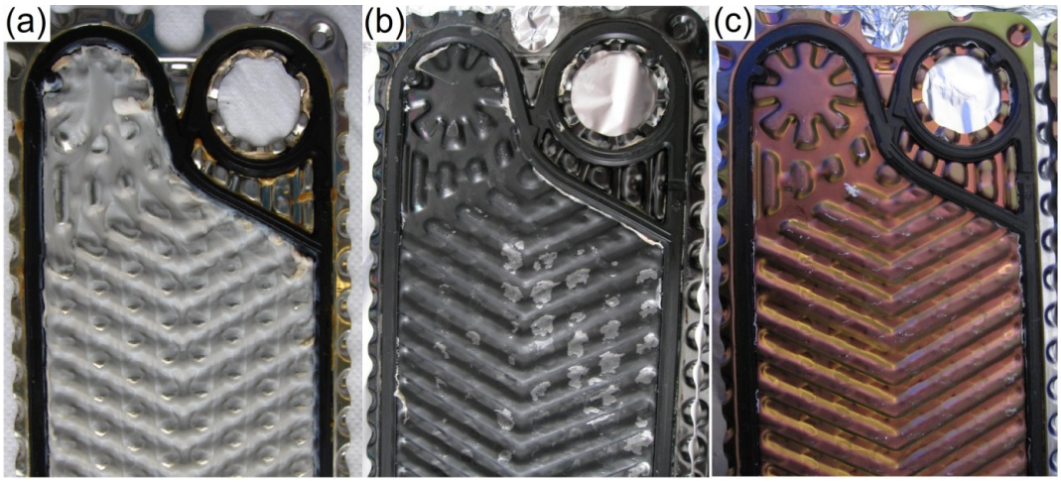

Fig. 4.52. Comparison of dry deposit on (a) stainless steel, (b) SICAN and (c) SICON®

The composition of the fouling layer on stainless steel and the coated surfaces is summarized in Table 4.26. A lower protein content of the deposit on DLC and SICAN and lower Ca and P contents on SICAN and SICON® were measured. On all surfaces, mineral attachment was greater than protein attachment. The influence of surface coating on the composition of deposits formed from calcium-rich whey protein solutions has not been reported in the literature. The results are in good agreement with the observations of Britten et al. (1988), who studied the influence of polymer coated surfaces on fouling of raw whole

milk. The authors found that the surface polar component affected the adhesion strength of such deposits, promoting more adhesion of mineral than protein.

Comparing the results of the batch-wise and continuous deposition (cp. Tables 4.19 and 4.26, for deposit composition), it can be noted that the amount of Ca and P was higher for the continuous fouling than for the batch-wise fouling, although the continous experiment was carried out in less time (continuous fouling = 120 min; batch-wise fouling = 360 min). While the protein content was lower for the continuous fouling than for the batch-wise fouling (initial concentration of β-lg in the bulk solution: continuous fouling = 30 g L^{-1}; batch-wise fouling = 3 g L^{-1}), that results from the different amount of native, denatured and agglomerate protein during the fouling experiments in both apparatus (see sections 4.2.1 and 4.2.2).

The molar Ca/P ratio varied for the different surfaces, as also previously observed for batch-wise fouling experiments. The molar Ca/P ratio was close to 0.7 for stainless steel and varied from 0.5 to 1.2 for the coated surfaces (1.2, 0.7 and 0.5, for DLC, SICAN and SICON®, respectively). The molar Ca/P ratio was lower than the values found in the literature (Lyster 1965; Daufin and Labbé 1998) for milk processing on uncoated stainless steel heat exchangers, which was close to 1.5, indicating the formation of tricalcium phosphate (Boxler et al., 2014a).

The fouling layers on the Si doped coatings not only differed in terms of the amount of deposit, which is reflected in the fouling resistance, but also the deposit composition (see protein/mineral ratio, Table 4.26) and most likely the deposit structure, as well as protein and mineral arrangements. Consequently, the fouling layers' adhesive and cohesive strengths were altered. These results are in accordance with Rosmaninho and Melo (2007), who found differences regarding the deposition rate, final deposit amount and morphology as well as adhesion of WPI plus SMUF deposits, depending on the surface energy. Their experiments were conducted under continuous flow conditions (Re = 6256), but at a lower wall temperature than in this work (ΔT = 1.5 K, T_{bulk} = 50 °C) and using TiN coated surfaces.

Table 4.26. Deposit chemical composition and final fouling resistance on modified surfaces

Surface	Protein [g m^{-2}]	Mineral [g m^{-2}]	Ca [g m^{-2}]	P [g m^{-2}]	Protein/ mineral [%]	$R_{f,end}$ [10^{-5} m^2 K W^{-1}]
SS	5.0 ± 0.5^{ab}	281 ± 23	41 ± 7^{c}	46 ± 4	1.8 ± 0.2^{f}	3.8 ± 0.1^{h}
DLC	2.1 ± 0.2^{a}	253 ± 22	58 ± 9^{cde}	36 ± 8	0.8 ± 0.2^{fg}	2.4 ± 0.2^{hij}
SICAN	2.9 ± 0.8^{b}	220 ± 11	35 ± 4^{d}	42 ± 9	1.3 ± 0.2	0.44 ± 0.06^{ik}
SICON®	4.2 ± 0.6	246 ± 16	20 ± 8^{e}	44 ± 10	1.7 ± 0.2^{g}	4.6 ± 0.2^{jk}

Letters *a* to *g* refer to statistically different values of fouling layer composition and letters *h* to *k* of final fouling resistance ($p \leq 0.05$).

The fouling progress for the modified surfaces is shown on Fig. 4.53. (Lines are shown to guide the eye and do not represent modelling results). A continuous increase of the thermal fouling resistance was observed during the 120 min experiment, except for the SICAN coated surface, upon which R_f decreased down to 45 min. In the first 15 min, a similar evolution of the fouling resistance could be measured for all surfaces. Thereafter, the fouling curves drifted apart, indicating that subsequent stages of deposition and removal were affected by the

surface properties. Fluctuations of the fouling curves of DLC, SICAN and SICON® show that the deposit was periodically removed from the surface due to the combination of shear stress and low adhesion on the coatings. Similar fouling behavior was observed by Geddert et al. (2009) for $CaSO_4$ fouling and by Boxler et al. (2011) for SMUF deposition on identically DLC-based coated surfaces under continuous flow conditions. Geddert et al. (2009) suggested the subdivision of the fouling process into two major influences: (*i*) for lower fluid velocities, the crystallization (amount of nucleis and growth) is the key factor; and (*ii*) with increasing Reynolds number, the interaction between surface and fouling layer becomes more important, with the adhesion now reflecting the key factor.

To compare the fouling on standard stainless steel versus coated steel, the average R_f value for the last 15 min was calculated ($R_{f,\ end}$) and is given in Table 4.26. SICAN showed the highest reduction in fouling resistance compared to the untreated stainless steel plate or SICON®, which revealed the highest R_f upon the experiments' conclusion (Boxler et al., 2013c).

Fig. 4.54 depicts the pressure drop profile by the deposition on the coated surfaces, giving further information about the fouling progress. Since the mean product and service flow rates as well as the service inlet temperature (specific heat flux $\dot{q}$ = constant) were kept constant during the deposition, the pressure drop increased due to the fouling layer formation. The pressure drop increase was higher on SS, followed by DLC, SICAN and SICON®. As with the fouling curves, fluctuations of the pressure drop were observed due to periodical deposit removal.

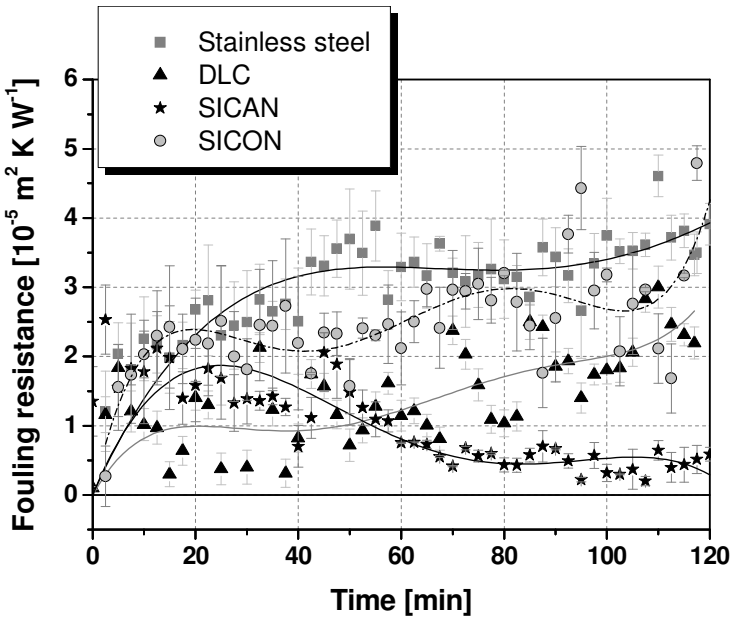

Fig. 4.53. Fouling resistance for WPI plus SMUF deposition on the coated surfaces

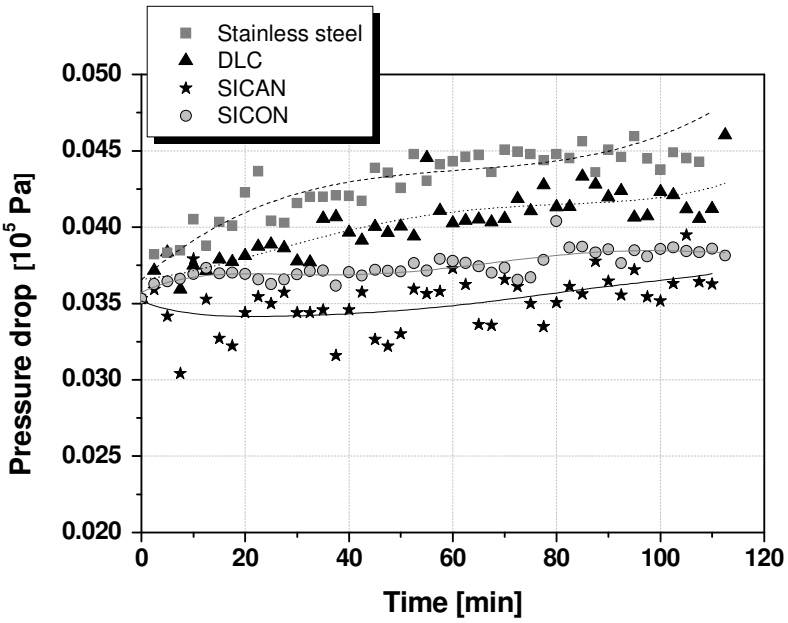

Fig. 4.54. Pressure drop profile for WPI plus SMUF deposition on the coated surfaces

4.4 Statistical fouling modelling

Since initial surface temperature, model fluid and surface modification significantly influenced the fouling, as previously shown, the separate and the simultaneous effect of these three variables on the final fouling resistance and the deposit mass is extensively analyzed in this section.

4.4.1 Batch-wise fouling

In this work, the γ_s^{LW} values were statistically identical, viz. the optimum surface tension is only dependent on the polar contribution. On the other hand, the electron donor component γ^- was the main energetic differentiating factor between the coated surfaces; therefore, a correlation of this component with the fouling behavior was considered. The roughness depth (R_z) reflected the further surface property considered in the analysis.

The analysis of variance (see Tables A3, A4, A9 and A10 for $R_{f,\,end}$, Tables A5, A6, A11 and A12 for mass and Tables A7, A8, A13 and A14 for $(dR_f/dt)_{1h}$) showed that the effect of T_0, γ^-, R_z, the quadratic terms of γ^-, T_0, fluid and R_z, as well as the combined effect of T_0 x fluid, T_0 x R_z, T_0 x γ^- and R_z x fluid were statistically significant ($p < 0.10$) for the final fouling resistance $R_{f,\,end}$, while the effects of T_0, and R_z, the quadratic terms of γ^- and R_z as well as the combined effect of T_0 x fluid, T_0 x R_z and T_0 x γ^- were statistically significant ($p < 0.10$) for the deposited mass and the effects of T_0, γ^-, R_z, the quadratic terms of γ^-, T_0 and fluid as well as the combined effect of T_0 x fluid and R_z x fluid were statistically significant ($p < 0.10$) for the initial fouling rate $(dR_f/dt)_{1h}$.

Fig. 4.55 depicts the most significant factors influencing $R_{f,\,end}$, while Fig. 4.56 shows the most significant factors influencing mass and Fig. 4.57 the most significant factors affecting $(dR_f/dt)_{1h}$ (see also the main effect plots, Figs. A8 – A10 in appendix). The absolute

values of T-Statistic (Eq. (3.39)) from the multiple regression analysis, also refered to as standardized effects, provide the heights of the bars that are arranged in descending order in the pareto diagram (Figs. 4.55 - 4.57). The value for T-Statistic = $T-\text{Statistic}_{(n_{sample}-2;2.5\%)}$ completes the diagram, providing the value as from which, the effects are significant.

In summary, the final fouling resistance $R_{f,\,end}$, the deposited mass and the initial fouling rate $(dR_f/dt)_{1h}$ increased with T_0 and decreased with R_z for the investigated parameter ranges ($80 < T_0 < 120$ °C; $0.8 < R_z < 1.9$ µm). Figs. 4.55 - 4.57 also show that the initial wall temperature had a large effect on the $R_{f,\,end}$, mass and $(dR_f/dt)_{1h}$ and that the simultaneous effect of the wall temperature and type of fluid, γ^- as well as surface roughness, and that the magnitude of the effect of T_0 and (T_0 x fluid), (T_0 x γ^-) or (T_0 x R_z) was diferrent on each fouling variable. The combined effect of type of fluid and surface roughness (fluid x R_z) was also significant for describing the data, indicating that protein and crystallization fouling will be diferrent for surfaces with different roughness. Furthermore, Figs. 4.55 - 4.57 show that the effect of the surface roughness was higher than the effect of the surface free energy parameter γ^- on the depedent variables, emphasizing again the importance of the initial substrate polish. $R_{f,\,end}$, mass and $(dR_f/dt)_{1h}$ also depended positively on $(\gamma^-)^2$ and negatively on $(\text{fluid})^2$, although this dependence was lower than the individual variables T_0 and R_z. The effect of γ^- or $(\gamma^-)^2$ alone was weaker than the effect of T_0 or R_z.

The experimental results were reflected in the results from the analysis of variance (Tables A9 – A14 in appendix). At higher initial surface temperature (T_0 = 120 °C), the factors γ^-, fluid and R_z affected the deposition less than at a lower temperature (T_0 = 80 °C). Moreover, working with more complex fouling fluid (milk salts were added to whey protein), the influence of surface roughness is expected to be lower on deposition. By increasing T_0 from 80 °C to 120 °C, $R_{f,\,end}$ was from 2 to 10 times higher for WPI and WPI plus SMUF, while $R_{f,\,end}$ was 2 to 2.5 times higher for the coated surfaces by T_0 = 80 °C when the substrate was electropolished. At T_0 = 120 °C, $R_{f,\,end}$ was approximately constant up to 1.2 times higher. At a lower initial temperature a significant influence of γ^- could be observed for SMUF and WPI plus SMUF deposition (Figs. 4.29 and 4.34 a-b), which was repeated for WPI plus SMUF deposition on pre-fouled surfaces with calcium phosphate (Fig. 4.38b). The statistical models (Eqs. (4.2) – (4.7)) show that the influenced of R_z was inverse to the fouling describing variables, i.e. the higher the roughness, lower was $R_{f,\,end}$, mass and $(dRf/dt)_{1h}$, that reflects the results of the fouling curves from Fig. 4.34 for WPI plus SMUF fouling. Note that the interaction γ^- x R_z was not significant to interpret the data of $R_{f,\,end}$, mass and $(dR_f/dt)_{1h}$,. As discussed in section 4.1.4, the parameters γ^- and R_z presented no correlation, viz. in the range of roughness investigated no influence on γ^- was detected.

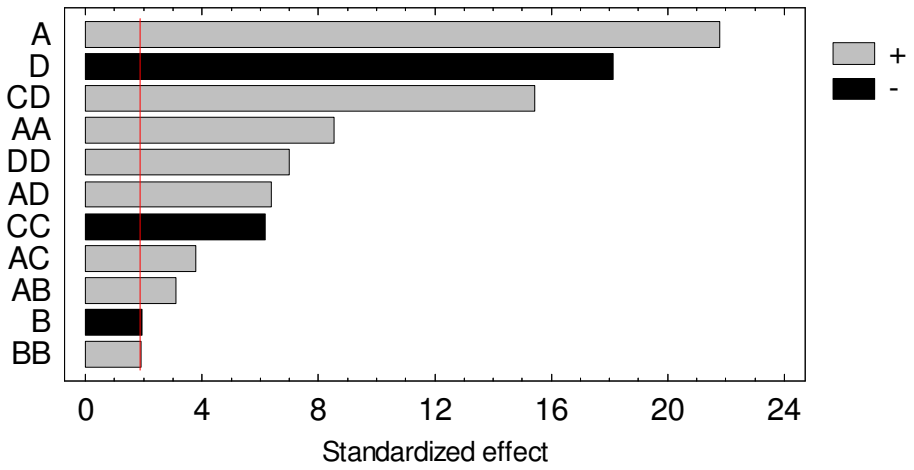

Fig. 4.55. Pareto diagram for $R_{f,\ end}$ with a pareto index of 5 %. A = T_0_cod; B = Base_cod; C = Fluid_cod; D = R_z_cod

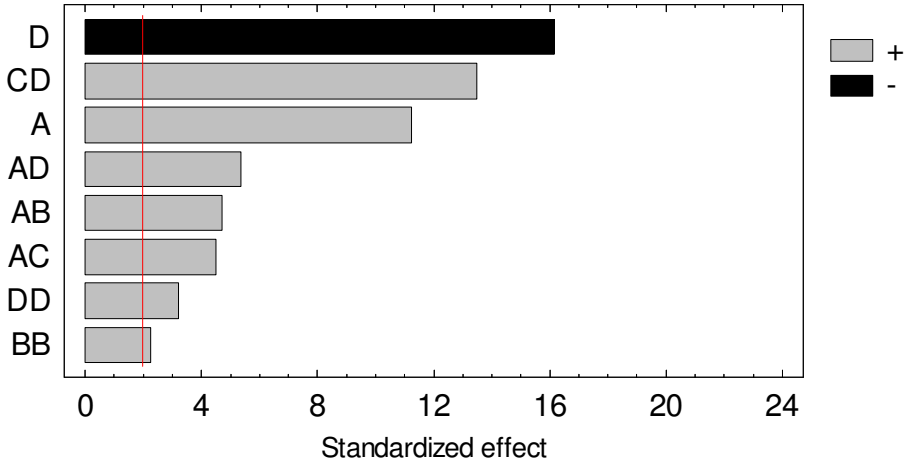

Fig. 4.56. Pareto diagram for Mass with a pareto index of 5%. A = T_0_cod; B = Base_cod; C = Fluid_cod; D = R_z_cod

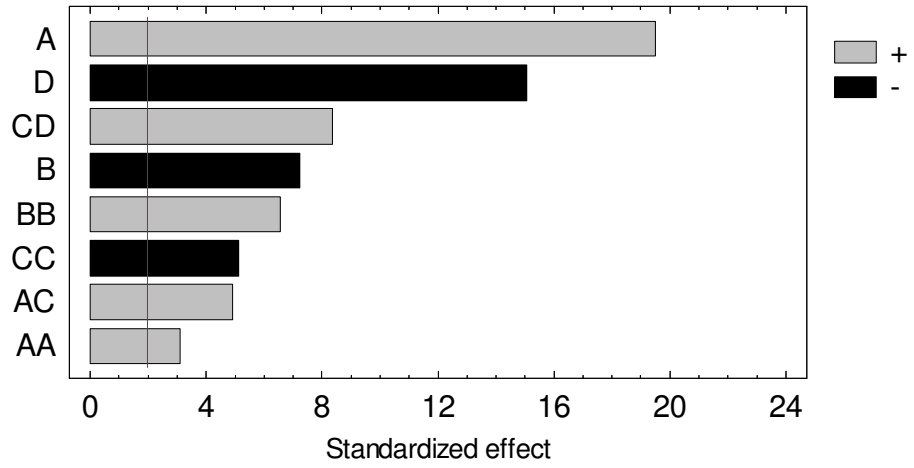

Fig. 4.57. Pareto diagram for $(dR_f/dt)_{1h}$ with a pareto index of 5 %. A = T_0_cod; B = Base_cod; C = Fluid_cod; D = R_z_cod

The corresponding simplified second-order polynomial model with coded variables is given in Eq. (4.2). The uncoded and corresponding coded values of the independent variables T_0, γ^-, R_z and fluid for the experimental design are given in Table 3.13.

$$R_{f,\,end}\,[10^{-4}\ K\ m^2\ W^{-1}] = 6.65\ (T_0\_cod)^2 + 0.78\ (\gamma^-\_cod)^2 + 5.58\ (R_z\_cod)^2 - 3.38\ (fluid\_cod)^2 + 0.69\ (T_0\_cod \times \gamma^-\_cod) + 0.73\ (T_0\_cod \times fluid\_cod) + 1.17\ (T_0\_cod \times R_z\_cod) + 3.96\ (R_z\_cod \times fluid\_cod) + 4.17\ T_0\_cod - 0.58\ \gamma^-\_cod - 5.31\ R_z\_cod + 4.24 \quad (4.2)$$

and with the uncoded variables T_0, R_z and γ^-, viz. T_0 is given in °C, R_z in µm and γ^- in mN m^{-1}, in Eq. (4.2):

$$R_{f,\,end}\,[10^{-4}\ K\ m^2\ W^{-1}] = 0.017\ (T_0)^2 + 0.0064\ (\gamma^-)^2 - 3.38\ (fluid\_cod)^2 + 17.40\ (R_z)^2 + 0.0036\ (T_0 \times \gamma^-) + 0.030\ (T_0 \times fluid\_cod) + 0.10\ (T_0 \times R_z) - 0.050\ (R_z \times fluid\_cod) - 3.31\ T_0 - 0.62\ \gamma^- - 58.48\ R_z + 202.57 \quad (4.3)$$

with a determination coefficient R^2 of 0.909, viz. the model explains 90.9 % of the total variance of the responses. The mean absolute error was 1.40 x 10^{-4} K m^2 W^{-1}.

The statistical model from Eq. (4.4) confirms the previously presented results, which had shown the influence of temperature, model fluid and surface on deposit mass. A second order equation with respect to γ^- was also obtained for deposit mass as dependent variable (Eqs. 4.3 and 4.4). The model for mass could be further simplified and the effect of $(T_0)^2$, $(fluid\_cod)^2$ and γ^- could be additionally excluded comparing to the model for $R_{f\,,\,end}$:

$$mass\ [g\ m^{-2}] = 18.60\ (\gamma^-\_cod)^2 + 41.02\ (R_z\_cod)^2 + 20.52\ (T_0\_cod \times \gamma^-\_cod) + 15.51\ (T_0\_cod \times fluid\_cod) + 20.66\ (T_0\_cod \times R_z\_cod) + 61.27\ (R_z\_cod \times fluid\_cod) + 39.45\ T_0\_cod - 74.98\ R_z\_cod + 108.18 \quad (4.4)$$

and with the uncoded variables T_0, R_z and γ^-, viz. T_0 is given in °C, R_z in µm and γ^- in mN m^{-1} :

$$mass\ [g\ m^{-2}] = -0.195\ (\gamma^-)^2 + 207.37\ (R_z)^2 + 0.074\ (T_0 \times \gamma^-) + 0.729\ (T_0 \times fluid\_cod) + 1.74\ (T_0 \times R_z) - 15.05\ (R_z \times fluid\_cod) - 1.56\ T_0 - 724.36\ R_z + 509.95 \quad (4.5)$$

The determination coefficient R^2 was 0.801 and the mean absolute error was 25.5 g m^{-2}.

The model for initial fouling rate $(dR_f/dt)_{1h}$ (Eqs. (4.6) and (4.7)) could be further simplified without loss of accuracy and the effect of $(R_z)^2$ and $(T_0 \times R_z)$ could be additionally excluded comparing to the model for mass, while the effect of $(T_0)^2$, $(fluid\_cod)^2$ and γ^- were significant.

$$(dRf/dt)_{1h}\ [10^{-4}\ m^2\ W^{-1}] = 2.47\ (T_0\_cod)^2 + 2.45\ (\gamma^-\_cod)^2 - 2.85\ (fluid\_cod)^2 + 0.92\ (T_0\_cod \times fluid\_cod) + 2.22\ (R_z \times fluid\_cod) + 3.63\ T_0\_cod - 1.73\ \gamma^-\_cod - 4.13\ R_z\_cod + 6.50 \quad (4.6)$$

and with the uncoded variables T_0, R_z and γ^-, viz. T_0 is given in °C, R_z in µm and γ^- in mN m^{-1} :

$$(dRf/dt)_{1h}\ [10^{-4}\ m^2\ W^{-1}] = 0.0063\ (T_0)^2 + 0.034\ (\gamma^-)^2 - 2.89\ (fluid\_cod)^2 + 0.040\ (T_0 \times fluid\_cod) - 1.38\ (R_z \times fluid\_cod) - 1.08\ T_0 - 2.15\ R_z - 1.29\ (\gamma^-) + 64.15 \quad (4.7)$$

The determination coefficient R^2 was 0.851 and the mean absolute error was 2.00 x 10^{-4} m^2 W^{-1}.

Figs. 4.58 - 4.60 give the fouling resistance, the deposit mass and the initial fouling rate as function of T_0 and γ^- for the SMUF-rich whey protein solution without consideration on R_z variation, which ranged narrowly from 0.8 to 1.9 µm. The higher the temperature, the higher the $R_{f,\ end}$, mass and $(dR_f/dt)_{1h}$, as expected, while $R_{f\ ,end}$, mass and $(dR_f/dt)_{1h}$ varied with γ^- in a quadratic form. The combined effect of T_0 and γ^- can also been seen in the figures. The effects of T_0 and the solutions' composition concerning the presence of calcium are known, having been reported by several authors (Changani et al., 1997; Christian et al., 2002; Bansal and Chen, 2006). However, the effect of surface free energy and principally the effect of the surface energy contribution terms have not yet been clearly established.

Fryer et al. (1996) used a statistical model to study the effect of amount of denatured whey protein, product flow rate and temperature difference across a test section on the rate of mass deposition, rate of change in the pressure drop and rate of change in the heat transfer coefficient in a PHE. After a multiple linear regression and elimination of the non-significant variables, they also found a quadratic dependence, as well as the interaction between the factors and the response variables.

A quadratic relationship of surface loading or deposit amount to total surface energy or to a surface energy component, as described in the statistical models (Eqs. (4.2) to (4.7)), has been reported by Baier (1980) and Zhao et al. (2004a, 2007) for bacteria adhesion, McGuire and Swartzel (1989) for milk protein, Rosmaninho et al. (2008) for calcium phosphate, Zhao et al. (2007) for calcium sulphate fouling, as well as Keijbets et al. (2009) for chocolate adhesion. Regarding the electron donor component, some works described it as attractive interaction force (Wu and Nancolas, 1998; Rosmaninho and Melo, 2008), whereas other works have contradicted these results and instead considered γ^- as a repulsive force (Liu et al., 2008; Al-Janabi et al., 2010). The statistical models according to Eqs. (4.2) – (4.7) can partially explain these contradictory conclusions, suggesting an optimum value of γ^- for which R_f is minimal.

Rosmaninho and Melo (2008) suggested a deposition mechanism in which protein and calcium phosphate were competing for the surface. In the presence of native proteins, calcium phosphate will preferentially attach to the surface. By contrast, in the presence of denatured proteins, less space is left for mineral attachments because the proteins more easily adhere to the surfaces (Rosmaninho and Melo, 2008). These observations can be complemented by the fact that on low γ^- surfaces calcium phosphate will prevail, while protein will preferentially attach to high γ^- surfaces, as previously discussed. The influence of the surface on the crystals and protein structures needs to be taken into account, as well as the bonding between protein and calcium. (Boxler et al., 2013b)

The consideration of further surface properties as well as the deposition under diverse flow and thermal conditions can improve the development of the models for $R_{f,\,end}$, mass and $(dR_f/dt)_{1h}$ and their determination coefficient. The surface energy parameters γ^{TOT} and γ^{+} were first omitted from the models for simplicity, despite showing statistically distinct values for the coated electropolished surfaces.

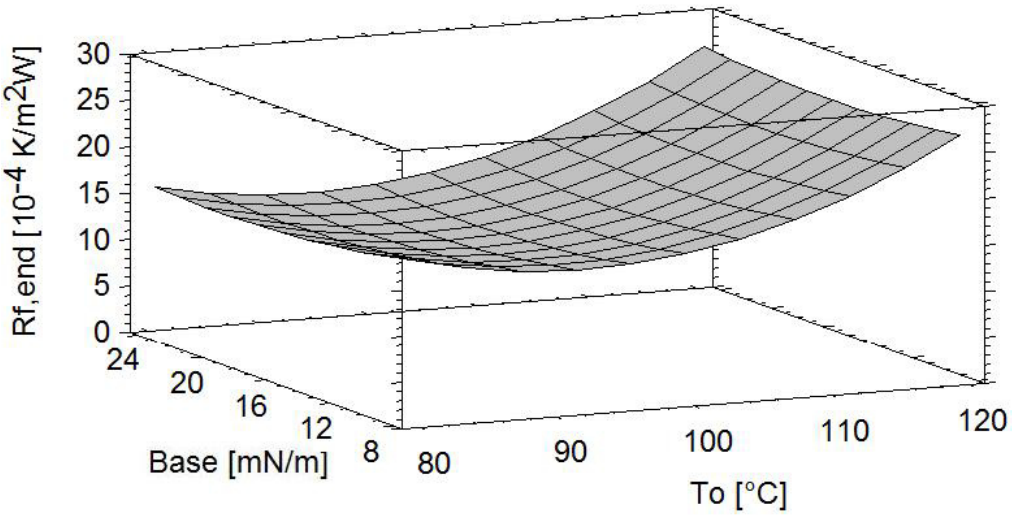

Fig. 4.58. $R_{f,\,end}$ as function of electron donor component (=Base) und T_0 for WPI plus SMUF on unpolished (Rz = 1.7 µm) plus unmodified and coated SS

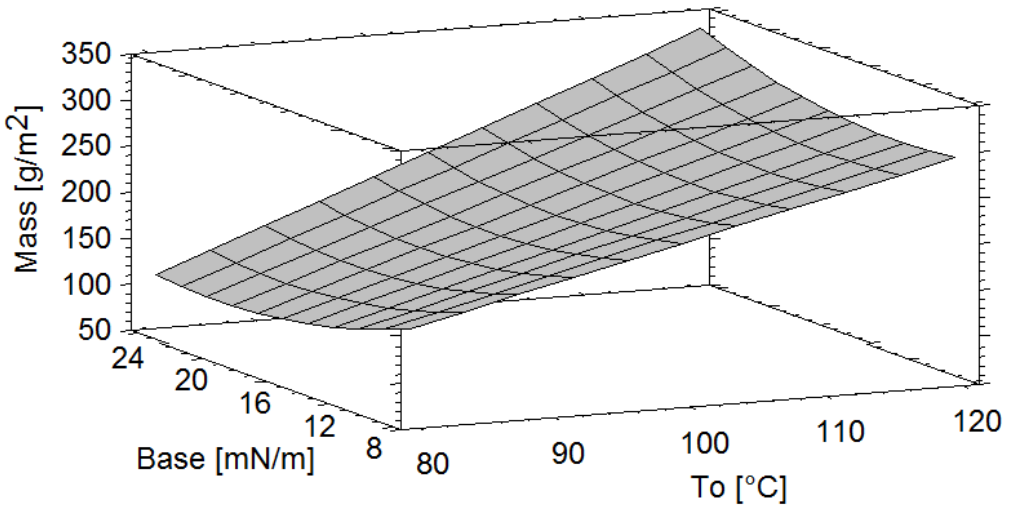

Fig. 4.59. Mass as function of electron donor component (=Base) und T_0 for WPI plus SMUF on a unpolished (R_z = 1.7 µm) plus unmodified and coated SS

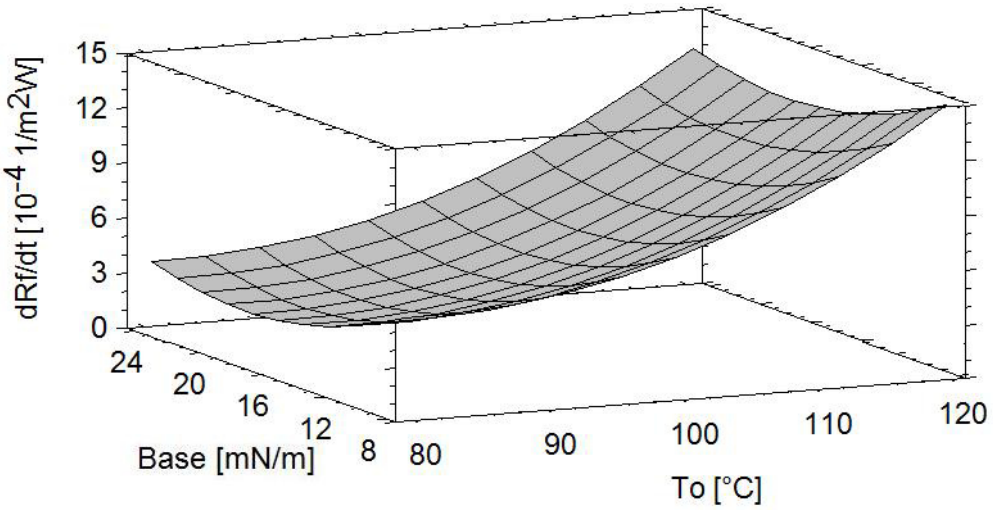

Fig. 4.60. $(dR_f/dt)_{1h}$ as function of electron donor component (=Base) und T_0 for WPI plus SMUF on unpolished (Rz = 1.7 µm) plus unmodified and coated SS

4.4.2 Continuous fouling

The relationship between the deposit formation on the plate heat exchanger and the surface properties was investigated. The analysis of variance (see Tables A.15 – A.26) indicated that the effect of the electron donor component γ^- and the quadratic term of γ^- on the final fouling resistance $R_{f,\,end}$, on the initial fouling rate $(dR_f/dt)_{0.5h}$ and on the protein/mineral ratio in the fouling layer were statistically significant ($p < 0.10$), while the influence of the roughness ($1.2 < R_z < 1.6$ µm) was not statistically significant at the 90 % or higher confidence level. A similar dependency of the $R_{f,\,end}$ and deposited mass from γ^- for whey protein and/or calcium phosphate batch-wise deposition was described for the batch-wise fouling (section 4.4.1).

A second-order polynomial equation for $R_{f,\,end}$, $(dR_f/dt)_{0.5h}$ and protein/mineral ratio could be obtained and the corresponding polynomials are given in Eqs. (4.8) - (4.10), with uncoded γ^- in mN m^{-1}:

$$R_{f,\,end}\ [10^{-5}\ m^2\ K\ W^{-1}] = 12.27 - 2.54\ \gamma^- + 0.15\ (\gamma^-)^2 \qquad (4.8)$$

The determination coefficient R^2 is 0.79 and the standard error 0.89 x 10^{-5} m^2 K W^{-1}.

The model for initial fouling rate $(dR_f/dt)_{0.5h}$ with uncoded γ^- in mN m^{-1} is given in Eq. (4.9):

$$(dR_f/dt)_{0.5h}\ [10^{-5}\ m^2\ W^{-1}] = 18.51 - 4.11\ \gamma^- + 0.23\ (\gamma^-)^2 \qquad (4.9)$$

The determination coefficient R^2 is 0.75 and the standard error 1.50 x 10^{-5} m^2 W^{-1}.

For the protein/mineral ratio, the corresponding polynomial could be established:

$$\text{Protein/mineral [-]} = 4.42 - 0.75\ \gamma^- + 0.042\ (\gamma^-)^2 \qquad (4.10)$$

The determination coefficient R^2 is 0.69 and the standard error 0.33.

Fig. 4.61 summarizes the effect of the electron donor component on $R_{f,\ end}$ and protein/mineral ratio, showing that a minimal deposition in the PHE occurred for γ^- between 8.5 and 9 mN m^{-1}. A similar graph has been shown by Boxler et al. (2014a) for the deposit protein content in function of γ^-. No statistically significant relationship between γ^- and the mineral content or mineral plus protein contents could be identified at the 90 % or higher confidence level.

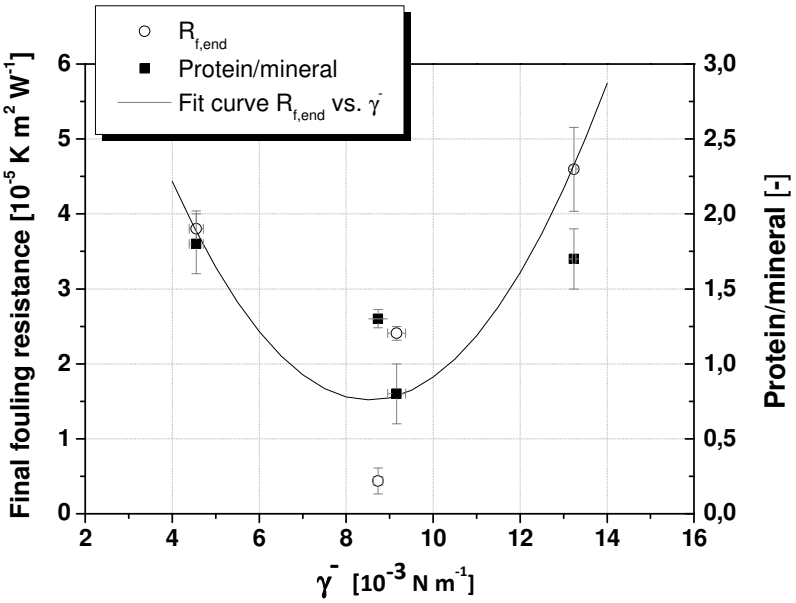

Fig. 4.61. Final fouling resistance and protein/mineral ratio as a function of the surface electron-donor component

Comparison of the absolute values of the T-Statistic, viz. the standardized effects, of the independent variable γ^- and the term $(\gamma^-)^2$ of the statistical models of Eq. (4.3) for the batch-wise fouling (Table A9) and Eq. (4.8) for the deposition on PHE (Table A17) show that for the depedent variable $R_{f,end}$ the effect of γ^- was almost the same in both models, but the effect of $(\gamma^-)^2$ was 1.8 times higher for the fouling on PHE than on the coupons.

For the SMUF-rich whey protein batch-wise deposition at T_0 = 85 °C, a γ^- value of 19 – 24 mN m^{-1} could be determined from Eqs. (4.3) and (4.7) for the roughness range R_z of 1.2 – 1.6 µm and no fouling ($R_{f,end}$ = 0 and $(dRf/dt)_{1h}$ = 0), while Eqs. (4.8) and (4.9) gave optimal values of γ^- of 8.5 – 9.8 mN m^{-1} for minimal fouling on the PHE (see also Fig. 4.61). It is noteworthy that the fluiddynamic and heat transfer conditions on both experiments were completely different: in the vessel, the fluid was stirred with an impeller Re of 12,360 and was heated at an initial temperature difference between the fluid and the wall of

ΔT = 30 – 70 K; while on PHE, the fluid flowed between two corrugated plates with Re = 870, following an initial temperature profile along the plate in which ΔT was up to 23 K. Therefore, the statistical models for the batch-wise and the continuous fouling cannot be compared, given that they do not include either heat transfer or fluiddynamic effects on fouling. However, the models reflect the first attempt in the literature to describe the combined influence of the surface free energy, initial surface temperature and roughness on milk fouling. Further experiments are required to expand and increase the scope of the models. The result of both statistical models again emphasizes the complexity of the deposition of milk components and that the studied parameters (T_0, surface free energy, roughness and fouling fluid) simultaneously affect its behavior.

In continuous flow experiments, Rosmaninho and Melo (2007) found an increase of the maximal fouling resistance with γ^- for SMUF-rich whey protein deposition on TiN coated surfaces, whose γ^- values varied from 23 mN m^{-1} to 55.3 mN m^{-1}. Otherwise, in batch-wise fouling (rotating disk apparatus), Rosmaninho and Melo (2008) found that in the presence of denatured protein, low γ^- surfaces (γ^- = 10 mN m^{-1}, Ni–P–PTFE) promoted more deposition than high γ^- surfaces (γ^- = 53.8 mN m^{-1}, SiO_x). These two works indicate that the influence of the flow conditions and further surface properties should also be considered for the understanding of the fouling process and the choice of the most efficient surface.

4.5 Cleaning of the DLC-coated surfaces

The fouling layers formed during the deposition process are evidently the starting material for any cleaning protocol, and likewise the state of the surface remaining after any cleaning stage holds crucial importance in later operation, given that it will dictate foulants' ability to attach (Wilson, 2005). Therefore, is essential that the coating not only reduces fouling deposition, but also improves its removal as well. Thus, a detailed analysis of the deposit cleaning behavior from the DLC-based coated surfaces is presented in this section.

4.5.1 Influence of coating on batch cleaning

After most fouling experiments, the fouled surfaces were cleaned batch-wise, as described in section 3.3.4, in order to: (*i*) prepare the surface for the surface energy analysis and consequently to next fouling run; or (*ii*) recover the deposits for chemical analysis.

In contact with NaOH, the color of the protein-rich deposit changed to translucent white, while the formation of a smooth, swollen gel was also evident. Mineral deposits were quite soft and could be rubbed off, but not removed by alkali or water. The amount of deposit remaining on each surface after each cleaning procedure differed according to the surface. The cleanability depends on the structure of the deposit formed, which in turn depends on the initial surface temperature and model fluid, as well as its attachment, which additionally depends on the surface properties. Pure protein and calcium phosphate deposits were easier to remove than deposits formed from protein and minerals in combination, as well as deposits formed at lower temperatures. Without shear stress, the cleaning procedure was repeated (= cleaning steps) until the surface was free from residuals.

Fig. 4.62 shows the influence of the coatings and the coating aging on the surface cleanability. Although the DLC coating appears to be most effective in mitigating protein plus mineral fouling (see Fig. 4.34 and Table 4.18), the cleaning procedure in batch often had to be repeated several times for this coating to achieve a microscopical clean surface. Beuf et al. (2003) observed similar difficulties in cleaning the DLC coating. In contrast, deposits on SICON® were easier to remove than from the other surfaces.

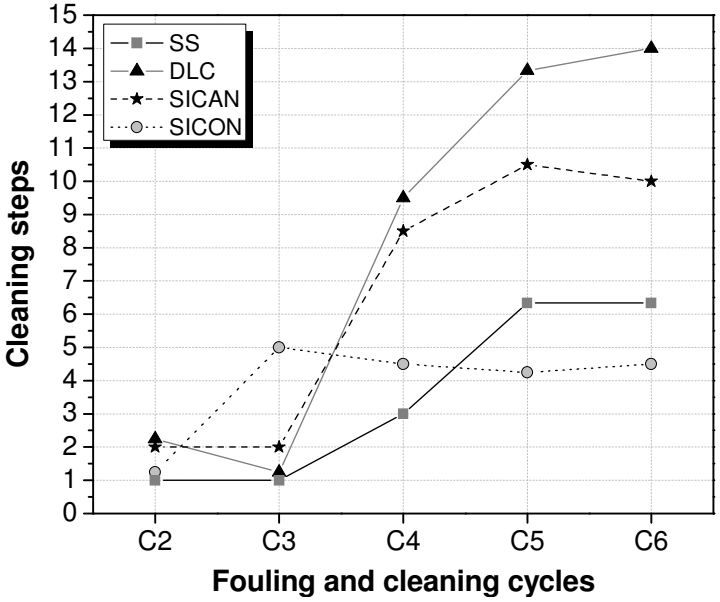

Fig. 4.62. Influence of coating on required cleaning steps (mean value for cleaning of protein, calcium phosphate as well as protein plus mineral deposits)

4.5.2 Influence of coating on continuous cleaning

Since the protein plus mineral deposits formed at T_0 = 120 °C were relatively similar in comparison with deposits generated under other conditions, repeatable and more difficult to remove by batch cleaning (as discussed in the previous section and observed in practice for all surfaces), these deposits were subsequently used to compare the cleaning behavior of the different coated surfaces under continuous flow conditions.

Fig. 4.63 schematically depicts the observed removal pattern of the different surfaces. Deposit color changed to translucent white and yellow/brownish close to the surface and the initial swelling was noticed for all surfaces. Initial cracks were formed and deposits' fracture could also be observed (stage b). Further swelling occurred (stage c). Protein deposits have been described as more adhesive than cohesive (Liu et al., 2006), resulting in their removal in smaller chunks. This behavior could be observed for the low γ^- surfaces (stage c + d, low γ^- surface). For these surfaces, large swollen chunks, supposedly more adhesive than the upper material, were still attached to the surface. However, on the SICON®, SICAN and ESICON® coated surfaces, the foulant was almost entirely removed by the flow within the first five minutes of the experiment (stage c, high γ^- surface), despite the low shear force. The resting

deposit was subsequently removed randomly in discrete clusters or as chunks by shear stress and mass transport (stage d, low γ^- surface). For the SS, ESS, DLC and EDLC surfaces, the complete swollen deposit could not be totally removed (Boxler et al., 2013a).

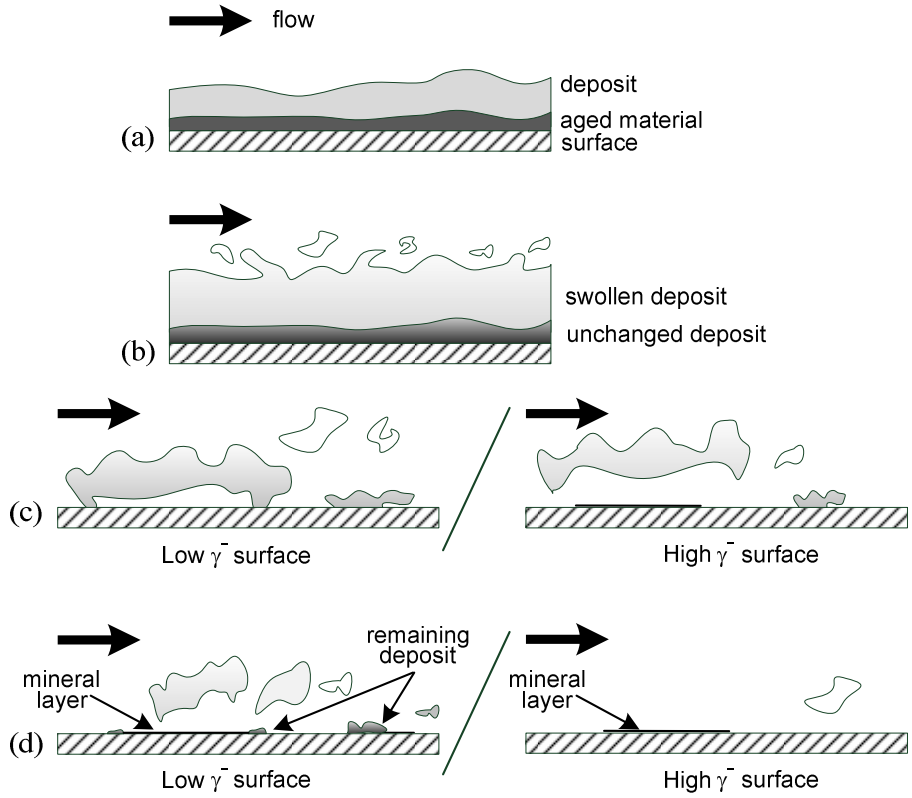

Fig. 4.63. Stages of milk deposits' removal on the different surfaces: (a) swelling of the covering layer; (b) uniform stage, protein-matrix break down and removal of swollen deposits' clumps; (c) further swelling of aged material (low γ^- surface) and removal of large swollen chunks (high γ^- surface); (d) decay phase, removal of chunks or isolated clusters. Whiteness of shading indicates extent of swelling. (Boxler et al., 2013a)

The thermal resistances during the cleaning procedure for the two alkali concentrations of the investigated surfaces are shown in Fig. 4.64. Different thermal resistance developments could be observed for the diverse surfaces. Through the heterogeneous microstructure of the fouling layer (and thus roughness), the film heat transfer coefficient h on the fluid side can be improved due to turbulence (Albert et al., 2011). For this reason, the thermal resistance (R_f) starts from negative values. The thermal resistance initially increases owing to the increased deposit thickness δ_f due to swelling. The extent of the swelling depends on: *(i)* the amount of deposit remaining; *(ii)* the diffusion of detergent in the deposit matrix; *(iii)* the reaction's kinetics of breaking peptide bonds; *(iv)* the interaction deposit-deposit; and *(v)* the chemical concentration used in the cleaning step. Simultaneous to swelling, the deposits' thermal conductivity also changes, depending on the deposits' thermal history and voidage (Davies et al, 1997). Note that R_f is a balance of three effects, namely the

increase of the deposit thickness (δ_f), increase of its' thermal conductivity (λ_f) and alter of the heat transfer coefficient (h):

$$\frac{1}{U_f} = \frac{\delta}{\lambda} + \frac{1}{h} + \frac{\delta_f}{\lambda_f} \tag{4.11}$$

The partial removal of swollen deposit due to wall shear stress results in the decrease of the thermal resistance, which can superimpose the swelling. A clear separation of the swelling phase from the start of removal, depending only on the thermal data, is therefore difficult. According to Gillham et al. (1999), the cleaning is initially limited by reaction of the protein matrix and diffusion of protein through the viscous swollen deposit.

The cleaning profiles in Fig. 4.64 a-b and Fig. 4.64 c-d indicate the influence of the cleaning solution concentration on the cleaning behavior. Raising the chemical concentration from 0.25 % w/w to 0.5 % w/w reduced the duration of the swelling stage and thus the thermal resistance, owing to the superimposed removal. The effect of the surface modification on adhesive and cohesive strengths, and consequently on the cleaning process, can be clearly seen for the higher sodium hydroxide concentration (Fig. 4.64 c, d). A maximum value of the thermal resistance R_f is reached earlier, particularly for the SICAN, SICON®, ESICAN and ESICON® coated surfaces. The maximum R_f varied from 2.6 x 10^{-4} m^2 K W^{-1} to 3 x 10^{-4} m^2 K W^{-1}, for the cleaning using 0.25 % w/w NaOH and from 0.75 x 10^{-4} m^2 K W^{-1} to 2.7 x 10^{-4} m^2 K W^{-1}, for the cleaning with 0.5 % w/w NaOH. Furthermore, the lowest value of R_f is reached earlier for the SICAN, SICON®, ESICAN and ESICON® coatings. The thermal measurements (R_f) remained at values from 0.25 x 10^{-4} m^2 K W^{-1} to 2.5 x 10^{-4} m^2 K W^{-1}, while the cleaning rate dropped down to 0.02 g m^{-2} s^{-1} (see Fig. 4.67). This shows that at the studied cleaning conditions (flow velocity, NaOH concentration and temperature), soil remained the surfaces and further deposit removal did not occur. In some cases, a further increase in the thermal resistance could be detected (Fig. 4.64b, Fig. 4.64d for ESS and EDLC after 20 min), indicating that the chemical reactions within the deposit still caused the deposit to swell (aged material deposit), although the efficiency of removal is minimal or constant. These results show that the deposit layer thickness slowly decreases after initial swelling and removal, suggesting that further cleaning is dominated by the reaction on the deposit-substrate interface (Boxler et al., 2013a).

Figs. 4.65 and 4.66 compare the initial wet deposit on the different surfaces and the remaining deposit after 60 min cleaning, respectively. On SS, DLC and ESS, there remained a large amount of deposit, as well as on the other electropolished and coated SS surfaces (images not shown). Given that type B deposit is high in calcium and phosphorus salts, NaOH alone was unable to remove mineral fouling. The alkaline solution will dissolve most of the protein and release some of the minerals bound in the protein matrix. However, the use of appropriate sequestrants in alkali formulations, or the circulation of acidic solutions before (to leach calcium from the deposit allowing it to swell easily (Morison and Larsen, 2005)) or after the NaOH stage (to dissolve remaining calcium phosphate) is required for the complete removal of minerals. A remaining mineral residue after removal of the other milk components (e.g. protein via alkaline solutions) is often described as a hard sandy deposit. Such hard sandy deposit could be observed on the SICAN and SICON® surfaces after the cleaning

experiment. This residual deposit could only be complete removed with acid cleaning (batch-wise cleaning, section 4.4.1). Rosmaninho et al. (2007b) reported that the residual mass of calcium phosphate deposits after rinsing with water generally increased with the surface γ^- value (18.4 mN m^{-1} < γ^- < 46.2 mN m^{-1}), as observed for the SICAN and SICON® surfaces. However, since the SICAN and SICON® coated surfaces were easier to clean than untreated stainless steel, it is expected that the surfaces will be cleaned completely at a cleaning solution temperature of 30 °C, that was the temperature of the solution in this work, or higher and at a higher flow velocity, using an industrial alkaline solution followed by acid solution.

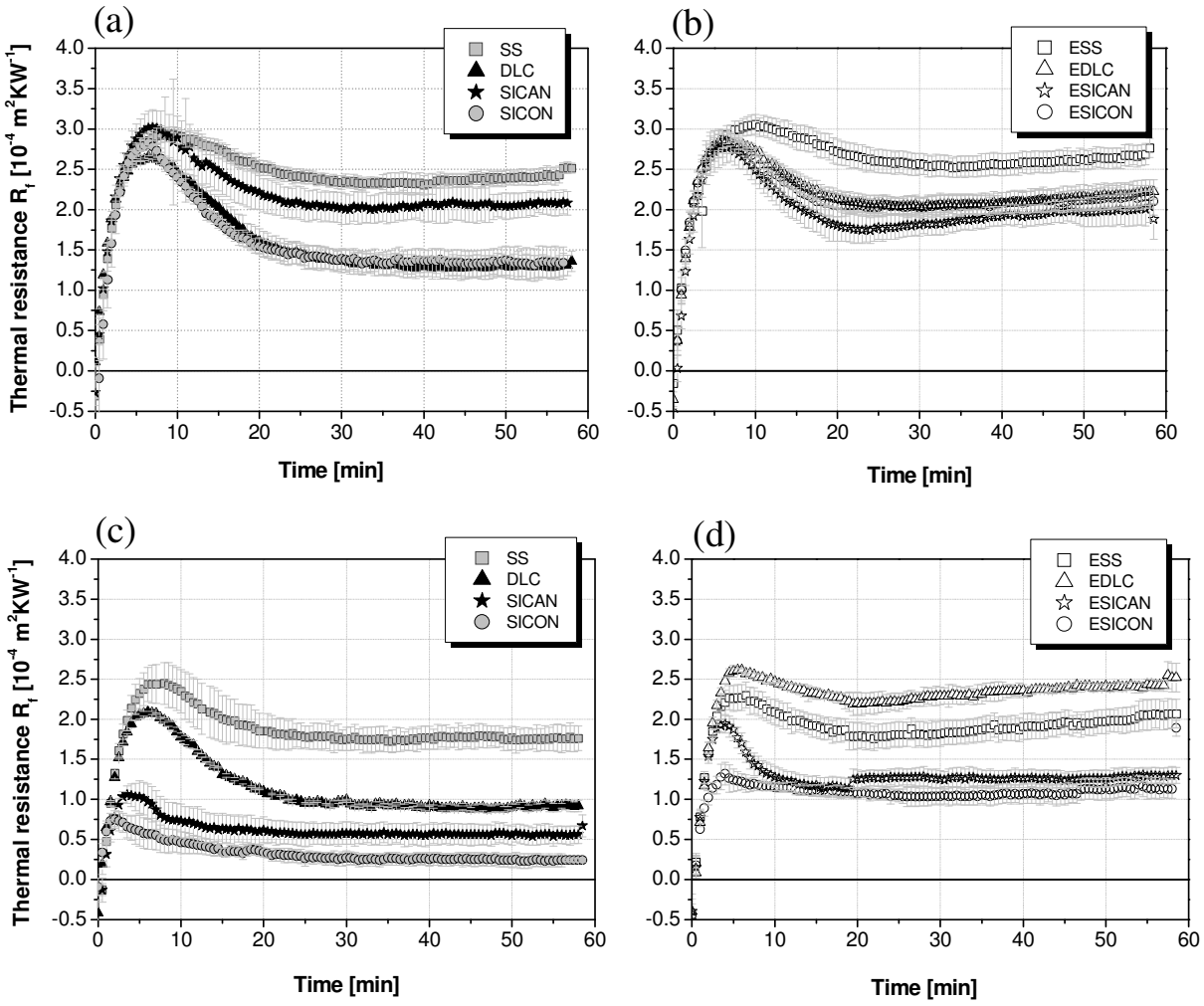

Fig. 4.64. Thermal resistance for the (a) coated surfaces and the (b) electropolished plus coated surfaces with 0.25 % w/w NaOH and for the (c) coated surfaces and the (d) electropolished plus coated surfaces with 0.5 % w/w NaOH

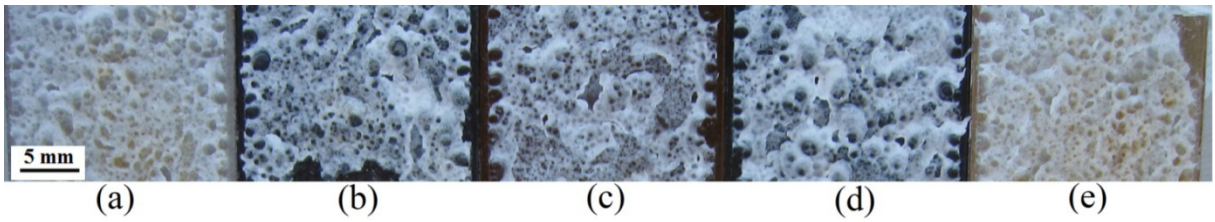

Fig. 4.65. Wet deposits on (a) SS, (b) SICAN, (c) SICON®, (d) DLC and (e) ESS before cleaning

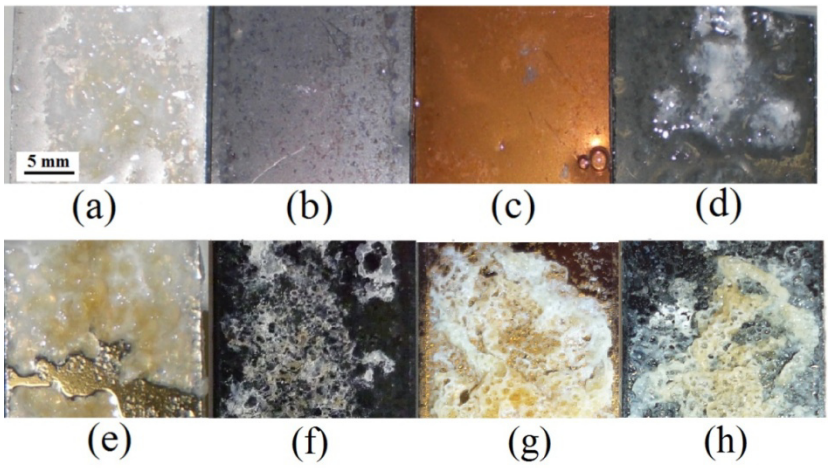

Fig. 4.66. Remaining deposit on (a) SS, (b) SICAN, (c) SICON®, (d) DLC, (e) ESS, (f) ESICAN, (g) ESICON® and (h) EDLC after 60 min cleaning using 0.5 % w/w NaOH at 30 °C

Fig. 4.67 depicts the cleaning rate over time for uncoated and coated, unpolished and electropolished stainless steel. The three different stages of the cleaning process (see Fig. 2.15) can be easily identified in these curves, namely swelling, uniform removal and decay period. The cleaning profiles are affected by the cleaning solution concentration, as well as the surface coating. Raising the chemical concentration from 0.25 % w/w to 0.5 % w/w the cleaning rate increased, the duration of the swelling stage decreased and therefore the thermal resistance (Fig. 4.64) decreased due to the superimposed removal. The results are in accordance with Plett (1985) and Tissier and Lalande (1986), who reported a nearly linear increase of the cleaning rate with increasing detergent concentration. An optimum NaOH concentration of 0.5 % w/w was found for the cleaning of WPC and milk deposits at 50 °C (Bird and Fryer, 1991). Above this optimum, a less open structure (Tissier and Lalande, 1986) or a glassy deposit (Fryer et al., 2006) can be formed.

The effect of the surface modification on adhesive and cohesive strengths and consequently on the cleaning process can be clearly seen for the higher sodium hydroxide concentration (Fig. 4.67 c - d). Comparing the cleaning profiles for all surfaces at each NaOH concentration, different maximal cleaning rates and different duration of the swelling and uniform stages could be observed. Again, an improved cleanability for SICON® and ESICON® could be identified, as indicated by the highest values of the cleaning rate for these surfaces.

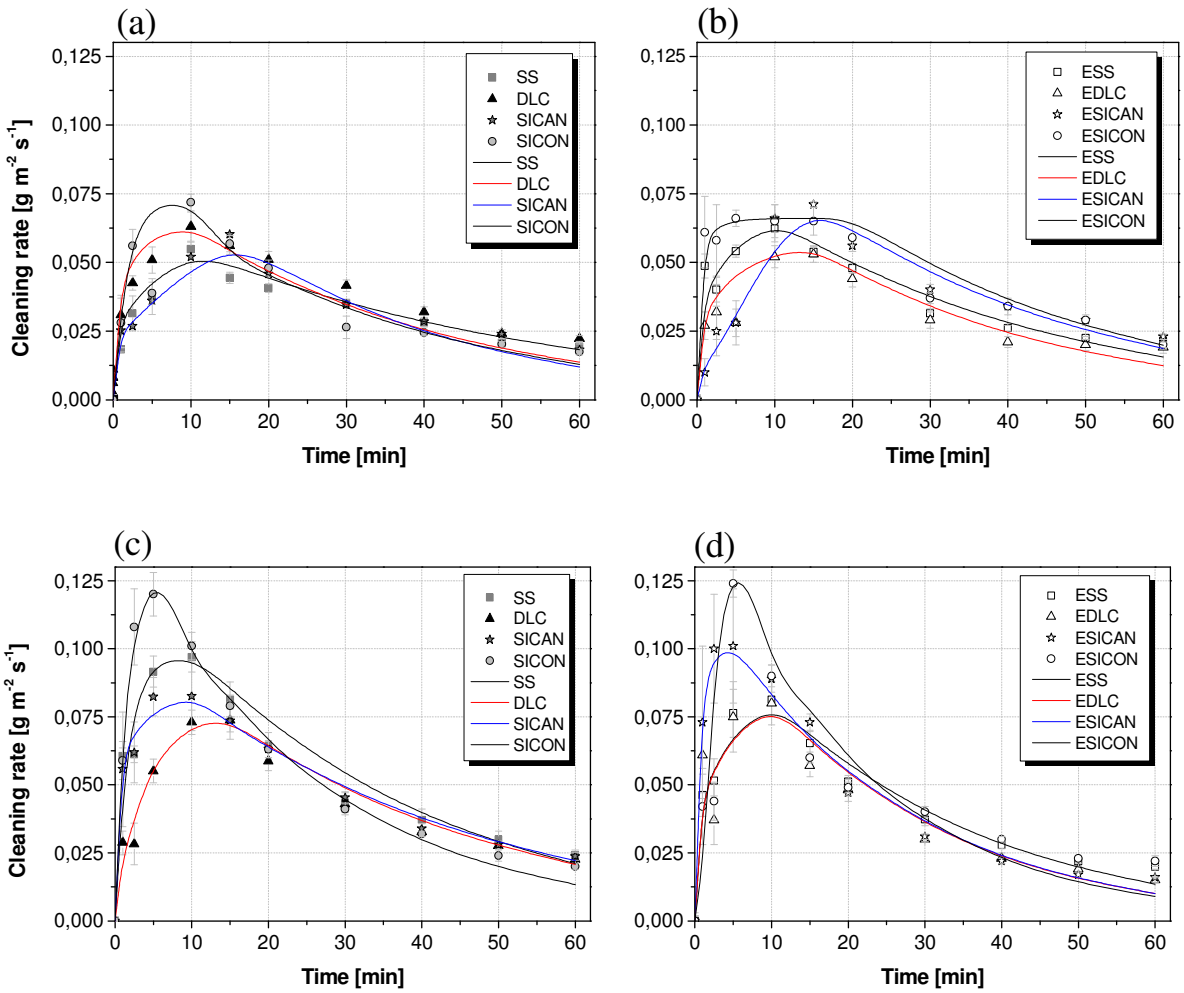

Fig. 4.67. Cleaning rate profiles for the (a) coated surfaces and for the (b) electropolished plus coated surfaces with 0.25 % w/w NaOH and for the (c) coated surfaces and for the (d) electropolished plus coated surfaces with 0.5 % w/w NaOH. Experimental (dots) and predicted results using the model from Xin et al. (2004) (Eqs. (2.14) and (2.15)) (lines)

The experimental results were fitted using the mathematical model from Xin et al. (2004), described in section 2.3.1, which is based on polymer dissolution theory and mass transfer mechanism. Experimental results and predictions showed a good accordance (Fig. 4.65), indicating that the disengagement of swollen soil and its' back-diffusion into the flowing fluid controlled the process. The influence of the alkali concentration and of the surface coating on the model parameters is summarized in Table 4.27. The cleaning rate $r_{c,m}$ and the kinetic constant ξ increased with γ^- (see also Fig. 4.68). Higher values of $r_{c,m}$ and ξ means that larger disengagement rates of the protein chains contribute to the initial stage of cleaning (Xin et al., 2004). Note that the values of $r_{c,m}$ and ξ were higher at higher NaOH concentration. The changes of $r_{c,m}$ and ξ could be attributed to variations in the deposit-deposit and deposit-surface interactions. The constant k_a rate was similar for all surfaces (Fig. 4.66), indicating that the transport of disengaged protein back into the cleaning solution was not affected by the energetic surface properties.

Table 4.27. Model parameters obtained from the analyses of experimental results

Surface	0.25 % w/w NaOH			0.5 % w/w NaOH		
	$r_{c,m}$ [g m^{-2} s^{-1}]	ξ [s^{-1}]	ka [s^{-1}]	$r_{c,m}$ [g m^{-2} s^{-1}]	ξ [s^{-1}]	ka [s^{-1}]
SS	0.055	0.0050	0.00037	0.097	0.017	0.00055
DLC	0.063	0.0088	0.00051	0.074	0.0088	0.00047
SICAN	0.060	0.0031	0.00060	0.085	0.0056	0.00044
SICON®	0.072	0.018	0.00052	0.12	0.018	0.00067
ESS	0.066	0.0059	0.00048	0.082	0.0059	0.00060
EDLC	0.055	0.0057	0.00055	0.082	0.0057	0.00070
ESICAN	0.072	0.0052	0.00050	0.10	0.014	0.00070
ESICON®	0.066	0.011	0.00050	0.125	0.023	0.00080

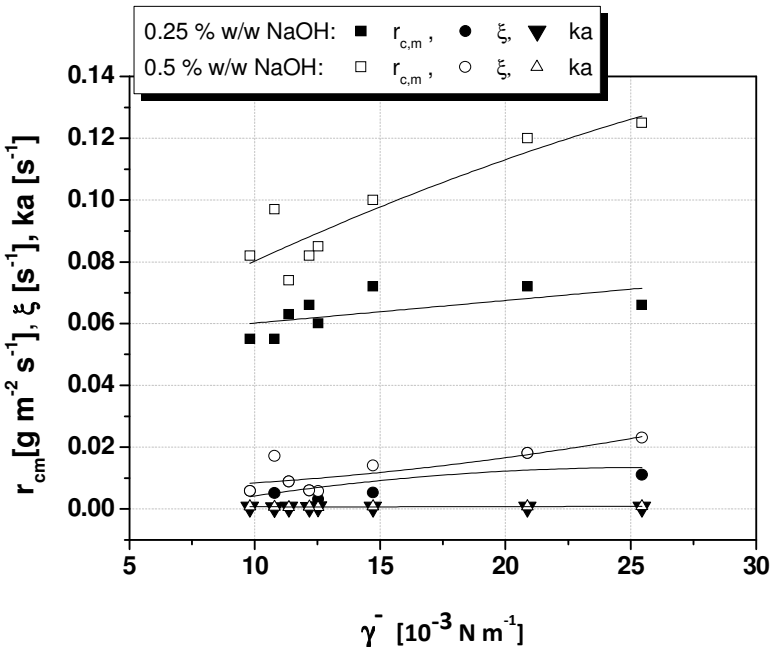

Fig. 4.68. Model parameters as function of the electron donor component

A comparison of the results from thermal data (Fig. 4.64) and chemical analysis of the cleaning solutions (Fig. 4.67) showed significant differences in the length of the uniform and the decay stages. These differences were more pronounced for the coated surfaces. The uniform/decay stage transition was always detected earlier by the thermal data and the length of the thermal decay stage was always shorter (i.e. the thermal resistance reaches its constant final value earlier) than the corresponding mass removal stage. A noticeable increase in the thermal cleaning rate (i.e. reduction in R_f) coincides with the onset of the decay stage in the chemically determined removal data. This phenomenon was also reported by Gillham et al. (1999). (Boxler et al. 2013a) Finally, it should be stressed that the coated surfaces achieved a lower thermal resistance after 30 min cleaning with 0.5 % w/w NaOH, thus indicating a better cleanability of these surfaces compared to the electropolished surfaces. However, this

information cannot be concluded based solely on the analysis of the cleaning rate profiles, and therefore a complementary approach as taken here is advisable.

In general, deposit-surface binding is weaker at low energy surfaces, which are easier to clean. However, a number of studies have contradicted this tendency (Detry et al., 2010; Liu and Zhao, 2011). For this reason, the γ^- component or the γ^{LW}/γ^- ratio has been used for surfaces with significantly different γ^{LW} values to correlate the formation and removal of diverse deposits on different surfaces. The studied DLC-based coatings have a very similar γ^{LW} value. Hence, the relationship between γ^- of the solid substrates and the cleanability was investigated.

The analysis of variance of the data showed that the maximal cleaning rate $r_{c,m}$ was significantly affected by the electron donor component ($p < 0.01$), while the effect of the surface roughness R_z or the combined effect of γ^- and R_z on $r_{c,m}$ was not statistically significant (see Tables A25 – A28). The cleaning rate increased with γ^-, as shown in Fig. 4.69a. This suggests that the polar contribution of the surface energy influenced the nature of the interactions between the initial layer and the surface, hence affecting the strength of deposit adhesion and the point of failure under stress. However, the effect of γ^- on the cleaning rate at 0.25 % w/w NaOH was lower than at the alkali concentration of 0.5 % w/w. The results are in agreement with the observations of Rosmaninho and Melo (2007). For deposition of calcium phosphate and proteins at 70 °C, they reported that the soil formed on low γ^- surfaces were more resistant to cleaning. Furthermore, in another work (Rosmaninho and Melo, 2008), the same authors observed that calcium phosphate structures will prevail on the low γ^- surfaces by the deposition of SMUF-rich whey protein solution, leading to more consistent deposits than on the high γ^- surface. Accordingly, this explains why more deposits remained on the low γ^- surfaces by cleaning using only sodium hydroxide. Liu and Zhao (2011) also showed that the biofilm removal rate decreases when increasing the γ^{LW}/γ^- ratio.

The cleaning rate is frequently found in the literature to compare the cleanability of surfaces or equipment under different operating conditions. However, the cleaning rate reaches the highest value earlier than the lowest value or the thermal resistance of zero is reached. Therefore, the ratio between the R_f after 30 min during the cleaning process and the final R_f after fouling experiment for all surfaces was also compared. The same tendency regarding the effect of the γ^- parameter on cleaning effort can be seen in Fig. 4.69b, with the exception of SICAN (marked on the figure). The higher the γ^-, the lower the thermal resistance for the same point in time (= 30 min).

Although no significant influence of the surface roughness ($0.8\ \mu m < R_z < 1.9\ \mu m$) on the cleaning rate could be detected (Fig. 4.70a), visual observation of the removal process (see Fig. 4.66 for remaining deposit) suggested that electropolished surfaces (coated or unmodified) were more difficult to clean than unpolished ones. Plotting the (R_f after 30 min cleaning/$R_{f,\ end}$ after fouling) ratio against R_z (Fig. 4.70b), the visual observations can be confirmed, making it clear that the cleaning process was also influenced by altering the surface topography. As with the energetic surface property γ^-, the influence of the surface roughness could be mainly observed at the higher alkali concentration, at which some surfaces have been almost complete cleaned (Fig. 4.66). At this concentration, the higher the R_z, the lower the thermal resistance $R_{f,cleaning,30\ min}$, again confirming the visual observations.

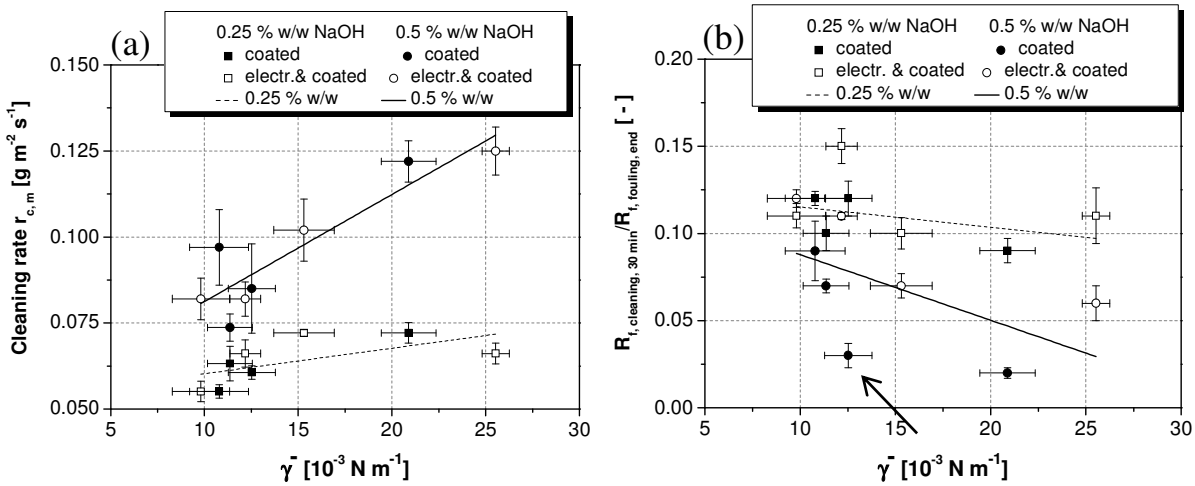

Fig. 4.69. Variation of the (a) highest cleaning rate and of the (b) (R_f after 30 min cleaning/$R_{f,\ end}$ fouling) rate with cleaning solution concentration and surface modification as function of the electron donor component for WPI plus SMUF soiled at 120 °C

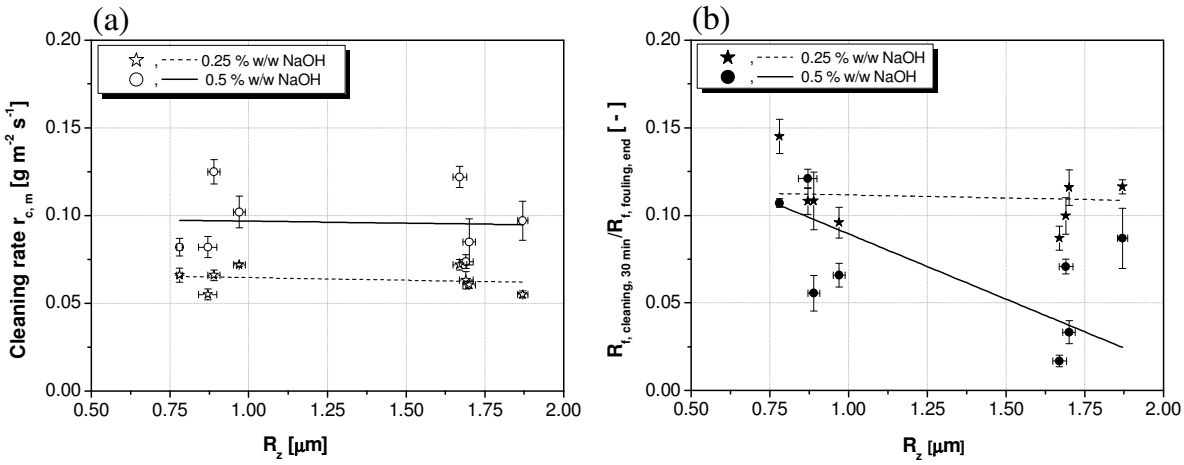

Fig. 4.70. Variation of the (a) highest cleaning rate and of the (b) (R_f after 30 min cleaning/$R_{f,\ end}$ fouling) rate with cleaning solution concentration and surface roughness as function of the roughness depth for WPI plus SMUF soiled at 120 °C

5 Conclusions

This study has addressed the effect of surface modification and conditioning, initial surface temperature and fluid/solution composition on deposition of raw milk, as well as the main constituents of milk soils, i.e. whey protein and calcium phosphate. Furthermore, the effect of surface modification on cleaning behavior of (hard) deposits formed by both constituents has also been investigated. Standard and electropolished stainless steel were modified by PECVD, resulting in amorphous hydrogen containing carbon coatings (a-C:H:X) with different topographic and energetic properties. The combined or synergistic influence of the parameters R_z, T_o and γ^- on the fouling and cleaning processes could be identified and quantified through the analysis of variance and modelling. A statistical model based on experimental fouling results was established and the cleaning kinetic results were adjusted to a model derived from the literature.

The fouling layer deposition resulted from a sequence of stages, summarized in the schema of Fig. 5.1, suggesting that fouling is controlled by fluid as well as surface reactions. The results suggest that mineral and protein were building the initial fouling layer simultaneously. Further deposition depended on the conditions favoring the protein denaturation near to the wall, as well as the presence or absence of calcium and phosphate ions in the solution.

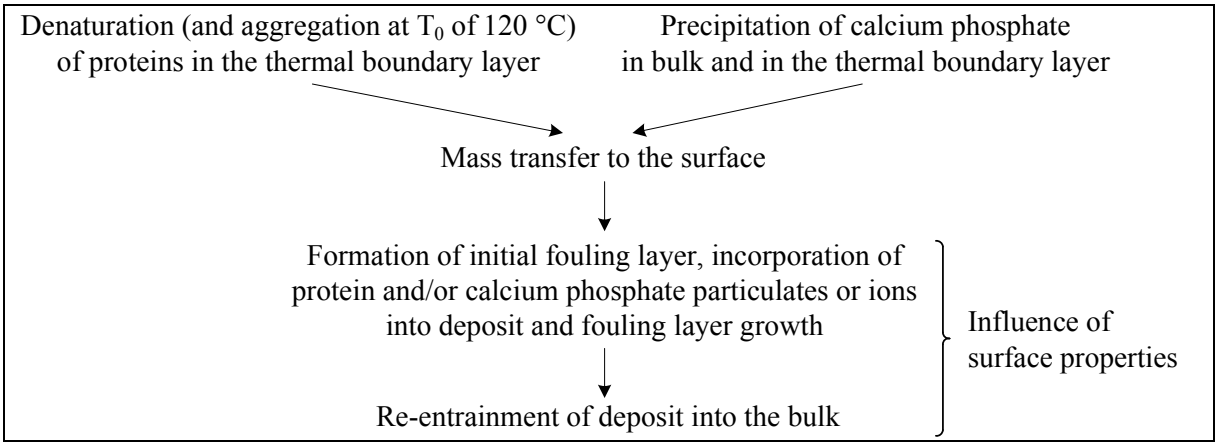

Fig. 5.1. Stages of whey protein, calcium phosphate and calcium phosphate-rich whey protein solution deposition process

The initial surface free energy and the zeta potential of new coatings varied due to repeated fouling and cleaning processes, consequently affecting the fouling behavior on these surfaces. However, the surface properties reached stable values after five fouling and cleaning cycles at the latest, which in turn resulted in quite reproducible measurements of thermal fouling resistance and deposit mass. The coatings showed similar surface dispersive components (γ^{dis} or γ^{LW}) after the initial aging, which contributed more significantly to γ^{TOT} than the polar components (γ^{pol} or γ^{AB}), whose values were significantly different for the diverse coated surfaces. The contribution of the electron acceptor component (γ^+) to γ^{AB} was very low and similar for all surfaces, whereas the contribution of the electron donor component (γ^-) was high and differentiated the surfaces. The combination of Si or Si and O

inside the a-C:H:X coating lead to an increase of γ^-. No dependence of surface roughness on γ^- could be found.

The results confirmed that the surface energetic properties, particularly γ^-, the surface roughness (R_z), the initial surface temperature (T_0), the solution composition and the flow conditions, influenced:

- the formation of the initial fouling layer and the subsequent deposit build-up, resulting in different final fouling resistances ($R_{f,\,end}$);
- the dry deposit mass;
- the fouling layer composition regarding protein, mineral, Ca and P contents and thereby the fouling type;
- the fouling layer structure; and
- the deposit cohesive strength and thus its removal during fouling.

Furthermore, the surface energetic properties, particularly γ^-, and the surface roughness, affected:

- the deposit cohesive and adhesive strengths and thus its removal kinetics during cleaning;
- the cleaning and thermal resistance profiles; and
- the cleaning parameters, such as maximal cleaning rate ($r_{c,m}$) and cleaning kinetic constant (ξ).

In the batch-wise experiments, fouling generally became more serious as the surface temperature increased, due to the enhancement of calcium phosphate precipitation and protein denaturation. The additional smoothing or electropolishing of the surface resulted in a higher deposit amount and fouling rate, while a slight decrease of Ca and P contents could be detected. The effect of γ^- was clearer especially when this was considered in combination with other parameters, e.g. for one T_0 or for one model solution. In batch and under flow conditions a quadratic correlation between γ^- and the $R_{f,end}$, deposit dry mass or protein/mineral could be detected. For deposition under low shear stress, the deposits at low surface temperature resembled those of type A described in the literature, whereas deposits at high surface temperature were more proteinaceous than deposit type B. Under flow conditions on all surfaces, mineral deposition was greater than protein deposition, which might be related to the fact that the model fluid recirculated in the PHE. Regarding the cleaning behavior, the surfaces with high γ^- value showed the highest cleaning rate, as well as the fastest reduction of the thermal resistance, whereas electropolished surfaces were more difficult to clean than rough surfaces.

An optimum γ^- value of around 9 mN m^{-1} for minimal continuous fouling and of around 22 mN m^{-1} for minimal batch-wise fouling as well as maximal cleaning effort was suggested from the statistical modelling of the experimental data. The different optimum γ-values for the batch-wise and continuous experiments indicates that the influence of further factors, such as flow conditions and ΔT or T profiles, should be also considered and included in the model.

This investigation has demonstrated the potentials and restrictions of DLC coatings on deposit growth mitigation, as well as the enhancement of cleaning efficiency in the food industry.

References

Adams, J. P.; Simunovic, J.; Smith, K. L. (1984). Temperature histories in a UHT indirect heat exchanger. *Journal of Food Science*, 49 (1), 273–277.

Adamson, A. W.; Gast, A. P. (1997). Physical Chemistry of Surfaces. John Wiley & Sons, Inc., New York.

Albert, F.; Augustin, W.; Scholl, S. (2011). Roughness and constriction effects on heat transfer in crystallization fouling. *Chemical Engineering Science*, 66, 499–509.

Al-Janabi, A.; Malayeri, M. R.; Müller-Steinhagen, H. (2010). Experimental fouling investigation with electroless Ni-P coatings. *International Journal of Thermal Science*, 49, 1063-1071.

Al-Malah, K.; McGuire, J.; Krisdhasima, V.; Suttiprasit, P.; Sproull, R. (1992). Ellipsometric evaluation of β-lactoglobulin adsorption onto low- and high-energy materials. *Biotechnology Progress*, 8, 58–66.

Altankov, G.; Richau, K.; Groth, T. (2003). The role of surface zeta potential and substratum chemistry for regulation of dermal fibroblasts interaction. *Materialwissenschaft und Werkstofftechnik*, 34, 1120–1128.

Alvarez, N.; Daufin, G.; Gésan-Guiziou, G. (2010). Recommendations for rationalizing cleaning-in-place in the dairy industry: Case study of an ultra-high temperature heat exchanger. *Journal of Dairy Science*, 93, 808–821.

Alvarez, N.; Gésan-Guiziou, G.; Daufin, G. (2007). The role of surface tension of re-used caustic soda on the cleaning efficiency in dairy plants. *International Dairy Journal*, 17, 403–411.

Andritsos, N.; Yiantsios, S. G.; Karabelas, A. J. (2002). Calcium phosphate scale formation from simulated milk ultrafiltrate solutions. *Food and Bioproducts Processing*, 80, 223–230.

Anema, S. G. (2009). Effect of milk solids concentration on the pH, soluble calcium and soluble phosphate levels of milk during heating. *Dairy Science and Technology*, *89*, 501–510.

Anema, S. G.; McKenna, A. B. (1996). Reaction kinetics of thermal denaturation of whey proteins in heated reconstituted whole milk. *Journal of Agricultural and Food Chemistry*, 44, 422–428.

Anema, S. G.; Li, Y. (2003). Association of denatured whey proteins with casein micelles in heated reconstituted skim milk and its effect on casein micelle size. *Journal of Dairy Research*, 70, 73–83.

AOAC (2005). Official Methods of Analysis of AOAC International. W. Horwitz, G. W. Latimer (Eds.). Association of Analytical Communities International, Gaithersburg, USA.

Apenten, R. K. O. (1995). A three-state heat-denaturation of bovine α-lactalbumin. *Food Chemistry*, 52, 131–133.

Application Note MRK379-01 (2005). The measurement of zta potential using an autotitrator: effect of conductivity. Malvern Instruments Ltd., Grovewood Road, UK

Arnebrant, T.; Barton, K.; Nylander, T. (1987). Adsorption of α-lactalbumin and β-lactoglobulin on metal surfaces versus temperature. *Journal of Colloid and Interface Science*, 119, 383–390.

Ashokkumar, S.; Adler-Nissen, J.; Møller, P. (2012). Factors affecting the wettability of different surface materials with vegetable oil at high temperatures and its relation to cleanability. *Applied Surface Science*, *263*, 86–94.

Augustin, M. A.; Udabage, P. (2007). Influence of processing on functionality of milk and dairy proteins. *Advances in Food and Nutrition Research*, 53, 1–38.

Ayadi, M. A.; Bénézech, T.; Chopard, F.; Berthou, M. (2008). Thermal performance of a flat ohmic cell under non-fouling and whey protein fouling conditions. *Lebensmittel-Wissenschaft und -Technologie*, 41, 1073–1081.

Azzi, M.; Amirault, P.; Paquette, M.; Klemberg-Sapieha, J. E.; Martinu, L. (2010). Corrosion performance and mechanical stability of 316L/DLC coating system: Role of interlayers. *Surface & Coatings Technology*, 204, 3986–3994.

Baier, R. E. (1980). Adsorption of micro-organisms to surface. Wiley-Interscience, New York.

Balasubramanian, S.; Puri, V. M (2008). Fouling mitigation during product processing using a modified plate heat exchanger surface. *Transactions of ASABE*, 51 (2), 629–639.

Balasubramanian, S.; Puri, V. M. (2009). Reduction of milk fouling in a plate heat exchanger system using food-grade surface coating. *Transactions of the ASABE*, 52, 1603–1610.

Bansal, B.; Chen, X. D. (2006). A critical review of milk fouling in heat exchangers. *Comprehensive Reviews in Food Science and Food Safety*, 5, 27–33.

Bansal, B.; Müller-Steinhagen, H. (1993). Crystallization fouling in plate heat exchangers. *Journal of Heat Transfer*, 115, 584–591.

Bargir, S.; Dunn, S.; Jefferson, B.; Macadam, J.; Parsons, S. (2009). The use of contact angle measurements to estimate the adhesion propensity of calcium carbonate to solid substrates in water. *Applied Surface Science*, *255*, 4873–4879.

Barish, J. A.; Goddard, J. M. (2013). Anti-fouling surface modified stainless steel for food processing, *Food and Bioproducts Processing*, 91 (4), 352–361.

Barkshire, I.; Karduck, P.; Rehbach, W. P.; Richter, S. (2000). High-spatial-resolution low-energy electron beam X-ray microanalysis. *Microchimica Acta*, 132 (2), 113–128.

Beck, U.; Bobe, U.; Gamer, N.; Reiners, G.; Sommer, K. (2005). Reinigung realer Oberflächen. *Chemie Ingenieur Technik*, 77 (12), 1942–1946.

Bell, R. W. (1925). The effect of heat on the solubility of the calcium and phophorus compounds in milk. *The Journal of Biological Chemistry*, 64, 391–400.

Bell, R. W.; Sanders, C. F. (1944). Prevention of milkstone formation in a High-Temperature-Short-Time heater by preheating milk, skim milk and whey. *Journal of Dairy Science*, 27, 499–504.

Bellmann, C.; Calvimontes, A.; Caspari, A.; Marx, S.; Mauermann, M. (2012). Innovative Oberflächen zur Verminderung des Anschmutzverhaltens in der Lebensmittelindustrie. *Chemie Ingenieur Technik*, 84, 1531–1537.

Bellmann, C.; Opfermann, A.; Jacobasch, H.; Adler, H. (1997). Characterisation of pure or coated metal surfaces with streaming potential measurements. *Fresenius' Journal of Analytical Chemistry*, 358, 255–257.

Belmar-Beiny, M. T.; Fryer. P. J. (1993). Preliminary stages of fouling from whey protein solutions. *Journal of Dairy Research*, 60, 467–483.

Belmar-Beiny, M. T.; Gotham, S. M.; Paterson, W. R.; Fryer, P. J. (1993). The effect of Reynolds number and fluid temperature in whey protein fouling. *Journal of Food Engineering*, 19, 119–139.

Beuf, M.; Rizzo, G.; Leuliet, J. C.; Müller-Steinhagen, H.; Yiantsios, S.; Karabelas A.; Bénézech, T. (2003). Fouling and cleaning of modified stainless steel plate heat exchangers processing milk products. In: P. Watkinson, H. Müller-Steinhagen, M. R. Malayeri (Eds.), *Proceedings of the International Conference on Heat Exchanger Fouling and Cleaning* (pp. 99–106). ECI Symposium Series, New York.

Bewilogua, K.; Bialuch, I.; Ruske, H.; Weigel, K. (2011). Preparation of a-C:H/a-C:H:Si:O and a-C:H/a-C:H:Si multilayer coatings by PACVD. *Surface Coating Technology*, 206 (4), 623–629.

Bird, M. R. (1994). Cost optimisation of dairy cleaning in place (CIP) cycles. *Transactions of the Institution of Chemical Engineers*, 72, 17–20.

Bird, M. R. (1995). CIP optimisation for the food industry: Relationships between detergent concentration, temperature and cleaning time. *Transactions of the Institution of Chemical Engineers*, 73, 63–70.

Bird, M. R.; Fryer, P. J. (1991). An experimental study of cleaning of surfaces fouled by whey proteins. *Transactions of the Institute of Chemical Engineers*, 69, 13–21.

Blanpain-Avet, P.; Hédoux, A.; Guinet, Y.; Paccou, L.; Petit, J.; Six, T.; Delaplace, G. (2012). Analysis by Raman spectroscopy of the conformational structure of whey proteins constituting fouling deposits during the processing in a heat exchanger. *Journal of Food Engineering*, *110*, 86–94.

Blel, W.; Legentilhomme, P.; Benezech, T.; Fayolle, F. (2013). Cleanabilty study of a scraped surface heat exchanger. *Food and Bioproducts Processing*, 91, 95–102.

Bobe, U.; Hofmann, J.; Sommer, K.; Beck, U.; Reiners, G. (2007). Adhesion – where cleaning starts. *Trends in Food Science & Technology*, 18, 36–39.

Bobe, U.; Wildbrett, G. (2006). Anforderungen an Werkstoffe und Werkstoffoberflächen bezüglich Reinigbarkeit und Beständigkeit. *Chemie Ingenieur Technik*, 78, 1615–1622.

Böhm, H. D.; Heeschen, W.; Teufel, P. (2000). Das neue Milch-Hygienerecht. Th. Mann, Gelsenkirchen-Buer, Germany.

Bohnet, M. (1987). Fouling of Heat Transfer Surfaces. *Chemical Engineering & Technology*, 10, 113–125.

Boinovich, L.; Emelyanenko, A. (2011). Wetting and surface forces. *Advances in Colloid and Interface Science*, 165, 60–69.

Bos, M. A.; Shervani, Z.; Anusiem, A. C. I.; Giesbers, M Norde W.; Kleijn, J. M. (1994). Influence of the electric potential of the interface on the adsorption of proteins. *Colloids and Surfaces B: Biointerfaces*, 3, 91–100.

Bott, T. R. (1990). Fouling Notebook. Institution of Chemical Engineers, Warwickshire, UK.

Bott, T. R. (1995). Fouling of heat exchangers. Elsevier, Amsterdam, NL.

Bott, T. R. (2011). Industrial biofouling. Elsevier, Oxford, UK.

Boulangé-Petermann, L.; Doren, A.; Baroux, B.; Bellon-Fontaine, M.-N (1995). Zeta potential measurements on passive metals. *Journal of Colloid and Interface Science*, 171 (1), 179-186.

Boulangé-Petermann, L.; Gabet, C.; Baroux, B. (2006). On the respective effect of the surface energy and micro-geometry in the cleaning ability of bare and coated steels. *Colloids and Surfaces A: Physicochemical and Engineering Aspects*, 272, 56–62.

Boulangé-Petermann, L.; Guio, M. J.; Bénézech, T.; Faille, C.; Jullien, C.; Bellon-Fontaine¸ M.N; De Christofaro, N. (2002). *Improvement of the cleanability and disinfection of stainless steel surfaces for the food industry (dairy and meat)*. Report Nr. EUR 20476. European Commission, Luxembourg.

Boulangé-Petermann, L.; Jullien, C.; Dubois, P. E. ; Bénézech, T.; Faille, C. (2004). Influence of surface chemistry on the hygienc status of industrial stainless steel. *Biofouling*, 20, 25–33.

Bouvier, L.; Moreau, A.; Ronse, G.; Six, T.; Petit, J.; Delaplace, G. (2014). A CFD model as a tool to simulate β-lactoglobulin heat-induced denaturation and aggregation in a plate heat exchanger. *Journal of Food Engineering*, 136, 56-63.

Boxler, C.; Augustin, W.; Scholl, S. (2013a). Cleaning of whey protein and milk salts soiled on DLC coated surfaces at high-temperature. *Journal of Food Engineering*, 114 (1), 29-38.

Boxler, C.; Augustin, W.; Scholl, S. (2013b). Fouling of milk components on DLC coated surfaces at pasteurization and UHT temperatures. *Food and Bioproducts Processing*, 91, 336-347.

Boxler, C.; Augustin, W.; Scholl, S. (2014a). Influence of surface modification on the composition of a calcium phosphate-rich whey protein deposit in a plate heat exchanger. *Dairy Science & Technology*, 94, 17–31.

Boxler, C.; Augustin, W.; Scholl, S. (2014b). Composition of milk fouling deposits in a plate heat exchanger under pulsed flow conditions. *Journal of Food Engineering*, 121, 1–8.

Boxler, C.; Kaup, F.; Teixeira, R.; Pereira, A.; Mendes, J.; Melo, L.; Augustin, W.; Scholl, S. (2011). On-line monitoring of deposition and removal of milk salts on coated surfaces. In: H. Müller-Steinhagen, M. R. Malayeri, P. Watkinson (Eds.), *Proceedings of the 9th International Conference on Heat Exchanger Fouling and Cleaning*, (pp. 414–420). Publico Publications, Essen.

Bradford, M. M. (1976). A rapid and sensitive method for the quantitation of microgram quantities of protein utilizing the principle of protein-dye binding. *Analytical Biochemistry*, 72, 248–254.

Bradley, S. E.; Fryer, P. J. (1992). A comparison of two fouling-resistant heat exchangers. *Biofouling*, 5 (4), 295–314.

Bramaud, C.; P. Aimar, G. D. (1997). Optimisation of a whey protein fractionation process based on the selective precipitation of α-Iactalbumin. *Le Lait*, 77, 411–423.

Britten, M.; Green, M. L.; Boulet, M.; Paquin, P. (1988). Deposit formation on heated surfaces – effect of interface energetics. *Journal of Dairy Research*, 55 (4), 551–562.

Brüesch, P.; Müller, K.; Atrens, A.; Neff, H. (1985). Corrosion of stainless steels in chloride solution: An XPS investigation of passive films. *Applied Physics A*, 38 (1), 1–18.

Bullen, A. J.; O'Hara, K. E.; Cahill, D. G.; Monteiro, O.; von Keudell, A. (2000). Thermal conductivity of amorphous carbon thin films. *Journal of Applied Physics*, 88, 6317–6320.

Burdett, M. (1974). The effect of phosphates in lowering the amount of deposit formation during the heat treatment of milk. *Journal of Dairy Research*, 41, 123–129.

Burton, H. (1966). A comparison between a hot wire laboratory apparatus and a plate heat exchanger for determining the sensitivity of milk to deposit formation. *Journal of Dairy Research*, 33 (3), 317-324.

Burton, H. (1968). Deposits from whole milk in heat treatment plant – a review and discussion. *Journal of Dairy Research*, 35, 317–330.

Burton, H. (1988). Ultra-high-temperature processing of milk and milk products. Elsevier, London, UK.

Cárcel, J.; García-Pérez, J.; Benedito, J.; Mulet, A. (2012). Food process innovation through new technologies: Use of ultrasound. *Journal of Food Engineering*, 110 (2), 200–207.

Cash, M. J.; Erazo-Majewicz, P.; Good, R. M. (2006) Process of reducing fouling during heat processing of foods and beverages. Patent Nr. WO2006102051 A1, 09/28/2006.

Casiraghi, C.; Robertson, J.; Ferrari, A. C. (2007). Diamond-like carbon for data and beer storage. *Materials Today*, 10 (1–2), 44–53.

Cassie, A. B. D.; Baxter, S. (1944). Wettability of porous surfaces. *Transactions of the Faraday Society*, 546–551.

Castner, D. G.; Ratner, B. D. (2002). Biomedical surface science: Foundations to frontiers. *Surface Science*, 500, 28–60.

Cattaneo, S.; Masotti, F.; Pellegrino, L. (2008). Effects of overprocessing on heat damage of UHT milk. *European Food Research and Technology*, 226, 1099–1106.

Chandrasekaran, N.; Dimartino, S.; Fee, C. J. (2013). Study of the adsorption of proteins on stainless steel surfaces using QCM-D. *Chemical Engineering Research and Design*, 91 (9), 1674–1683.

Changani, S. D.; Belmar-Beiny, M. T.; Fryer, P. J. (1997). Engineering and chemical factors associated with fouling and cleaning in milk processing. *Experimental Thermal and Fluid Science*, 14 (4), 392–406.

Chapman, D.L. (1913). Theory of electrocapillarity. *Philosophical Magazine and Journal of Science*, 6 (25), 475–481.

Chapple, D.; Kresta, S. M; Wall, A.; Afacan, A. (2002). The effect of impeller and tank geometry on power number for a pitched blade turbine. *Chemical Engineering Research and Design*, 80 (4), 364–372.

Charitidis, C. A. (2010). Nanomechanical and nanotribological properties of carbon-based thin films: A review. *International Journal of Refractory Metals & Hard Materials*, 28, 51–70.

Chen J. R.; Wakida, T. (1997). Studies on the surface free energy and surface structure of PTFE film treated with low temperature plasma. *Journal of Applied Polymer Science*, 63, 1733–1739.

Chen, X. D.; Chen, J.; Wilson, D. I. (2002). Modelling whey protein based fouling of heat exchangers – further examining the deposition mechanisms. In: H. Müller-Steinhagen, R. Malayeri, P. Watkinson (Eds.), *Proceedings of the 4th International Conference on Heat Exchanger Fouling - Fundamental approaches & technical solutions* (pp. 153–162). Publico Publications, Essen.

Chenoweth, J. M. (1990). Final Report of the HTRI/TEMA Joint Committee to review the fouling section of the TEMA standards. *Heat Transfer Engineering*, 11 (1), 73–107.

Cherepy, N.; Shen, T.; Esposito, A.; Tillotson, T. (2005). Characterization of an effective cleaning procedure for aluminum alloys: surface enhanced Raman spectroscopy and zeta potential analysis. *Journal of Colloid and Interface Science*, 282, 80–86.

Chibowski, E. (2007). On some relations between advancing, receding and Young's contact angles. *Advances in Colloid and Interface Science*, 133, 51–59.

Christian, C. K.; Changani, S. D.; Fryer, P. J. (2002). The Effect of adding minerals on fouling from whey protein concentrate - Development of a Model Fouling Fluid for a Plate Heat Exchanger. *Food and Bioproducts Processing*, 80, 231–239.

Christoffersen, J.; Christoffersen, M. R.; Kibalczyc, W.; Andersen, F. A. (1989). A contribution to the understanding of the formation of calcium phosphates. *Journal of Crystal Growth*, 94, 767–777.

Compton, S. J.; Jones, C. G. (1985). Mechanism of dye response and interference in the Bradford protein assay. *Analytical Biochemistry*, 151, 369–374.

Considine, T.; Patel, H. A.; Anema, S. G.; Singh, H.; Creamer, L. K. (2007). Interactions of milk proteins during heat and high hydrostatic pressure treatments - A Review. *Innovative Food Science and Emerging Technologies*, 8 (1), 1–23.

Corredig, M.; Dalgleish, D. G. (1998). Effect of heating of cream on the properties of milk fat globule membrane isolates. *Journal of Agricultural and Food Chemistry*, 46, 2533–2540.

Correia, N. T.; Ramos, J. J. M.; Saramago, B. J. V. ; Calado, J. C. G. (1997). Estimation of the surface tension of a solid: application to a liquid crystalline polymer. *Journal of Colloid and Interface Science*, 189, 361–369.

Cosimo, B.; Khellil, S.; Luigi, B.; Song, L. (2005). Heat transfer enhancement in heat pipe applications using surface coating. *Journal of Enhanced Heat Transfer*, 12 (1), 21–36.

Council of Europe (2002). Guidelines on metals and alloys used as food contact materials. Council of Europe, Strasbourg, FR.

Croguennec, T.; O'Kennedy, B. T.; Mehra, R. (2004). Heat-induced denaturation/aggregation of β-lactoglobulin A and B: kinetics of the first intermediates formed. *International Dairy Journal*, 14, 399–409.

Cucci, M. W. (1954). The use of radioactive phosphorus to measure the amounts of milkstone deposited on rubber, pyrex glass, and tygon tubings. *Journal of Milk and Food Technology*, 17 (11), 332–333.

Dannenberg, F. (1986). Zur Reaktionskinetik der Molkeproteindenaturierung und deren technologischer Bedeutung. PhD thesis. Technische Universität München, Freising.

Dannenberg, F.; Kessler, H.-G. (1988). Reaction kinetics of the denaturation of whey proteins in milk. *Journal of Food Science*, 53 (1), 258–263.

Daufin, G.; Labbé, J. P.; Quemerais, A.; Brulé, G.; Michel, F.; Roignant, M.; Priol, M. (1987). Fouling of a heat exchange surface by whey, milk and model fluids. An analytical study. *Le Lait*, 67, 339–364.

Daufin, G.; Labbé, J-P. (1998). Equipment in the dairy application: problem and pretreatment. In: Z. Amjad (Ed.), *Calcium Phosphates in Biological and Industrial Systems*, (pp. 437 – 463). Kluwer Academic Publishers, Massachusetts, USA.

Davey, K.; Chandrakash, S.; O'Neill, B. (2013). A new risk analysis of clean-in-place milk processing. *Food Control*, 29, 248–253.

Davies, T. J.; Henstridge, S.C; Gillham, C.R.; Wilson, D.I. (1997). Investigation of whey protein deposit properties using heat flux sensors. *Food and Bioproducts Processing*, 75 (2), 106–110.

Davies, W. (1936). The effect of heat on milk. In: The chemistry of milk (pp. 343–364). D. Van Nostrand Co., New York.

de Jong, P. (1997). Impact and control of fouling in milk processing. *Trends in Food Science & Technology*, *8*, 401–405.

de Jong, P., Bouman, S.; van der Linden, H. J. L. J. (1992). Fouling of heat treatment equipment in relation to the denaturation of β-lactoglobulin. *The Journal of the Society of Dairy Technology*, 45 (1), 3–8.

de Jong, P.; te Giffel, M.; Straatsma, H.; Vissers, M. M. M. (2002). Reduction of fouling and contamination by predictive kinetic models. *International Dairy Journal*, 12, 285–292.

de Jong, P.; van der Linden, H. J. L. J. (1992). Design and operation of reactors in the dairy industry. *Chemical Engineering Science*, 47 (13/14), 3761–3768.

de la Fuente, M. A.; Singh, H.; Hemar, Y. (2002). Recent advances in the characterisation of heat-induced aggregates and intermediates of whey proteins. *Trends in Food Science & Technology*, 13, 262–274.

de Wit, J. N. (1990). Thermal stability and functionality of whey proteins. *Journal of Dairy Science*, 73, 3602–3612.

de Wit, J. N. (2009). Thermal behaviour of bovine β-lactoglobulin at temperatures up to 150°C. a review. *Trends in Food Science & Technology*, 20 (1), 27–34.

de Wit, J. N.; Klarenbeek, G. (1984). Effects of various heat treatments on structure and solubility of whey proteins. *Journal of Dairy Science*, 67, 2701–2710.

Dearnaley, G.; Arps, J. H. (2005). Biomedical applications of diamond-like carbon (DLC) coatings: A review. *Surface & Coatings Technology*, 200, 2518–2524.

Delgado, A.; González-Caballero, F.; Hunter, R.; Koopal, L.; Lyklema, J. (2007). Measurement and interpretation of electrokinetic phenomena. *Journal of Colloid and Interface Science*, 309, 194–224.

Delplace, F.; Leuliet, J. C.; Levieux; D. (1997). A reaction engineering approach to the analysis of fouling by whey proteins of a six-channels-per-pass plate heat exchanger. *Journal of Food Engineering*, 34, 91–108.

Delplace, F.; Leuliet, J. C.; Tissier, J. P. (1994). Fouling experiments of a plate heat exchanger by whey proteins solutions. *Trans IChemE*, *72*, 163–169.

Delsing, B. M. A.; Hiddink, J. (1983). Fouling of heat transfer surfaces by dairy fluids. *Netherlands Milk Dairy Journal,* 37, 139–148.

Derjaguin, B.; Landau, L. (1941). Theory of the stability of strongly charged lyophobic sols and of the adhesion of strongly charged particles in solutions of electrolytes. *Acta Physico Chemica URSS*, 14, 633–662.

Derksen, J. (2001). Assessment of large eddy simulations for agitated flows. *Chemical Engineering Research and Design*, 79 (8), 824–830.

Detry, J. G.; Sindic, M.; Deroanne, C. (2010). Hygiene and Cleanability: A Focus on surfaces. *Critical Reviews in Food Science and Nutrition*, 50 (7), 583–604.

Dey, A.; Bomans, P. H. H.; Müller, F. A.; Will, J.; Frederik, P. M.; With, G.; Sommerdijk, N. A. J. M. (2010). The role of prenucleation clusters in surface-induced calcium phosphate crystallization. *Nature Materials*, *9*, 1010–1014.

DIN 4760 (1982). Form deviations, Concepts, Classification system. Deutsche Institut für Normung e.V.. Beuth Verlag, Berlin.

DIN EN 10027-1 (2005). Designation systems for steels - Part 1: Steel names. Deutsche Institut für Normung e.V.. Beuth Verlag, Berlin.

DIN EN 1672-2 (2009). Food processing machinery - Basic concepts - Part 2: Hygiene requirements. Deutsche Institut für Normung e.V.. Beuth Verlag, Berlin.

DIN EN ISO 14891 (2002). Milk and milk products - Determination of nitrogen content - Routine method using combustion according to the Dumas principle. Deutsche Institut für Normung e.V.. Beuth Verlag, Berlin.

DIN EN ISO 25178-2 (2008). Geometrical product specifications (GPS) - Surface texture: Areal - Part 2: Terms, definitions and surface texture parameters. Deutsche Institut für Normung e.V.. Beuth Verlag, Berlin.

DIN EN ISO 4287 (2010). Geometrical product specifications (GPS) - Surface texture: Profile method - Terms, definitions and surface texture parameters. Deutsche Institut für Normung e.V.. Beuth Verlag, Berlin.

DIN ISO 3534-1 (2009). Statistics – Vocabulary and symbols – Part 1: General statistical terms and terms used in probability. Deutsche Institut für Normung e.V.. Beuth Verlag, Berlin.

Donnet, C. (1998). Recent progress on the tribology of doped diamond-like and carbon alloy coatings: a review. *Surface and Coating Technology*, 100-101, 180–186.

Douillard, J. M. (1997). Concerning the Thermodynamic Consistency of the “Surface Tension Components" Equations. *Journal of Colloid and Interface Science*, 188, 511–515.

Douillard, J. M. (1997). Concerning the thermodynamic consistency of the “surface tension components" equations. *Journal of Colloid and Interface Science*, 188 (2), 511–515.

Driedger, O.; Neumann, A. W.; Sell, P.-J. (1965). Über die grenzflächenenergetische Zustandsfunktion, II. *Kolloid-Zeitschrift und Zeitschrift für Polymere*, 204 (1/2), 101–105.

Dürr, H. (2002). Milk Heat Exchanger Cleaning - Modelling of deposit removal II. *Food and Bioproducts Processing*, *80*, 253–259.

Dürr, H. (2007). Influence of surface roughness and wettability of stainless steel on soil adhesion, cleanability and microbial inactivation. *Food and Bioproducts Processing*, 85, 49–56.

Dürr, H.; Graßhoff, A. (1999). Milk heat exchanger cleaning: modelling of deposit removal. *Food and Bioproducts Processing*, 77, 114–118.

Dumas, J. B. (1870). Determination of the nitrogen in organic componds: Determination of the nitrogen from the volume. In C. Remigius Fresenius (Ed.), *A system of instruction in quantitative chemical analysis*, (pp. 440–442). J. Wiley & Son, New York, USA.

Dupeyrat, M.; Labbé, J.-P.; Michel, F.; Billoudet, F.; Daufin, G. (1987). Mouillabilité et interactions solide-liquide dans l'encrassement de divers matériaux par du lactosérum et du lait. *Le Lait*, 67 (4), 465–486.

Epstein, N. (1981). Thinking about heat transfer fouling: A 5 × 5 matrix. *Heat Transfer Engineering*, 4 (1), 43–56.

FDA (2012) U.S Food and Drug Administration, CFSAN/Office of Food Additive Safety, Inventory of effective food contact substances, FDA - FCN No. 301.

Feng, H.-P.; Hsu, C.-H.; Lu, J.-K.; Shy, Y.-H. (2003). Effects of PVD sputtered coatings on the corrosion resistance of AISI 304 stainless steel. *Materials Science and Engineering*, A347, 123–129.

Fillaudeau, L.; Winterton, P.; Leuliet, J. C.; Tissier, J. P.; Maury, V.; Semet, F.; Debreyne, P.; Berthou, M.; Chopard, F. (2006). Heat treatment of whole milk by the direct Joule effect – Experimental and numerical approaches to fouling mechanisms. *Journal of Dairy Science*, 89, 4475–4489.

Fink, A.; Kessler, H. G. (1985). Changes in the fat globule membrane produced by heating. *Milchwissenschaft*, 40, 261–264.

Floris, R.; Bodnár, I.; Weinbreck, F.; Alting, A. C. (2008). Dynamic rearrangement of disulfide bridges influences solubility of whey protein coatings. *International Dairy Journal*, 18, 566–573.

Förster, M.; Augustin, W.; Bohnet, M. (1999). Influence of the adhesion force crystal/heat exchanger surface on fouling mitigation. *Chemical Engineering and Processing*, 38, 449–461.

Föste, H.; Schöler, M.; Majschak, J.-P.; Augustin, W.; Scholl, S. (2013). Modeling and validation of the mechanism of pulsed flow cleaning. *Heat Transfer Engineering*, 34, 753–760.

Foster, C. L.; Britten, M.; Green, M. L. (1989). A model heat-exchange apparatus for the investigation of fouling of stainless steel surfaces by milk I: Deposition formation at 100°C. *Journal of Dairy Research*, 56, 201–209.

Foster, C. L.; Green, M. L. (1990). A model heat exchange apparatus for the investigation of fouling of stainless steel surfaces by milk II: Deposition of fouling material at 140°C, its adhesion and depth profiling. *Journal of Dairy Research*, 57, 339–348.

Fowkes, F. M. (1964). Attractive forces at interfaces. *Industrial and Engineering Chemistry*, 56 (12), 40–52.

Fox, P.; Brodkorb, A. (2008). The casein micelle: historical aspects, current concepts and significance. *International Dairy Journal*, 18, 677–684.

Fryer, P. J.; Belmar-Beiny, M. T. (1991). Fouling of heat exchangers in the food industry: a chemical engineering perspective. *Trends in Food Science & Technology*, 2, 33–37.

Fryer, P. J.; Bird, M. R. (1994). Factors which affect the kinetics of cleaning dairy solids. *Food Science and Technology Today*, 8, 36–42.

Fryer, P. J.; Christian, G. K. (2005). Improving the cleaning of heat exchangers. In: H. L. M. Lelieveld, M. A. Mostert, J. Holah (Eds.), *Handbook of hygiene control in the food industry*, (pp. 425 - 496). Woodhead Publishing Ltd., Boca Raton, USA.

Fryer, P. J.; Christian, G. K.; Liu, W. (2006). How hygiene happens: physics and chemistry of cleaning. *International Journal of Dairy Technology*, 59, 76–84.

Fryer, P. J.; Robbins, P.T.; Green, C.; Schreier, P. J. R.; Pritchard, A. M.; Hasting, A. P. M.; Royston, D. G.; Richardson, J. F. (1996). A statistical model for fouling of a plate heat exchanger by whey protein solution at UHT conditions. *Food and Bioproducts Processing*, *74*, 189–199.

Fryer, P. J.; Slater, N. K. H. (1984). Reaction fouling from food fluids. *American Society of Mechanical Engineers*, *35*, 65–73.

Fryer, P. J.; Slater, N. K. H. (1986). The simulation of heat exchanger control with tube-side chemical reaction fouling. *Chemical Engineering Science*, 41, 2363–2372.

Fukuzaki, S.; Urano, H.; Nagata, K. (1995). Adsorption of protein onto stainless-steel surfaces. *Journal of Fermentation and Bioengineering*, *80*, 6–11.

Galani, D.; Apenten, R. K. O. (1997). The comparative heat stability of bovine β-lactoglobulin in buffer and complex media. *Journal of the Science of Food and Agriculture*, 74, 89–98.

Galani, D.; Apenten, R. K. O. (1999a). Beta-lactoglobulin denaturation by dissociation-coupled unfolding. *Food Research International*, 32, 93–100.

Galani, D.; Apenten, R. K. O. (1999b). Heat-Induced denaturation and aggregation of β-lactoglobulin: kinetics of formation of hydrophobic and disulphide-linked aggregates. *International Journal of Food Science and Technology*, 34, 467–476.

Gallot – La Vallée, T.; Lalande, M. (1985). A mechanistic approach of pasteurized milk deposit cleaning. In: D. B. Lund, E. Plett, C. Sandu (Eds.), *Proceedings of the 2nd Conference on Fouling and Cleaning in Food Processing*, (pp. 374–394). Madison, Wisconsin, USA.

Gallot – LaVallée, T.; Lalande, M.; Corrieu, G. (1982). An optical method to study the kinetics of cleaning milk deposits by sodium hydroxide. *Journal of Food Process Engineering*, 5, 131–143.

Gallot – LaVallée, T.; Lalande, M.; Corrieu, G. (1984). Cleaning kinetics modeling of holding tubes fouled during milk pasteurization. *Journal of Food Process Engineering*, 7, 123–142.

Gao, R.; van Halsema, F. E. D.; Temminghoff, E. J. M.; van Leeuwen, H. P.; van Valenberg, H. J. F.; Eisner, M. D.; van Boekel, M. A. J. S. (2010). Modelling ion composition in simulated milk ultrafiltrate (SMUF). II. Influence of pH, ionic strength and polyphosphates. *Food Chemistry*, 122, 710–715.

Garrett-Price, B. A; Smith, S. A.; Watts, R. L.; Knudsen, J. G. (1985). Fouling of heat exchangers – Characteristics, costs, prevention, control and removal. Noyes Publications, New Jersey.

Geddert, T.; Augustin, W.; Scholl, S. (2011a). Influence of surface defects and aging of coated surfaces on fouling behavior. *Heat Transfer Engineering*, 32 (3–4), 300–306.

Geddert, T.; Augustin, W.; Scholl, S. (2011b). Induction time in crystallization fouling on heat transfer surfaces. *Chemical Engineering Technology*, 34, 1303–1310.

Geddert, T.; Bialuch, I.; Augustin, W.; Scholl, S. (2009). Extending the induction period of crystallization fouling through surface coating. *Heat Transfer Engineering*, 30 (10–11), 868–875.

Georgiadis, M. C.; Macchietto, S. (2000). Dynamic modelling and simulation of plate heat exchangers under milk fouling. *Chemical Engineering Science*, *55*, 1605–1619.

Gillham, C. R.; Fryer, P. J.; Hasting, A. P. M.; Wilson, D. I. (1999). Cleaning-in-place of whey protein fouling deposits: Mechanisms controlling cleaning. *Trans IChem, 77C*, 127–136.

Good, R. J.; Girifalco, L. A. (1960). A theory for estimation of surface and interfacial energies. III. Estimation of surface energies of solids from contact angle data. *Journal of Physical Chemistry B*, 64, 561–565.

Gordon, K. P.; Hankinson, D. J.; Carver, C. E. (1968). Deposition of milk solids on heated surfaces. *Journal of Dairy Science*, 51, 520–526.

Gotham, S. M.; Fryer, P. J.; Paterson, W. R. (1988). The measurement of insoluble proteins using a modified Bradford assay. *Analytical Biochemistry*, 173, 353–358.

Gotham, S. M.; Fryer., P. J.; Pritchard, A. M. (1992). β-lactoglobulin denaturation and aggregation reactions and fouling deposit formation: a DSC study. *International Journal of Food Science and Technology*, *27*, 313–327.

Gouy, G. (1910). Sur la constituition de la charge électrique à la surface d'un électrolyte. *Journal de Physique Théorique et Appliquée*, 4 (9), 457–467.

Grant, C. S.; Webb, G. E.; Jeon, Y. W. (1996). Calcium phosphate decontamination of stainless steel surfaces. *AIChE Journal*, 42 (3), 861–875.

Graßhoff, A. (1997). Cleaning of heat treatment equipment. *Bulletin of the International Dairy Federation*, 328, 32–44.

Graßhoff, A. (1998). Methoden der Reinigung in milchwirtschaftlichen Betrieben. *SÖFW-Journal*, 124, 1037–1042.

Graßhoff, A. (2006). Reinigungsverfahren. In: G. Wildbrett (Ed.), *Reinigung und Desinfektion in der Lebensmittelindustrie*, (pp. 193–240). B. Behr's Verlag GmbH & Co. KG, Hamburg.

Grijspeerdt, K.; Mortier, L.; de Block, J., van Renterghem, R. (2004). Applications of modelling to optimise ultra high temperature milk heat exchangers with respect to fouling. *Food Control*, *15*, 117–130.

Grill, A. (1993). Review of the tribology of diamond-like carbon. *Wear*, 168, 143–153.

Grill, A. (1999). Diamond-like carbon: state of the art. *Diamond and Related Materials*, 8, 428–434.

Grill, A. (2003). Diamond-like carbon coatings as biocompatible materials - an overview. *Diamond and Related Materials*, 12 (2), 166–170.

Grischke, M.; Bewilogua, K.; Trojan, K.; Dimigen, H. (1995). Application-oriented modification of deposition processes for diamond-like-carbon based coatings. *Surface and Coatings Technology*, 74-75, 739–745.

Guérin R.; Ronse, G.; Bouvier, L.; Debreyne, P.; Delaplace, G. (2007). Structure and rate of growth of whey protein deposit from in situ electrical conductivity during fouling in a plate heat exchanger. *Chemical Engineering Science*, 62, 1948–1957.

Guideline VDI 2840 (2005). Carbon films. Basic knowledge, film types and properties, Association of German Engineers. VDI-Gesselschaft, Düsseldorf.

Guignard, C.; Verones, F.; Loerincik, Y.; Jolliet, O. (2009). Environmental/Ecological impact of the dairy sector. *Bulletin of the International Dairy Federation*, 436, 1–60.

Gynning, K.; Thome, K. E.; Samuelsson, E.-G. (1958). Das Anbrennen in Plattenerhitzern. *Milchwissenschaft*, 13, 62–70.

Harper (1972). Sanitation in dairy food plants. In: R. K. Guthrie (Ed.), *Food Sanitation* (pp. 112). AVI Publishing Company Inc., Westport.

Harper, W. J. (1972). Sanitation in dairy food plants. In: R. K. Guthrie (Ed.), *Food Sanitation*. The AVI Publishing Company, Inc, West-Port.

Hasebe, T.; Hotta, A.; Kodama, H.; Kamijo, A.; Takahashi, K.; Suzuki, T. (2007). Recent advances in diamond-like carbon in the medical and food packing fields. *New Diamond and Frontier Carbon Technology*, 17, 263–279.

Hasson, D.; Avriel, M.; Resnick, W.; Rozenman, T.; Windreich, S. (1968). Mechanism of calcium carbonate scale deposition on heat-transfer surfaces. *Industrial & Engineering Chemistry Fundamentals*, 7 (1), 59–65.

Hauert, R. (2003). A review of modified DLC coatings for biological applications. *Diamond and Related Materials*, 12, 583–589.

Hauser, G.; Curiel, G. J.; Bellin, H.-W.; Cnossen, H.J.; Hofmann, J.; Kastelein, J.; Partington, E.; Peltier, Y.; Timperley, A. W. (2004). Equipment design criteria, Doc. 08. European Hygienic Engineering and Design Group, Frankfurt.

Haynes, C. A.; Norde, W. (1994). Globular proteins at solid/liquid interfaces. *Colloids and Surfaces B: Biointerfaces*, 2 (6), 517–566.

Hege, W. U. (1984). Über die Bildung von Ablagerungen beim Erhitzen von Milch und Molke. PhD thesis. Technische Universität München, Freising.

Hegg, P.-O.; Castberg, H. B.; Lundh, G. (1985). Fouling of whey proteins on stainless steel at different temperatures. *Journal of Dairy Research*, 52, 213–218.

Hegg, P.O.; Larsson, K. (1981). Ellipsometry studies of adsorbed lipids and milk proteins on metal surfaces. In: Hallström, B., Lund, D.B., Trägrådh, C. (Eds.), *Proceedings of Fundamentals and applications of surface phenomena associated with fouling and cleaning in food processing*, (pp. 250–255). Tylösand, Sweden.

Hejda, F.; Solar, P.; Kousal, J. (2010). Surface Free Energy Determination by Contact Angle Measurements – A Comparison of Various Approaches. In: J. Šafránková, J. Pavlů (Eds.), *Proceedings of the 19th Annual Conference of Doctoral Students – WDS*, (pp. 25–30). Matfyz Press, Prague.

Henry, D. C. (1931). The cataphoresis of suspended particles, Part 1, The equation of cataphoresis. *Proceedings of the Royal Society London*, 133A, 106–129.

Herreid, E. O.; Le Luetscher, R. (1963). Cleaning and sanitizing dairy equipment. *Journal of Dairy Science*, 46, 1309–1314.

Herrmann, P. S. P.; Yoshida, C. M. P. ; Antunes, A. J.; Marcondes, J. A. (2004). Surface evaluation of whey protein films by atomic force microscopy and water vapour permeability analysis. *Packaging Technology and Science*, 17, 267–273.

Hieke, A. (2001). Verschleissfeste Antihaftschichten auf Basis modifizierter diamantähnlicher Kohlenstoffschichten. *Vakuum in Forschung und Praxis*, 13, 9–13.

Hoffmann, W.; Reuter, H. (1984). Wandschubspannung als Bezugsgröße für die für Strömungsmechanik beim Zirkulationsreinigen von geraden Rohren. *Milchwissenschaft*, 39, 645–647.

Hoffmann, W.; Reuter, H. (1984). Zirkulationsreinigen (CIP) von den geraden Rohren in Abhängigkeit von der Oberflächenrauheit und anderen Einflußfaktoren. *Chemie Ingenieur Technik*, 56, 328–329.

Höfling, V. (2004). Kristallisationsfouling auf wärmeübertragenden Flächen durch Mehrkomponentensysteme. PhD thesis. Technische Universität Braunschweig.

Holsinger, V. H.; Rajkowski, K. T.; Stabe, J. R. (1997). Milk pasteurisation and safety: a brief history and update. *Rev. sci. tech. Off. int. Epiz*, 16, 441–451.

Hooper, R. J.; Paterson, W. R.; Wilson, D. I. (2006). Comparison of whey protein model foulants for studying cleaning of milk fouling deposits. *Food and Bioproducts Processing*, 84, 329–337.

Horne, D. S. (1998). Casein interactions: casting light on the black boxes, the structure in dairy products. *International Dairy Journal*, 8, 171-177.

Hunter, R. J. (1981). *Zeta potential in colloid science. Principles and applications*. Academic Press, Inc, London.

Iametti, S.; De Gregori, B.; Vecchio, G.; Bonomi, F. (1996). Modifications occur at different structural levels during the heat denaturation of β-lactoglobulin. *European Journal of Biochemistry*, 237 (1), 106-112.

Informationsstelle Edelstahl Rostfrei (2006). Edelstahl Rostfrei – Eigenschaften, Merkblatt 821. Düsseldorf.

Irwin, D.; Warren, S.; Danne, M.; Weeks, M. (2006). Cleaning the cleaning solution - an industry approach to CIP recovery. In: D. I. Wilson, J. Y. M. Chew, P. J. Fryer, A. P. M. Hasting (Eds.), *Proceedings of the Conference Fouling, Cleaning and Disinfection in Food Processing*, (pp. 307–314). Cambridge, UK.

ISO 22412 (2008). Particle Size Analysis – Dynamic Light Scattering. International Organisation for Standardisation, Geneva, Switzerland.

Itoh, H.; Nagata, A.; Toyomasu, T.; Sakiyama, T.; Nagai, T.; Saeki, T.; Nakanishi, K. (1995). Adsorption of β-lactoglobulin onto the surface of stainless steel particles. *Bioscience Biotechnology & Biochemistry*, 59, 1648–1651.

Jackson, A. T.; Low, W. M.. (1982). Circulation cleaning of a plate heat exchanger fouled by tomato juice. III. The effect of fluid flow rate on cleaning efficiency. *Journal of Food Technology*, *17*, 745–752.

Jennings, W. G. (1959). Circulation cleaning. III. The kinetics of a simple detergent system. *Journal of Dairy Science*, 42, 1763–1771.

Jennings, W. G. (1965). Theory and practice of hard-surface cleaning. *Advances in Food Research*, 14, 325–458.

Jennings, W. G.; McKillop, A. A.; Luick, J. K. (1957). Circulation cleaning. *Journal of Dairy Science*, 40, 1471–1479.

Jeurnink, T. J. M. (1995a). Fouling of heat exchangers in relation to the serum protein concentration in milk. *Milchwissenschaft*, 50 (5), 257–260.

Jeurnink, T. J. M. (1995b). Fouling of heat exchangers by fresh and reconstituted milk and the influence of air bubbles. *Milchwissenschaft*, 50 (4), 189–193.

Jeurnink, T. J. M.; de Kruif, K. G. (1995). Calcium concentration in milk in relation to heat stability and fouling. *Netherlands Milk and Dairy Journal*, 49, 151–165.

Jeurnink, T. J. M.; Walstra, P.; de Kruif, C. G. (1996a). Mechanisms of fouling in dairy processing. *Netherlands Milk and Dairy Journal*, *50*, 407–426.

Jeurnink, T.; Brinkman, D. W. (1994). The cleaning of heat exchangers and evaporators after processing milk or whey. *International Dairy Journal*, 4, 347–368.

Jeurnink, T.; Verheul, M.; Stuart, M. C.; de Kruif, C. G. (1996b). Deposition of heated whey proteins on a chromium oxide surface. *Colloids and Surfaces B: Biointerfaces*, 6, 291–307.

Jimenez, M.; Delaplace, G.; Nuns, N.; Bellayer, S.; Deresmes, D.; Ronse, G.; Alogaili, G.; Collinet-Fressancourt, M.; Traisnel, M. (2013). Toward the understanding of the interfacial dairy fouling deposition and growth mechanisms at a stainless steel surface: a multiscale approach. *Journal of Colloid and Interface Science*, *404*, 192–200.

Jin, S.; Atrens, A. (1987). ESCA-studies of the structure and composition of the passive folm formed on stainless steel by various immersion times in 0,1 M sodium chloride solution. *Applied Physics A*, 42 (2),149–165.

Johnson, J. J.; Roland, C. T. (1940b). Study of dairy cleaning problems. II. Effectiveness of alkalies in removing heat-deposited milk solids and butterfat films. *Journal of Dairy Science*, 23, 463–469.

Johnson, J. J.; Roland, C. T. (1940a). Study of dairy cleaning problems I. Films and deposits on hot-milk equipment. *Journal of Dairy Science*, 23, 457–461.

Jullien, C.; Bénézech, T.; Carpentier, B.; Lebret, V.; Faille, C. (2002). Identification of surface characteristics relevant to the hygienic status of stainless steel for the food industry. *Journal of Food Engineering*, 56, 77–87.

Jun, S.; Puri, V. M. (2005). Fouling models for heat exchangers in dairy processing: a review. *Journal of Food Process Engineering*, 28, 1–34.

Jun, S.; Puri, V. M. (2007). Plate heat exchanger: Thermal and fouling analysis. In: D.-W. Sun (Ed.), *Computational Fluid Dynamics in Food Processing*, (pp. 417–432). CRC Press, Boca Raton, USA.

Kaelble, D. H. (1970). Dispersion-polar surface tension properties of organic solids. *The Journal of Adhesion*, 2, 66–81.

Khaldi, M.; Blanpain-Avet, P.; Guérin, R.; Ronse, G.; Bouvier, L.; André, C.; Bornaz, S.; Croguennec, T.; Jeantet, R.; Delaplace, G. (2015). Effect of calcium content and flow regime on whey protein fouling and cleaning in a plate heat exchanger. *Journal of Food Engineering*, 147, 68‑78.

Kananeh, A. B.; Scharnbeck, E.; Kück, U. D.; Räbiger, N. (2010). Reduction of milk fouling inside gasketed plate heat exchanger using nano-coatings. *Food and Bioproducts Processing*, 8 (4), 349–356.

Kane, D. R.; Middlemiss, N. E. (1985). Cleaning chemicals-state of the knowledge. In: D. Lund, E. Plett, C. Sandu (Eds.), *Proceedings of the 2nd International Conference of Fouling and Cleaning in Food Processing*, (pp. 312–335), Madison, USA.

Karlsson, C. A.-C.; Wahlgren, M. C.; Trägårdh, A. C. (1996). β-lactoglobulin fouling and its removal upon rinsing and by SDS as influenced by surface characteristics, temperature and adsorption time. *Journal of Food Engineering*, 30, 43–60.

Kastanas, P.; Lewis, M. J.; Grandison, A. S. (1995). Design and development of a miniature UHT Plant for fouling studies and its evaluation using milk adjusted to different pH values, goat's milk and milk permeate. *Transactions of the Institution of Chemical Engineers*, 73, 83–91.

Kazi, S.; Duffy, G.; Chen, X. (2012). Fouling and fouling mitigation on heated metal surfaces. *Desalination*, 288, 126–134.

Keijbets, E. L.; Chen, J.; Dickinson, E.; Vieira, J. (2009). Surface energy investigation of chocolate adhesion to solid mould materials. *Journal of Food Engineering*, 92 (2), 217–225.

Kern, D. Q.; Seaton, R. E. (1959). A theoretical analysis of thermal surface fouling. *British Chemical Engineering*, 4, 258–262.

Keshani, S.; Daud, W. R. W.; Woo, M. W.; Nourouzi, M. M.; Talib, M. Z. M.; Luqman Chuah, A.; Russly, A. R. (2013). Reducing the deposition of fat and protein covered particles with low energy surfaces. *Journal of Food Engineering*, 116 (3), 737–748.

Kessler, H. G. (1996). Lebensmittel- und Bioverfahrenstechnik – Molkereitechnologie. A. Kessler Verlag, München.

Kessler, H.; Fiedler, J.; Hege, W. (1986). Produktansatzbildung beim Erhitzen und Eindampfen flüssiger Lebensmittel. *Chemie Ingenieur Technik*, 58, 475–485.

Kessler, H.-G.; Beyer, H.-J. (1991). Thermal denaturation of whey proteins and its effect in dairy technology. *International Journal of Biological Macromolecules*, 13, 165–173.

Kim, J. C.; Lund, D. B. (1997). Adsorption behavior of β-lactoglobulin onto stainless steel surfaces. *Journal of Food Processing and Preservation*, 21, 303–317.

Kim, J. C.; Lund, D. B. (1989). Adsorption of β-lactoglobulin onto stainless steel surfaces. In: H. G. Kessler, K. Welchner, D. B. Lund (Eds.), *Proceedings of the 3rd International Conference on Fouling and Cleaning in Food Processing*, (pp. 187–199). Druckerei Walch, Augsburg.

Kim, J.; Lund, D. (1998a). Kinetics of β-lactoglobulin adsorption onto stainless steel surfaces. *Biotechnology Progress*, 14, 951–958.

Kim, J.; Lund, D. (1998b). Milk protein/stainless steel interaction relevant to the initial stage of fouling in thermal processing. *Journal of Food Process Engineering*, 21, 369–386.

Kirtley, S. A.; McGuire, J. (1989). On differences in surface constitution of dairy product contact materials. *Journal of Dairy Science*, 72 (7), 1748–1753.

Knudsen, J. G. (1980). Apparatus and techniques for measurement of fouling of heat transfer surfaces. In: J. G. Knudsen, E. F. C. Somerscales (Eds.), *Proceedings of the International Conference on the Fouling of Heat Transfer Equipment*, (pp. 57–81). Hemisphere, Washington, DC, USA.

Koch, C.; Kraft, K.; Leipertz, A. (1998). Parameter study on the performance of dropwise condensation. *Revue Générale de Thermique*, 37, 539–548.

Kouider, N.; Hamadi, F.; Mallouki, B.; Bengoram, J.; Mabrouki, M.; Zekraoui, M.; Ellouali, M; Latrache, H. (2010). Effect of stainless steel surface roughness on Staphylococcus aureus adhesion. *International Journal of Pure and Applied Science*, 4 (1), 1–7.

Kresta, S. M; Wood, P. E. (1993). The mean flow field produced by a 45° pitched blade turbine: Changes in the circulation pattern due to off bottom clearance. *The Canadian Journal of Chemical Engineering*, 71, 42–53.

Krüss GmbH (2004). Drop Shape Analysis DSA1 v 1.90 für Kontaktwinkelmesssystem DSA100 - Benutzerhandbuch. Krüss GmbH, 15021. Hamburg.

Kulkarni, S. M.; Maxcy, R. B.; Arnold, R. G. (1975). Evaluation of soil deposition and removal processes: An Interpretive Review. *Journal of Dairy Science*, 58, 1922–1936.

Kuncewicz, Cz.; Pietrzykowski, M. (2001). Hydrodynamic model of a mixing vessel with pitched-blade turbines. *Chemical Engineering Science*, 56 (15), 4659-4672.

Kuwata, K.; Shastry, R.; Cheng, H.; Hoshino, M.; Batt, C. A.; Goto, Y.; Roder, H. (2001). Structural and kinetic characterization of early folding events in β-lactoglobulin. *Nature Structural Biology*, 8, 151–155.

la Fuente, M. A.; Singh, H.; Hemar, Y. (2002). Recent advances in the characterisation of heat-induced aggregates and intermediates of whey proteins. *Trends in Food Science & Technology*, 13 (8), 262–274.

Lalande, M.; Tissier, J.-P; Corrieu, G. (1984). Fouling of a plate heat exchanger used in ultra-high-temperature sterilization of milk. *Journal of Dairy Research*, 51, 557–568.

Lalande, M.; Tissier, J.-P; Corrieu, G. (1985). Fouling of heat transfer surfaces related to β-lactoglobulin denaturation during heat processing of milk. *Biotechnology Progress*, 1, 131–139.

Leclercq-Perlat, M. N.; Tissier, J. P.; Bénézech, T. (1994). Cleanability of stainless steel in relation to chemical modifications due to industrial cleaning procedures used in the dairy industry. *Journal of Food Engineering*, 23 (4), 449–465.

Leclercq-Perlat, M.-N.; Lalande, M. (1991). A review of the modeling of the removal of porous contaninants deposited on heat transfer surfaces. *International Chemical Engineering*, 31, 74–93.

Leclercq-Perlat, M.-N.; Lalande, M. (1994). Cleanability in relation to surface chemical composition and surface finishing of some materials commonly used in food industries. *Journal of Food Engineering*, 23, 501–517.

Lee, S. J.; Sherbon, J. W. (2002). Chemical changes in bovine milk fat globule membrane caused by heat treatment and homogenisation of whole milk. *The Journal of Dairy Research*, 69, 555–567.

Leeder, J. G. (1956). Milkstone - It can be controlled. *Journal of Dairy Science*, 39, 229–231.

Lenges, J. (1982). Etude des coefficients de diffusion d'agents de surface et de la cinétique de micellisation d'un colorant. Thèse de Docteur en Science, Universitaté de Bruxelles.

Li, D.; Neumann, A. (1990). A reformulation of the equation of state for interfacial tensions. *Journal of Colloid and Interface Science*, 137, 304–307.

Lieske, B.; Konrad, G.; Faber, W. (1997). A new spectrophotometric assay for native β-lactoglobulin in raw and processed bovine milk. *International Dairy Journal*, 7, 805–812.

Lin, S. X. Q.; Chen, X. D. (2007). A laboratory investigation of milk fouling under the influence of ultrasound. *Food and Bioproducts Processing*, 85, 57–62.

Liu, C.; Zhao, Q. (2011). The CQ ratio of surface energy components influences adhesion and removal of fouling bacteria. *Biofouling*, 27 (3), 275–285.

Liu, C.; Zhao, Q.; Liu, Y.; Wang, S.; Abel, E. W. (2008). Reduction of bacterial adhesion on modified DLC coatings. *Colloids and Surfaces B: Biointerfaces*, 61, 182–187.

Liu, W.; Fryer, P. J.; Zhang, Z.; Zhao, Q.; Liu, Y. (2006a). Identification of cohesive and adhesive effects in the cleaning of food fouling deposits. *Innovative Food Science and Emerging Technologies*, 7, 263–269.

Liu, W.; Zhang, Z.; Fryer, P. J. (2006b). Identification and modelling of different removal modes in the cleaning of a model food deposit. *Chemical Engineering Science*, 61, 7528–7534.

Liu, Y.; Zou, Y.; Zhao, L.; Liu, W.; Cheng, L. (2011). Investigation of adhesion of $CaCO_3$ crystalline fouling on stainless steel surfaces with different roughness. *International Communications in Heat and Mass Transfer*, 38, 730–733.

Long, J.; Chen, P. (2006). On the role of energy barriers in determining contact angle hysteresis. *Advances in Colloid and Interface Science*, 127, 55–66.

Lowe, E. K.; Anema, S. G.; Bienvenue, A.; Boland, M. J.; Creamer, L. K.; Jiménez-Flores, R. (2004). Heat-induced redistribution of disulfide bonds in milk proteins. 2. Disulfide bonding patterns between bovine β-lactoglobulin and κ-casein. *Journal of Agricultural and Food Chemistry*, 52, 7669–7680.

Lucey, J. A.; Horne, D. S. (2009). Milk salts: technological significance. In: P. L. H. McSweeney, P. F. Fox (Eds.), *Advanced Dairy Chemistry: Volume 3: Lactose, Water, Salts and Minor Constituents*, (pp. 351–389). Springer, New York.

Lund, D.; Sandu, C. (1981). Chemical reaction fouling due to foodstuffs. In: E. F. C. Somerscales, J. G. Knudsen (Eds.), *Fouling of heat transfer equipment*, (pp. 437–476). Hemisphere Publishing Corporation, Washington, DC.

Ly, M.; Aguedo, M.; Goudot, S.; Le, M.; Cayot, P.; Teixeira, J.; Le, T.; Belin, J.-M.; Waché, Y. (2008). Interactions between bacterial surfaces and milk proteins, impact on food emulsions stability. *Food Hydrocolloids*, *22*, 742–751.

Lyster, R. L. J. (1965). The composition of milk deposits in an ultra-high-temperature plant. *Journal of Dairy Research*, 32, 203–208.

Lyster, R. L. J. (1979). The equilibria of calcium and phosphate ions with the micellar calcium phosphate in cow's milk. *Journal of Dairy Research*, 46, 343–346.

MacRitchie, F. (1978). Proteins at interfaces. *Advanced Protein Chemistry*, 32, 283–326.

Maguire, P. D.; McLaughlin, J. A.; Okpalugo, T. I. T.; Lemoine, P.; Papakonstantinoua, P.; McAdams, E. T.; Needham, M.; Ogwu, A. A.; Ball, M.; Abbas, G. A. (2005). Mechanical stability, corrosion performance and bioresponse of amorphous diamond-like carbon for medical stents and guidewires. *Diamond and Related Materials*, 14, 1277–1288.

Mahdi, Y.; Mouheb, A.; Oufer, L. (2009). A dynamic model for milk fouling in a plate heat exchanger. *Applied Mathematical Modelling*, 33, 648–662.

Maller, R. R. (2007). Passivation of stainless steel (EHEDG Update). *Trends in Food Science & Technology*, 18 (1), 112–115.

Malvern (2004). Zetasizer Nano Series - User Manual, Issue 2.1. Malvern Instruments Ltd., Worcestershire, UK.

Marchand, S.; de Block, J.; de Jonghe, V.; Coorevits, A.; Heyndrickx, M.; Herman, L. (2012), Biofilm formation in milk production and processing environments. Influence on milk quality and safety. *Comprehensive Reviews in Food Science and Food Safety*, 11: 133–147.

Marsh, R. J.; Jones, R. A. L.; Sferrazza, M. (2002). Adsorption and displacement of a globular protein on hydrophilic and hydrophobic surfaces. *Colloids and Surfaces B: Biointerfaces*, 23 (1), 31–42.

Martínez, M. J.; Carrera-Sánchez, C.; Rodríguez-Patino, J. M.; Pilosof, A. M. R. (2009). Interactions in the aqueous phase and adsorption at the air–water interface of caseino-glycomacropeptide (GMP) and β-lactoglobulin mixed systems. *Colloids and Surfaces B: Biointerfaces*, 68(1), 39–47.

Masurovsky, E. B.; Jordan, W. K. (1958). Studies on the relative bacterial cleanability of milk-contact surfaces. *Journal of Dairy Science*, 41, 1342–1358.

Maubois, J. L. (1984). Separation, extraction and fractionation of milk protein components. *Le Lait*, 64, 485–495.

Mauermann, M.; Eschenhagen, U.; Bley, T.; Majschak, J.-P. (2009). Surface modifications – Application potential for the reduction of cleaning costs in the food processing industry. *Trends in Food Science & Technology*, 20, S9–S15.

Maxcy, R. B. (1973). Nature and cause of yellow film occurring on dairy equipment. *Journal of Dairy Science*, 56, 164–167.

Mayer, M.; Augustin, W; Scholl, S. (2012). Adhesion of single crystals on modified surfaces in crystallization fouling. *Journal of Crystal Growth*, 361, 152–158.

McGuire, J. (1989). A predictive model for food particle interactions with contact surfaces. Journal of Food Science, 54 (1), 22–24, 29.

McGuire, J.; Lee, E.; Sproull, R. D. (1990). Temperature influences on surface energetic parameters evaluated at solid-liquid interfaces. *Surface and Interface Analysis*, 15, 603–608.

McGuire, J.; Swartzel, K. R. (1989). The influence of solid surface energetics on macromolecular adsorption from milk. *Journal of Food Processing and Preservation*, 13, 145–160.

McLaughlin, J. A.; Maguire, P. D. (2008). Advances on the use of carbon based materials at the biological and surface interface for applications in medical implants. *Diamond & Related Materials*, 17, 873–877.

Mekmene, O.; Quillard, S.; Rouillon, T.; Bouler, J.-M.; Piot, M.; Gaucheron, F. (2009). Effects of pH and Ca/P molar ratio on the quantity and crystalline structure of calcium phosphates obtained from aqueous solutions. *Dairy Science and Technology*, 89 (3-4), 301–316.

Michalski, M.; Ollivon, M.; Briard, V.; Leconte, N.; Lopez, C. (2004). Native fat globules of different sizes selected from raw milk: thermal and structural behavior. *Chemistry and Physics of Lipids*, 132, 247–261.

Milledge, J. J. (2010). The cleanability of stainless steel used as a food contact surface: an updated short review. *Food Science and Technology*, 24 (3): 18–20

Milledge, J. J.; Jowitt, R. (1980). The cleanability of stainless steel used as a food contact surface. *Institut of Food Science and Technology Proceedings*, 13, 57–62.

Molkerei Weihenstephan (2005). Umwelterklärung 2005, Molkerei Weihenstephan GmbH & Co. KG, Freising.

Molkerei Weihenstephan (2008). Umwelterklärung 2008, Molkerei Weihenstephan GmbH & Co. KG, Freising.

Monahan, F. J.; German, J. B.; Kinsella, J. E. (1995). Effect of pH and temperature on protein unfolding and thiol/disulfide interchange reactions during heat-induced gelation of whey protein. *Journal of Agricultural and Food Chemistry*, 43, 46–52.

Montgomery (1997). Introduction to statistical quality control. John Wiley & Sons, Inc., New York.

Morison, K. R.; Larsen, S. (2005). Spinning disc measurement of two-stage cleaning of heat transfer fouling deposits of milk. *Journal of Food Process Engineering*, 28, 539–551.

Morison, K. R.; Tie, S. R. (2002). The development and investigation of a model milk mineral fouling solution. *Food and Bioproducts Processing*, 80 (4), 326–331.

Morrissey, B. W.; Smith, L. E.; Stromberg, R. R.; Fenstermaker, C. A. (1976). Ellipsometric investigation of the effect of potential on blood protein conformation and adsorbance, *Journal of Colloid and Interface Science*, 56 (3), 557–563.

Mottar, J.; Moermans, R. (1988). Optimization of the forewarming process with respect to deposit formation in indirect ultra high temperature plants and the quality of milk. *Journal of Dairy Research*, 55, 563–568.

Moulin, P.; Roques, H. (2003). Zeta potential measurement of calcium carbonate. *Journal of Colloid and Interface Science*, 261, 115–126.

Mounsey, J. S.; O'Kennedy, B. T. (2009). Stability of β-lactoglobulin/micellar casein mixtures on heating in simulated milk ultrafiltrate at pH 6.0. *International Journal of Dairy Technology*, *62*, 493–499.

Müller, R. H.; Nitzsche, R.; Paulke, B.-R. (1996). Zetapotential und Partikelladung in der Laborpraxis: Einführung in die Theorie, praktische Meßdurchführung, Dateninterpretation. Wissenschaftliche Verlagsgesellschaft, Stuttgart.

Müller-Steinhagen, H. (2000). Heat exchanger fouling – Mitigation and cleaning technologies. Publico Publications, Essen.

Mullin, J. W. (1997). Crystallization. Butterworth-Heinemann, London, UK.

Murray, B. S.; Cros, L. (1998). Adsorption of β-lactoglobulin and β-casein to metal surfaces and their removal by a non-ionic surfactant, as monitored via a quartz crystal microbalance. *Colloids and Surfaces B: Biointerfaces*, 10 (4), 227–241.

Nakanishi, K.; Sakiyama, T.; Imamura, K. (2001). On the adsorption of proteins on solid surfaces, a common but very complicated phenomenon. *Journal of Bioscience and Bioengineering*, 91, 233–244.

Nam, N. D.; Lee, S. H.; Kim, J. G.; Yi, J. W.; Lee, K. R. (2009). Effect of stress on the passivation of Si-DLC coating as stent materials in simulated body environment. *Diamond and Related Materials*, 18, 1145–1151.

Napper, D. (2007). Hygiene in food factories of the future. *Trends in Food Science & Technology*, *18*, S74–S88.

Nassauer, J. (1985). Adsorption und Haftung an Oberflächen und Membranen. Dissertation. Technische Universität München, Freising.

Nassauer, J.; Kessler, H. G. (1986). The effect of electrostatic phenomena on the cleaning of surfaces. *Chemical Engineering and Processing*, 20, 27–32.

Navarra, G.; Leone, M.; Militello, V. (2007). Thermal aggregation of β-lactoglobulin in presence of metal ions. *Biophysical Chemistry*, 131, 52–61.

Ndoye, F. T.; Erabit, N.; Flick, D.; Alvarez, G. (2013). In-line characterization of a whey protein aggregation process: Aggregates size and rheological measurements. *Journal of Food Engineering*, 115 (1), 73–82.

Nicolai, T.; Britten, M.; Schmitt, C. (2011). β-lactoglobulin and WPI aggregates: Formation, structure and applications. *Food Hydrocolloids*, 25, 1945–1962.

O'Kennedy, B. T.; Mounsey, J. S.; Murphy, F.; Pesquera, L.; Mehra, R. (2006). Preferential heat-induced denaturation of bovine β-lactoglobulin variants as influenced by pH. *Milchwissenschaft*, *61*, 366–369.

O'Kennedy, B. T.; Mounsey, J. S. (2009). The dominating effect of ionic strength on the heat-induced denaturation and aggregation of β-lactoglobulin in simulated milk ultrafiltrate. *International Dairy Journal*, 19, 123–128.

Oldfield, D. J.; Singh, H.; Taylor, M. W. (1998b). Association of β-lactoglobulin and α-lactalbumin with the casein micelles in skim milk heated in an ultra-high temperature plant. *International Dairy Journal*, 8, 765–770.

Oldfield, D. J.; Singh, H.; Taylor, M. W. (2005). Kinetics of heat-induced whey protein denaturation and aggregation in skim milks with adjusted whey protein concentration. *Journal of Dairy Research*, 72, 369–378.

Oldfield, D. J.; Singh, H.; Taylor, M. W.; Pearce, K. N. (1998a). Kinetics of denaturation and aggregation of whey proteins in skim milk heated in an ultra-high temperature (UHT) pilot plant. *International Dairy Journal*, 8, 311–318

Oldfield, D. J.; Singh, H.; Taylor, M. W.; Pearce, K. N. (2000). Heat-induced interactions of β-lactoglobulin and α-lactalbumin with the casein micelle in pH-adjusted skim milk. *International Dairy Journal*, 10, 509–518.

Oliveira, R. (1997). Understanding adhesion: A means for preventing fouling. *Experimental Thermal and Fluid Science*, 14, 316–322.

Owens, D. K.; Wendt, R. C. (1969). Estimation of the surface free energy of polymers. *Journal of Applied Polymer Science*, 13, 1741–1747.

Palethorpe, S. J.; Bridgwater, J. (1988). The influence of surface finish on calcium sulphate fouling. In: *Proceedings of the International Conference on Fouling in Process Plants* (pp. 355-372). Oxford, UK.

Palzer, S.; Hiebl, C.; Sommer, K.; Lechner, H. (2001). Einfluss der Rauhigkeit einer Feststoffoberfläche auf den Kontaktwinkel. *Chemie Ingenieur Technik*, 73, 1032–1038.

Panchal, C. B.; Knudsen, J. G. (1998). Mittigation of Water Fouling: Technology Status and Challenges. *Advances in Heat Transfer*, 31, 431–474.

Parbhu, A.; Hendy, S.; Danne, M. (2006). Reducing milk protein adhesion rates: a transient surface treatment of stainless steel. *Food and Bioproducts Processing*, 84, 274–278.

Parker, M. E.; Johnson, A. H. (1930). Notes on the prevention and removal of milkstone. In: *Proceedings of the 23th Annual Convention International Association Milk Dealers, Plant Sect.*, 5–15.

Parker, T. G.; Horner, D. S. (1980). Factors influencing the stability of milk dialysate. *Journal of Dairy Research*, 47 (3), 337–342.

Patel, J. S.; Bansal, B.; Jones, M. I.; Hyland, M. (2013). Fouling behaviour of milk and whey protein isolate solution on doped diamond-like carbon modified surfaces. *Journal of Food Engineering*, 116 (2), 413–421.

Paterson, W. R.; Fryer, P. J. (1988). A reaction engineering approach to the analysis of fouling. *Chemical Engineering Science*, 43 (7), 1714–1717.

Patil, G. R.; Reuter, H. (1986). Deposit formation in UHT plants. I. Effect of forewarming in indirectly heated plats. *Milchwissenschaft*, 41, 337 – 339.

Paul, E. L.; Atiemo-Obeng, V. A.; Kresta, S. M. (2004). Handbook of industrial mixing: science and practice. Wiley-Interscience, Hoboken, USA.

Paulsson, M.; Dejmek, P. (1990). Thermal denaturation of whey proteins in mixtures with caseins studied by differential scanning calorimetry. *Journal of Dairy Science*, 73, 590–600.

Paulsson, M.; Hegg, P.-O.; Castberg, H. B. (1985). Thermal stability pf whey proteins studied by differential scanning calorimetry. *Thermodinamica Acta*, 95, 435–440.

Petit, J.; Herbig, A.-L.; Moreau, A.; Delaplace, G. (2011). Influence of calcium on β-lactoglobulin denaturation kinetics: Implications in unfolding and aggregation mechanisms. *Journal of Dairy Science*, *94*, 5794–5810.

Petit, J.; Six, T.; Moreau, A.; Ronse, G.; Delaplace, G. (2013). β-lactoglobulin denaturation, aggregation, and fouling in a plate heat exchanger: Pilot-scale experiments and dimensional analysis. *Chemical Engineering Science*, *101*, 432–450.

Pflug, I. J.; Hedrick, T. I.; Kaufmann, O. W.; Keppeler, R. A.; Pheil, C. G. (1961). Studies on the deposition and removal of radioactive soil. *Journal of Milk and Food Technology*, 24, 390–396.

Plett, E. A. (1985). Cleaning of fouled surfaces. In: D. Lund, E. Plett, C. Sandu (Eds.), *Proceedings of the 2nd International Conference of Fouling and Cleaning in Food Processing*, (pp. 286–311), Madison, USA.

Prematilaka, S. S.; Hyland, M. M.; Chen, X. D.; Watkins, L. R.; Bansal, B. (2007). Interaction of whey protin with modified stainless steel surfaces. In: H. Müller-Steinhagen, M. R. Malayeri, A. P. Watkinson (Eds.), *Proceedings of 7th International Conference on Heat Exchanger Fouling and Cleaning - Challenges and Opportunities*, (pp. 150–161). ECI Symposium Series, New York.

Prematilaka, S.; Hyland, M.; Chen, X.; Bansal, B. (2006). A Study of the effects of surface chemistry on the initial deposition mechanisms of dairy fouling. *Food Bioproducts and Processing*, 84 (4), 265–273.

Purwanti, N.; Fox, M.; Schroën, K.; Jong, P. de (2009). The microheater: A new tool for rapid determination of food kinetics. *Journal of Food Engineering*, 91, 78–84.

QUANTAX Manual (2008). Bruker AXSMicroanalysis GmbH, Berlin.

Rabe, M.; Verdes, D.; Seeger, S. (2011). Understanding protein adsorption phenomena at solid surfaces. *Advances in Colloid and Interface Science*, 162, 87–106.

Rabel, W. (1971). Einige Aspekte der Benetzungstheorie und ihre Anwendung auf die Untersuchung und Veränderung der Oberflächeneigenschaften von Polymeren. *Farbe und Lack*, 77, 997–1005.

Ramachandra, S. S.; Wiehe, S.; Hyland, M. M.; Chen, X. D.; Bansal, B. (2005). A preliminary study of the effect of surface coating on the initial deposition mechanisms of dairy fouling, In: H. Müller-Steinhagen, M. R. Malayeri, A. P. Watkinson (Eds.),

Proceedings of 6th International Conference on Heat Exchanger Fouling and Cleaning - Challenges and Opportunities, (pp. 88–96). ECI Symposium Series, New York.

Rasmussen, L. M.; Maxcy, R. B. (1979). Quantitation of proteinaceous soil removal from clean-in-place systems. *Journal of Dairy Science*, 62, 249–252.

Regulation EU No. 605/2010 (2010). Laying down animal and public health and veterinary certification conditions for the introduction into the European Union of raw milk and dairy products intended for human consumption. European Union, 2 July 2010, Brussels.

Robbins, P. T.; Elliott, B. L.; Fryer, P. J.; Belmar, M. T.; Hasting, A. P. M. (1999). A comparison of milk and whey fouling in a pilot scale plate heat exchanger: implications for modelling and mechanistic studies. *Food and Bioproducts Processing*, *77*, 97–106.

Robertson, J. (2002). Diamond-like amorphous carbon. *Materials Science and Engineering: R: Reports*, 37, 129–281.

Roscoe, S. G.; Fuller, K. L. (1993). Fouling of model surfaces: Adsorption and removal of κ-casein and β-lactoglobulin. *Food Research International*, 26, 343–353.

Rosmaninho, R.; Melo, L. (2006a). The effect of citrate on calcium phosphate deposition from simulated milk ultrafiltrate (SMUF) solution. *Journal of Food Engineering*, 73 (4), 379–387.

Rosmaninho, R.; Melo, L. F. (2006b). Calcium phosphate deposition from simulated milk ultrafiltrate on different stainless steel-based surfaces. *International Dairy Journal*, 16 (1), 81–87.

Rosmaninho, R.; Melo, L. F. (2007). Effect of proteins on calcium phosphate deposition in turbulent flow as a function of surface properties. *Experimental Thermal and Fluid Science*, 32 (2), 375–386.

Rosmaninho, R.; Melo, L. (2008). Protein-calcium phosphate interactions in fouling of modified stainless-steel surfaces by simulated milk. *International Dairy Journal*, 18, 78–80.

Rosmaninho, R.; Rizzo, G.; Müller-Steinhagen, H.; Melo, L. F. (2003). Study of the influence of bulk properties and surface tension on the deposition process of calcium phosphate on modified stainless steel. In: P. Watkinson, H. Müller-Steinhagen, M. R. Malayeri (Eds.), *Proceedings of Heat Exchanger Fouling and Cleaning: Fundamentals and Applications*, (pp. 115–120), ECI Symposium Series, New York.

Rosmaninho, R.; Rizzo, G.; Müller-Steinhagen, H.; Melo, L. F. (2007b). Calcium phosphate fouling on TiN-coated stainless steel surfaces: Role of ions and particles. *Chemical Engineering Science*, 62 (14), 3821–3831.

Rosmaninho, R.; Rizzo, G.; Müller-Steinhagen, H.; Melo, L. F. (2008). Deposition from a milk mineral solution on novel heat transfer surfaces under turbulent flow conditions, *Journal of Food Engineering*, 85, 29–41.

Rosmaninho, R.; Santos, O.; Nylander, T.; Paulsson, M.; Beuf, M.; Bénézech, T.; Yiantsios, S.; Andritsos, N.; Karabelas, A.; Rizzo, G.; Müller-Steinhagen, H.; Melo, L. F. (2007a) Modified stainless steel surfaces targeted to reduce fouling – Evaluation of fouling by milk components. *Journal of Food Engineering*, 80 (4), 1176–1187.

Rosmaninho, R.; Visser, H.; Melo, L. (2004). Influence of the surface tension components of stainless steel on fouling caused by calcium phosphate. *Progress in Colloid and Polymer Science*, 123, 203–209.

Rostagno, M.; Cartasegna, F. (2010). Anti-wear coatings for the food processing. In: R. Rauscher, M. Perucca, G. Buyle (Eds.), *Plasma technology for hyperfuncional surfaces. Food, biomedical and textile applications* (pp. 263-294). Wiley-VCH Verlag GmbH, Weinheim.

Roy, S.; Acharya, S. (2012). Scalar mixing in a turbulent stirred tank with pitched blade turbine: Role of impeller speed perturbation. *Chemical Engineering Research and Design*, 90 (7), 884–898.

Roy, S.; Acharya, S.; Cloeter, M. D. (2010). Flow structure and the effect of macro-instabilities in a pitched-blade stirred tank. *Chemical Engineering Science*, 65 (10), 3009–3024.

Rozzi, S.; Massini, R.; Paciello, G.; Pagliarini, G.; Rainieri, S.; Trifirò, A. (2007). Heat treatment of fluid foods in a shell and tube heat exchanger: Comparison between smooth and helically corrugated wall tubes. *Journal of Food Engineering*, 79, 249–254.

Rüegg, M.; Moor, U.; Blanc, B. (1977). A calorimetric study of the thermal denaturation of whey proteins in simulated milk ultrafiltrate. *Journal of Dairy Research*, 44 (3), 509–520.

Rungraeng, N.; Cho, Y.-C.; Yoon, S. H.; Jun, S. (2012). Carbon nanotube-polytetrafluoroethylene nanocomposite coating for milk fouling reduction in plate heat exchanger. *Journal of Food Engineering*, 111 (2), 218–224.

Sadeghinezhad, E.; Kazi, S. N.; Badarudin, A.; Zubair, M. N. M.; Dehkordi, B. L.; Oon, C. S. (2013). A review of milk fouling on heat exchanger surfaces. *Reviews in Chemical Engineering*, 29 (3), 169–188.

Saikhwan, P.; Geddert, T.; Augustin, W.; Scholl, S.; Paterson, W. R.; Wilson, D. I. (2006). Effect of surface treatment on cleaning of a model food soil. *Surface and Coating Technology*, 201, 943–951.

Sander, M. (1993). Oberflächenmesstechnik für den Praktiker. Feinprüf Perthen GmbH, Göttingen

Sandu, C. (1989). Chemical reaction fouling due to milk: defects - growth model. In: H. G. Kessler, K. Welchner, D. B. Lund (Eds.), *Proceedings of the 3rd International Conference on Fouling and Cleaning in Food Processing*, (pp. 46–58). Druckerei Walch, Augsburg.

Sandu, C.; Lund, D. (1985). Minimizing fouling in heat exchanger design. *Biotechnology Progress*, 1, 10–17.

Santos, O. (2004). Whey protein adsorption and aggregation on modified stainless steel surfaces in relation to fouling. PhD thesis. Lund, Sweden.

Santos, O.; Nylander, T.; Paulsson, M.; Trägårdh, C. (2006b). Whey protein adsorption onto steel surfaces-effect of temperature, flow rate, residence time and aggregation. *Journal of Food Engineering*, 74, 468–483.

Santos, O.; Nylander, T.; Rosmaninho, R.; Rizzo, G.; Yiantsios, S.; Andritsos, N.; Karabelas, A.; Müller-Steinhagen, H.; Melo, L.; Boulangé-Petermann, L.; Gabet, C.; Braem, A.; Trägårdh, C.; Paulsson, M. (2004). Modified stainless steel surfaces targeted to reduce fouling - surface characterization. *Journal of Food Engineering*, 64, 63–79.

Santos, O.; Nylander, T.; Schillén, K.; Paulsson, M.; Trägårdh, C. (2006a). Effect of surface and bulk solution properties on the adsorption of whey protein onto steel surfaces at high temperature. *Journal of Food Engineering*, 73, 174–189.

Sapan, C. V.; Lundblad, R. L.; Price, N. C. (1999). Colorimetric protein assay techniques. *Biotechnology and Applied Biochemistry,* 29, 99–108.

Schafer, M.; Yianneskis, M.; Wachter, P.; Durst, F. (1998). Trailing vortices around a 45° pitched blade impeller. *AIChE Journal*, 44 (6), 1233–1246.

Schlüssler, H. J. (1970). Zur Reinigung fester Oberflächen in der Lebensmittelindustrie. *Milchwissenschaft*, 25 (3), 133–145.

Schlüssler, H. J. (1976). Zur Kinetik von Reinigungsvorgängen an festen Oberflächen. *Brauwissenschaft*, 29, 263–268.

Schokker, E. P.; Singh, H.; Creamer, L. K. (2000). Heat-induced aggregation of β-lactoglobulin A and B with α-lactoalbumin. *International Dairy Journal*, 10, 843–853.

Schokker, E. P.; Singh, H.; Pinder, D. N.; Norris, G. E.; Creamer, L. K. (1999). Characterization of intermediates formed during heat-induced aggregation of β-lactoglobulin AB at neutral pH. *International Dairy Journal*, 9, 791–800.

Schramm, G.; Hieke, A.; Bialuch, I. (2004). Niedrige Reibwerte. Verschleißfeste Antihaftbeschichtungen für produktberührende Flächen. *Lebensmitteltechnik*, 1–2, 47–49.

Schreier, P. J. R.; Fryer, P. J. (1995). Heat exchanger fouling: A model study of the scale up of laboratory data. *Chemical Engineering Science*, *50*, 1311–1321.

Schultz, J.; Tsutsumi, K.; Donnet, J.-B. (1977a). Surface properties of high-energy solids. II. Determination of the nondispersive component of the surface free energy of mica and its energy of adhesion to polar liquids. *Journal of Colloid and Interface Science*, 59, 277–282.

Schultz, J.; Tsutsumi, K.; Donnet, J.-B. (1977b). Surface properties of high-energy solids. I. Determination of the dispersive component of the surface free energy of mica and its energy of adhesion to water and n-alkanes. *Journal of Colloid and Interface Science*, 59, 272–276.

Schurz, J.; Erk, G.; Schempp, W.; Ribitsch, V. (1990). Zeta potential as an analytical tool for graft copolymers and for polymer surfaces. *Journal of Macromolecular Science: Part A - Chemistry*, 27, 1673–1692.

Sheikholeslami, R. (1999). Composite fouling - inorganic and biological: A Review. *Environmental Progress,* 18, 113–122.

Simons, J.-W. F.; Kosters, H. A.; Visschers, R. W.; de Jongh, H. H. (2002). Role of calcium as trigger in thermal β-lactoglobulin aggregation. *Archives of Biochemistry and Biophysics*, 406, 143–152.

Sinner, H. (1960). Über das Waschen mit Haushaltwaschmaschinen in welchem Umfange erleichtern Haushaltwaschmaschinen und -geräte das Wäschehaben im Haushalt? Haus+Heim-Verlag, Hamburg.

Skudder, P. J.; Brooker, B. E.; Bonsey, A. D.; Alvarez-Guerrero, N. R. (1986). Effect of pH on the formation of deposit from milk on heated surfaces during ultra high temperature processing. *Journal of Dairy Research*, 53, 75–87.

Skudder, P. J.; Thomas, E. L.; Pavey, J. A.; Perkin, A. J. (1981). Effects of adding potassium iodate to milk before UHT treatment: I. Reduction in the amount of deposit on the heated surfaces. *Journal of Dairy Research*, 48, 99-113.

Smyth, E.; Clegg, R.; Holt, C. (2004). A biological perspective on the structure and function of caseins and casein micelles. *International Journal of Dairy Technology*, 57, 121–126.

Spanos, N.; Patis, A.; Kanellopoulou, D.; Andritsos, N.; Koutsoukos, P. G. (2007). Precipitation of calcium phosphate from Simulated Milk Ultrafiltrate solutions. *Crystal Growth & Design*, 7, 25–29.

Spiro, M.; Chong, Y. Y. (1997). Surface films formed by milk in hard water. *Food Chemistry*, 59, 237–245.

Spreer, E. (2005). Technologie der Milchverarbeitung. B. Behr's Verlag GmbH & Co. KG, Hamburg.

Srichantra, A.; Newstead, D. F.; Mccarthy, O. J.; Paterson, A. H. J. (2006). Effect of preheating on fouling of a pilot scale UHT sterilizing plant by recombined, reconstituted and fresh whole milks. *Food and Bioproducts Processing*, 84, 279–285.

Stancl, J.; Zitny, R. (2010). Milk fouling at direct ohmic heating. *Journal of Food Engineering*, 99, 437–444.

Steinhagen, R; Müller-Steinhagen, H.; Maani, K. (1993). Problems and costs due to heat exchanger fouling in New Zealand industries. *Heat Transfer Engineering*, 14 (1), 19–30.

Stern. O. (1924). Zur Theorie der elektrolytischen Doppelschicht. *Zeitschrift für Elektrochemie*, 30, 508-516.

Ström, G.; Fredriksson, M.; Stenius, P. (1987). Contact angles, work of adhesion, and interfacial tensions at a dissolving hydrocarbon surface. *Journal of Colloid and Interface Science*, 119, 352–361.

Suttiprasit, P.; Krisdhasima, V.; McGuire, J. (1992). The surface activity of α-lactalbumin, β-lactoglobulin, and bovine serum albumin: I. Surface tension measurements with single-component and mixed solutions. *Journal of Colloid and Interface Science*, 154, 316–326.

Swain, P. S.; Lipowsky, R. (1998). Contact angles on heterogeneous surfaces: A New Look at Cassie's and Wenzel's Laws. *Langmuir*, 14, 6772–6780.

The World Dairy Situation (2010). *Bulletin of the International Dairy Federation*, 446, International Dairy Federation, Brussels.

Theilen, U.; Goldbach, H. (2000). Umwelt-Handbuch - Umweltkatalog: Molkereien, Bundesministerium für wirtschaftliche Zusammenarbeit und Entwicklung, Bonn.

Timperley, D. A.; Smeulders, C. N. M. (1987). Cleaning of dairy HTST plate heat exchangers: Comparison of single- and two-stage procedures. *The Journal of the Society of Dairy Technology*, 40(1), 4–7.

Tissier, J. P.; Lalande, M. (1986). Experimental device and methods for studying milk deposit formation on heat exchanger surfaces. *Biotechnology Progress*, *2*, 218–229.

Toepfl, S.; Mathys, A.; Heinz, V.; Knorr, D. (2006). Review: Potential of high hydrostatic pressure and pulsed electric fields for energy efficient and environmentally friendly food processing. *Food Reviews International*, 22 (4), 405–423.

Tolkach, A.; Kulozik, U. (2007). Reaction kinetic pathway of reversible and irreversible thermal denaturation of β-lactoglobulin. *Le Lait*, 87 (4-5), 301–315.

Töpel, A. (2004). Chemie und Physik der Milch. B. Behr‘s Verlag, Hamburg.

Trojan, K.; Grischke, M.; Dimigen, H. (1994). Network modification of DLC coatings to adjust a defined surface energy, *Physica Status Solidi A*, 145, 575–586.

Tscharnuter, W. W. (2001). Mobility measurements by phase analysis. *Applied Optics*, 40, 3995–4003.

Tsuge, H.; Tanaka, Y.; Yoshizawa, S.; Kuraishi, T. (2002). Reactive crystallization behaviour of calcium phosphate with and without whey protein addition. *Chemical Engineering Research and Design*, 80, 105–110.

Tuckey, S. I. (1931). Milkstone formation, control and removal. *Milk Plant Monthly*, 20: 6, 46–47, 69.

Tuladhar, T. R.; Paterson, W. R.; Wilson, D. I. (2002). Thermal conductivity of whey protein films undergoing swelling – Measurement by dynamic gauging. *Food and Bioproducts Processing*, 80, 332–339.

Tung, M. S. (1998). Calcium phosphates: Structure, composition, solubility, and stability. In: Z. Amjad (Ed.), *Calcium Phosphates in Biological and Industrial Systems*, (pp. 1–19). Kluwer Academic Publishers, Massachusetts, USA.

Umweltbundesamt (2005). BVT - Merkblatt über die besten verfügbaren Techniken in der Nahrungsmittel-, Getränke- und Milchindustrie. Umweltbundesamt, Dessau-Roßlau.

Unterhaslberger, G.; Schmitt, C.; Sanchez, C.; Appolonia-Nouzille, C.; Raemy, A. (2006). Heat denaturation and aggregation of β-lactoglobulin enriched WPI in the presence of arginine HCl, NaCl and guanidinium HCl at pH 4.0 and 7.0. *Food Hydrocolloids*, 20, 1006–1019.

Unterhaslberger, G.; Schmitt, C.; Sanchez, C.; Appolonia-Nouzille, C.; Raemy, A. (2006). Heat denaturation and aggregation of β-lactoglobulin enriched WPI in the presence of arginine HCl, NaCl and guanidinium HCl at pH 4.0 and 7.0. *Food Hydrocolloids*, 20, 1006–1019.

van Asselt, A. J.; van Houwelingen, G.; te Giffel, M. C. (2002). Monitoring system for improving cleaning eficiency of cleaning-in-place processes in dairy environments. *Food and Bioproducts Processing*, 80, 276–280.

van Claeys, W. L.; Ludikhuyze, L. R.; Loey, A. M.; Hendrickx, M. E.. (2001). Inactivation kinetics of alkaline phosphatase and lactoperoxidase, and denaturation kinetics of β-lactoglobulin in raw milk under isothermal and dynamic temperature conditions. *Journal of Dairy Research*, 68, 95–107.

van Creamer, L. K.; Bienvenue, A.; Nilsson, H.; Paulsson, M.; Wanroij, M.; Lowe, E. K.; Anema, S. G.; Boland, M. J.; Jiménez-Flores, R. (2004). Heat-induced redistribution of disulfide bonds in milk proteins. 1. Bovine β-lactoglobulin. *Journal of Agricultural and Food Chemistry*, 52, 7660–7668.

van Kemenade, M. J. J. M.; de Bruyn, P. L. (1989). The influence of casein on the kinetics of hydroxyapatite precipitation. *Journal of Colloidal and Interface Science*, 129, 1–14.

van Morr C. V.; German, B.; Kinsella, J. E.; Regenstein, J. M.; Buren, J. P.; Kilara, A.; Lewis, B. A.; Mangino, M. E. (1985). A collaborative study to develop a standardized food protein solubility procedure. *Journal of Food Science*, 50, 1715–1718.

van Oss, C. J. (1994). Interfacial forces in aqueous media. M. Dekker, New York.

van Oss, C. J. (1995). Hydrophobicity of biosurfaces - origin, quantitative determination and interaction energies. *Colloids and Surfaces B: Biointerfaces*, 5, 91–110.

van Oss, C. J. (2006). Interfacial forces in aqueous media. CRC Press. Boca Raton, USA.

van Oss, C. J.; Chaudhury, M. K.; Good, R. J. (1988). Interfacial Lifshitz-van der Waals and polar interactions in macroscopic systems. *Chemical Reviews*, 88, 927–941.

van Oss, C. J.; Good, R. J.; Chaundhury, M. K. (1987). Determination of the hydrophobic interaction energy-application to separation processes. *Separation Science and Technology*, 22 (1), 1–24.

van Oss, C. J.; Good, R.; Chaudhury, M. (1986). The role of van der Waals forces and hydrogen bonds in "hydrophobic interactions" between biopolymers and low energy surfaces. *Journal of Colloid and Interface Science*, 111, 378–390.

VDI-Wärmeatlas (2006). Verein Deutscher Ingenieure (Ed.). Springer Verlag GmbH, Berlin.

Vedantam, S.; Panchagnula, M. V. (2008). Constitutive modeling of contact angle hysteresis. *Journal of Colloid and Interface Science*, 321, 393–400.

Verein Deutscher Ingenieure (2005). Kohlenstoffschichten. Grundlagen, Schichtypen und Eigenschaften. Richtlinie VDI 2840. Beuth Verlag, Berlin.

Verheul, M.; Roefs, S. P. F. M.; de Kruif, K. G. (1998). Kinetics of heat-induced aggregation of β-lactoglobulin. *Journal of Agricultural and Food Chemistry*, 46, 896–903.

Verran, J.; Rowe, D. L.; Cole, D.; Boyd, R. D. (2000). The use of the atomic force microscope to visualise and measure wear of food contact surfaces. *International Biodeterioration & Biodegradation*, 46, 99–105.

Verwey, E. J. W.; Overbeek, J. T. G. (1948). Theory of the stability of lyophobic colloids. Elsevier, Amsterdam.

Vieira, E. P.; Rocha, S.; Carmo Pereira, M.; Möhwald, H.; Coelho, M. A. N. (2009). Adsorption and diffusion of plasma proteins on hydrophilic and hydrophobic surfaces: Effect of Trifluoroethanol on protein structure. *Langmuir*, 25, 9879–9886.

Villamiel, M.; López-Fandino, R.; Corzo, N.; Olano, A. (1997). Denaturation of β-lactoglobuIin and native enzymes in the plate exchanger and holding tube section during continuous flow pasteurization of milk. *Food Chemistry*, 58, 49–52.

Visser, H. (2001). Improvement of construction materials used in the food industry to lengthen processing time - a new European project (MODSTEEL). In: H. M. Steinhagen, M. R. Malayeri, A. P. Watkinson (Eds.), *Proceedings of the 4th International Conference on Heat Exchanger Fouling and Fundamental Approaches and Technical Solutions*, (pp. 3–10). Davos, Switzerland.

Visser, H.; Jeurnink, T. J. M. (1997b). General aspects of fouling and cleaning. Introduction. Economics. *Bulletin of the International Dairy Federation*, 328, 5–6.

Visser, H.; Jeurnink, T. J. M.; Schraml, J. E.; Fryer, P.; Delplace, F. (1997). Fouling of heat treatment equipment. *Bulletin of the International Dairy Federation*, 328, 7–31.

Visser, J. (1998). Reducing fouling of heat exchangers in the dairy industry by process optimization. In: D. I. Wilson, P. J. Fryer, A. P. M. Hasting (Eds.), *Proceedings of the Conference Fouling and Cleaning in Food Processing* , (pp. 180 – 188). Cambridge, UK.

Visser, J.; Jeurnink, T. J. M. (1997a). Fouling of heat exchangers in the dairy industry. *Experimental Thermal and Fluid Science*, 14, 407–424.

Wahlgren, M.; Arnebrant, T. (1990). Adsorption of β-lactoglobulin onto silica, methylated silica, and polysulfone. *Journal of Colloid and Interface Science*, 136 (1), 259–265.

Wahlgren, M.; Arnebrant, T. (1991). Protein adsorption to solid surfaces. *Trends in Biotechnology*, 9 (1), 201–208.

Walkling-Ribeiro, M.; Rodríguez-González, O.; Jayaram, S.; Griffiths, M. (2011). Microbial inactivation and shelf life comparison of 'cold' hurdle processing with pulsed electric fields and microfiltration, and conventional thermal pasteurisation in skim milk. *International Journal of Food Microbiology*, 144, 379–386.

Walstra, P. (1990). On the stability of casein micelles. *Journal of Dairy Science*, 73, 1965–1979.

Walstra, P.; Geurts, T. J.; Noomen, A.; Jellema, A.; van Boekel, M. A. J. S. (1999). Dairy technology, principles of milk properties and processes. Marcel Dekker, Inc., New York.

Walstra, P.; Jenness, R. (1984). Dairy chemistry and physics. John Wiley & Sons, Inc., New York.

Wang, L.; Sundén, B.; Manglik, R. M. (2007). Plate Heat Exchangers. Design, applications and performance. WIT Press, Ashurst, UK.

Wang, Z.; Wang, C.; Wang, Q.; Zhang, J. (2008) Electrochemical corrosion behaviors of a-C:H and and a-C:Nx:H films. *Applied Surface Science*, 254, 3021–3025.

Wei, J.; Ravn, D. B.; Gram, L.; Kingshott, P. (2003). Stainless steel modified with poly(ethylene glycol) can prevent protein adsorption but not bacterial adhesion. *Colloids and Surfaces B: Biointerfaces*, 32, 275–291.

Wenzel, R. N. (1936). Resistance of solid surfaces to wetting by water. *Industrial & Engineering Chemistry*, 28, 988–994.

Westhoff, D. C. (1978). Heating milk for microbial destruction: a historical outline and update. *Journal of Food Protection*, *41*, 122–130.

Whyman, G.; Bormashenko, E.; Stein, T. (2008). The rigorous derivation of Young, Cassie–Baxter and Wenzel equations and the analysis of the contact angle hysteresis phenomenon. *Chemical Physics Letters*, 450, 355–359.

Wildbrett, G.; Sauerer, V. (1989). Cleanability of PMMA and PP compared with stainless steel. In: In: H. G. Kessler, K. Welchner, D. B. Lund (Eds.), *Proceedings of the 3rd International Conference on Fouling and Cleaning in Food Processing*, (pp. 163–177). Druckerei Walch, Augsburg.

Wilson, D. I. (2005). Challenges in cleaning: recent developments and future prospects. *Heat Transfer Engineering*, 26 (1), 51–59.

Wohlfahrt, M. (2012). ZMB Jahrbuch Milch 2012. ZMB Zentrale Milchmarkt Berichterstattung GmbH, Berlin.

Wu, S. (1973). Polar and nonpolar interactions in adhesion. *The Journal of Adhesion*, 5, 39–55.

Wu, W.; Nancollas, G. H. (1998). Kinetics of heterogeneous nucleation of calcium phosphates on anatase and rutile surfaces. *Journal of Colloid and Interface Science*, 199, 206–211.

Wu, W.; Zuang, H.; Nancollas G. H. (1997). Heterogeneous nucleation of calcium phosphate on solid surfaces in aqueous solution. *Journal of Biomedical Materials Research*, 35 (1), 93–100.

Xin, H.; Chen, X. D.; Özkan, N. (2002). Cleaning rate in the uniform cleaning stage for whey protein gel deposits. *Trans IChemE*, 80, 240–246.

Xin, H.; Chen, X. D.; Özkan, N. (2004). Removal of a model protein foulant from metal surfaces. *AIChE Journal*, *50*, 1961–1973.

Xu, Z.-M.; Zhang, Z.-B; Yang, S.-R. (2007). Costs due to utility fouling in China. In: H. Müller-Steinhagen, M. R. Malayeri, A. P. Watkinson (Eds.), *Proceedings of 7th International Conference on Heat Exchanger Fouling and Cleaning - Challenges and Opportunities* (pp. 113–118). ECI Symposium Series, New York.

Yoon, J.; Lund, D. B. (1989). Effect of operating conditions, surface coatings and pretreatment on milk fouling in a plate heat exchanger. In: In: H. G. Kessler, K. Welchner, D. B. Lund (Eds.), *Proceedings of the 3rd International Conference on Fouling and Cleaning in Food Processing*, (pp. 59–80). Druckerei Walch, Augsburg.

Yoon, J.; Lund, D. B. (1994). Magnetic treatment of milk and surface treatment of plate heat exchangers: effects on milk fouling. *Journal of Food Science*, 59 (5), 964–969, 980.

Young, T. (1804). An essay on the cohesion of fluids. *Philosophical Transactions of the Royal Society of London*, 95, 65–87.

Zeng, A.; Liu, E.; Annergren, I. F.; Tan, S. N.; Zhang, S.; Hing, P.; Gao, J. (2002). EIS capacitance diagnosis of nanoporosity effect on the corrosion protection of DLC films. *Diamond and Related Materials*, 11, 160–168.

Zettler, H. U.; Weiß, M.; Zhao, Q.; Müller-Steinhagen, H. (2005). Influence of surface properties and characteristics on fouling in plate heat exchangers. *Heat Transfer Engineering*, 26, 3–17.

Zhang, H.; Li, W.; Cui, D.; Hu, Z.; Xu, L. (2012). Design of lotus-simulating surfaces: Thermodynamic analysis based on a new methodology. *Colloids and Surfaces A: Physicochemical and Engineering Aspects*, 413, 314–327.

Zhao, Q.; Liu, Y.; Abel, E. (2004b). Effect of temperature on the surface free energy of amorphous carbon films. *Journal of Colloid and Interface Science*, 280, 174–183.

Zhao, Q.; Liu, Y.; Wang, C.; Wang, S. (2007). Bacterial adhesion on silicon-doped diamond-like carbon films. *Diamond and Related Materials*, 16 (8), 1682–1687.

Zhao, Q.; Liu, Y.; Wang, C.; Wang, S.; Müller-Steinhagen, H. (2005b). Effect of surface free energy on the adhesion of biofouling and crystalline fouling. *Chemical Engineering Science*, *60*, 4858–4865.

Zhao, Q.; Liu, Y.; Wang; S. (2005a). Surface modification of water treatment equipment for reducing CaSO4 scale formation. Desalination, 180 (1–3), 133–138.

Zhao, Q.; Müller-Steinhagen, H. (2002). Intermolecular and adhesion forces of deposits on modified heat transfer surfaces. In: H. Müller-Steinhagen, M. R. Malayeri, P. Watkinson (Eds.), *Heat Exchanger Fouling - Fundamental Approaches and Technical Solutions* (pp. 41–46). PUBLICO Publications, Essen.

Zhao, Q.; Wang, S.; Müller-Steinhagen, H. (2004a). Tailored surface free energy of membrane diffusers to minimize microbial adhesion. *Applied Surface Science*, 230 (1–4), 371–378.

Zisman, W. A. (1964). Relation of the equilibrium contact angle to liquid and solid constitution. *Advances in Chemistry*, 1–51.

Zúñiga, R. N.; Tolkach, A.; Kulozik, U.; Aguilera, J. M. (2010). Kinetics of formation and physicochemical characterization of thermally-induced β-lactoglobulin aggregates. *Journal of Food Science*, 75 (5), E261–E268.

Appendix

A1. Fluid properties

The specific heat capacity of whey (Kessler, 1996) and water (VDI-Wärmeatlas, 2006) are given by:

$$c_{p,whey} = 1.3076\ DM + (1 - DM)\ c_{p,water} \quad (a.1)$$

$$c_{p,water} = 4.214 - 2.153*10^{-3}\left(\frac{T_{in}+T_{out}}{2}\right) + 3.646*10^{-5}\left(\frac{T_{in}+T_{out}}{2}\right)^2 - 1.4948*10^{-7}\left(\frac{T_{in}+T_{out}}{2}\right)^3 \quad (a.2)$$

where DM [%] is the dry matter of the whey protein solution (=0.055 kg kg^{-1}), c_P is given in kJ kg^{-1} K^{-1} and T in °C.

The density of whey and water (Kessler, 1996) could be written as:

$$\rho_{whey} = 4.039\ DM + 1.273*10^{-2}\ DM^2 + 9.62*10^{-5}\ DM^3 + \rho_{water} \quad (a.3)$$

$$\rho_{water} = 100022 + 1.0205*10^{-2}\left(\frac{T_{in}+T_{out}}{2}\right) - 5.8149*10^{-3}\left(\frac{T_{in}+T_{out}}{2}\right)^2 + 1.496*10^{-5}\left(\frac{T_{in}+T_{out}}{2}\right)^3 \quad (a.4)$$

where DM [%] is the dry matter of the whey protein solution, ρ is given in kg m^{-3} and T in °C.

The dynamic viscosity of whey (Kessler, 1996) and water (VDI-Wärmeatlas, 2006) could be written as:

$$\mu_{whey} = \exp\left[3.03*10^{-5}\left(\frac{T_{in}+T_{out}}{2}\right)^2 - 1.813*10^{-2}\left(\frac{T_{in}+T_{out}}{2}\right) + 0.609\right] \quad (a.5)$$

$$\mu_{water} = 10^3 * \exp\left[-22.968 + \left(\frac{T_{in}+T_{out}}{2}\right) + 3275.89 \Big/ \left(\frac{T_{in}+T_{out}}{2}\right) + 0.017637\left(\frac{T_{in}+T_{out}}{2}\right) + 0.000693*10^{-3}\left(\frac{T_{in}+T_{out}}{2}\right)^2 - 0.0012933*10^{-6}\left(\frac{T_{in}+T_{out}}{2}\right)^3\right] \quad (a.6)$$

where μ is given in mPa.s and T in °C for whey and in K for water.

The thermal conductivity of whey and water (Kessler, 1996) are given by:

$$\lambda_{whey} = 0.65 \text{ W m}^{-1} \text{ K}^{-1}$$

$$\lambda_{water} = \left[568.96 + 1.88\left(\frac{T_{in}+T_{out}}{2}\right) - 8.2*10^{-3}\left(\frac{T_{in}+T_{out}}{2}\right)^2 + 6.02*10^{-6}\left(\frac{T_{in}+T_{out}}{2}\right)^3\right]*10^{-3} \quad (a.7)$$

where λ is given in W m^{-1} K^{-1} and T in °C.

The density (digital density meter DE 51, Mettler-Toledo GmbH, Giessen, Germany), the dynamic viscosity (Rheometer Physica MCR 101, Anton Paar Germany GmbH,

Ostfildern, Germany), and the pH value of the sodium hydroxide solutions at 30 °C were measured and are given in Table A1.

Table A1. Psychochemical properties of the NaOH solution

Concentration [% w/w]	ρ [kg m^3]	μ [Pa s]	pH [-]
0.25	998.57	856.54	12.57 ± 0.02
0.5	1001.06	868.36	12.80 ± 0.02

A2. Surface characterization

Table A2. Zeta potential of new and used surfaces at pH 6.70 ± 0.05 at 40.0 ± 0.1 °C in diverse solutions

Solution	Surface	Zeta potential [mV]	
		new	used
10^{-3} mol L^{-1} KCl	SS	- 27.0 ± 0.2	–
	DLC	- 15.2 ± 0.5	–
	SICAN	- 32.4 ± 0.3	–
	SICON®	- 30.0 ± 0.3	–
5.5 g L^{-1} WPI	SS	- 21 ± 1	- 21 ± 2
	DLC	- 41 ± 1	- 9 ± 1
	SICAN	- 35.8 ± 0.5	- 34.0 ± 0.4
	SICON®	- 23.1 ± 0.3	- 12.8 ± 0.6
SMUF	SS	12.5 ± 0.6	13 ± 2
	DLC	27 ± 3	24 ± 2
	SICAN	13 ± 1	23.8 ± 0.4
	SICON®	24 ± 1	27.3 ± 0.8
5.5 g L^{-1} WPI plus SMUF	SS	19.5 ± 0.5	17.6 ± 0.5
	DLC	25 ± 2	19 ± 2
	SICAN	20 ± 2	22.2 ± 0.8
	SICON®	26.1 ± 0.6	27.3 ± 0.3

A3. Particle size distribution during fouling

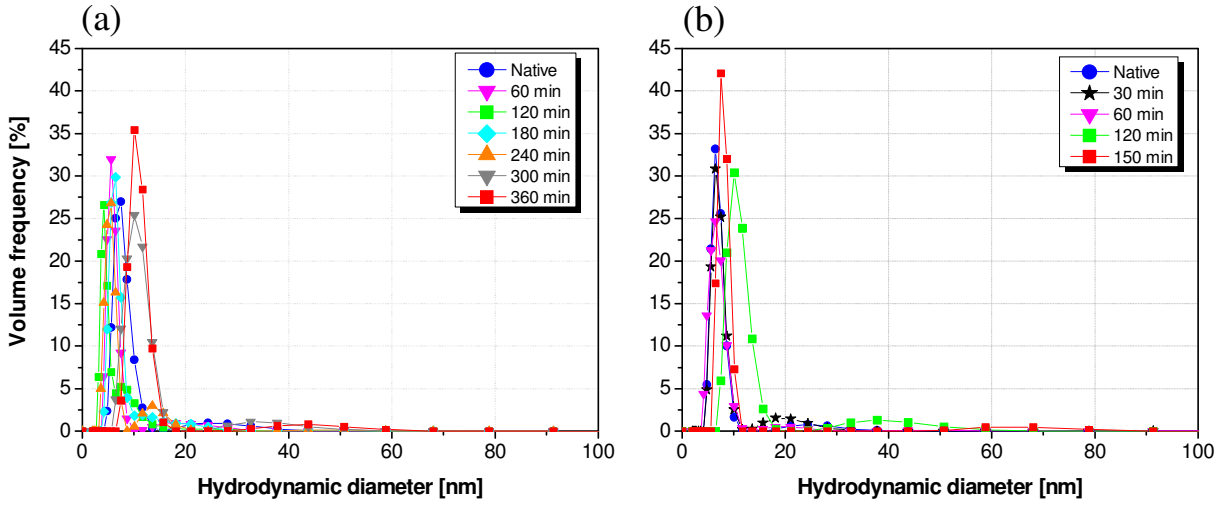

Fig. A1. Particle size distribution of bulk solution for WPI fouling at a wall temperature T_0 = (a) 80 °C and (b) 120 °C

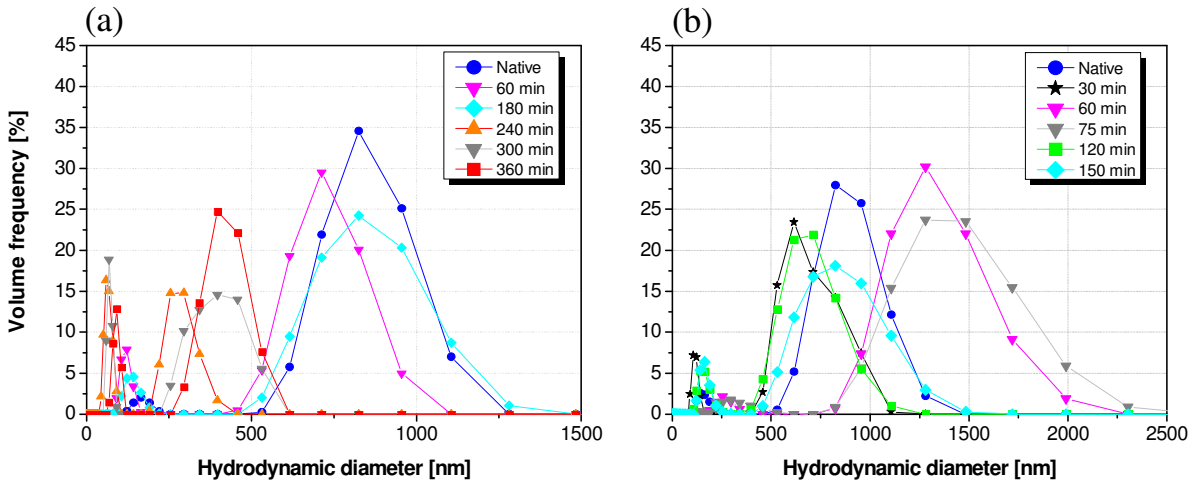

Fig. A2. Particle size distribution of bulk solution for WPI plus SMUF fouling at a wall temperature T_0 = (a) 80 °C and (b) 120 °C

A4. Statistical analysis of results from batch-wise fouling experiments

Fig. A3 gives the deposit mass and the final fouling resistance for the fouling of all model solutions: whey protein, calcium phosphate and SMUF-rich whey protein, at the initial surface temperatures of 80 and 120 °C (for SMUF, 105 °C) on the studied surfaces as function of the electron donor component. No clear/defined correlation between the two dependent variables (mass and $R_{f,\ end}$) and the independent variable can be found. It emphasizes that a statistical analysis of the data is necessary to identify possible effect of the initial surface temperature and roughness, no linear effect, as well as the combined effect of all independent variables (T_0, R_z and γ^-) on mass and $R_{f,\ end}$.

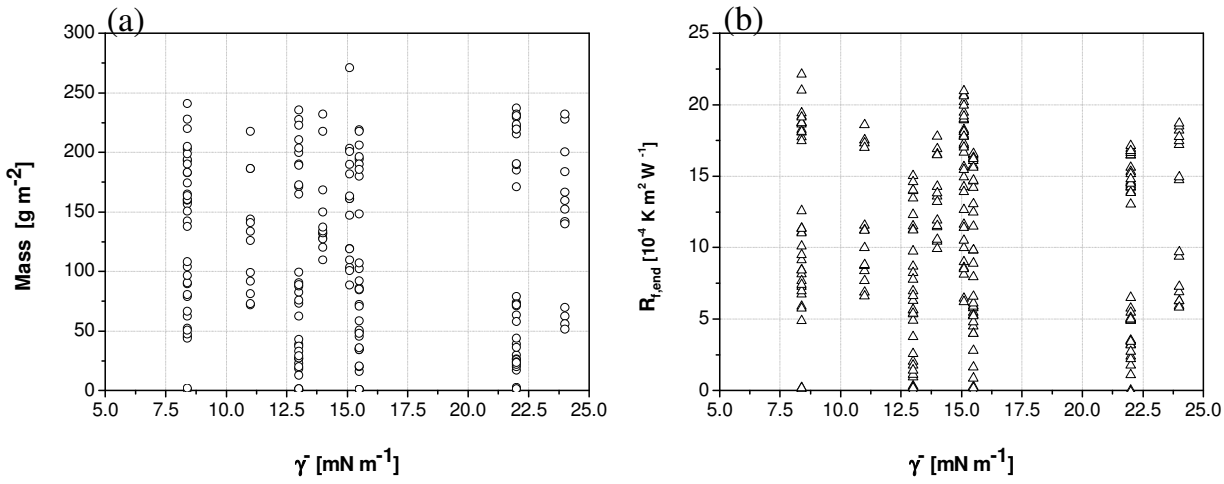

Fig. A3. (a) Deposit mass and (b) $R_{f,\ end}$ for fouling of whey protein, SMUF and WPI plus SMUF at initial temperatures of 80 and 120 °C (for SMUF, 105 °C) as a function of γ^-

The statistical tests of the data require the assumption that the data come from a normal distribuition (Montgomery, 1997). Therefore, the normal probability plotting of the original data is shown in Fig. A4 as well as in Figs. A9, A11 and A13 for the residuals of the estimated models. The data of $R_{f,\,end}$, deposited mass and $(dR_f/dt)_{1h}$ for whey protein, calcium phosphate and SMUF-rich whey protein fouling, at initial wall temperatures of T_0 = 80, 105 and 120°C, on the studied surfaces (coated and untreated unpolished and electropolished stainless steel coupons) is approximately normally distributed (Fig. A4). The extreme points (highest and lowest limits) for $R_{f,\,end}$, for mass as well as for $(dR_f/dt)_{1h}$ depart from normality. They represent: (i) the whey protein fouling at low temperature (T_0 = 80 °C), in which the thermal boundary layer has not hot sufficiently to protein denaturation, aggregation and further deposition as well as (ii) the SMUF-rich whey protein fouling at T_0 = 120°C, in which deposit aging probably occurred. According to Montgomery (1997) moderate departures from normality do not seriously affect the statistical tests.

Tables A3 and A4 show the Multiple Regression Analysis and the Analysis of Variance, respectively for the $R_{f,\,end}$, Tables A5 and A6 for the mass and Tables A7 and A8 for $(dR_f/dt)_{1h}$ for the complete models, including the quadratic and linear effects of T_0, γ^-, model solution (fluid) and R_z as well as the combined effect of these fators on $R_{f,\,end}$, mass and $(dR_f/dt)_{1h}$. Figs. A5 – A7 show the corresponding pareto diagrams and Figs. A8 – A10 the main effect plots. The pareto and the main effect diagrams give the magnitude of the factors on the dependent variables.

In determining whether the models can be simplified, it was noticed that the highest p value on the independent variables varied from 0.13 to 0.98 for $R_{f,\,end}$, mass and $(dR_f/dt)_{1h}$, the belonging to the interaction terms Cod_γ^- x Cod_R_z for all dependent variables, Cod_T_0 x Cod_γ^- for $(dR_f/dt)_{1h}$ as well as Cod_γ^- x Cod_fluid for deposit mass and $(dR_f/dt)_{1h}$, to the quadratic terms $(Cod\_T_0)^2$ and $(Cod\_fluid)^2$ for mass, Cod_γ^- for mass and Cod_fluid for $R_{f,\,end}$, mass and $(dR_f/dt)_{1h}$. Since the p value is greater or equal to 0.10, that term is not statistically significant at the 90% or higher confidence level. Consequently, these terms were removed from the models, with exception for $(Cod\_\gamma^-)^2$ for the $R_{f,\,end}$ and mass model, for Cod_fluid x Cod_R_z for mass and $(dR_f/dt)_{1h}$ and Cod_γ^- for $(dR_f/dt)_{1h}$. Tables A7 – A12 show the Multiple Regression Analysis and the Analysis of Variance for the $R_{f,\,end}$, mass and $(dR_f/dt)_{1h}$ for the reduced models with p values lower than 0.10. Figs. A9, A10 and A12 plot the observed versus the estimated values for the variables $R_{f,\,end}$ and mass. The normal probability plot of the residuals is shown in Figs. A9, A11 and A13. Since the residuals lie approximately along a straight line, any severe non-normality of the data is given.

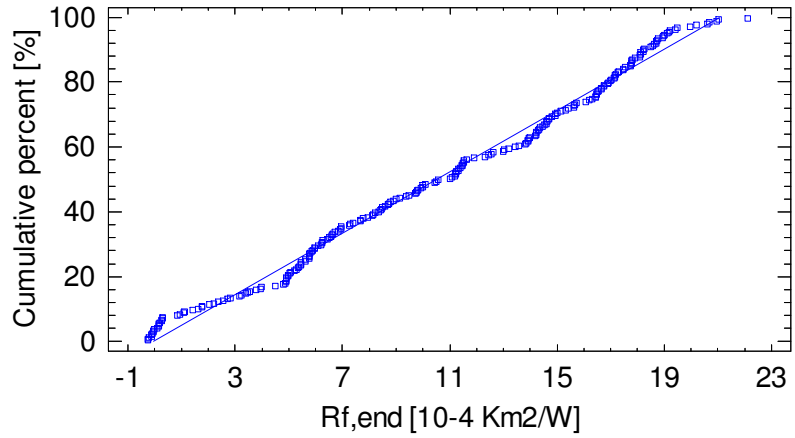

(a)

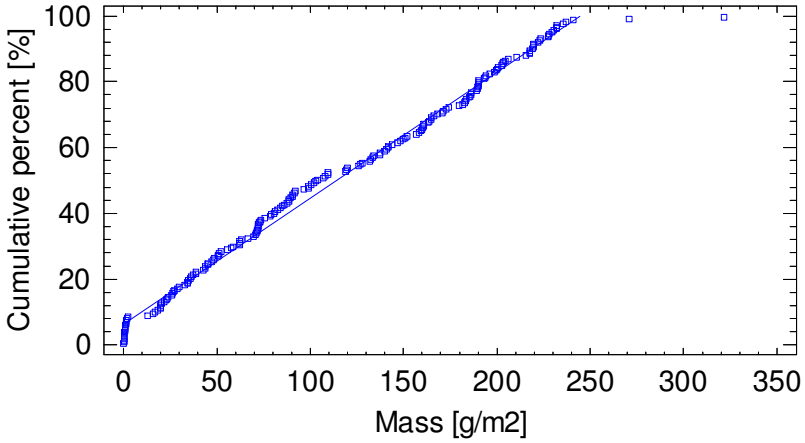

(b)

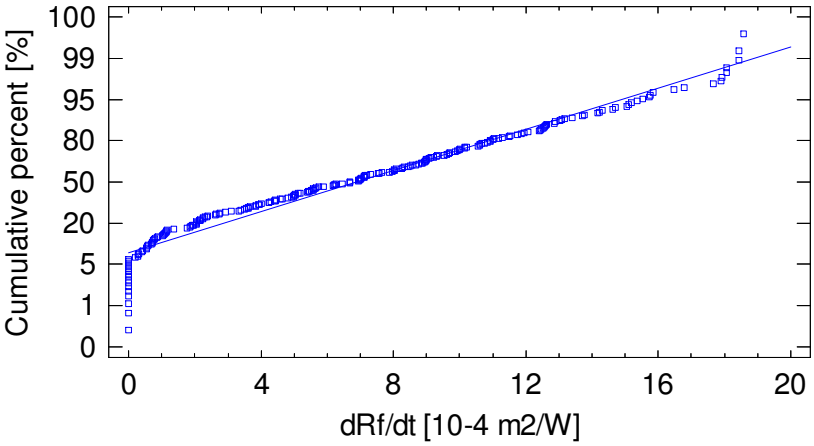

(c)

Fig. A4. Normal probably plot of (a) $R_{f,\,end}$, (b) mass and (c) $(dR_f/dt)_{1h}$

Table A3. Multiple Regression Analysis for the dependent variable $R_{f,\,end}$

Parameter	Estimate	Standard Error	T-Statistic	P value
Constant	6.50429	1.57186	4.13797	0
Cod_T_0 x Cod_T_0	6.70479	0.778164	8.61617	0
Cod_γ^- x Cod_γ^-	0.862589	0.553351	1.55885	0.1205
Cod_fluid x Cod_fluid	-3.4241	0.547153	-6.25802	0
Cod_Rz x Cod_Rz	5.82039	0.87461	6.65484	0
Cod_T_0 x Cod_γ^-	0.671227	0.228204	2.94134	0.0036
Cod_T_0 x Cod_fluid	0.70187	0.192933	3.6379	0.0003
Cod_T_0 x Cod_Rz	1.15969	0.183252	6.32839	0
Cod_γ^- x Cod_fluid	1.03999	0.600689	1.73133	0.0848
Cod_γ^- x Cod_Rz	-0.012427	0.477151	-0.0260442	0.9792
Cod_fluid x Cod_Rz	7.58565	2.34955	3.22856	0.0014
Cod_T_0	4.19459	0.192015	21.8451	0
Cod_γ^-	-1.44075	0.593019	-2.42951	0.0159
Cod_fluid	-2.45636	1.64225	-1.49573	0.1362
Cod_Rz	-8.89003	2.30649	-3.85435	0.0002

Table A4. ANOVA for $R_{f,\,end}$

Source	Sum of Squares	Df	Mean Square	F-Ratio	P value	R-squared
Model	8020.97	14	572.926	162.42	0	91.14 %
Residual	779.556	221	3.5274			
Total	8800.52	235				

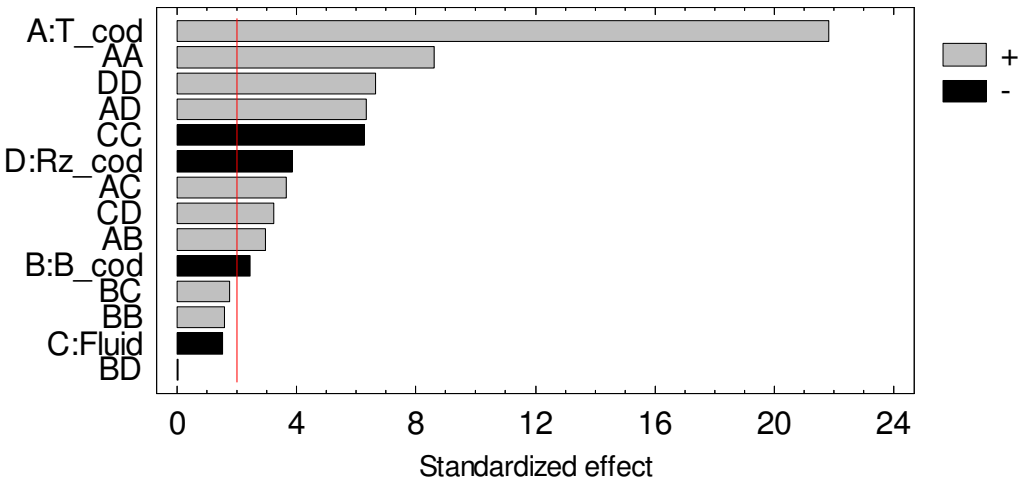

Fig. A5. Pareto diagram for $R_{f,\,end}$ (pareto index = 5%). A = T_cod; B = Base_cod; C = Fluid_cod; D = Rz_cod

Table A5. Multiple Regression Analysis for the dependent variable mass

Parameter	Estimate	Standard Error	T-Statistic	P value
Constant	109.635	28.4162	3.85817	0.0002
Cod_T_0 x Cod_T_0	15.2214	13.3493	1.14024	0.2557
Cod_γ^- x Cod_γ^-	16.3716	11.2843	1.45084	0.1486
Cod_fluid x Cod_fluid	-6.61328	9.66512	-0.684242	0.4947
Cod_Rz x Cod_Rz	31.8142	19.5386	1.62827	0.1052
Cod_T_0 x Cod_γ^-	20.6337	4.49923	4.58605	0
Cod_T_0 x Cod_fluid	14.9854	3.531	4.24394	0
Cod_T_0 x Cod_Rz	21.2592	3.96014	5.36829	0
Cod_γ^- x Cod_fluid	4.84001	11.0679	0.437302	0.6624
Cod_γ^- x Cod_Rz	-4.96206	9.44354	-0.525445	0.5999
Cod_fluid x Cod_Rz	68.151	42.6293	1.59869	0.1116
Cod_T_0	40.4596	3.70065	10.9331	0
Cod_γ^-	-5.86647	10.8727	-0.539557	0.5902
Cod_fluid	-3.86196	29.7371	-0.12987	0.8968
Cod_Rz	-83.6525	41.7039	-2.00587	0.0464

Table A6. ANOVA for mass

Source	Sum of Squares	Df	Mean Square	F-Ratio	P value	R-squared
Model	921020	14	65787.1	58.4	0	81.88 %
Residual	203881	181	1126.42			
Total	1.1249 x 10^6	195				

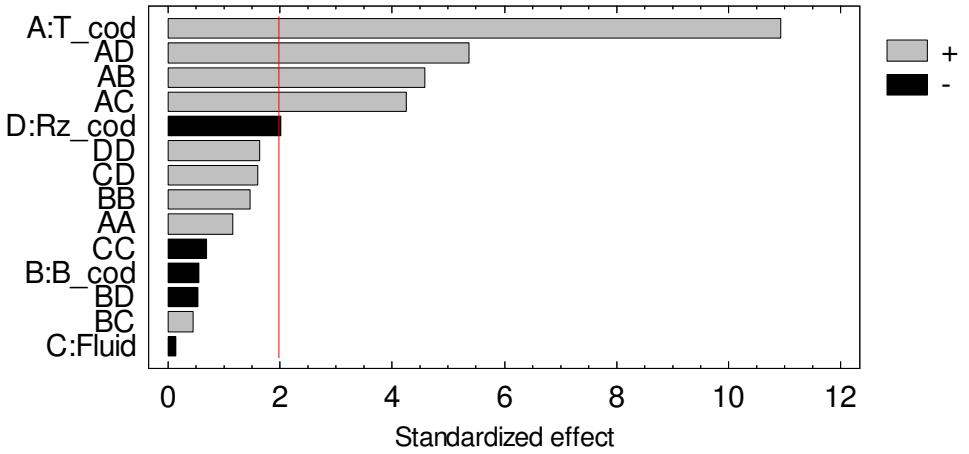

Fig. A6. Pareto diagram for mass (pareto index = 5%). A = T_cod; B = Base_cod; C = Fluid_cod; D = Rz_cod

Table A7. Multiple Regression Analysis for the dependent variable $(dR_f/dt)_{1h}$

Parameter	Estimate	Standard Error	T-Statistic	P value
Constant	5.96496	1.58571	3.76171	0.0002
Cod_T_0 x Cod_T_0	2.19785	0.778829	2.82199	0.0052
Cod_γ^- x Cod_γ^-	1.98494	0.582912	3.40522	0.0008
Cod_fluid x Cod_fluid	-2.56608	0.548212	-4.68083	0
Cod_Rz x Cod_Rz	2.51349	0.910266	2.76127	0.0063
Cod_T_0 x Cod_γ^-	-0.00862156	0.24071	-0.0358173	0.9715
Cod_T_0 x Cod_fluid	0.727068	0.193616	3.7552	0.0002
Cod_T_0 x Cod_Rz	-0.501905	0.193058	-2.59976	0.01
Cod_γ^- x Cod_fluid	-0.288785	0.598446	-0.482558	0.6299
Cod_γ^- x Cod_Rz	0.0225045	0.494102	0.0455462	0.9637
Cod_fluid x Cod_Rz	3.42869	2.36715	1.44844	0.149
Cod_T_0	3.80905	0.197151	19.3205	0
Cod_γ^-	-0.969599	0.606662	-1.59825	0.1115
Cod_fluid	-0.94351	1.65349	-0.570618	0.5689
Cod_Rz	-4.76988	2.32658	-2.05017	0.0416

Table A8. ANOVA for $(dR_f/dt)_{1h}$

Source	Sum of Squares	Df	Mean Square	F-Ratio	P value	R-squared
Model	4957.9	14	354.136	100.3	0	86.93 %
Residual	745.01	211	3.53085			
Total	1.1249×10^6	195				

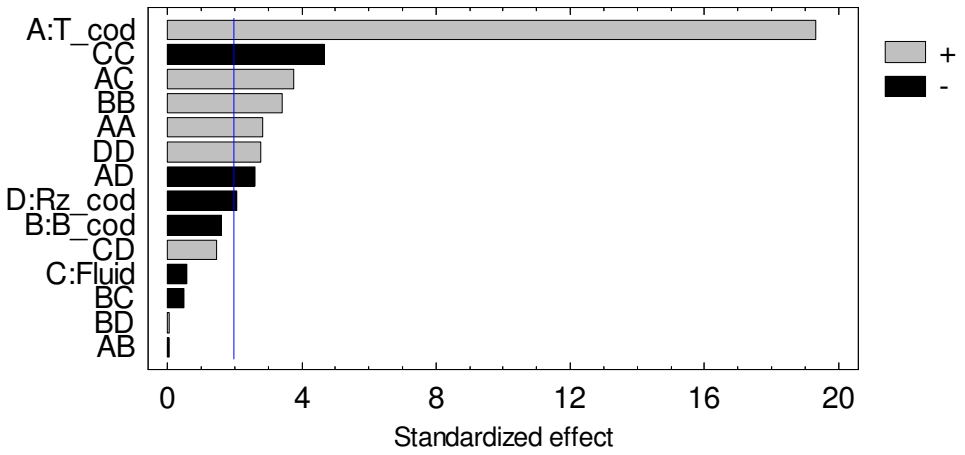

Fig. A7. Pareto diagram for $(dR_f/dt)_{1h}$ (pareto index = 5%). A = T_cod; B = Base_cod; C = Fluid_cod; D = Rz_cod

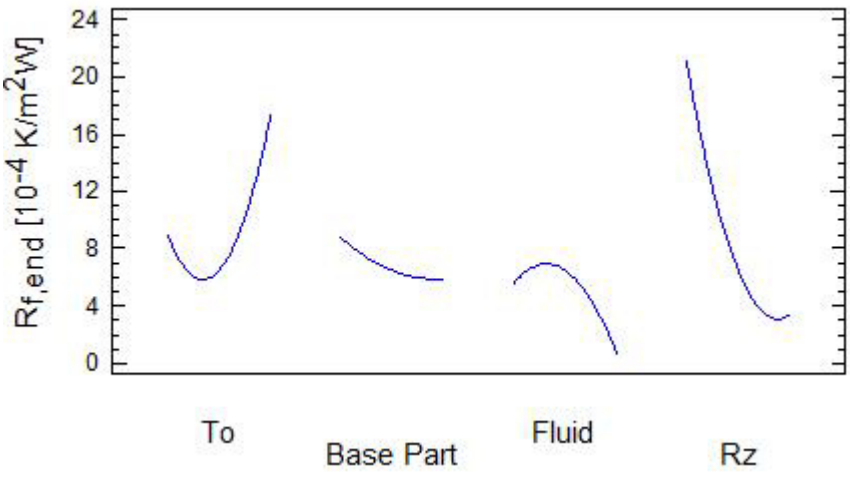

Fig. A8. Main effect plot for $dR_{f,end}$

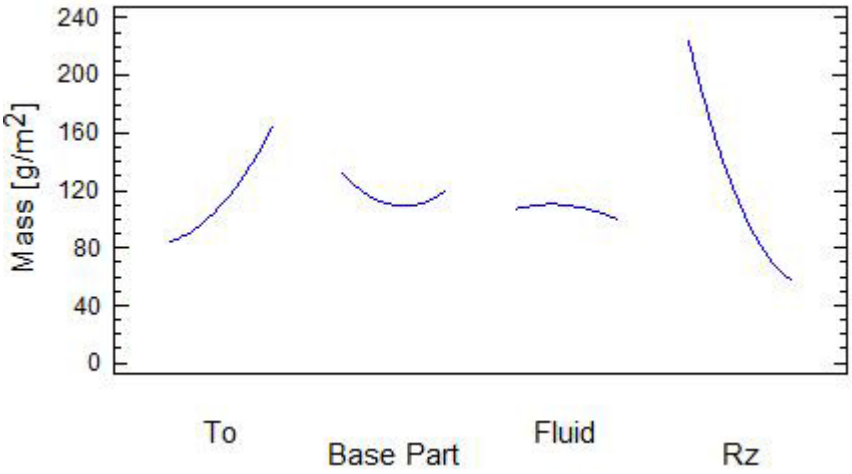

Fig. A9. Main effect plot for mass

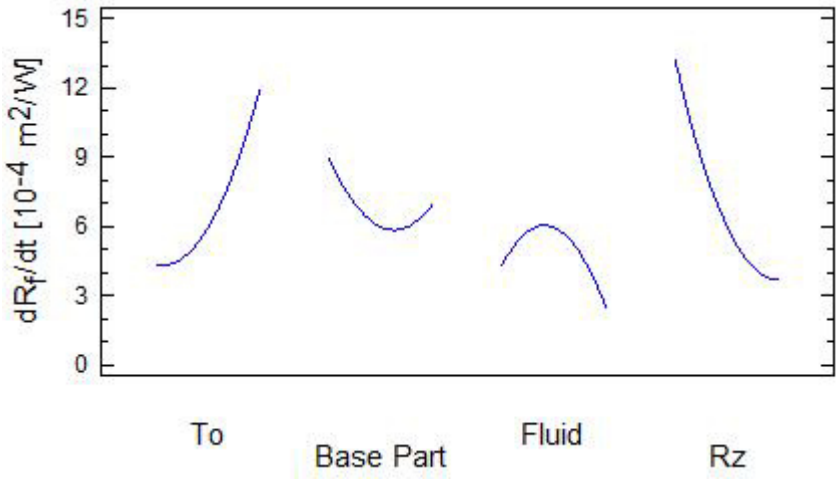

Fig. A10. Main effect plot for $(dR_f/dt)_{1h}$

Table A9. Multiple Regression Analysis for the dependent variable $R_{f,\,end}$ (simplified model)

Parameter	Estimate	Standard Error	T-Statistic	P value
Constant	4.23846	0.715554	5.92332	0
Cod_T_0 x Cod_T_0	6.64607	0.778505	8.53696	0
Cod_γ^- x Cod_γ^-	0.77858	0.409365	1.90192	0.0585
Cod_fluid x Cod_fluid	-3.37888	0.547609	-6.17024	0
Cod_Rz x Cod_Rz	5.57369	0.795791	7.00396	0
Cod_T_0 x Cod_ γ^-	0.696036	0.225144	3.09152	0.0022
Cod_T_0 x Cod_ fluid	0.729368	0.192388	3.79114	0.0002
Cod_T_0 x Cod_ Rz	1.16763	0.182557	6.39601	0
Cod_fluid x Cod_ Rz	3.95951	0.256315	15.4478	0
Cod_T_0	4.17371	0.191447	21.8008	0
Cod_γ^-	-0.583108	0.300018	-1.94358	0.0532
Cod_R_z	-5.30614	0.292606	-18.1341	0

Table A10. ANOVA for $R_{f,\,end}$ (simplified model)

Source	Sum of Squares	Df	Mean Square	F-Ratio	P value	R-squared
Model	8007.55	11	727.959	205.64	0	90.99 %
Residual	792.969	224	3.54004			
Total	8800.52	235				

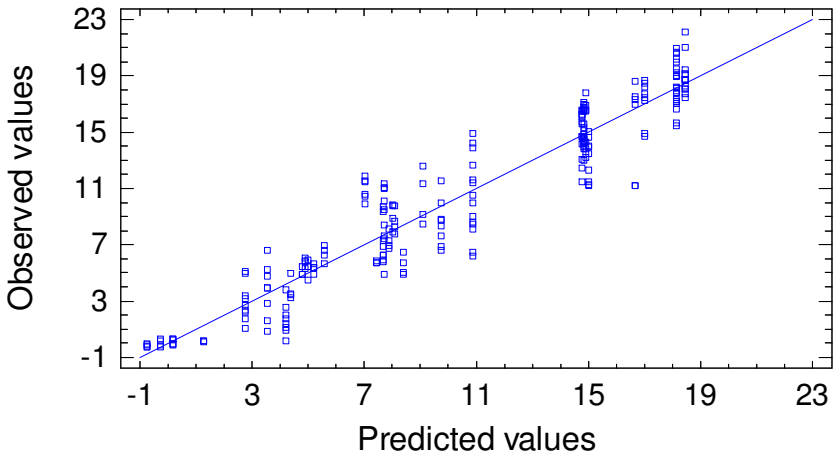

Fig. A11. Observed versus predicted values for the dependent variable $R_{f,\,end}$ (simplified model)

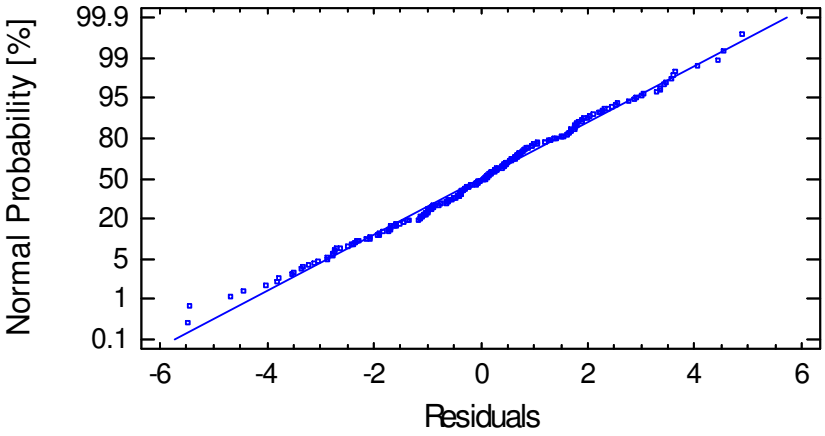

Fig. A12. Normal probability plot of residuals for the variable $R_{f,\,end}$ (simplified model)

Table A11. Multiple Regression Analysis for the dependent variable mass (simplified model)

Parameter	Estimate	Standard Error	T-Statistic	P value
Constant	108.18	7.12306	15.1873	0
Cod_γ^- x Cod_γ^-	18.5994	8.29851	2.24129	0.0262
Cod_Rz x Cod_Rz	41.0196	12.8179	3.20018	0.0016
Cod_T_0 x Cod_ γ^-	20.5183	4.35274	4.71389	0
Cod_T_0 x Cod_ fluid	15.512	3.44899	4.49755	0
Cod_T_0 x Cod_ Rz	20.6622	3.8598	5.35316	0
Cod_fluid x Cod_ Rz	61.2672	4.54503	13.48	0
Cod_T_0	39.4447	3.51612	11.2182	0
Cod_R_z	-74.9799	4.6384	-16.165	0

Table A12. ANOVA for mass (simplified model)

Source	Sum of Squares	Df	Mean Square	F-Ratio	P value	R-squared
Model	918046	8	114756	103.74	0	81.6 %
Residual	206855	187	1106.18			
Total	1.1249×10^6	195				

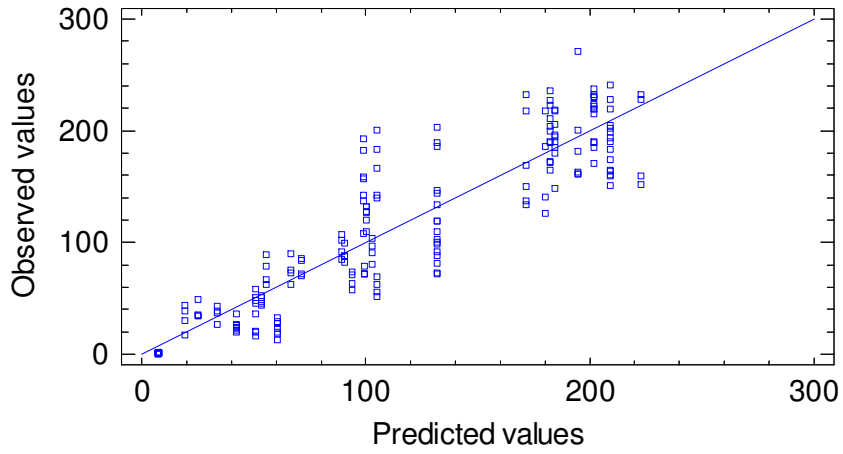

Fig. A13. Observed versus predicted values for the dependent variable mass (simplified model)

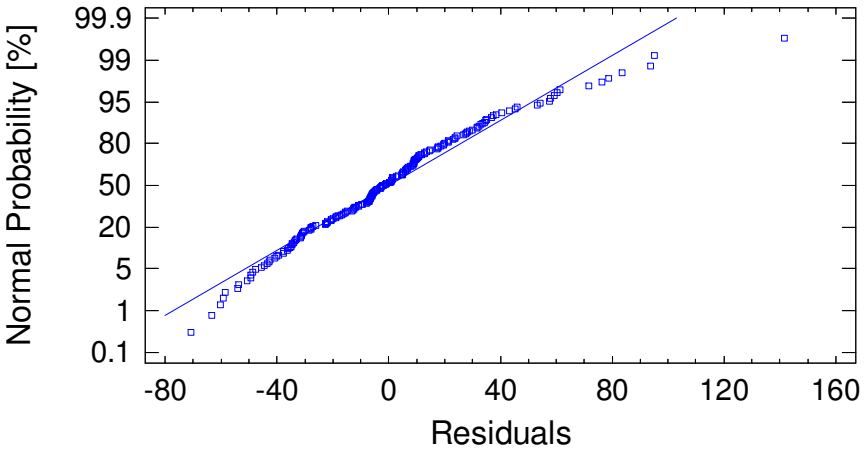

Fig. A14. Normal probability plot of residuals for the variable mass (simplified model)

Table A13. Multiple Regression Analysis for the dependent variable $(dR_f/dt)_{1h}$ (simplified model)

Parameter	Estimate	Standard Error	T-Statistic	P value
Constant	6.50302	0.596542	10.9012	0
Cod_T_0 x Cod_T_0	2.47259	0.796124	3.10578	0.0022
Cod_γ^- x Cod_γ^-	2.45704	0.375556	6.54241	0
Cod_fluid x Cod_fluid	-2.85397	0.55729	-5.12116	0
Cod_T_0 x Cod_ fluid	0.917003	0.186372	4.92028	0
Cod_fluid x Cod_R_z	2.21575	0.264504	8.37703	0
Cod_T_0	3.62807	0.186015	19.5042	0
Cod_γ^-	-1.7306	0.23884	-7.24587	0
Cod_R_z	-4.1283	0.274089	-15.0619	0

Table A14. ANOVA for $(dR_f/dt)_{1h}$ (simplified model)

Source	Sum of Squares	Df	Mean Square	F-Ratio	P value	R-squared
Model	4888.53	8	611.066	162.82	0	85.7 %
Residual	814.384	217	3.75292			
Total	1.1249×10^6	195				

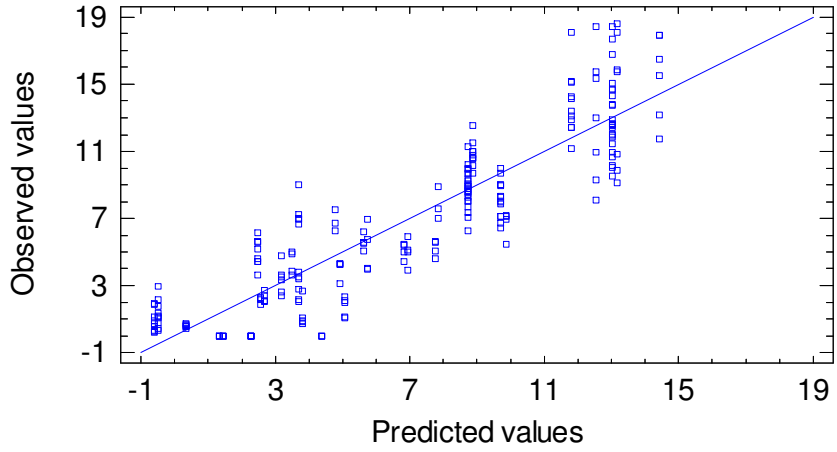

Fig. A15. Observed versus predicted values for the dependent variable $(dR_f/dt)_{1h}$ (simplified model)

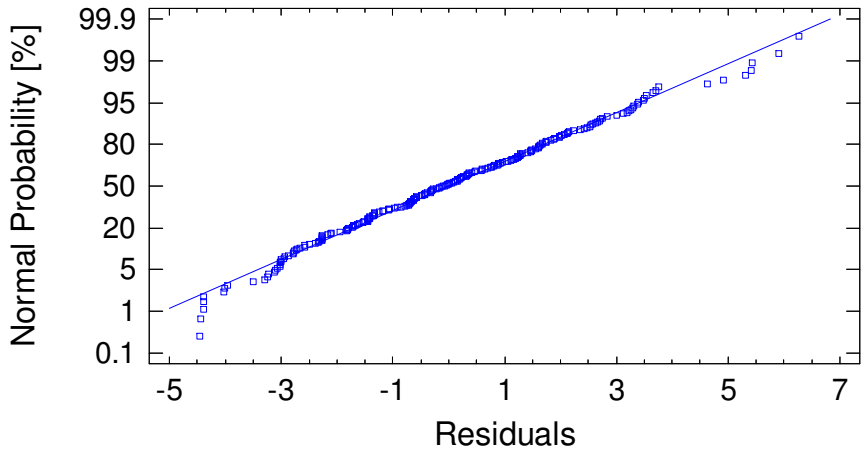

Fig. A16. Normal probability plot of residuals for the variable $(dR_f/dt)_{1h}$ (simplified model)

A5. Statistical analysis of results from continuous fouling experiments (PHE)

This section gives the statistical analysis for the WPI plus SMUF deposition experiments on the plate heat exchanger. Tables A15, A16, A19, A20, A23 and A24 show the statistical analysis for the complete models, including the plate roughness (R_z) as a factor influencing the final fouling resistance, $(dR_f/dt)_{0.5h}$ and the protein/mineral ratio. Since the p value for $(R_z)^2$, γ^- x R_z and R_z in the ANOVA table (Table A15) is greater than 0.10, there is not a statistically significant relationship between these terms and the dependent variable $R_{f,\,end}$ at the 90% or higher confidence level. As shown in the section A4 for the coupons, the effect of

roughness on $R_{f,\,end}$ was also not statistically significant. Therefore, the model was simplified and the results of the statistical analyses were depicted on Tables A17 and A18. A similar procedure as for analysis of the $R_{f,\,end}$ was performed for the dependent variables $(dR_f/dt)_{0.5h}$ and deposit protein/mineral ratio. Again, no influence of the roughness on the fouling behavior was found. Tables A21 – A22 and Tables A25 – A26 show the multiple regression analysis and the ANOVA of the simplified models for $(dR_f/dt)_{0.5h}$ and protein/mineral ratio, respectively. Figs. A17, A18 and A21 plot the observed versus the estimated values for the variables $R_{f,\,end}$, $(dR_f/dt)_{0.5h}$ and mineral/protein ratio. The normal probability plots of the residuals are shown in Figs. A18, A20 and A22. Since the residuals lie approximately along a straight line, any severe non-normality of the data is given. Thus, the specifications of the models are satisfied.

Table A15. Multiple Regression Analysis for the dependent variable $R_{f,\,end}$ (complete model)

Parameter	Estimate	Standard Error	T-Statistic	P value
Constant	-39.7867	46.6068	-0.853669	0.4832
γ^- x γ^-	0.214839	0.0613132	3.50396	0.0727
Rz x Rz	-41.1647	31.434	-1.30956	0.3206
γ^- x Rz	2.29852	2.13087	1.07867	0.3935
γ^-	-6.42239	3.31074	-1.93987	0.1919
Rz	95.9455	75.9354	1.26352	0.3337

Table A16. ANOVA for $R_{f,\,end}$ (complete model)

Source	Sum of Squares	Df	Mean Square	F-Ratio	P value	R-squared
Model	18.4583	5	3.69166	3.73	0.225	90.3083 %
Residual	1.98091	2	0.990453			
Total	20.4392	7				

Table A17. Multiple Regression Analysis for the dependent variable $R_{f,\,end}$ (simplified model)

Parameter	Estimate	Standard Error	T-Statistic	P value
Constant	11.838	2.51977	4.69806	0.0033
γ^- x γ^-	0.14164	0.0359255	3.9426	0.0076
γ^-	-2.41823	0.632808	-3.82143	0.0087

Table A18. ANOVA for $R_{f,\,end}$ (simplified model)

Source	Sum of Squares	Df	Mean Square	F-Ratio	P value	R-squared
Model	15.6629	2	7.83143	7.86	0.0211	72.3701 %
Residual	5.97987	6	0.996644			
Total	21.6427	8				

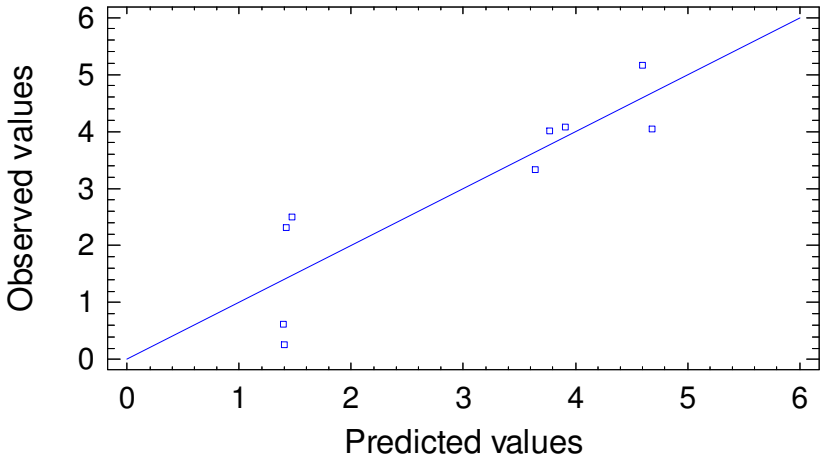

Fig. A17. Observed versus predicted values for the dependent variable $R_{f,\,end}$ (PHE)

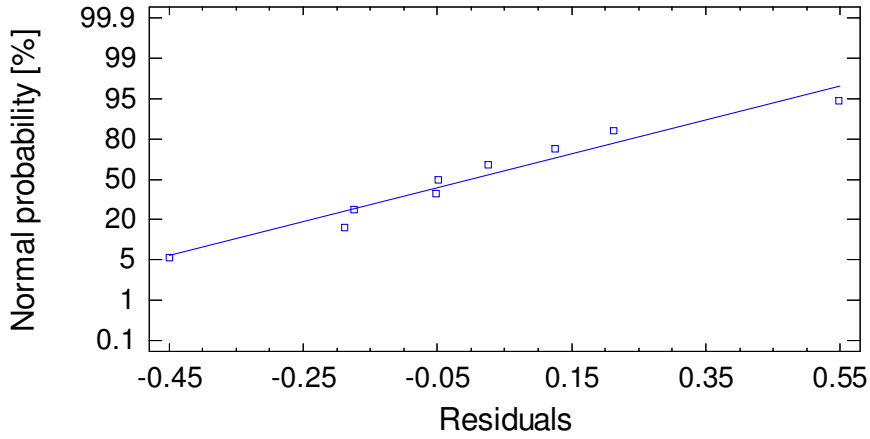

Fig. A18. Normal probability plot of residuals for the dependent variable $R_{f,\,end}$ (PHE)

Table A19. Multiple Regression Analysis for the dependent variable $(dR_f/dt)_{0.5h}$ (complete model)

Parameter	Estimate	Standard Error	T-Statistic	P value
Constant	-25.578	254.487	-0.100508	0.9362
γ^- x γ^-	0.380477	0.288477	1.31892	0.413
Rz x Rz	8.24561	120.532	0.0684102	0.9565
γ^- x Rz	-4.47885	7.12108	-0.628956	0.6426
γ^-	-1.5649	4.70754	-0.332423	0.7957
Rz	35.2222	362.472	0.0971722	0.9383

Table A20. ANOVA for $(dR_f/dt)_{0.5h}$ (complete model)

Source	Sum of Squares	Df	Mean Square	F-Ratio	P value	R-squared
Model	32.5372	5	6.50744	1.55	0.5336	88.567 %
Residual	4.20006	1	4.20006			
Total	36.7372	6				

Table A21. Multiple Regression Analysis for the dependent variable $(dR_f/dt)_{0.5h}$ (simplified model)

Parameter	Estimate	Standard Error	T-Statistic	P value
Constant	18.5059	4.47691	4.13364	0.0145
$\gamma^- \times \gamma^-$	0.226046	0.0669211	3.3778	0.0278
γ^-	-4.1066	1.1834	-3.47018	0.0256

Table A22. ANOVA for $(dR_f/dt)_{0.5h}$ (simplified model)

Source	Sum of Squares	Df	Mean Square	F-Ratio	P value	R-squared
Model	27.6992	2	13.8496	6.13	0.0605	75.398 %
Residual	9.03801	4	2.2595			
Total	36.7372	6				

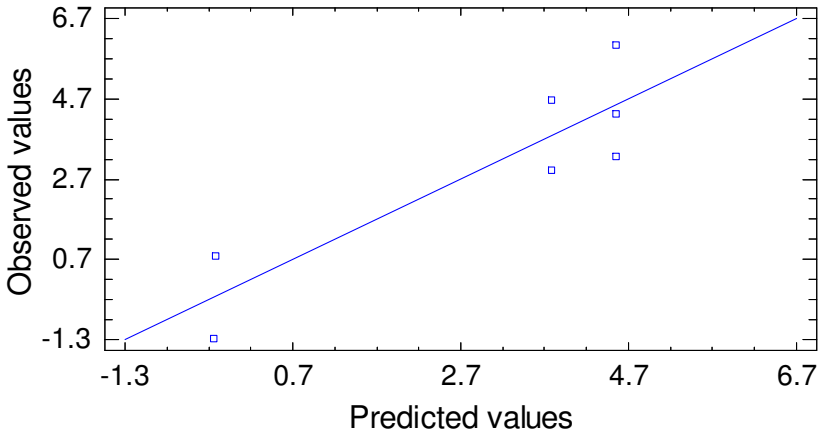

Fig. A19. Observed versus predicted values for the dependent variable $(dR_f/dt)_{0.5h}$ (PHE)

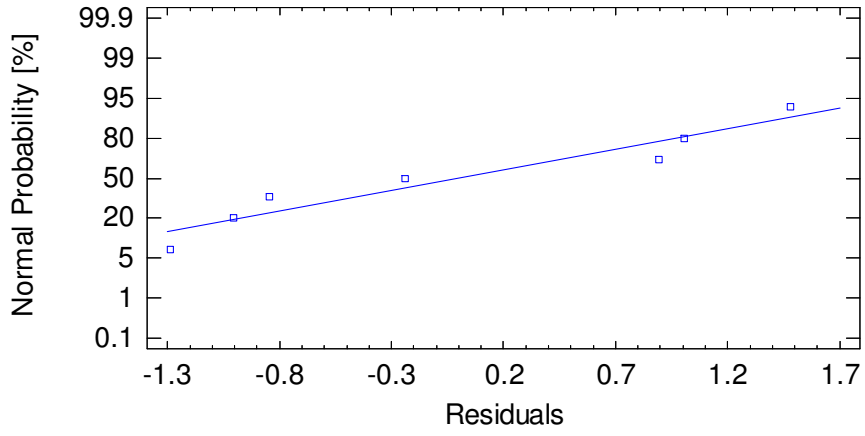

Fig. A20. Normal probability plot of residuals for the dependent variable $(dR_f/dt)_{0.5h}$ (PHE)

Table A23. Multiple Regression Analysis for the dependent variable protein/mineral ratio (complete model)

Parameter	Estimate	Standard Error	T-Statistic	P value
Constant	-19.6722	147.877	-0.133031	0.9026
γ^- x γ^-	0.0682149	0.243663	0.279956	0.7977
Rz x Rz	-0.660558	65.5484	-0.0100774	0.9926
γ^- x Rz	-2.13597	5.98939	-0.356625	0.745
γ^-	1.32797	8.31409	0.159726	0.8832
Rz	22.344	209.233	0.10679	0.9217

Table A24. ANOVA for protein/mineral ratio (complete model)

Source	Sum of Squares	Df	Mean Square	F-Ratio	P value	R-squared
Model	1.6665	5	0.3333	2.76	0.2165	82.138 %
Residual	0.362389	3	0.120796			
Total	2.02889	8				

Table A25. Multiple Regression Analysis for the dependent variable protein/mineral ratio (simplified model)

Parameter	Estimate	Standard Error	T-Statistic	P value
Constant	4.42148	0.815348	5.42282	0.0016
γ^- x γ^-	0.0415014	0.0116284	3.56897	0.0118
γ^-	-0.748447	0.204805	-3.65444	0.0106

Table A26. ANOVA for protein/mineral ratio (simplified model)

Source	Sum of Squares	Df	Mean Square	F-Ratio	P value	R-squared
Model	1.4015	2	0.70075	6.7	0.0296	69.077 %
Residual	0.627389	6	0.104565			
Total	2.02889	8				

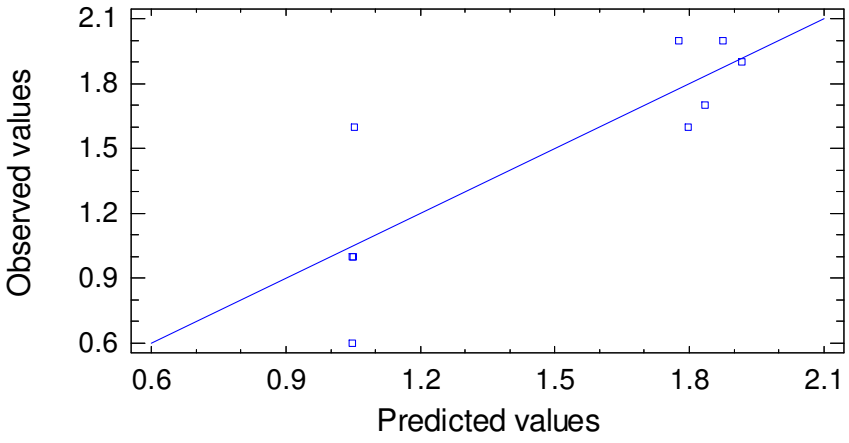

Fig. A21. Observed versus predicted values for the dependent variable protein/mineral content (PHE)

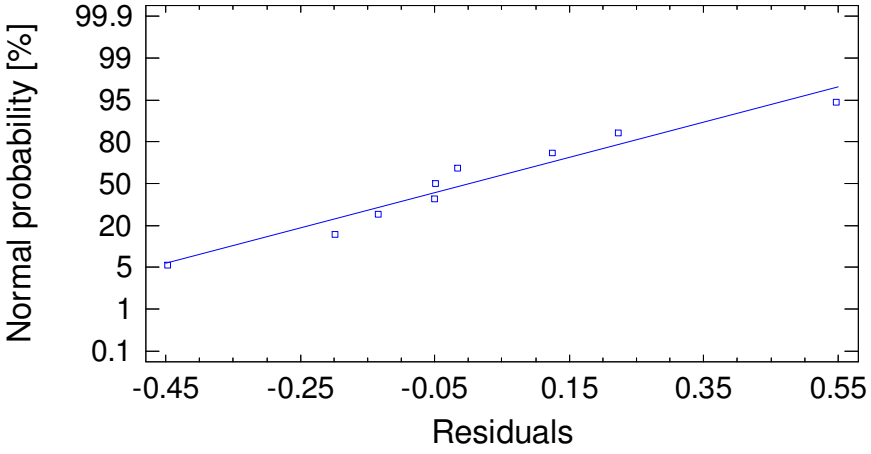

Fig. A22. Normal probability plot of residuals for the variable protein/mineral ratio (PHE)

A6. Statistical analysis of results from cleaning experiments

Tables A27, A28, A31, A32 and Tables A35, A36, A39, A40 show the statistical analysis for the maximal cleaning rate and the fouling resistance, respectively, at the NaOH concentrations of 0.25 % w/w and 0.50 % w/w, with the coupon roughness and the electron donor component as factors influencing $r_{c,m}$ and (R_f after 30 min cleaning/$R_{f,\,end}$ after fouling). Since the p value for $(R_z)^2$, $(\gamma^-)^2$, γ^- x R_z and R_z in the ANOVA table is greater than 0.10, there is not a statistically significant relationship between these terms and the dependent variable. A further simplification of the models resulted in non statistically significant effect of the factors γ^- and R_z on the dependent variables $r_{c,m}$ and (R_f after 30 min cleaning/$R_{f,\,end}$ after fouling) at 0.25 % w/w NaOH (Tables A29, A30, A37 and A38) or no fitting of the model for the variable $r_{c,m}$ at 0.50 % w/w NaOH (Tables A33 and A34), viz. low R^2. However, the ANOVA show a statistically significant effect of the factors γ^- and R_z on the dependent (R_f after 30 min cleaning/$R_{f,\,end}$ after fouling) at 0.50 % w/w NaOH (Tables A41 and A42, Figs. A23 and A24) and a linear model could be fitted to the data:

$$\frac{R_{f,cleaning,30\,min}}{R_{f,fouling,end}} = 0.20 - 0.0045\,\gamma^{-1} - 0.048\,R_z \qquad \text{(a.8)}$$

The determination coefficient R^2 is 70.2 % and the standard error 0.014.

Table A27. Multiple Regression Analysis for the dependent variable cleaning rate ($r_{c,m}$) with 0.25 % w/w NaOH

Parameter	Estimate	Standard Error	T-Statistic	P value
Constant	-0.0784999	0.0623155	-1.25972	0.2161
γ^- x γ^-	-0.00021971	0.00015961	-1.37658	0.1774
R_z x R_z	-0.0562297	0.039679	-1.41711	0.1653
γ^- x R_z	-0.00031744	0.0013812	-0.229829	0.8196
γ^-	0.00806333	0.00651631	1.23741	0.2242
R_z	0.147099	0.102037	1.44162	0.1583

Table A28. ANOVA for the dependent variable cleaning rate ($r_{c,m}$) with 0.25 % w/w NaOH

Source	Sum of Squares	Df	Mean Square	F-Ratio	P value	R-squared
Model	0.00157122	5	0.00031424	1.52	0.209	17.83 %
Residual	0.00723893	35	0.00020683			
Total	0.00881015	40				

Table A29. Multiple Regression Analysis for the dependent variable cleaning rate ($r_{c,m}$) with 0.25 % w/w NaOH (simplified model)

Parameter	Estimate	Standard Error	T-Statistic	P value
Constant	0.0571623	0.00959777	5.95579	0
γ^-	0.00057696	0.00050497	1.14255	0.2604
R_z	0.00060606	0.0052769	0.114851	0.9092

Table A30. ANOVA for the dependent variable cleaning rate ($r_{c,m}$) with 0.25 % w/w NaOH (simplified model)

Source	Sum of Squares	Df	Mean Square	F-Ratio	P value	R-squared
Model	0.00030408	2	0.00015204	0.68	0.5131	3.45 %
Residual	0.00850607	38	0.00022384			
Total	0.00881015	40				

Table A31. Multiple Regression Analysis for the dependent variable cleaning rate ($r_{c,m}$) with 0.50 % w/w NaOH

Parameter	Estimate	Standard Error	T-Statistic	P value
Constant	-0.0479604	0.170749	-0.280882	0.7806
γ^- x γ^-	-0.00067758	0.00043359	-1.56272	0.1277
R_z x R_z	0.0805105	0.100004	0.805077	0.4265
γ^- x R_z	-0.00225079	0.003523	-0.638885	0.5273
γ^-	0.0310603	0.0184624	1.68236	0.1019
R_z	-0.192736	0.253959	-0.758924	0.4533

Table A32. ANOVA for the dependent variable cleaning rate ($r_{c,m}$) with 0.50 % w/w NaOH

Source	Sum of Squares	Df	Mean Square	F-Ratio	P value	R-squared
Model	0.0201353	5	0.00402706	3.59	0.0105	35.25 %
Residual	0.0369705	33	0.00112032			
Total	0.0571058	38				

Table A33. Multiple Regression Analysis for the dependent variable cleaning rate ($r_{c,m}$) with 0.50 % w/w NaOH (simplified model)

Parameter	Estimate	Standard Error	T-Statistic	P value
Constant	0.047902	0.0159757	2.99842	0.0048
γ^-	0.00382963	0.00097691	3.92014	0.0004

Table A34. ANOVA for the dependent variable cleaning rate ($r_{c,m}$) with 0.50 % w/w NaOH (simplified model)

Source	Sum of Squares	Df	Mean Square	F-Ratio	P value	R-squared
Model	0.016758	1	0.016758	15.37	0.0004	29.35 %
Residual	0.0403478	37	0.00109048			
Total	0.0571058	38				

Table A35. Multiple Regression Analysis for the dependent variable (R_f after 30 min cleaning/$R_{f,\,end}$ after fouling) with 0.25 % w/w NaOH

Parameter	Estimate	Standard Error	T-Statistic	P value
Constant	0.325618	0.130504	2.49507	0.0317
$\gamma^- \times \gamma^-$	-0.00021959	0.00028205	-0.778566	0.4543
$R_z \times R_z$	0.17954	0.0727639	2.46744	0.0333
$\gamma^- \times R_z$	-0.001611	0.0025432	-0.633455	0.5407
γ^-	0.00903829	0.0117146	0.771539	0.4582
R_z	-0.463557	0.197019	-2.35286	0.0404

Table A36. ANOVA for the dependent variable (R_f after 30 min cleaning/$R_{f,\,end}$ after fouling) with 0.25 % w/w NaOH

Source	Sum of Squares	Df	Mean Square	F-Ratio	P value	R-squared
Model	0.00316852	5	0.0006337	2.36	0.1158	54.15 %
Residual	0.00268202	10	0.0002682			
Total	0.00585054	15				

Table A37. Multiple Regression Analysis for the dependent variable (R_f after 30 min cleaning/$R_{f, end}$ after fouling) with 0.25 % w/w NaOH (simplified model)

Parameter	Estimate	Standard Error	T-Statistic	P value
Constant	0.149213	0.0219401	6.8009	0
γ^-	-0.0013575	0.000923	-1.47075	0.1651
R_z	-0.0151499	0.0110307	-1.37343	0.1928

Table A38. ANOVA for the dependent variable (R_f after 30 min cleaning/$R_{f, end}$ after fouling) with 0.25 % w/w NaOH (simplified model)

Source	Sum of Squares	Df	Mean Square	F-Ratio	P value	R-squared
Model	0.00122834	2	0.00061417	1.73	0.2161	20.99 %
Residual	0.0046222	13	0.00035555			
Total	0.00585054	15				

Table A39. Multiple Regression Analysis for the dependent variable (R_f after 30 min cleaning/$R_{f, end}$ after fouling) with 0.50 % w/w NaOH

Parameter	Estimate	Standard Error	T-Statistic	P value
Constant	0.538395	0.115016	4.68106	0.0009
$\gamma^- \times \gamma^-$	0.00054353	0.00024857	2.18659	0.0536
$R_z \times R_z$	0.12928	0.064128	2.01597	0.0715
$\gamma^- \times R_z$	0.00088955	0.00224136	0.396881	0.6998
γ^-	-0.0238754	0.0103243	-2.31255	0.0433
R_z	-0.391566	0.173636	-2.2551	0.0478

Table A40. ANOVA for the dependent variable (R_f after 30 min cleaning/$R_{f, end}$ after fouling) with 0.50 % w/w NaOH

Source	Sum of Squares	Df	Mean Square	F-Ratio	P value	R-squared
Model	0.0162895	5	0.00325791	15.64	0.0002	88.66 %
Residual	0.00208317	10	0.00020832			
Total	0.0183727	15				

Table A41. Multiple Regression Analysis for the dependent variable (R_f after 30 min cleaning/$R_{f, end}$ after fouling) with 0.50 % w/w NaOH (simplified model)

Parameter	Estimate	Standard Error	T-Statistic	P value
Constant	0.198124	0.0238941	8.29175	0
γ^-	-0.00448375	0.0010052	-4.46056	0.0006
R_z	-0.0479082	0.012013	-3.98802	0.0015

Table A42. ANOVA for the dependent variable (R_f after 30 min cleaning/$R_{f,\,end}$ after fouling) with 0.50 % w/w NaOH (simplified model)

Source	Sum of Squares	Df	Mean Square	F-Ratio	P value	R-squared
Model	0.0128906	2	0.00644529	15.28	0.0004	70.16 %
Residual	0.00548214	13	0.0004217			
Total	0.0183727	15				

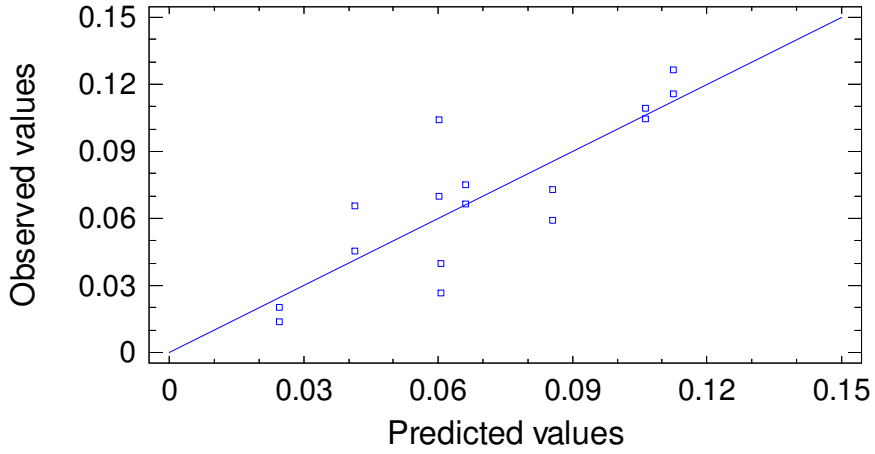

Fig. A23. Observed versus predicted values for the dependent variable (R_f after 30 min cleaning/$R_{f,\,end}$ after fouling) with 0.50 % w/w NaOH

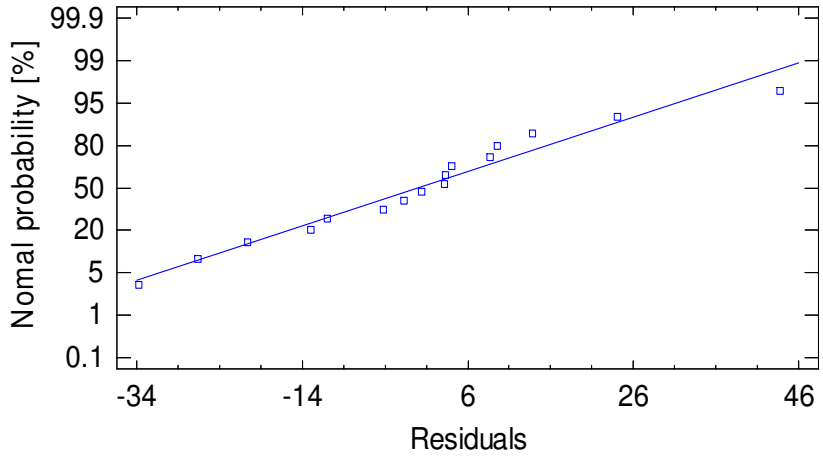

Fig. A24. Normal probability plot of residuals for the dependent variable (R_f after 30 min cleaning/$R_{f,\,end}$ after fouling) with 0.50 % w/w NaOH

Curriculum Vitae

Personal data

Name:	Cristiane Boxler, born Vieira Ferreira
Date of birth:	02/26/1975
Place of birth:	Belo Horizonte, Brazil
Family status:	married, a son (04/24/2003)
Nationality:	Brazilian and German

Academic studies

01/2008 – 05/2014	Doctoral studies in Engineering, Institute of Chemical and Thermal Process Engineering, Technische Universität Braunschweig
03/1999 – 07/2001	Master studies in Food Engineering, State University of Campinas, Brazil M.Sc. Thesis: Influence of tangential flow velocity and trans-membrane pressure on separation of casein from skim milk by microfiltration
02/1993 – 12/1997	Graduate studies in Chemical Engineering, Federal University of Minas Gerais, Brazil

Academic professional experience

since 06/2014	Process Engineer, Milchwerke “Mittelelbe” GmbH, Stendal
10/2006 – 07/2012	Research assistant, Institute of Chemical and Thermal Process Engineering, Technische Universität Braunschweig Guest researcher at the University of Porto, Portugal
10/2008 – 09/2010	Advising of graduate and undergraduate students/researchers
04/2008 – 06/2011	Teaching assistant
10/2001 – 02/2003	Research assistant, Institute for Food Process Engineering, Technische Universität München Project: Fermentation and vacuum drying of starter cultures
05/1998 – 02/1999	Research assistant, Institute of Food Technology, Brazil Project: Deodorization of “soymilk” to reduce off-flavors
03/1997 – 08/1997	Research assistant, Department of Production Engineering, Federal University of Minas Gerais, Brazil Project: Supply and demand logistics of the Brazilian milk industries
03/1995 – 06/1997	Research assistant, Department of Chemical Engineering, Federal University of Minas Gerais, Brazil Project: Synthesis, characterization and structural study of polymer systems consisting of/with polyacrylamide and poly(ethylenoglycol)

Journal Referee

Journal of Food Engineering, Heat and Mass Transfer, Colloids and Surfaces B: Biointerfaces Scientific Research and Essay, Chemical Product and Process Modeling